8 Physical processes and tools for levee assessment and design

Courtesy E Durand

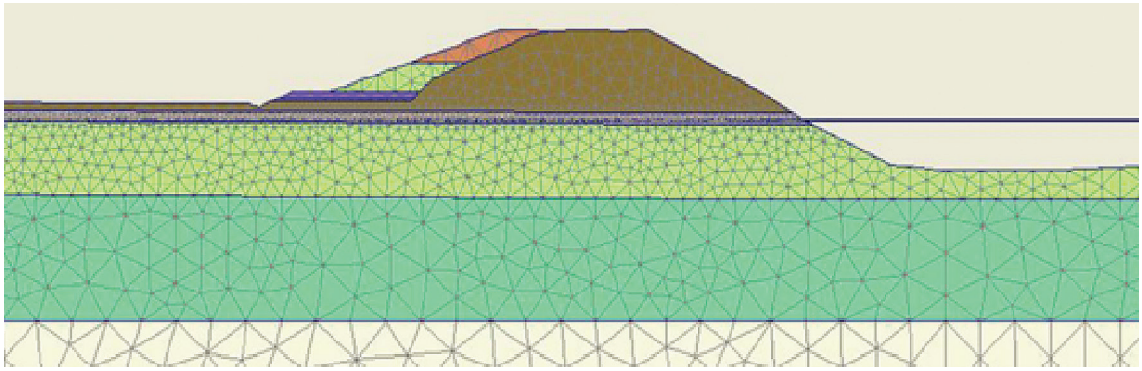

Courtesy E Durand

CHAPTER 8 CONTENTS

8 PHYSICAL PROCESSES AND TOOLS FOR LEVEE ASSESSMENT AND DESIGN

Chapter 8 details the morphological, hydraulic and geotechnical analysis tools needed to assess performance of a levee.

Key inputs from other chapters

- Chapter 3 ⇨ **functions, forms and failure mechanisms**
- Chapter 5 ⇨ **requirements for analysis**
- Chapter 7 ⇨ **morphological, hydraulic and geotechnical parameters**
- Chapter 9 ⇨ **requirements for analysis.**

Key outputs to other chapters

- **Tools for levee assessment, design and construction** ⇨ Chapters 5, 9 and 10

Note: The reader should **revisit Chapters 2 and 3** throughout the levee life cycle for a reminder of important issues.

This flow chart shows where to find information in the chapter and how it relates to other chapters. Use it in combination with the contents page to navigate the manual.

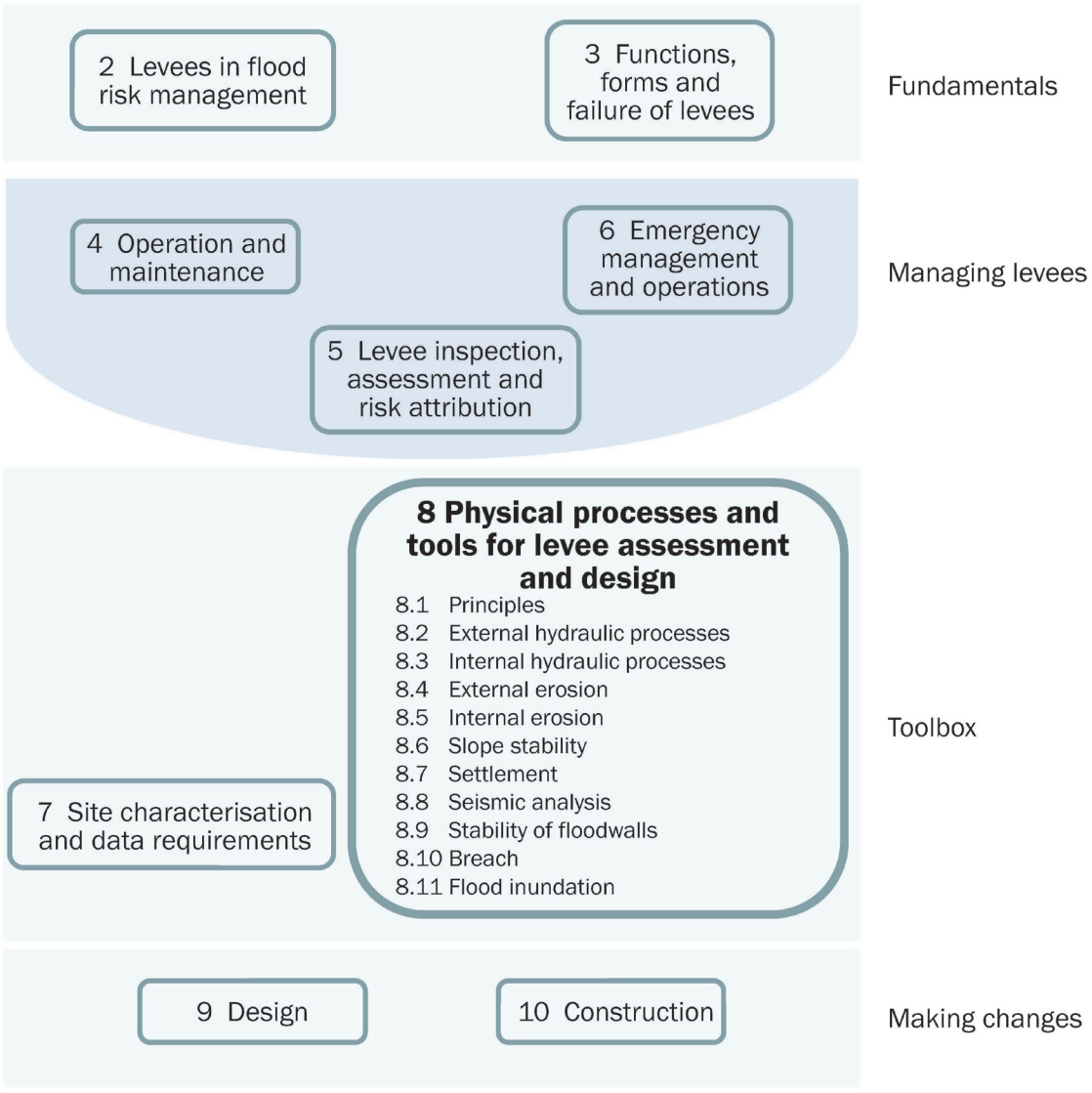

CHAPTER CONTENTS AND TARGET USER

This chapter is divided into 11 sections, and serves as a toolbox, which gives a thorough analysis of levee performance. The chapter first discusses the external and internal hydraulic processes that impose loading on the levee, through to the basic failure mechanisms of external erosion, internal erosion and slope instability. Additionally, the chapter addresses several critical issues including settlement, seismic loading, and stability of flood walls. The chapter concludes with a treatment of breaching and inundation modelling.

Principles

Section 8.1 introduces the key principles discussed in the chapter, and issues relating to levee analysis. It also provides links with other chapters.

External hydraulic processes

Section 8.2 describes the multiple hydraulic processes that impose loading on a levee. These processes include wave run-up and overtopping, overflow, and scour in river channels, on beaches and in front of coastal levees.

Internal hydraulic processes

Section 8.3 details multiple hydraulic processes that occur within the levee, which can lead to deterioration and damage. These processes include seepage and pore pressure and their impacts.

External erosion

Section 8.4 describes the principles and concepts of external erosion. The section details resistance to erosion from grass systems and other erosion resistant systems. Resistance of protection systems to erosion due to currents and waves is also presented.

Internal erosion

Section 8.5 discusses the principles of internal erosion including backward erosion, concentrated leak erosion, suffusion, contact erosion, as well as use and stability of filters.

Slope stability

Section 8.6 details methods to analyse slope stability from simplified methods, design charts, limit equilibrium methods, limit analysis approaches, and stress deformation analysis.

Settlement

Section 8.7 presents the principles of settlement analysis, assumptions and approximations, settlement calculation, verification of settlement prediction and use of finite element methods (FEM).

Seismic analysis

Section 8.8 details the analysis of a levee from seismic loading. This includes the governing parameters, slope stability with inclusion of dynamics, crest settlement, and liquefaction.

Stability of flood walls

Section 8.9 provides information related to the analysis of flood wall stability from hydraulic forces acting on flood walls. Analysis for stability of T-walls and I-walls is further detailed in the section.

Breach

Section 8.10 aids in understanding the breaching process, determining the parameters necessary for performing a breach analysis, and details methods for modelling breach growth.

Flood inundation

Section 8.11 provides information related to the end users of inundation modelling, parameters and data requirements, types of inundation models, modelling approaches, model outputs, and treatment of uncertainties.

8.1 PRINCIPLES

8.1.1 Links to other parts of the handbook

Levee assessment and design are often complex steps in a project since these require multidisciplinary engineering approaches, especially for levee stability assessment (for existing levees or for a new levee) where geotechnical and hydraulic issues are intimately linked and interact very strongly. For such projects, designers and engineers are often specialised in one discipline, so levee projects require integrated management (Chapter 5).

In a new levee project, for all phases of the project from feasibility to design, after the levee alignment has been selected (Chapter 9) and the site properly characterised (Chapter 7), engineers analyse levee stability with regard to various physical processes. These physical processes form a levee failure scenario (Chapter 3) and their analysis ensures the levee will be stable for all stages of construction (Chapter 10), and for all loads and hydraulic situations defined in the design process (Chapter 9) to reach a protection level chosen by owners or stakeholders (Chapter 2).

For stakeholders, engineers and designers, Chapter 8 can be considered a 'tool box', which details several actual methods to analyse stability for various physical processes that could lead to levee deterioration or failure as defined in Chapter 3. Each of these individual mechanisms is treated from the simplest to the more complex existing approaches so that the proper analysis model may be found at each stage of the project. The experimental and theoretical bases of the approaches are briefly described and the advantages and disadvantages of each method are discussed in terms of conditions of use and accuracy of the results. The different approaches are expressed, following a gradual complexity, through rule of thumbs, empirical formulae, analytical models or numerical methods.

8.1.2 Analyses issues for levees

In a simple way, levees could be defined as civil works projects designed to resist 'hydraulic' loading. The assessment of levees includes several aspects related to geotechnical, structural, and hydraulic domains. Figure 8.1 gives an illustration of those issues. For levees, both disciplines are intimately linked and even if there are purely geotechnical stability situations to analyse, the main critical situations for levees often depend on external hydraulic steady or transient loads.

Levees are built in river or coastal settings that continually change. The movement of water over and through the landscape shapes and forms the stream channel network or beach/dune complex as it interacts with the geologic formations that form the landscape. The levee will alter this interaction, sometimes in a negative way.

Stream flow path and planform variability can have significant consequences if not allowed for in the evaluation of levees. Lateral instability can change the angle or point of attack for a river on a nearby levee, possibly accentuating local and contraction scour and inducing bank instability. This instability may have direct and indirect impacts on the levee. For example, direct impacts may be the result of increased stream bank height that leads to slope failure, which extends through the levee embankment. Indirect impacts may result where changed stream alignment alters currents toward the levee embankment.

Changes in stream or beach planform may be gradual or the result of a single flood event. The directions and magnitudes of such changes are difficult to predict. However, it is essential to assess potential planform changes and how they relate to the levee to ensure its successful performance over the design life. Bank erosion and lateral migration analyses should be carried out, for example, to identify the erosion potential of the foundation near to or at the levee. The importance of lateral instability assessments is emphasised by Graham (1983) and Simon (1994) who observed that increased discharge in rivers leads to changes in channel width in preference to depth in unconstrained sections. According to Simon (1995), width adjustment processes may represent the dominant mode of adjustment in coarse-grained streams with cohesionless banks.

Lateral instability in rivers can be in the form of general channel bank erosion, bend scour, channel widening, and channel shift. General channel bank erosion can result from erosion by current flow, the action of waves generated by wind, or human weathering mechanisms such as freeze-thaw and desiccation, seepage effects, surface runoff, and mass failure mechanisms. There is potential for significant change in both coastal and riverine settings, which can result in substantial changes in planforms and profiles for example.

Tools for estimating meteorological, morphologic, hydrologic and hydraulic loads are given in Chapter 7. These loads are the drivers in changed boundary conditions. Boundary characteristics including bed material size and composition interact with these loads over time. Chapter 7 also describes methods for assessing the interaction between the boundary and the movement of water over the land surface (whether river channels or coastal features). Sediment transport, also covered in Chapter 7, describes methods for assessing long-term system response. Localised erosion and scour that may occur near or at the levee embankment are addressed in Section 8.2.

Whether assessing the condition of an existing levee or designing a new levee, the interaction between the water, the landscape and the levee embankment typically requires an iterative process using site condition information and hydraulic modelling tools (found in Chapter 7), local boundary condition calculations (Chapter 8), and any constraints defined for the system (Chapter 5 for existing levees or Chapter 9 for new levees).

The principle relationships between relevant boundary conditions associated with assessing watershed and stream characteristics and hydraulic loads for levee projects are shown in Figure 8.1. The diagram also indicates relevant design parameters that should be determined.

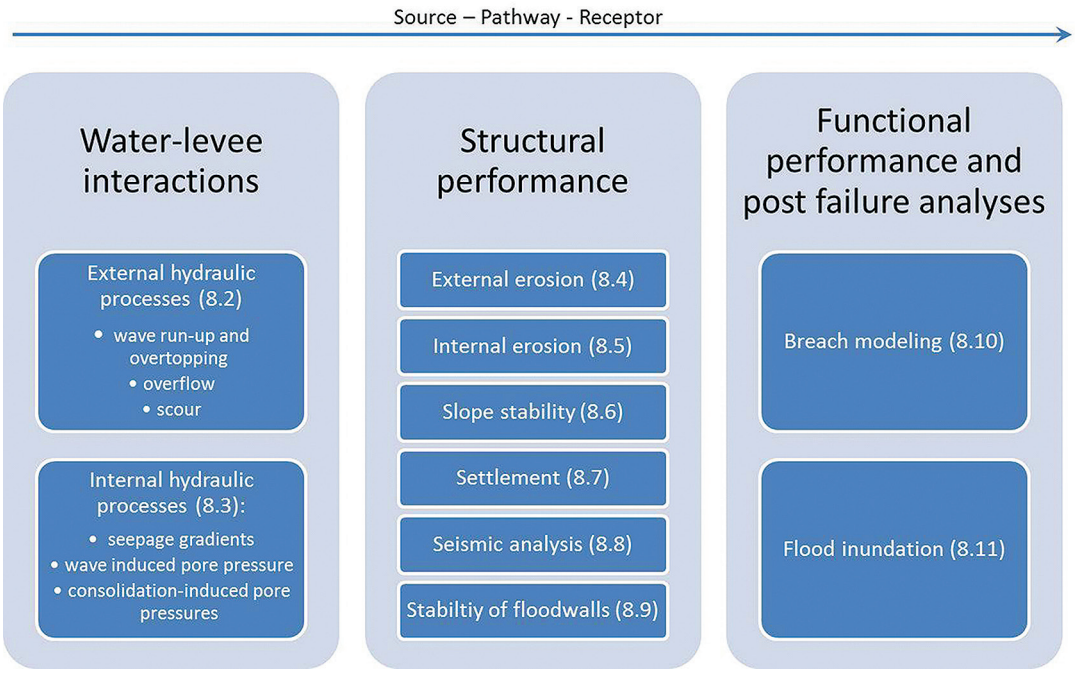

Figure 8.1 Geotechnical and hydraulic issues for levee section analysis

8.1.3 Links with other chapters

Chapter 8 is designed as a toolbox, using data mainly derived from processes described in Chapter 7. However, Chapter 8 can be useful for several adjustments required during design process (Chapter 9) or construction process of a levee (Chapter 10). Table 8.1 lists the main data required for the calculation process and relation with other chapters.

Table 8.1 Data used during calculation process

Type of data	Description of data and its use in construction	Chapter refs
Geometry of levee and its environment	**Description:** topographic and bathymetric data **Use:** required to determinate typical cross-sections of the levee and the suite of models used for stability analysis	7
Design loads	**Description:** external loads (geotechnical, hydraulic, permanent or transient loads etc) and their evolution versus time (hydrograms) need to be defined **Use:** required for determinate levee induced loads as internal loads in order to perform the levee stability analysis	7
Design situations	**Description:** hydraulic situations (depending on choices made by the levee owner or stakeholders in relation to the protection level objectives) **Use:** required to determinate levee internal loads and perform levee stability analysis	5, 7, 9
Feasibility, project or design site analysis and characterisation reports	**Description:** site characterisation during feasibility, project or design phases **Use:** during calculation phases, data are used to define geometric and geotechnical models. Affects the choice of methods related to processes that have to be studied	7, 9
Project programme (schedule)	**Description:** project programme (schedule) **Use:** affects design choices and construction methods and then calculation steps (for example, necessity of settlement acceleration techniques or soil reinforcement techniques)	5, 9
Construction phases	**Description:** project phases of construction of levee **Use:** affects calculation steps (intermediate steps etc)	10
As-built drawings	**Description:** documentation of levee constructed condition including changes to design, site conditions and constructed work **Use:** provides written records for local specific calculations	10

8.2 EXTERNAL HYDRAULIC PROCESSES

There are several external hydraulic processes that have to be accounted for in the proper design or assessment of a levee. These processes will be detailed in this section and include wave reflection, wave run-up and run-down, wave overtopping, overflow and scour. The layout of this section is shown in the following flow chart.

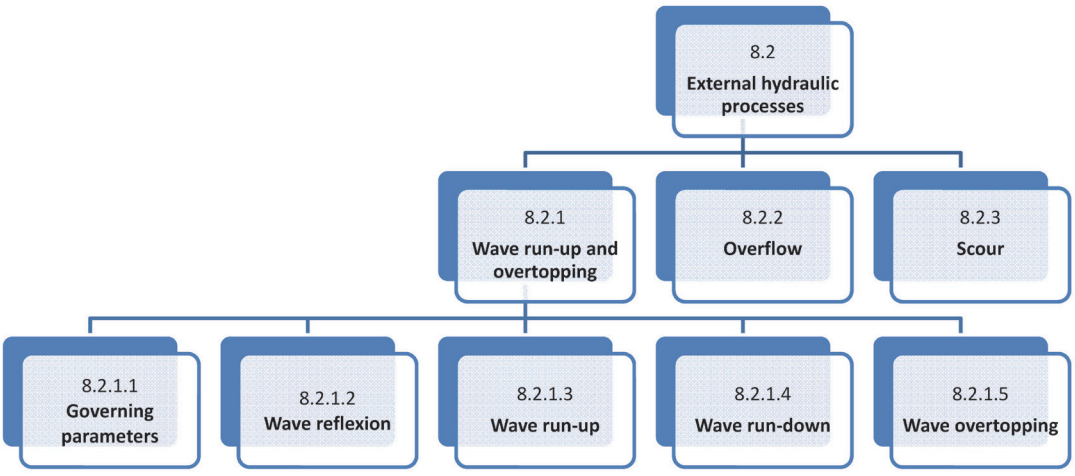

8.2.1 Wave run-up and overtopping

8.2.1.1 Governing parameters

Many hydraulic and structural responses on levees depend on the form and severity of wave action

before, and after it reaches the levee. Design methods generally use empirical equations or graphs based originally on results of hydraulic model tests. These relate the required response (eg wave run-up level, or limiting armour mass) to parameters describing the incident wave conditions (height, period, wavelength), and the structure geometry (water depth, slope angle of the structure). These are generally grouped to form dimensionless parameters that have physical meaning, some of which are summarised as follows:

Wave steepness

Wave steepness s_0 (-) is a parameter defined to integrate the influence of the wave period. It is defined as the ratio of wave height to wave length:

$$s_0 = \frac{H_s}{L_0} = \frac{2\pi}{g}\frac{H_s}{T^2} \tag{8.1}$$

where:

g = gravitational constant (9.81 m/s^2)
H_s = significant local wave height (m)
T = wave period (s)
L_0 = deep-water wavelength (m)

In random wave terms, mean and peak wave steepness are introduced, which are defined to consider the mean wave period T_m and the peak wave period T_p respectively in Equation 8.1. It is worth noting that this definition is not itself complete as both H and L can vary with position and depth (in turn varying with water and sea/lake/river bed level).

Surf similarity or Iribarren number

Wave breaking on a slope, whether approach or revetment slopes, can be categorised by a parameter known as the surf similarity parameter or Iribarren number, ξ (-). It is defined as:

$$\xi = \frac{\tan\alpha}{\sqrt{s_0}} \tag{8.2}$$

where α is the slope angle of the structure (°).

As for wave steepness, this parameter can be adapted by substituting, s_{0m} or s_{0p} to s_0 to obtain surf similarity related to mean (ξ_m) or peak (ξ_p) waves.

Relative water depth

Many wave processes depend on the water depth at the toe of the structure h (m), not as an absolute value, but when related to the waves. The most useful wave parameter here is generally the wave length, usually given as L_{0m} or L_{0p}. The relative water depth may then be expressed as h/L_{0m} or h/L_{0p}.

Structure geometry

One of the most important responses of a levee or seawall is the overtopping performance given by the proportion of waves overtopping, the mean overtopping discharge per unit length of defence, or the coefficient of wave transmission. Each of these depends on the crest elevation above the still water level (SWL). This structure freeboard, R_c (m), is often related to the incident wave height as R_c/H_{si}.

The other controlling parameter is the waterside slope angle. Levee slopes of 1:1 (difficult to achieve in practice) or 1:2 (cot α = 2.0) have very similar run-up/overtopping performance. Overtopping falls quite rapidly as the slope is reduced to 1:4 (cot α = 4.0) or beyond.

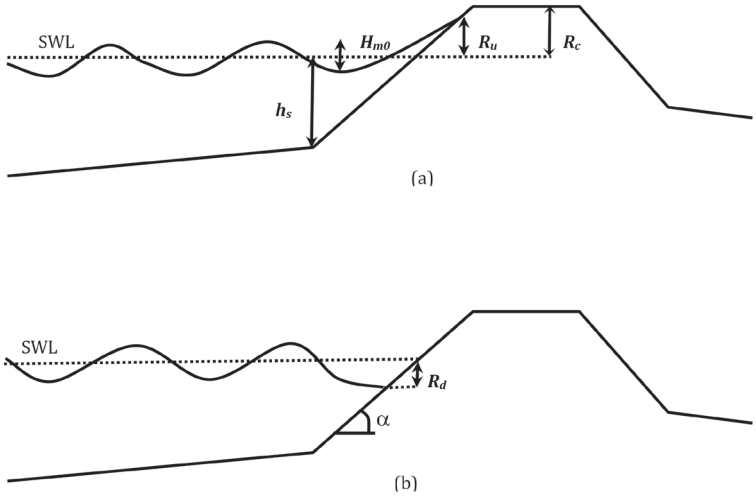

Note

R_c = freeboard, R_u = wave run-up, R_d = wave run-down, H_{m0} = wave height at the toe of the levee, h_s = water depth of the toe of the levee as regards to the still water level (SWL)

Figure 8.2 *Definition of run-up (a), and run-down (b) situations*

8.2.1.2 Wave reflection

All waves encountering any structure will reflect (at least in part) back from that structure. The most useful measure of wave reflection performance is the reflection coefficient, C_r , defined by the ratio of reflected H_r (m) to incident H_i (m) wave heights:

$$C_r = \frac{H_r}{H_i} \tag{8.3}$$

For vertical walls, reflections from plain vertical walls generally fall in $C_r \approx 0.85$ to 0.9, with relatively little influence of incident wave height or period. On typical levees, some wave energy will be dissipated on the slope, so C_r will be less, and this reduction will be greatest for shallower slopes. Reflections may also be reduced by roughness and/or porosity on the levee/revetment surface.

Upperbound estimation of reflection ratio

A very simple method describes an upper bound to these results:

$$C_r = 0.79 + 0.11\frac{R_c}{H_s} \qquad \text{for } R_c/H_s < 1.0 \tag{8.4}$$

$$C_r = 0.90 \qquad \text{for } R_c/H_s \geq 1.0 \tag{8.5}$$

Seelig formula

Reflections from smooth or armoured slopes may be described by a simple formula derived by Seelig (1983) and adapted by Allsop (1990) for random waves.

$$C_r = \frac{a\,\xi_m^2}{b + \xi_m^2} \tag{8.6}$$

where a and b are constant parameters depending on surface roughness and permeability. Allsop and Channel (1989) derived coefficients for smooth and armoured slopes, with wave conditions in the ranges $0.004 < s_m < 0.052$, and $0.6 < H_s/\Delta D_{n50} < 1.9$ where Δ is the relative buoyant density and D_{n50} the median nominal diameter. Some typical values are given in Table 8.2 and represented in Figure 8.3.

Table 8.2 *Values of the coefficient a and b in equation*

Slope type	*a*	*b*
Smooth	0.96	4.80
Armourstone – two layers	0.64	8.85
Armourstone – one layer	0.64	7.22

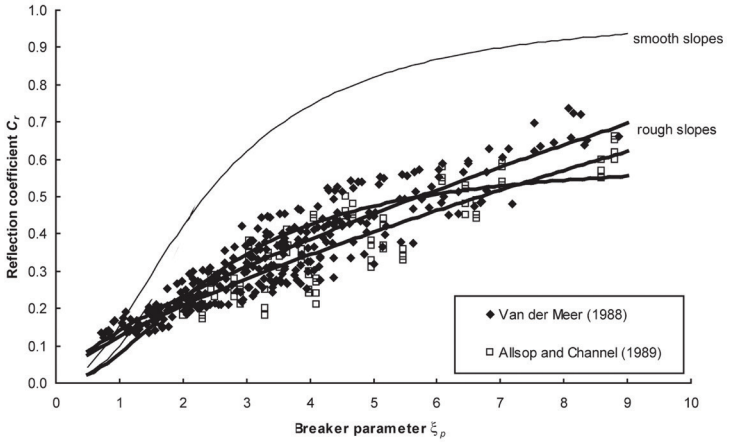

Figure 8.3 *Wave reflections for slopes (CIRIA; CUR; CETMEF, 2007)*

8.2.1.3 Wave run-up

The process of wave up-rush on a slope will reach a run-up level at its upward extent. Run-up levels (R_u) are defined vertically relative to the static water level used for those calculations(Figure 8.2). The run-up level most closely associated with setting levee crest levels is the two per cent exceedance level, $R_{u2\%}$. The run-down level at the same exceedance level, $R_{d98\%}$, may be useful in determining the lower extent of armouring on the levee/revetment face. For structures where methods are not available to estimate overtopping, estimates of extreme wave run-up level(s) may be required. Wave run-up depends primarily on the structure slope angle, and the incident wave steepness. Two methods for estimating run-up are presented. One method is based solely on geometry of the slopes (Box 8.1), while the other is based on surf similarity.

Box 8.1 *Geometrical methods for run-up calculation*

Wassing formula (1957)

For many years, the Netherlands used a simple formula for estimating irregular wave run-up for milder slopes verifying tanα ≤ 1/3 (Wassing, 1957):

$$R_{u,2\%} = 8\, H_{1/3}\, \tan\alpha \tag{8.7}$$

where α is the slope angle of the structure (°) as previously defined and $H_{1/3}$ is average of the highest one-third of the waves.

Saville method (1958)

It is one of the most widely-used methods for predicting run-up over complex geometries (Saville, 1957). It is based on the preliminary definition of a hypothetical average or 'effective' slope β of the entire active surf zone, extending between the wave break point and the run-up limit.

$$\tan\beta = \frac{R_u + h_b}{X_{Ru} + X_b} \tag{8.8}$$

where X_b is the horizontal distance from the shoreline to the breakpoint (m), and h_b is the incipient breaking depth (m).

Box 8.1 *Geometrical methods for run-up calculation (contd)*

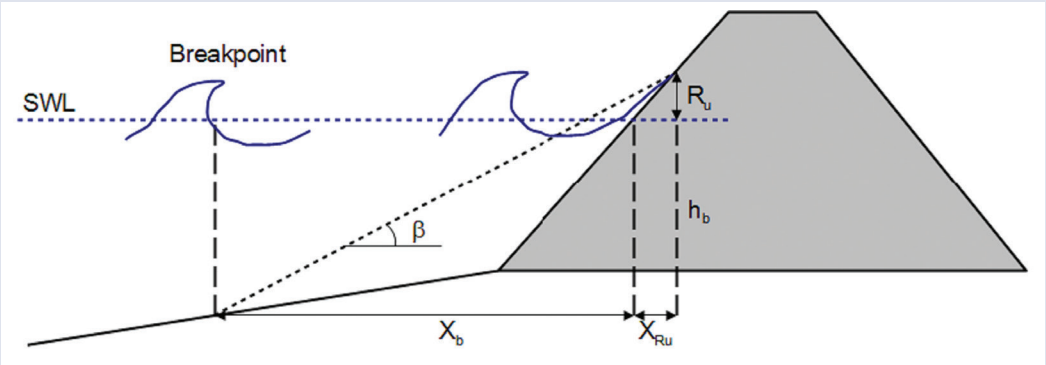

Figure 8.4 *Definition of effective slope for idealised beach profiles*

Combining the slope equation with Hunt's formula:

$$R_u = \tan\beta\sqrt{H_0 L_0} \tag{8.9}$$

where L_0 is the deep-water wave length and H_0 the deep-water wave height. For general application over arbitrary beach geometries, the run-up is estimated iteratively by following the procedure:

1 A run-up limit is assumed.
2 An average slope is calculated from the break point to the assumed run-up limit.
3 Run-up is estimated using an average slope in empirical design curves.
4 Calculated run-up is compared to the initially assumed value.

This general procedure is time-consuming. However, in the case of a known uniform slope, the problem is simplified and it exists as an analytical solution:

$$R_u = \frac{\tan\beta}{2}\left(X_b - \sqrt{H_0 L_0}\right)\left[\sqrt{1 + \frac{4\,h_b\sqrt{H_0 L_0}}{\tan\beta\,\left(X_b - \sqrt{H_0 L_0}\right)^2}} - 1\right] \tag{8.10}$$

This approach is applicable to smooth slopes (following Table 8.3). Generalisation of this approach to rough slopes may be done by considering a reduction factor γ_f = 0.67.

Table 8.3 *Run-up estimation for smooth slopes, from (CFBR, 2012)*

Slope	1/3	1/2.5	1/2
H_0/L_0 = 0.1	1.15	1.40	1.90
H_0/L_0 = 0.08	1.37	1.64	2.00
H_0/L_0 = 0.07	1.49	1.73	2.00

Surf similarity methods

The relative run-up level, R_u/H_s may be related to the peak surf similarity parameter or Iribarren number ξ. Taking into account the influence of berms (γ_b), of slope roughness (γ_f) and wave obliquity (γ_β) the relative run-up level may take the general form:

$$\frac{R_{u,p}}{H_s} = \gamma_b\,\gamma_f\,\gamma_\beta\,(A\,\xi + B) \tag{8.11}$$

where A and B are fitting coefficients depending on slope permeability and target probability p for run-up estimation (%). This formula may be completed by an upper bound fit to the data.

Hunt's method (1959)

For surging regular waves on plane, impermeable slopes, Hunt recommended the following equation:

$$R_{u,2\%} = 2.3\,H_s\,\xi_0 \tag{8.12}$$

Ahrens method (1981)

This method accounts for wind-induced waves following a Rayleigh distribution. The run-up level for a probability of exceedance p, $R_{u,p}$, may be calculated using the following equation:

$$R_{u,p} = 0.67\, H_s\, \xi_0^{0.51} \sqrt{\frac{-\ln p}{2}} \tag{8.13}$$

EurOtop method (Pullen *et al*, 2007)

For example, run-up level at two per cent exceedance level, given by $R_{u2\%}$ may be calculated using equations from Pullen *et al* (2007):

$$R_{u,2\%} = \gamma_f\, \gamma_\beta\, H_{m0}\, \min\left[1.65\, \gamma_b\, \xi_{m-1.0}\,;\, 4.00 - \frac{1.50}{\sqrt{\xi_{m-1.0}}}\right] \tag{8.14}$$

where:

$R_{u,2\%}$ = wave run-up height exceeded by two per cent of incoming waves (m)
H_{m0} = spectral significant wave height (m)
γ_b = influence factor for a berm (-)
γ_f = influence factor for roughness on the slope (-)
γ_β = influence factor for oblique wave attack (-)
$\xi_{m-1,0}$ = surf similarity parameter (-)

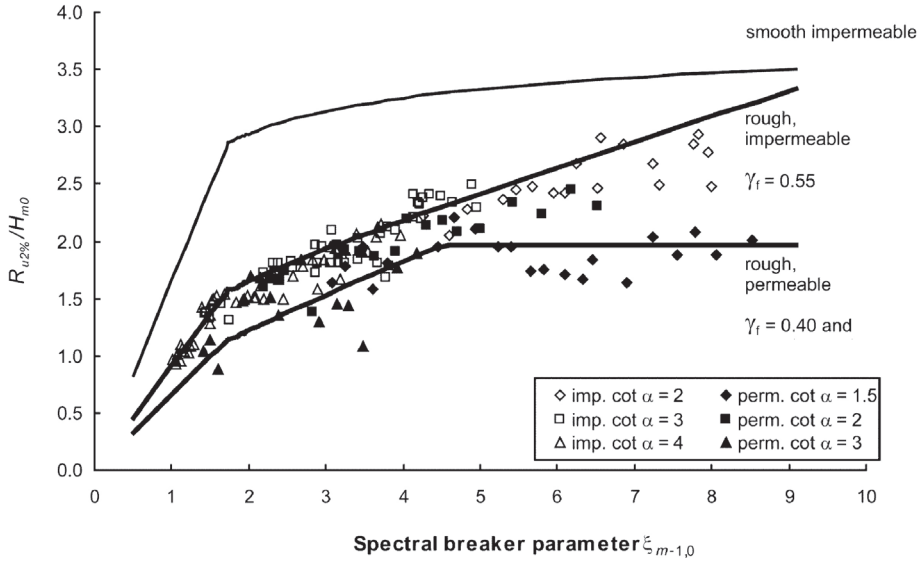

Figure 8.5 *Relative run-up on rock slopes (permeable or impermeable core), compared to smooth impermeable slopes (from CIRIA; CUR; CETMEF, 2007)*

Pohl method (1997)

The surf parameter is also used for the classification of breaking behaviour and breaker types. For small surf parameters breaking waves (spilling, plunging, surging) can be expected whereas for $\xi_{m-1,0} > 2$ to 3 nonbreaking waves (reflection) are typical. As in a wave spectrum a wide spread of wave parameters may be included as there are both breaking and nonbreaking waves influencing the run-up process in the transition zone. This was taken into account by the formula (Pohl 1997, Pohl and Heyer 2005, Figure 8.6):

$$R_{u,2\%} = P\, R^{nb}_{u,2\%} + (1 - P)\; R^{b}_{u,2\%} \tag{8.15}$$

with

$P = 1 - \exp(\xi_0/3.6)^{2.25}$

This formula considers the statistical $R_{u,2\%}$ run-up height to consist of a fraction P of nonbreaking waves and a fraction $1-P$ of breaking waves. In other words P is assumed to be the probability that no breaking takes place and $1-P$ is the breaking probability.

For example, the run-up of 'breaking waves' on smooth slopes may be calculated by means of the Hunt/Battjes formula:

$$R^{b}_{u,x\%} = k_r\, k_x \sqrt{H_m L_m}\, \tan\alpha \tag{8.16}$$

Using k_r = 1.0 on smooth slopes and k_x = 2.23 as a dimensionless parameter for the run-up exceedance probability of two per cent yields, with $H_m = 0.63 H_s$:

$$R^{b}_{u,x\%} = 1.77\, H_{m0}\, \xi_{m-1.0} \tag{8.17}$$

For 'nonbreaking waves', the run-up may be calculated as:

$$R^{nb}_{u,x\%} = 1.89\, H_{m0} \sqrt{\frac{\pi}{2\alpha}} \tag{8.18}$$

This yields almost identical results for breaking waves ($\xi_{m-1,0}$<2). In the transition zone this gives a local maximum for the normalised run-up $R_{2\%}/H_{m0}$ at $\xi_{m-1,0} \approx 3$. The weakness of other approaches, that the results either tend to infinity with growing (breaking) or dropping (nonbreaking) $\xi_{m-1,0}$ or that different formulae have to be used for different ranges of validity, could be overcome with this approach (Figure 8.6). For large $\xi_{m-1,0}$ (nonbreaking, vertical wall) the $R_{2\%}/H_{m0}$ curve by Pohl und Heyer (2005) goes asymptotically towards the value of $R_{2\%}/H_{m0} \to 2$, which stands for full reflection and is known as standing wave (clapotis), from theory.

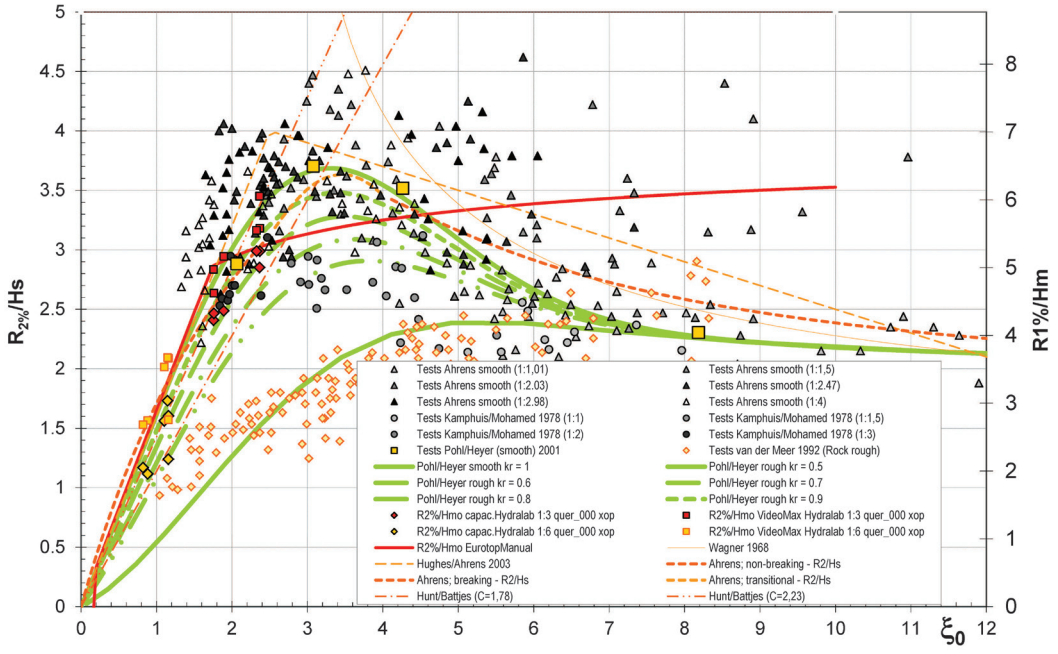

Figure 8.6 Normalised wave run-up on smooth and rough slopes (Pohl et al, 2012)

Van der Meer method (2002)

$$\frac{R_{u,2\%}}{H_{m0}} = \gamma_f\, \gamma_\beta\, \gamma_b\, \gamma_p \begin{cases} 1.77\, \xi_{m0} & 0.50 \le \gamma_b\, \xi_{m0} \le 1.80 \\ 4.30 - \dfrac{1.60}{\sqrt{\xi_{m0}}} & 1.80 \le \gamma_b\, \xi_{m0} \end{cases} \tag{8.19}$$

where γ_p is an influence factor for structure permeability (-).

For the consideration of further influences on the wave run-up the coefficients γ_b for the influence of a berm, γ_f for the slope roughness, and γ_β for oblique incident waves are used.

Van Gent formula (2000 and 2001)

An alternate form of the run-up equation was recommended by Melby (2012) after evaluating several popular empirical methods for predicting wave run-up on structures and beaches. Melby recommended the run-up equation by Van Gent (2000 and 2001) as the best predictor for impermeable coastal structures such as levees. It gives potentially smaller values than Pullen *et al* (2007) and is defined as:

$$\frac{R_{u,2\%}}{H_{m0}} = \gamma_f \gamma_\beta \gamma_b \gamma_p \begin{cases} 1.35\xi_{m-1.0} & \xi_{m-1.0} \le 1.7 \\ 4.7 - 4.1/\xi_{m-1.0} & \xi_{m-1.0} \ge 1.7 \end{cases} \tag{8.20}$$

Influence of slope roughness

Different values of γ_f are suggested by Pullen *et al* (2007), and a few examples are listed in Table 8.4.

Table 8.4 Examples of influence factor accounting roughness on the slope

Type of armour	Reduction factor, γ_f
Smooth concrete/asphalt	1.0
Concrete with roughness elements	0.7–0.95
Grass slope	0.9–1.0
One layer rock armour	0.55–0.6
Two layers rock armour	0.50–0.55

Influence of wave obliquity

The angle of wave attack, β (°), is defined as the angle between the direction of propagation of waves and the axis perpendicular to the structure (for normal wave attack: $\beta = 0°$). There are many approaches existing for the estimation of γ_β for the oblique wave approach. The coefficient γ_β is defined as the quotient of normalised run-up height with incident wave angle $\beta \neq 0°$ and the normalised run-up height for straight approaching $\beta = 0°$. This can be calculated using the equations by Wagner and Bürger:

$$\gamma_\beta = 0.35 + 0.65 \cos\beta \tag{8.21}$$

and by de Waal and van der Meer for a short-crested sea:

$$\gamma_\beta = 1 - 0.022\,|\beta| \tag{8.22}$$

Particularly for a very oblique wave approach ($\beta \to \pm 90°$) the limiting values are partly not plausible, so the application of these equations should be limited to angles $\to \beta < |\pm 50°|$.

Influence of berms

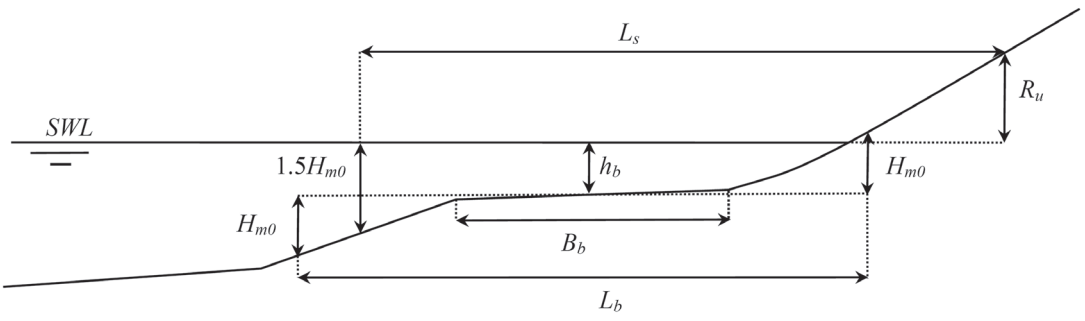

Figure 8.7 Definition for geometrical parameters of the berm

The berm influence area (Figure 8.7) is defined by the horizontal distance L_s (m) between the point corresponding to the level $SWL–1.5H_{m0}$ and the level $SWL+R_u$. The first step consists of defining the representative slope. For bermed slopes, it may be estimated as:

$$\tan\alpha = \frac{R_u + 1.5H_{m0}}{L_s - B_b} \tag{8.23}$$

For slopes with complex profiles, using an average structure slope given by:

$$\tan\alpha = \frac{4\,H_{m0}}{L} \tag{8.24}$$

where L is the horizontal distance between points on the levee at 2 H_{m0} above and 2 H_{m0} below the still water line.

So, the surf similarity parameter may be defined as $\xi_{m-1,0}$. The berm reduction factor is determined by the expression:

$$0.6 \leq \gamma_b = 1 - \frac{B_b}{L_b}(1 - k_h) \leq 1.0 \tag{8.25}$$

with k_h defined according to the following equation:

$$k_h = \frac{1}{2}\left[1 - \cos\left(\frac{\pi\, h_b}{x}\right)\right] \tag{8.26}$$

where:

x = R_u if berm level is above SWL or $2H_{m0}$ if berm level is below SWL
k_h = 1 if berm is outside influence area
H_b = the incipient breaking depth (m)

8.2.1.4 Wave run-down

Run-down is usually not as important as run-up, which can lead to overtopping, but both give an idea of total water excursion on a slope. Run-down is usually larger on impermeable slopes (ie concrete or reveted) as the water cannot percolate into the bottom as it does for permeable slopes (ie grassy or dirt). According to van der Meer (1988), wave period and bottom slope angles also have an effect on run-down. So, depending on the wave and slope characteristics, there may be a possibility of erosion on the slope due to the run-down velocity on the levee.

8.2.1.5 Wave overtopping

For coastal or lake seawalls/levees, the hydraulic response of most concern is wave overtopping, commonly expressed by the mean overtopping discharge per unit length along the defence q (Box 8.2), but sometimes as the number or percentage of incident waves overtopping the crest, $N_{wo\%}$. Noting that wave heights are distributed randomly, it will be seen that most practical levees on a sea or lake shore may experience some wave overtopping under extreme conditions. So, calculations of wave run-up levels are generally less useful in design than overtopping discharges. The simple method developed by Owen (1980) is described in Box 8.3.

Box 8.2 ***Wave overtopping on coastal flood embankments (from Hewlett et al, 1987)***

Conventional coastal engineering practice is to adopt an embankment crest level and profile, which limits the mean overtopping discharge intensity at design upslope wave and water level conditions to a maximum acceptable value. Mean overtopping discharge intensity has been determined by laboratory tests for regular embankment profiles under various upslope wave and water level conditions.

There are no universally accepted values for maximum allowable mean overtopping discharge intensity for coastal defences. Goda (1971) recommends the following maximum values of mean overtopping discharge intensity, $\overline{q}$, for stability of grassed and paved protection to the crest and downslope face of coastal flood embankments:

	$\overline{q}$ (m³/s/m)
Crest and downslope paved	0.05
Crest paved, downslope grassed	0.02
Crest and downslope grassed only	0.005

Box 8.3 Simple method of assessing overtopping (from Owen, 1980)

Around the UK, many rural seawalls have a simple cross-section, with slopes of 1:2–1:4. The overtopping performance of these structures under random waves was studied intensively in the late 1970s. Overtopping discharges under random waves were related to freeboard R_c, and wave parameters H_s and T_m. The prediction method developed by Owen (1980 and 1982) relates dimensionless parameters Q* and R* by an exponential equation with a roughness coefficient, r, and coefficients *A* and *B* for each slope angle:

$$Q^* = A \exp\left(-B \frac{R^*}{r}\right) \tag{8.27}$$

where:

$Q^* = q/(gT_m H_s)$

$R^* = R_c/T_m(gH_s)^{0.5}$

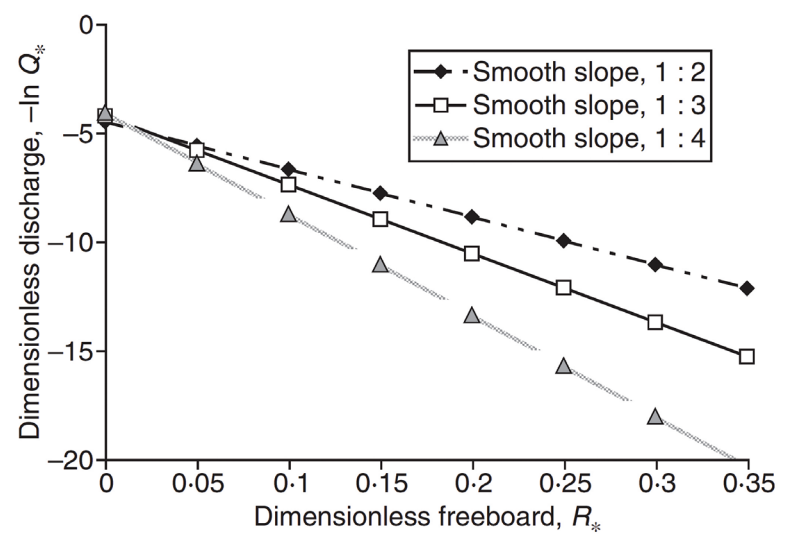

Figure 8.8 Overtopping for simple slopes (after Allsop et al, 2005)

and values of coefficients *A* and *B* are:

Slope	A	B
1: 1.0	0.0079	20.1
1: 1.5	0.0102	20.1
1: 2.0	0.0125	22.1
1: 3.0	0.0163	31.9
1: 4.0	0.0192	47.0

The form of Equation 8.27 is illustrated in Figure 8.8 where *Q** is plotted against *R**. For levees with particularly small relative freeboards and/or large wave heights, the prediction lines come together at one point, indicating that the slope angle no longer has much influence in controlling overtopping. At this point, the slope is said to be 'drowned out'. Over the normal range of freeboards, the discharge characteristics for slopes 1:1, 1:1.5 and 1:2 are similar, but overtopping reduces significantly for slopes shallower than 1:2.

Owen's method (1980) was developed initially for smooth slopes only, but the use of the roughness factor, *r*, allowed its use for rough, and even armoured slopes. The main advantages of Owen's method are its simplicity, and availability of data to support particular coefficients. The disadvantages are that the method was not explicitly developed for armoured slopes, the coefficient *r* is not always constant, and values of r have not been measured for some types of armour. The range of validity of this approach generally considered is $0.05 < R^* < 0.3$. Other approaches have been developed for configurations or armour not covered by Owen's original analysis:

1 Use Owen's method (1980) and coefficients *A* and *B* with values of *r* derived from tests with the appropriate armour and slope geometry.

2 Use Owen's general equation, but with new values of *A* and *B* derived for similar section geometry and armouring, and with $r = 1$

Overtopping configurations

There are four configurations of overtopping (Figure 8.9) that can affect levees:

- wave-only overtopping with positive freeboard
- wave-only overtopping with zero freeboard
- surge-only overflow with negative freeboard
- combined surge and wave overtopping with negative freeboard.

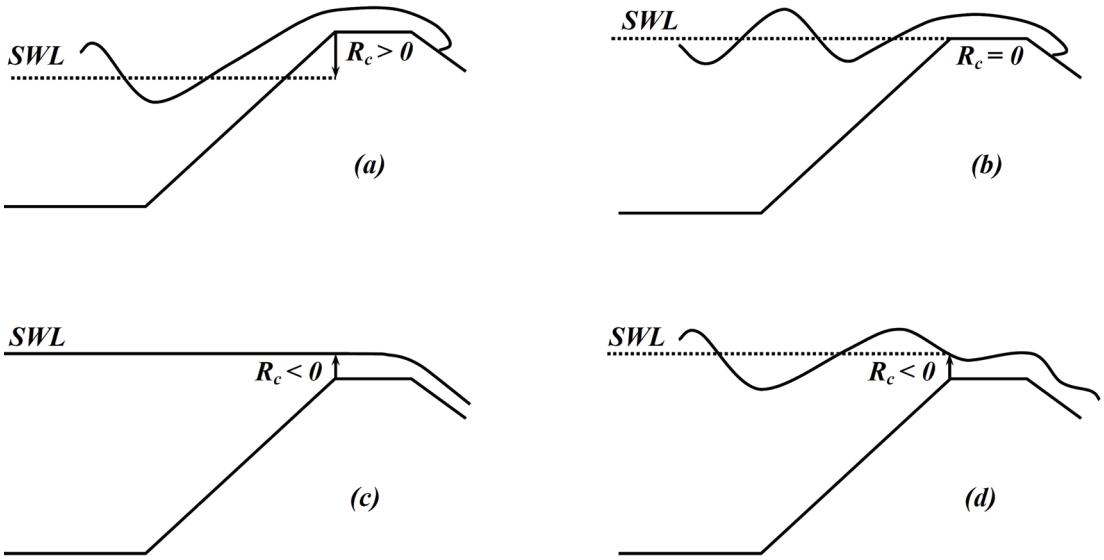

Figure 8.9 ***Four types of overtopping on levees: wave overtopping for positive freeboard (a), wave overtopping for zero freeboard (b), overflow for negative freeboard (c), overflow and overtopping for negative freeboard (d) (from Pullen et al, 2007)***

Wave-only overtopping with positive freeboard

Van der Meer (2002) and Pullen *et al* (2007) revised the average wave overtopping discharge q_w developed by van der Meer and Janssen (1995) for probabilistic design. In cases where heavy breaking is present (ie $\xi_{m-1.0} > 5.0$), long waves influence the predictions leading to underestimation of wave overtopping. When $\xi_{m-1.0} > 7.0$, the following equation should be used for wave-only overtopping with positive freeboard:

$$Q = \frac{q_w}{\sqrt{g\,H_{m0}^3}} = \begin{cases} \dfrac{0.067\,\gamma_b\,\xi_{m-1.0}}{\sqrt{\tan\alpha}} \exp\left(-\left\{\dfrac{4.75\,R_c}{\gamma_f\gamma_b\gamma_\beta H_{m0}\xi_{m-1.0}}\right\}\right) & \xi_{m-1.0} < 5.0 \\ 10\exp\left(-\left\{\dfrac{R_c}{\gamma_f\gamma_b H_{m0}\,(0.33+0.22\xi_{m-1.0})}\right\}\right) & \xi_{m-1.0} > 7.0 \end{cases} \tag{8.28}$$

Use linear interpolation between these two equations for breaking waves $5 < \xi_{m-1.0} < 7$. The following equation is the maximum value that the dimensionless average wave overtopping discharge Q should not exceed.

$$Q < 0.2\exp\left(-\left\{\frac{2.60\,R_c}{\gamma_f\gamma_b H_{m0}}\right\}\right) \tag{8.29}$$

Wave-only overtopping with zero freeboard

Schüttrumpf (2001) and Schüttrumpf *et al* (2001) derived equations for average wave overtopping discharge q_w based on model tests with smooth slopes between 1:3 and 1:6. His results are also presented in Pullen *et al* (2007) for overtopping resistant levees when the water level comes close to the crest as:

$$Q = \frac{q_w}{\sqrt{g\,H_{m0}^3}} = \begin{cases} 0.0537\,\xi_{m-1.0} & \xi_{m-1.0} < 2.0 \\ 0.136 - \dfrac{0.226}{\xi_{m-1.0}^3} & \xi_{m-1.0} \geq 2.0 \end{cases} \tag{8.30}$$

Surge-only overflow with negative freeboard

If the water level is higher than the crest, then overtopping can be modelled as flow over a broad-crested weir as described for open channel flow (Henderson, 1966). The surge-only overflow discharge q_s is defined as:

$$q_s = 0.5443\sqrt{g\,|-R_c^3|} \approx 0.6\sqrt{g\,|-R_c^3|} \tag{8.31}$$

where R_c is the negative relative crest height or overflow depth (ie difference between surge elevation and levee crest elevation). The second half of this equation is the approximation used by Pullen *et al* (2007).

Combined surge and wave overtopping with negative freeboard

The last form of levee overtopping is the combined wave and surge overtopping. In this condition, both the wave only and the surge only conditions occur together. Every wave has the possibility of overtopping the levee and the peak instantaneous discharge can be several times the value of the steady overflow discharge. The overtopping flow is unsteady in time and spatially non-uniform. Pullen *et al* (2007) suggests an approximation of the average combined wave and surge discharge q_{ws} for $\xi_{m-1.0}$ <2.0 as a superposition of the wave only with zero freeboard and surge only with negative freeboard equations given as:

$$\frac{q_{ws}}{\sqrt{gH_{m0}^3}} = 0.034 + 0.53\left(\frac{-R_c}{H_{m0}}\right)^{1.58} \qquad R_c < 0 \tag{8.32}$$

Hughes and Nadal (2008) conducted laboratory experiments of a trapezoidal levee at a 1:25 scale. Their experiments covered 27 overtopping conditions consisting of three water levels above crest elevation and nine irregular wave height and period combinations. They developed a new empirical equation that expresses the average overtopping discharge per unit length along the levee crest q_{ws} as a function of negative freeboard and incident energy-based significant wave height. The new equation fits the data very well. It was compared with Schüttrumpf *et al* (2001) and Reeve *et al* (2008) overtopping equations and gave lower overtopping rates, but following the same trends. Their combined overtopping q_{ws} is given as:

$$q_{ws} \equiv q_w + q_s = 0.0537\xi_{m-1.0}\sqrt{gH_{m0}^3} + 0.5443\sqrt{g|-R_c^3|} \qquad \xi_{m-1.0} < 2.0 \tag{8.33}$$

Note that R_c has to be entered as a negative number to ensure that the quantity in brackets is positive.

Landward slope erosion potential

The toe of the landward slope is the most common location for the initiation of erosion. The flow accelerates to reach supercritical and proceeds down slope until it reaches the base of the slope where a hydraulic jump develops. Erosion occurs due to the high velocities and turbulence under the hydraulic jump. The erosion typically advances upslope as a headcut develops.

In flow conditions typical of surge only overtopping, the flow becomes steady as a balance is reached between the water momentum and the frictional resistance of the slope material. The Manning equation for the steady flow velocity v_b is defined as:

$$v_b = \left(\frac{\sqrt{\sin\beta}}{n}\right)^{0.6} q_s^{0.4} \tag{8.34}$$

where:

β = the landward slope angle
q_s = steady critical discharge
n = Manning's coefficient

Hewlett *et al* (1987) recommended $n = 0.03$ for slopes of 1:10, decreasing linearly to $n = 0.02$ for 1:3 slopes and steeper. Since the Manning equation was derived for mild slopes, this equation is not strictly valid for steep slopes and significant air entrainment.

The flow down a landward slope for combined wave and surge overtopping is unsteady and more difficult to analyse. Hughes and Nadal (2008) developed an expression for the mean flow thickness h_b and flow velocity v_b on the landward slope as:

$$h_b = 0.4 \left(\frac{q_{ws}^2}{g \sin \beta} \right)^{1/3} \tag{8.35}$$

$$v_b = 2.5 \left(q_{ws}\, g \sin \beta \right)^{1/3} \tag{8.36}$$

Strictly speaking, these equations are only valid for the 1:3 slope and roughness used in the experiments until further research validates the results. In general, the friction factors for grass-covered slopes should be similar to the laboratory roughness, but armoured slopes would have significantly higher roughness factors.

Wave overtopping at flood walls

Waves can overtop a vertical flood wall even when the storm surge elevation is below the top elevation of the wall as illustrated in Figure 8.10. That portion of the wave above the flood wall will tumble over the wall and plunge to the ground under the force of gravity. The quantity of water will vary in time, and the unsteady discharge will be a function of wave height, wave period, and surge elevation relative to the wall. Erosion of unprotected soil will occur as the waves cascade over the wall, but the unsteadiness of the process, coupled with the variation of impact point due to irregular waves, makes scour estimation difficult, if not impossible.

The hydrodynamics of this phenomenon are quite complex because a substantial portion of the incident wave is reflected by the flood wall, and the reflected wave will interact nonlinearly with the incident wave. So, a few simplifying assumptions are necessary for the approximation given here.

Assume the incident waves are reasonably approximated as shallow water waves. Also, assume the incident wave crest height reaches the flood wall without being modified by the reflected wave, ie there is no nonlinear interaction between the incident and reflected wave. Waves in deeper water are symmetrical about the still water level (SWL) with the vertical distance between the wave crest and SWL being the same as the vertical distance between the wave trough and SWL. However, in shallow water the wave crests become more peaked and the troughs become flatter, and the vertical distance between the wave crest and the SWL becomes proportionally larger. For this simple development, assume the distance of the wave crest above the SWL is 70 per cent of the wave height, H, as shown in Figure 8.10.

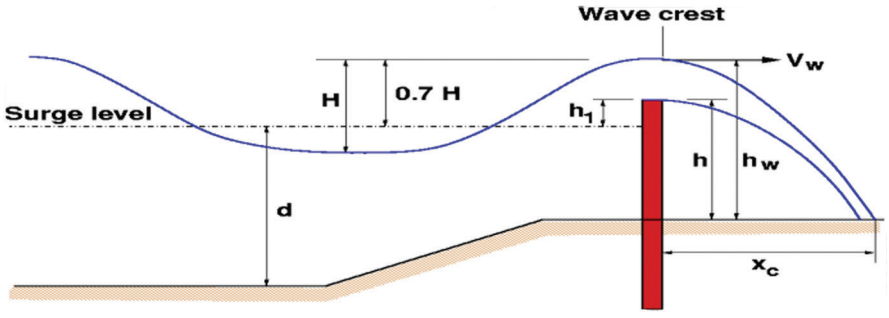

Figure 8.10 Definition sketch of wave overtopping flood wall (USACE, 2008)

As the wave crest passes over the flood wall, the orbital velocity of water particles at the free surface will be nearly the same as the wave celerity. Using the expression for wave celerity given by third-order theory for nonlinear, shallow water waves, the horizontal velocity V_w is given by:

$$V_w = \sqrt{g\,(d + H)} \tag{8.37}$$

where:

g = gravitational constant (9.81 m/s^2)
d = water depth at the toe of the structure (m)
H = incident wave height (m)

Note that wave celerity is independent of wave period in shallow water, and instead depends only on water depth and wave height. The distance from the wall to where the plunging wave crest impacts the ground level is found using the formulae for an object in free fall having an initial horizontal velocity of V_w and falling a vertical distance h_w.

$$h_w = h + 0.7\,H + h_1 \tag{8.38}$$

where h is the vertical distance between the top of the flood wall and the ground level, h_1 (m, positive or negative depending on surge level relative to the top of the wall) is the distance between the top of the wall and the surge level. If the surge level is lower than the flood wall, h_1 is negative. When the surge overtops the flood wall, h_1 is positive. The vertical fall distance is a function of fall time and gravitation acceleration $h_w = gt^2/2$. So, the fall time for a water particle at the wave crest free surface to fall to the ground level is given by:

$$t_f = \sqrt{\frac{2\,h_w}{g}} \tag{8.39}$$

The horizontal distance traversed by the water particle during this freefall time is simply $x_C = V_w\,t_f$, so that combination of the above equations yields:

$$x_C = \sqrt{2\,(d + H)\,(h + 0.7\,H + h_1)} \tag{8.40}$$

Additional details can be found in USACE (2008). Details for calculating nappe trajectories under wave or surge conditions are similar to those presented in Section 8.2.2.4 for flow over a flood wall. In the presence of waves, the equations shown in Section 8.2.2.4 have to be adjusted to include a variable horizontal velocity produced by the oscillatory wave action. This results in an unsteady, time-dependent estimate of jet position and jet velocity. The force and plunge position will vary over the length of the wave cycle, and landward protection should be designed based on the maximum range of fluctuation over that cycle.

8.2.2 Overflow

Overflow occurs when water on one side of a levee is higher than the top of levee elevation at point(s) along the levee profile. Overflow most often results from the waterside (or coastal) water level being greater than the top of levee elevation. However, it is possible for interior runoff to cause the reverse effect. Overflow can be continuous for a period of time where a design flood level is exceeded, or it may be intermittent as in the case of waves. Overflow may occur for both earthen embankment levees and flood walls of various types. Consequences of overflow range from minor erosion of the landward levee slope to entire failure of the levee component due to progressive erosion that leads to a breach.

In levee analysis and design processes the ability of the levee section to resist erosive forces caused by overflow has to be checked. The potential for erosion depends on the peak flow velocity as well as the depth and duration of overflow. Analysis and design should assess the potential for erosion due to overflow even where overflow is not likely under expected service conditions.

All levee systems are subject to overflow because of natural phenomena. The probabilistic methods used and uncertainties in estimating the water level needed to set top of levee elevations lead to potential overflow. Even where low probability discharges are used for determining levee height, there is risk that a greater magnitude event may happen over the project life (Box 2.8).

Assessment of an existing levee has to consider hydrologic and hydraulic conditions of the watershed and their influence on water levels that may cause overflow. Section 7.3 describes hydrologic and hydraulic models to accomplish this analysis.

The designer of a new levee has to decide on the site conditions and the combination of extreme events under which overflow occurs. Section 9.3.5 describes design considerations for overflow. The main consideration affecting the design decision is the likely consequence of failure and, more importantly, of any effect on life, property and land downstream.

8.2.2.1 Overflow discharge

Overflow discharge is the amount of water transferred across a levee segment and is usually expressed as a unit discharge, q ($m^3/s/m$). Unit discharge is a function of the height of water above the levee crest and physical characteristics of the levee crown and length of overflow section. Because levees are generally aligned parallel to a river's main flow direction overflow is similar to a lateral diversion. This means that flow over a levee is unsteady and gradually varied due to the slope of the water surface profile along the river (Figure 8.11). This is compounded further if there is a non-level crest elevation as in the case of levee overflow. The addition of waves adds additional complexity in unsteady flow conditions (Figure 8.12).

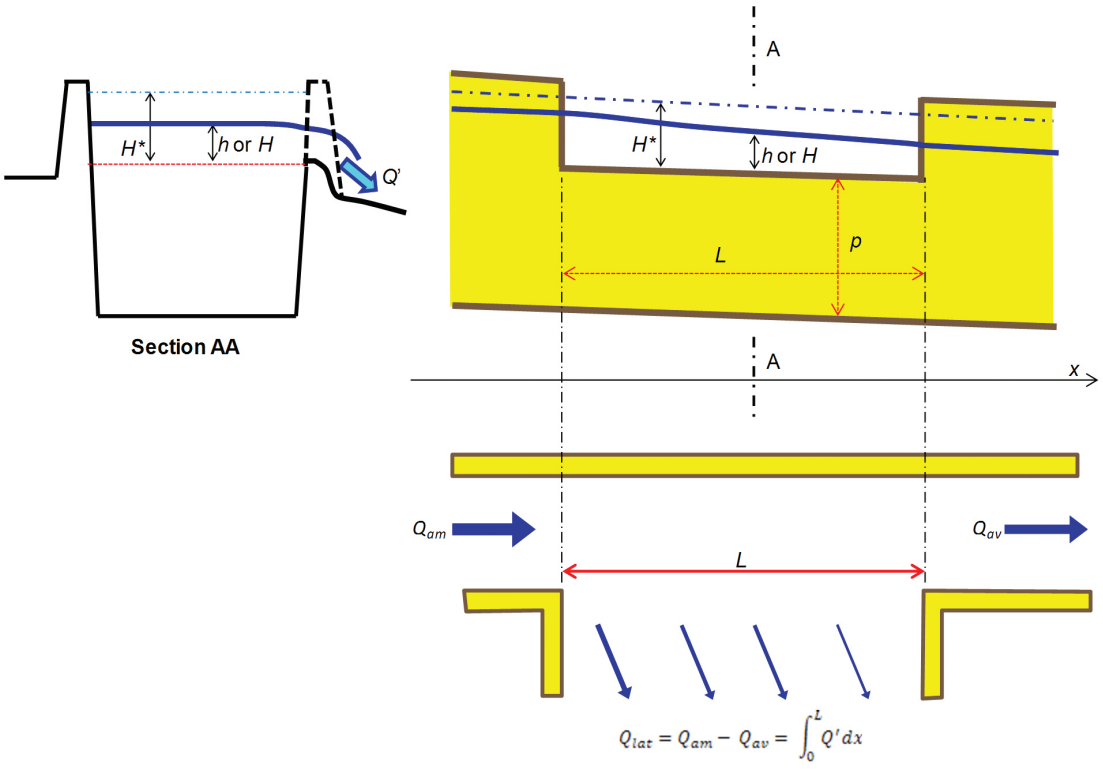

Figure 8.11 Illustration of gradually varied discharge over lateral overflow section (from Degoutte, 2012)

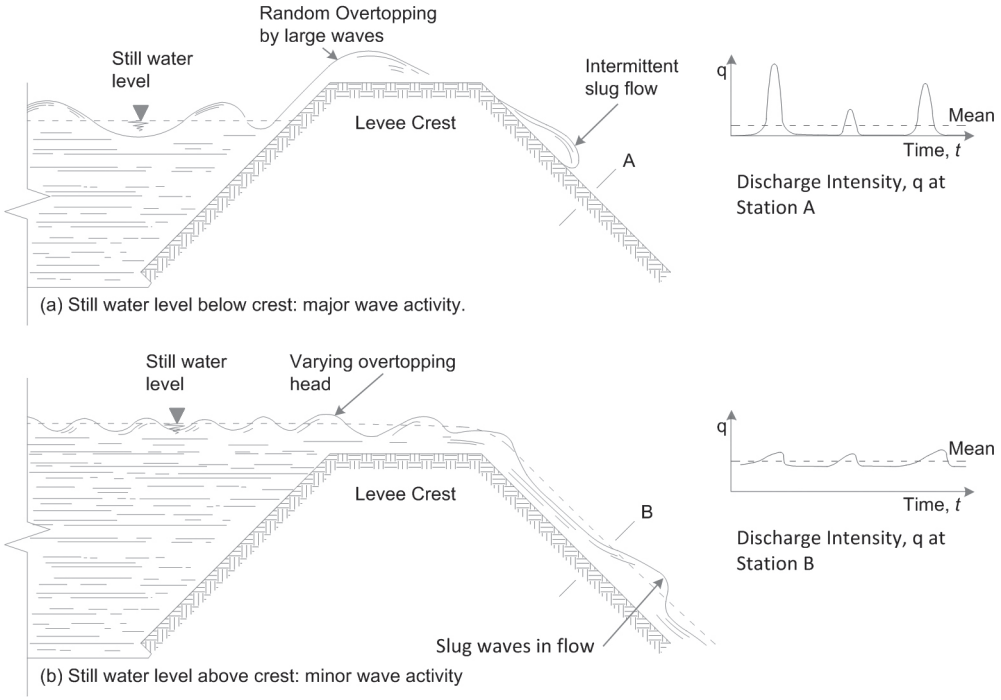

Figure 8.12 Wave effects on creating unsteady overtopping discharge (from Hewlett et al, 1987)

A simplified method for estimating uniform overflow discharge at a levee embankment cross-section is the standard broad-crested weir equation:

$$Q = C_d\, L\, H^{3/2} \tag{8.41}$$

$$q = C_d\, H^{3/2} \tag{8.42}$$

where Q (m³/s) is total discharge, q (m³/s/m) is unit discharge per length of overtopping section, C_d is a weir discharge coefficient, L (m) is the length of the overflow section, and H (m) is the head above the crest of the weir.

Basic approach

Assuming that the crest has a constant top elevation, the overflow is well approximated by the classic hydraulics problem of flow over a weir. Also, consider an additional head H_a corresponding to the velocity of approach V_a defined by:

$$H_a = \alpha \frac{V_a^2}{2\,g} \tag{8.43}$$

where α is the kinetic energy correction factor allowing non uniformity of velocity in the cross-section model. The linear discharge is given by:

$$q = \frac{2}{3}\, C\, \sqrt{2\,g}\, \left[H^{*3/2} - H_a^{3/2}\right] \tag{8.44}$$

where:

q = flow rate per unit length (m²/s)
C = flow coefficient (-)
g = gravitational constant (9.81 m/s²)
H = head over the crest (m)
H^* = $H+H_a$, equivalent head over the crest (m)

Experience suggests that typical values for C may range from 0.5 to 2.6 for levee overflowing situations. The lower value represents conditions where overflow is perpendicular, or nearly so, to the main channel flow direction. Higher values for C may be used when overtopping occurs on the convex side of bends where overflow is more closely aligned with the main channel flow direction (Figure 8.13).

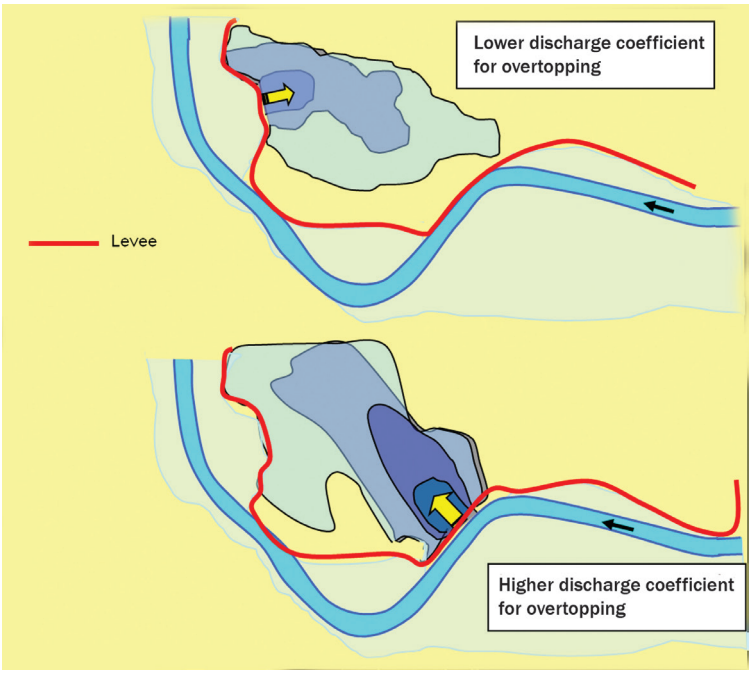

Figure 8.13 ***Angle of main channel current direction and its effect on overflow weir coefficient (from Degoutte, 2012***

The difficulty of this approach is that there is a longitudinal water surface slope along the river's length and levee crest elevations are rarely constant, both resulting varying head along the length of levee that is subject to overflow. Estimated overflow rates determined from the simplified approach should be compared to numerical model results obtained during site characterisation (Section 7.3), or from detailed numerical models of the overflow or spillway segment. Numerical model results obtained from site characterisation are required to determine the overflowing head, H (m). Unsteady model results also provide the overtopping discharges (Q m^3/s or q m^3/s/m) and heads that occur at various time steps through the flood hydrograph.

Hager procedure

Hager (1987) developed a procedure for calculating a value for weir coefficient C_d to be used with the standard weir Equation 8.41 as:

$$C_d = \frac{3}{5}\sqrt{g}\,C_0\sqrt{\frac{1-W}{3-2y-W}}\left\{1-(\beta+s_0)\sqrt{\frac{3\,(1-y)}{y-W}}\right\} \tag{8.45}$$

with:

W = $p/(H_t+p)$, $y = (H+p)/(H^*+p)$

where:

H = height of water surface above the weir (m)

p = height of weir above the ground (m)

H^* = height of the energy gradeline above the weir = $H+ H_a$ (m)

s_0 = average main channel bed slope (rd)

β = main channel contraction angle (0 if the weir is parallel to the main channel) (rd)

C_0 = f (weir shape), base discharge coefficient as shown in Table 8.5

The main channel contraction angle used in Equation 8.45 is shown graphically in Figure 8.14.

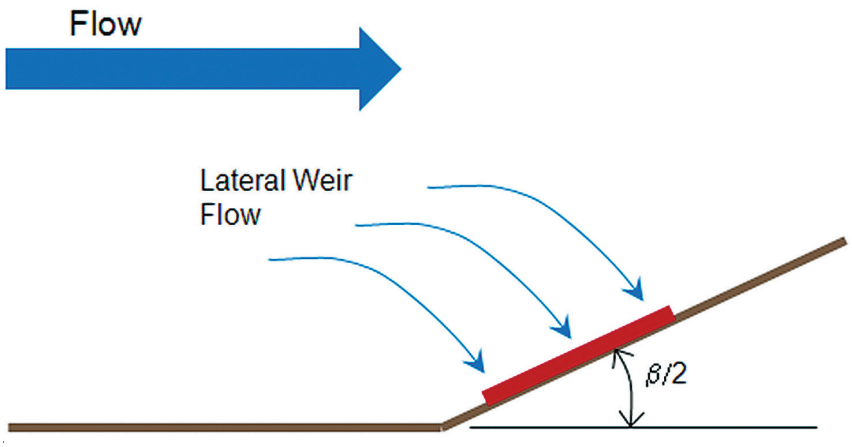

Figure 8.14 *Angle β for calculation of Hager (1987) weir coefficient*

Table 8.5 *Values for C_0 (from Hager, 1987)*

Weir type	Value of C_0
Sharp crested	1.0
Zero height	$\frac{8}{7}$
Broad crested (b = weir width in direction of flow)	$1-\frac{2}{9\left[1+\left(\frac{H_t}{b}\right)^4\right]}$
Round or ogee crested (r = weir crest radius)	$\frac{\sqrt{3}}{2}\left[1+\frac{\frac{22}{81}\left(\frac{H_t}{r}\right)^2}{1+\frac{1}{2}\left(\frac{H_t}{r}\right)^2}\right]$

Hager's (1987) equation takes into consideration the effects of flow depth, approaching velocity, lateral outflow direction and side weir channel shape in determining a value for the coefficient of discharge.

Sharp-crested levees

A similar approach can be applied where overflow occurs at a flood wall where the crest is narrow. Flow over wall type structures creates a jet that does not remain in full contact with the landside face of the wall.

Although viscous and surface tension effects are usually of secondary importance, such effects cannot be entirely neglected when the flood wall width (B) is not negligible relative to the head (H). Values of C_o range from approximately 0.58 to 0.78. Empirical formulae may be able to assess this phenomenon.

Francis' formula

This is one of the most commonly used formulae for calculating discharge. The flow coefficient is expressed, excluding lateral contraction due to end effects, as:

$$C_d = 0.623 \tag{8.46}$$

Bazin's formula

Based on this formula, the flow coefficient is given by

$$C_d = 0.405 + \frac{0.003}{H + H_a} \tag{8.47}$$

Rehbock's formula

Based on this formula, the flow coefficient is given by:

$$C_d = 0.605 + 0.08\frac{H}{z} + \frac{0.001}{H} \tag{8.48}$$

where z is the crest height (m).

The principal concern for flow over a structural flood wall is the potential for scour where the overflow jet impinges on the landside of the structure (Section 8.2.2.4).

8.2.2.2 Spillways and fuse plugs

Design calculations take hydraulic models developed during site characterisation (Chapter 7) and expand them to assess spillway/fuse plug components of a levee system. Models developed during site characterisation include solution of weir flow equations and an assessment of the effects of overflow (if any occurs) on the flood hydrograph but do not typically optimise spillway or fuseplug design (Figure 8.15). Additional detail is added during design in order to evaluate the spillway/fuse plug. Results from the unsteady flow models are used to proportion spillway/fuse plug features. In some cases, physical models are used to evaluate spillway/fuse plug performance and to adjust the design obtained from numeric calculations.

In basic terms, flow hydrographs that describe current conditions in the watershed (developed during site characterisation in Chapter 7) are routed through the system with desired levee alignments to evaluate how the levee may alter the magnitude and timing of discharges. Figure 8.15 shows this as the 'hydrograph with spillway'. If necessary, to manage and control overflow due to this hydrograph, a purpose designed overflow section may be included as a part of the levee plan. The capacity of the overflow section is determined by the depth of water above the overflow section crest, the length of section that overflows, and the length of time that overflow occurs (Figure 8.15). Water diverted by overflow reduces the discharge rates in the main conveyance system (Figure 8.15). The effects of an adequately designed overflow section prevents the riverward stage from exceeding top of levee elevations along other parts of the levee. However, water levels on the landward side of the overflow section experience increased water levels as depicted in the lower stage hydrographs in Figure 8.15.

The weir equations (8.46 to 8.48) above represent the simplest case for calculating overflow discharge. The equations provide a reasonable estimate for overflow discharge when the levee embankment or spillway configuration is in the form of a weir. There are spillways that use various types of gates and even explosives to control and regulate flow into the spillway outlet. Where gates are used the discharge characteristics of the gates and associated structures and their operation will determine the amount of water that leaves the primary conveyance system and enters the landward area. Fuse plugs are segments of a levee embankment designed to a lower crest elevation to permit overflow. In some cases, fuse plugs incorporate provisions for erosion and eventual breach of the embankment. Analysis of fuse plug overflow sections is complex due to the largely unknown rate of breach development.

Detailed hydraulic design for spillways/fuse plugs are beyond the scope of the handbook. Specific approaches and methodology for spillway design can be found in Degoutte (2012) and USACE (1992). Spillway/fuse plug detailing for levee systems will typically involve an iterative process to achieve a balance in spillway performance and required spillway structural requirements with respect to unit discharges, frequency of use and resulting erosive forces.

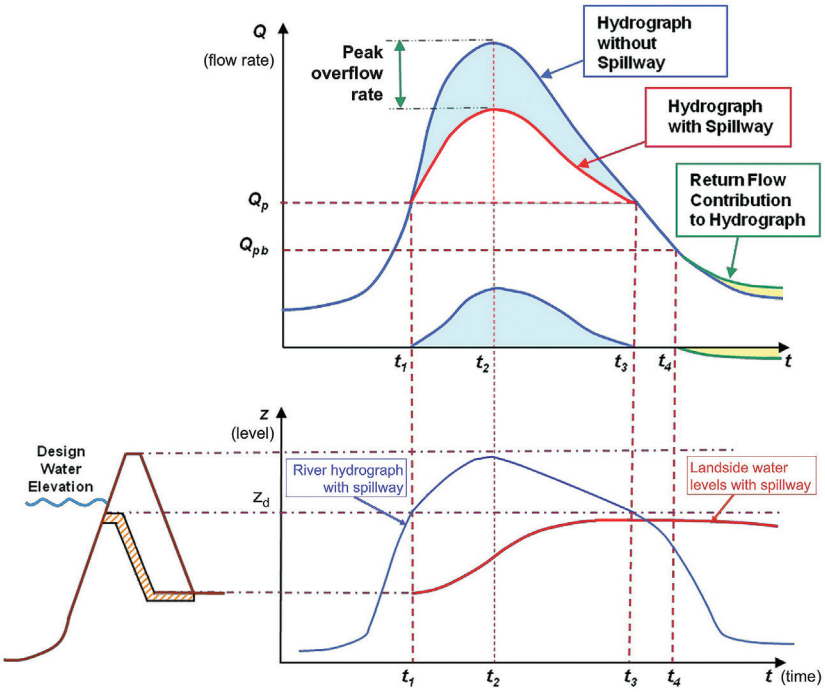

Figure 8.15 Effect of spillway/fuse plug on flood hydrograph (from Degoutte, 2012)

Blue shaded segments of hydrographs in Figure 8.15 are diverted by overflow at the spillway. The yellow segment represents where diverted water returns to the river. Depicted spillway hydrographs would be obtained if there is no limit on spillway (infinite storage volume downstream).

With intended overflow sections and with overtopping of embankments where wave activity on the waterside slope is limited (such as those associated with small lakes or river flood defences), threshold discharge conditions and design discharge are usually related to events with a defined probability of occurrence (or risk).

Where embankments are subject to substantial wave activity on the waterside slope (lakes, estuaries or large river systems with considerable wind fetch), overflow conditions are likely to be caused by a combination of extreme water level and wave action. In such cases, overflow discharge will fluctuate and the value of peak design discharge for protection measures is a matter of engineering judgment. Owing to the random nature of wind generated waves, the local peak discharge intensity, when a particular section of the embankment is overtopped by a large wave, could be between one and two orders of magnitude larger than the time-averaged mean discharge intensity (Figure 8.12).

8.2.2.3 Hydraulic performance of overflow spillways at levee embankments

Once overflow discharge and duration of overflow have been estimated (Section 7.3), the flow characteristics over the crest and along the landward face of the levee have to be calculated. First, critical depth (where Froude number, **Fr**, equals unity) (Section 7.3.6.1) is calculated for the overtopping discharge. Critical depth occurs at or very near the landward side of the levee crest.

Provided the landward slope is steep and the tailwater is low, the flow continues to accelerate until the normal depth is reached. Normal depth can be calculated using an iterative solution of the Manning's equation shown in Equation 7.17 using the estimated overflow discharge (Equations 8.46 or 8.47). As tailwater increases, the location of the jump moves further up the landward slope until the crest is submerged (Figure 8.16). Once normal depth is achieved for a given overflow discharge, flow continues down the levee slope at this state (depth and velocity) until there is a change in slope or downstream water levels begin to increase. At this point the flow decelerates rapidly resulting in significant energy loss through a 'hydraulic jump' (Figure 8.17). At this point the landside area is fully inundated to nearly the same level as in the river. Figure 8.18 shows possible states of overflow at the landward toe of a levee.

Mississippi River: Birds Point-New Madrid Floodway activation during 2011 flood

Figure 8.16 ***Water overflowing a levee with significant energy dissipation where accelerated flow interacts with tailwater the levee crown has been substantially eroded by the overflow (courtesy USACE)***

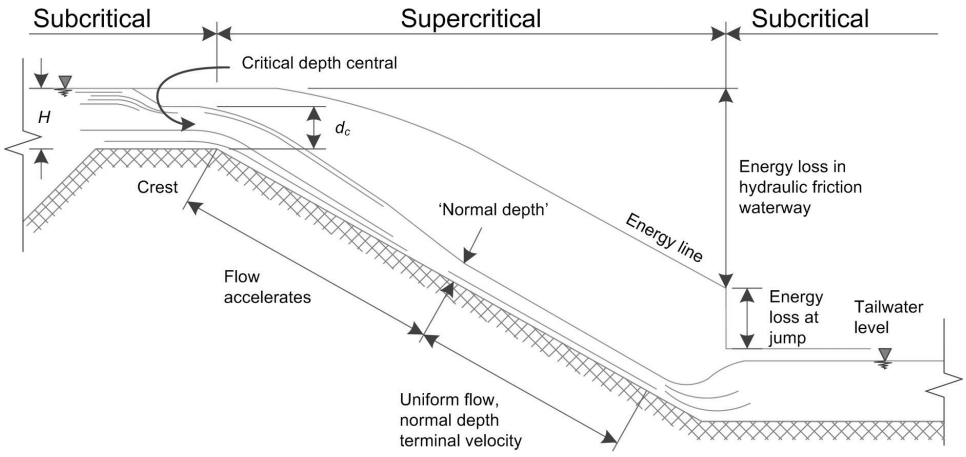

Figure 8.17 ***Elevation showing flow states down face of levee or spillway due to overflow (Hewlett et al, 1987)***

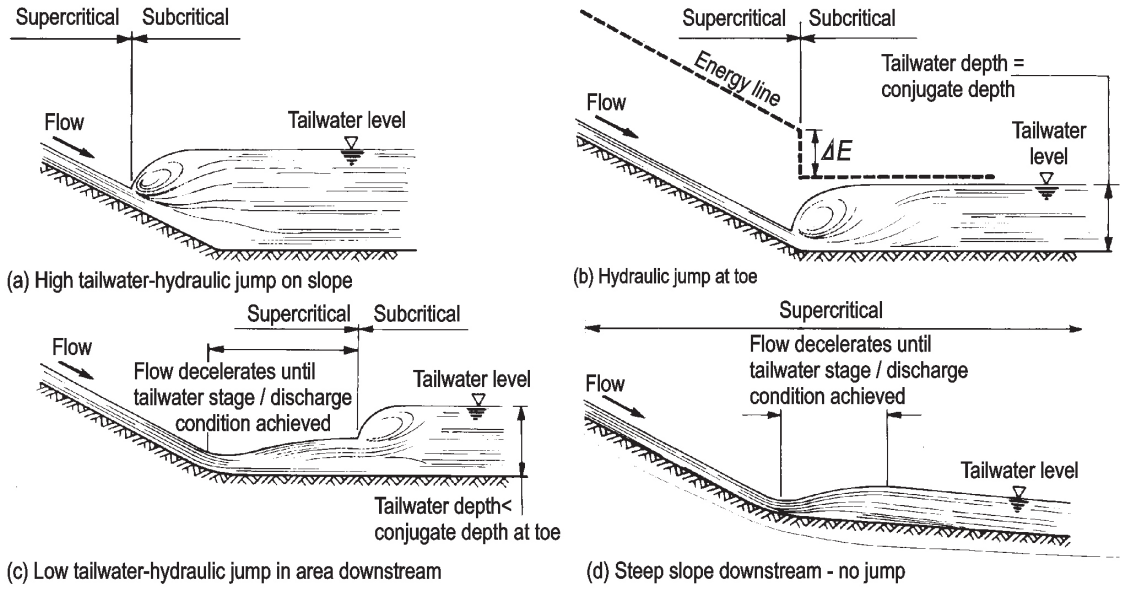

Figure 8.18 Different combinations of overflow near landward toe of levee (Hewlett et al, 1987)

Two critical concerns for levee overflow are velocity of flow on the downstream levee slope (here downstream may be either the riverward or landside slope depending on the direction of overtopping) and the high turbulence and energy dissipation at the hydraulic jump. Velocity on the slope has been addressed through calculation of the normal depth using Equation 7.17. It becomes necessary to determine the dimensions of the hydraulic jump so that adequate protection measures may be designed. The reader is referred to standard hydraulics text books, notably Chow (1959) for full details of the hydraulic jump.

The amount of energy dissipated through a jump depends on the Froude number (**Fr**) of the upstream supercritical flow (see Box 8.4). The downstream depth required to fully form the jump can be calculated by:

$$y_2 = \frac{y_1}{2}\left(\sqrt{1+8Fr_1^2}-1\right) \tag{8.49}$$

where y is depth, subscript 1 denotes upstream conditions and subscript 2 denotes downstream conditions. For a fully formed jump, the jump length can be estimated by:

$$L_{jump} = 220\, y_1 \tanh\left[\frac{Fr_1 - 1}{22}\right] \tag{8.50}$$

where L_{jump} is in metres, subscript 1 denotes upstream conditions and tan h the hyperbolic tangent.

Tailwater depth should also be calculated using the Manning equation and this value compared to y_2 computed from Equation 8.53. If the calculated tailwater depth is less than y_2, then the jump will not fully develop. One measure to ensure full jump development is to extend the levee slope to a lower elevation so that the full y_2 depth is achieved before continuing downstream (Figure 8.19).

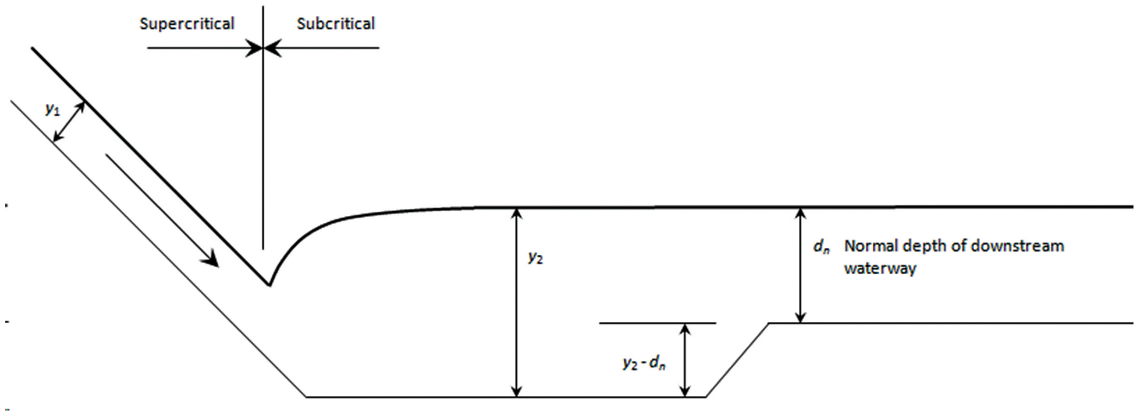

Figure 8.19 Measures to ensure full jump development where normal depth downstream may be limited

Box 8.4 Energy loss in a hydraulic jump (Hewlett et al, 1987)

For a given slope and roughness, Froude number, **Fr**, does not vary greatly with discharge. For example, in a hydraulically wide waterway, substituting Manning's equation for mean velocity of flow:

$$Fr \cong \frac{V}{\sqrt{g\,h}} = \frac{h^{1/6}}{n}\sqrt{\frac{S}{g}} \qquad (8.51)$$

Typical values of Froude number for grassed waterway applications (as for a grassed levee slope) are:

Slope, S	Fr
1V: 2.5H	5 to 6
1V: 5H	4 to 5
1V: 10H	3 to 4
1V: 25H	2 to 3
1V: 50H	2

Energy loss, ΔE, in a hydraulic jump is usually considered in relation to the specific energy, E, of the incoming flow. $\Delta E/E$ varies from about 65 per cent for **Fr**=7, to about 15 per cent for **Fr**=2. Below Froude numbers of about 2, the hydraulic jump is weak and relatively little energy dissipation occurs.

An example of issues to consider during the operation of a levee fuse plug or spillway, or when overtopping occurs is presented in Box 8.5.

Box 8.5 *Subsurface flow (from Hewlett et al, 1987)*

During the operation of a levee fuse plug or spillway or when overtopping occurs, the flow field in the underlayer and/or the subsoil below the armour layer is determined by the hydraulic boundary conditions at the interface with the open channel above.

In uniform flow conditions, the hydrostatic head due to open channel flow in the waterway can give rise to:

1 Infiltration into the unsaturated subsoil.
2 Seepage flow parallel to the slope (with hydraulic gradient equal to the slope of the waterway)

Infiltration is determined by the infiltration rate at the open channel boundary (ie the armour layer) and seepage flow is governed by the permeability of the underlayer/subsoil.

The turbulent flow conditions in the waterway will give rise to dynamic fluctuations in water pressure at the boundary, but in general (and within the limitations of velocity recommended herein) subsurface flow is relatively steady, and its direction is into or parallel to the open channel boundary. Within the limitations of waterway flow velocity and subsoil composition recommended in Hewlett *et al* (1987), piping or entrainment of soil particles in the underlayer/subsoil by subsurface flow is therefore unlikely.

Conditions of subsurface flow during operation of a reinforced grass waterway has to be distinguished from those below an armour layer or any other surface that is subject to wave attack. With wave action, the hydraulic boundary conditions are unsteady and during part of each wave cycle the direction of subsurface flow is out of the open channel boundary. This cyclic 'pumping action' in the subsoil with repeatedly high exit gradients gives rise to onerous requirements for a filter that can:

1 Retain the subsoil particles from migration.[box lists to be styled]
2 Maintain a sufficiently high permeability throughout its service life to avoid excessive head loss through the filter with consequent failure by uplift.

Further information on subsurface flow and filter requirements associated with wave action and navigational waterways is given in ICE (1984), CIRIA CUR CETMEF (2007), and PIANC (1987).

8.2.2.4 Hydraulic performance of flood walls

Flood walls that might be subject to overflow by rising water should be designed with erosion protection on the protected (dry) side capable of resisting the force of the free-falling water jet. Figure 8.20 illustrates flow discharging over a flood wall and plunging (in this case) into standing water on the protected side of the flood wall. The plunging jet penetrates the water and creates large eddies that erode material from the unprotected soil surface. The same mechanism will scour bed material when there is no standing water on the protected side of the flood wall.

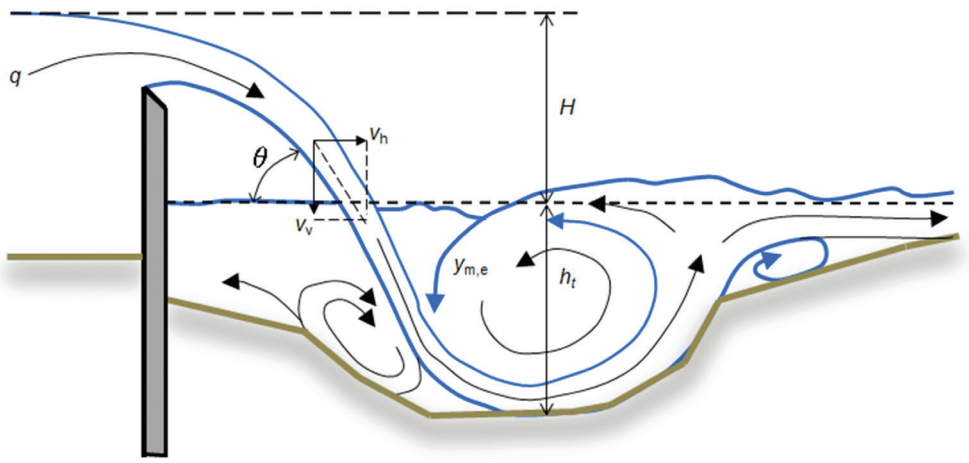

Figure 8.20 *Scour hole formation by overtopping jet (from Hoffmans and Verheij, 1997)*

This scouring action removes material that may be providing critical lateral support pressure against the protected side of the vertical flood wall. Failure occurs if the remaining undamaged portion of the foundation adjacent to the wall cannot withstand either the shear force or the overturning moment exerted on the flood wall by the elevated water on the flood side of the wall.

The jet of water passing over the vertical flood wall has two surface profiles referred to as 'nappes' (meaning 'a continuous surface'). The lower nappe is closest to the backside of the flood wall, and the upper nappe is the extension of the flow free surface as it spills over the wall. The trajectories of the lower and upper nappes are given in most open channel flow literature (eg Chow, 1959, and Morris and Wiggert, 1963).

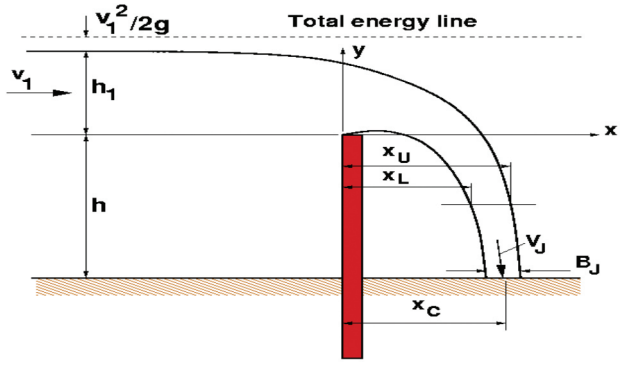

Figure 8.21 Flow over a flood wall approximated as a sharp-crested weir (USACE, 2008)

In dimensionless form, the equations are as follows with the x-y co-ordinate system as defined in Figure 8.21.

Lower nappe
$$\frac{y_L}{H^*} = A\left(\frac{x}{H^*}\right)^2 + B\left(\frac{x}{H^*}\right) + C \tag{8.52}$$

Upper nappe
$$\frac{y_U}{H^*} = \frac{y_L}{H^*} + D \tag{8.53}$$

where the parameters are defined as follows:

A = -0.425+0.25G
B = 0.4111–1.603G–(1.568G^2+0.892G+0.127)$^{1/2}$
C = 0.150–0.45G
D = 0.57–0.02[10 (G–0.208)]^2 exp [10(G–0.208)] with $G = V_a^2/2gH^*$

This yields equations for x_L and x_U as:

Lower nappe
$$\frac{x_L}{h_1} = \frac{-B - \sqrt{B^2 - 4A\,(C - y/h_1)}}{2A} \tag{8.54}$$

Upper nappe
$$\frac{x_U}{h_1} = \frac{-B - \sqrt{B^2 - 4A\,(C + D - y/h_1)}}{2A} \tag{8.55}$$

The distance to the centre of the jet at impact with the ground surface is the arithmetic average of x_L and x_U. The intersection points of the lower and upper nappes with the horizontal ground level on the landward side of the flood wall are found by setting $y=^{-}h$ in Equations 8.52 to 8.55. The horizontal width of the overflowing jet at impact is given by $B_x = x_U(y=-h) - x_L(y=-h)$.

If there is no venting, the air pressure in the space between the flood wall and lower nappe may become less than atmospheric as air is entrained into the jet during sustained overtopping. The decreased pressure will draw the plunging jet closer to the wall, however, this decrease in plunge point location away from the vertical wall is difficult to predict. This is likely not to be a problem because the scour protection will probably cover the entire region from the base of the wall out past the location of jet impact.

The overtopping jet impacts the ground at an angle less than vertical (which is given by -90° in the co-ordinate system defined in Figure 8.21). The jet entry angle is well approximated by the average of the angles of the lower and upper nappe profiles when they intersect the horizontal ground level. The entry angles of the nappe profiles are found by taking the derivative of Equations 8.52 and 8.53 and evaluating the result at $x=x_L$ and $x=x_U$, respectively, to get:

$$\theta_L = \arctan\left(\frac{dy}{dx}\right)_L = \arctan\left(\frac{2\,A\,x_L}{h_1} = B\right) \tag{8.56}$$

$$\theta_U = \arctan\left(\frac{dy}{dx}\right)_U = \arctan\left(\frac{2\,A\,x_U}{h_1} = B\right) \tag{8.57}$$

The jet entry angle is estimated as:

$$\theta_J = \frac{\theta_L + \theta_U}{2} \tag{8.58}$$

From geometric considerations the width of the impinging jet normal to the flow streamlines can be estimated with reasonable accuracy by the formula:

$$B_J = B_x \sin\left(-\theta_J\right) \tag{8.59}$$

Discharge over the flood wall remains constant for steady flow, and the discharge per unit length of the plunging jet at impact with the ground surface is given simply as the jet velocity parallel to the flow streamlines times the width of the jet normal to the flow. Therefore, the jet entry velocity can be estimated as:

$$V_J = \frac{q}{B_J} \tag{8.60}$$

Finally, the total force (thrust) exerted by the overtopping jet on the scour protection per unit length along the wall is given in inviscid jet theory (Milne and Thompson, 1960) as:

$$F_J = \rho\, B_J\, V_J^2 \tag{8.61}$$

where ρ is the water density.

This equation is an expression of the momentum flux of the jet, and the force is directed parallel to the jet streamlines.

The force of the overflow jet at impact creates high pressures because the jet width is narrow. The impact force given from Equation 8.61 can be resolved into vertical and horizontal components using the estimated jet entry angle from Equation 8.58. So, the apportioning of force between vertical and horizontal components will vary with overflow condition, and successful scour protection has to be able to resist the expected range of vertical and horizontal forces. For high discharges over low walls, the jet entry angles are far from vertical, and the water after impact will retain a substantial horizontal velocity as it flows down the protected side of the earthen levee.

Depending on the elevation of the adjacent land on the protected side of the flood wall, there may be standing water at the base of the wall. The impact force of an overflow jet will be dissipated to some degree as it enters the standing water but it still retains sufficient force to erode unprotected foundation soil. Scour protection that relies on self-weight for stability will be less stable when submerged, and the overflow jet may be able to dislodge submerged components of the protection. The highly turbulent conditions that exist in the plunge area make estimation of scour extent and depth difficult. It is necessary to use multi-dimensional numerical models with capability to simulate an erodible boundary or physical models should be used. Use of cohesive materials typical for levee construction further complicates estimating the rate and extent of erosion in the situation depicted in Figure 8.21. Current good practice is to provide continuous paving that incorporates a structural design so that the paving can withstand the expected impact forces from the jet.

8.2.3 Scour in river channels

This section will provide information related to evaluating scour in river channels and the relationship to a levee system. The flow of subsections is shown in Figure 8.22.

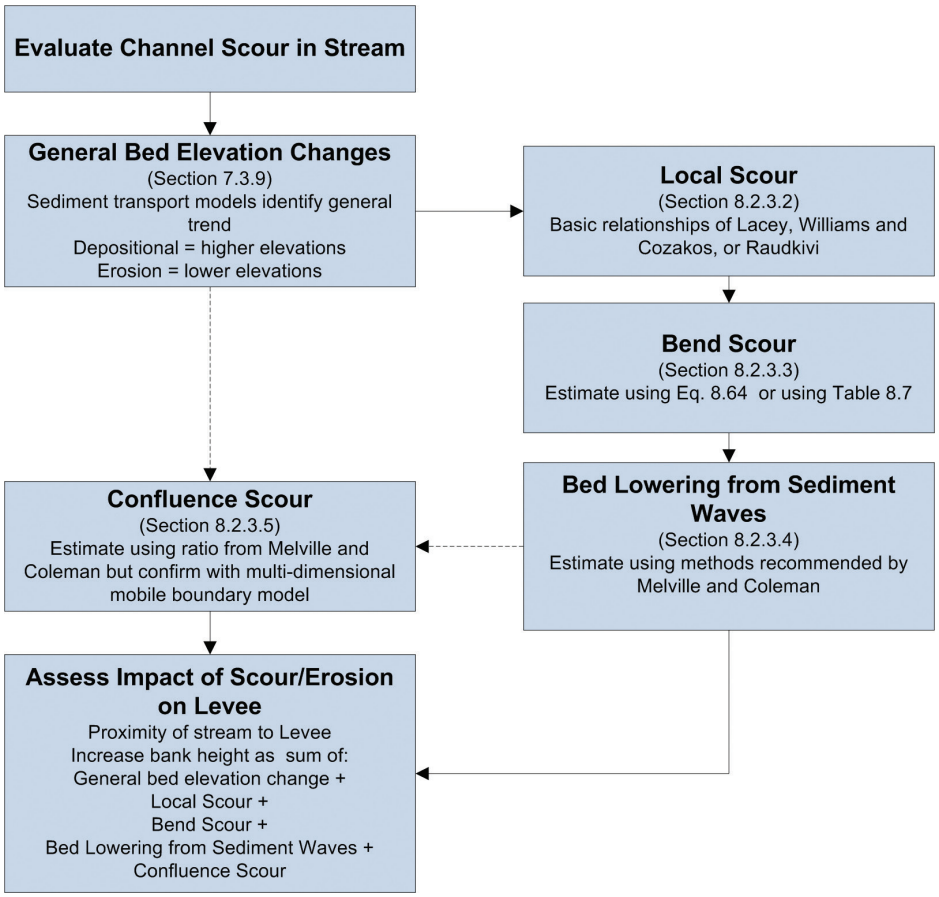

Figure 8.22 Basic approach to evaluating scour

8.2.3.1 General

Introduction of levees into a stream system will produce a system response. Evaluation of long-term channel stability was discussed in Section 7.3. Part of this analysis involves use of sediment transport models to estimate deposition or erosion trends in the stream over the project life. The analysis provides an indication of the amount and rate of vertical change that could be expected to occur. Adjustment of the stream bed elevation over time influences the design water level as described in Section 7.3. It is also necessary to assess how long-term (over the project life) trends in bed elevation may impact levee stability. When levees are set back from the stream channel any downward change predicted by sediment transport studies should pose no threat to levee structural integrity. This is not true when levees are close to the stream top bank. In this case, general erosion depths have to be included in the slope stability analysis. Adjustments in the levee alignment and/or embankment slopes may be required if calculated erosion depths create a bank height that is unstable.

Stream channels are not always straight with regular cross-section geometry. There is considerable variability, particularly in natural channels. Part of this variability is a result of shifts in the channel alignment and cross-section in response to the various boundary conditions that exist in the watershed. This introduces a requirement to evaluate both general trends in bed elevation change and local influences due to thalweg shifts and the presence of bends. Confluence scour occurs where two channels combine, and it should be considered as necessary.

8.2.3.2 Local scour

While not as apparent as a shift in channel location for braided streams, a shift in the thalweg will alter local bed elevations and can change the point and/or angle of attack for a flow. This can lead to markedly increased scour at the bank, which in turn may result in bank failure and increased threat to a levee located near the main stream channel. So, it is necessary to assess local scour depths in the vicinity of

the levee alignment so that appropriate protection measures can be included to ensure long-term levee integrity.

For flow around a bend, the interaction between the vertical gradient of streamwise velocity and the curvature of primary flow creates secondary currents. These secondary currents lead to larger flow depths, velocities and shear stresses along the outside of the bend, and so increased deepening at the toe of the outside bank. The position of the greatest depth in a bend is affected by changes in flow characteristics and channel-forming processes, flow variability, and bank conditions. The general observations shown in Table 8.6 apply.

Table 8.6 Influences on local scour depth at bends

Condition	Bend scour is principally a function of:
Abrupt change in flow direction/sharp bend angles	• degree of direction change
Eroding bends/migrating bank on outside	• bank material.

Once average bed elevations have been assessed at a site (Section 7.3), allowance needs to be made for the effect of variations in bed elevation across the site on local scour depths. The critical consideration for levees involves stream types that migrate over time. For meandering channels, estimates of bend scour will allow for lowered bed elevations due to the presence of the thalweg in the bend.

Lacey (1930) remarks that stable reaches of rivers frequently present a semi-elliptical cross-section. Lacey gives the relationship that for a truly semi-elliptical section the maximum flow depth, y_{max} is given by multiplying mean depth by 1.27. If a channel has a constricted width, Lacey indicates that y_{max} is equal to the mean depth.

In estimating design scour depths for protecting levee toes, Williams and Cozakos (1994) allow for thalweg formation based on the Lacey relationship of 25 per cent of flow depth for straight reaches. Raudkivi (1990) suggest that maximum channel depth equals $1.69R$ or $1.58y$ where R is the hydraulic radius and y is obtained by dividing cross-sectional area by channel top width if the channel is assumed to be of a cosine cross-section.

8.2.3.3 Bend scour

Lacey (1930) considered different classes of cross-section, for a semi-elliptical cross-section shape, that may develop in a river for varying bend radius of curvature. Lacey used a relationship where a constant wetted perimeter and cross-section area existed for various degrees of lateral adjustment on the channel boundary due to increasing scour depths (Figure 8.23). Lacey summarises the influence of bend curvature on maximum flow depth as shown in Table 8.7 where y_{bs} is maximum flow depth in the bend and R is the hydraulic radius for the channel only. Neil (1973) provided coefficients as recommended by the Indian Roads Congress (1966).

Table 8.7 Some coefficients relating bend curvature and maximum flow depth for a cross-section

Degree of bend curvature	Lacey (1930), y_{bs}/R	Neill (1973), y_{bs}/R
Greatly constricted	1.00	–
Straight	1.27	1.25
Moderate bend	1.50	1.50
Severe bend	1.75	1.75
Right-angled bend	2.00	2.00
At cliffs and walls	–	2.25

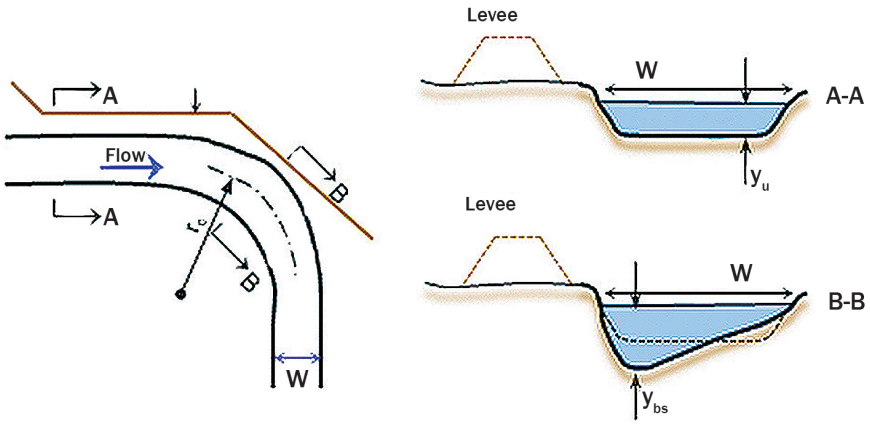

Figure 8.23 Bend scour and variables (from Melville and Coleman, 2000)

Various investigators include an allowance for the influence of bend angle on maximum bend flow depth (Galay *et al*, 1987, Apmann, 1972, Thorne, 1988, Thorne *et al*, 1995, Thorne and Abt, 1993, and Maynord and Hubbard, 1993). Thorne (1988) used data from 70 bends along the Red River between Arkansas and Louisiana in the USA to develop a relationship between y_u and y_{bs} as:

$$\frac{y_{bs}}{y_u} = 2.07 - 0.19 \ln\left[\left(\frac{r_c}{W} - 2\right)\right] \tag{8.62}$$

for $r_c/W > 2$ where y_u is the average flow depth (Area, A/Width, W) in the channel upstream of the bend.

Thorne *et al* (1995) includes a comparison of flume data and data for 257 bends on natural rivers, which varied widely in type and size, located in different physiographic regions and different parts of the world. The dataset included maximum flow depths of a few centimetres in the flumes up to about 17 m to cover all but the world's principal rivers. Equation 8.62 was found to be in reasonable agreement with the larger dataset with the majority of predictions falling between +30 per cent to -25 per cent of observed values.

Based on bend-scour data from the Mississippi River, USACE (1994) presents a 'safe' design curve for maximum bend flow depths of:

$$\frac{y_{bs}}{y_u} = 3.37 - 0.66 \ln\left[\left(\frac{r_c}{W}\right)\right] \tag{8.63}$$

The USACE equation is designated a 'safe' design curve because only five per cent of data used to derive the curve fall above predicted values. Maynord (1996) expressed concern that Equation 8.63 is conservative for the vast majority of measured data, particularly for relatively small streams. Incorporating channel aspect ratio into the expressions for bend scour, regression analyses of the Thorne and Abt (1993) and Maynord and Hubbard (1993) data yields, for $1.5 < (r_c/W) < 10$ and $20 < (W/y_u) < 125$:

$$\frac{y_{bs}}{y_u} = 1.80 - 0.051 \ln\left[\left(\frac{r_c}{W}\right)\right] + 0.0084\left(\frac{W}{y_u}\right) \tag{8.64}$$

Maynord (1996) suggests that the preceding empirical methods are valid up until there is significant interaction between main channel flow and overbank flow. Recommended use where overbank flow conditions exist is limited to where overbank depths are less than 20 per cent of the main channel depth, y_u.

Melville and Coleman (2000) recommend use of Equation 8.64 to estimate bend scour. Alternative methods described in Equations 8.62 and 8.63 may also be used if appropriate. Use of these equations together with coarse indications from Table 8.7 may be used as a guideline in estimating bend scour for use in slope stability analysis and in developing bank stabilisation requirements associated with levees. These equations may also be used where the low flow channel is sinuous within a larger channel cross-section.

8.2.3.4 Bed lowering from sediment waves

For flood flows associated with levee performance, sediment waves will be migrating through the river channel. The magnitudes of these waves influence bank height because wave troughs momentarily and locally lower bed elevations as the sediment waves propagate through a reach (Figure 8.24).

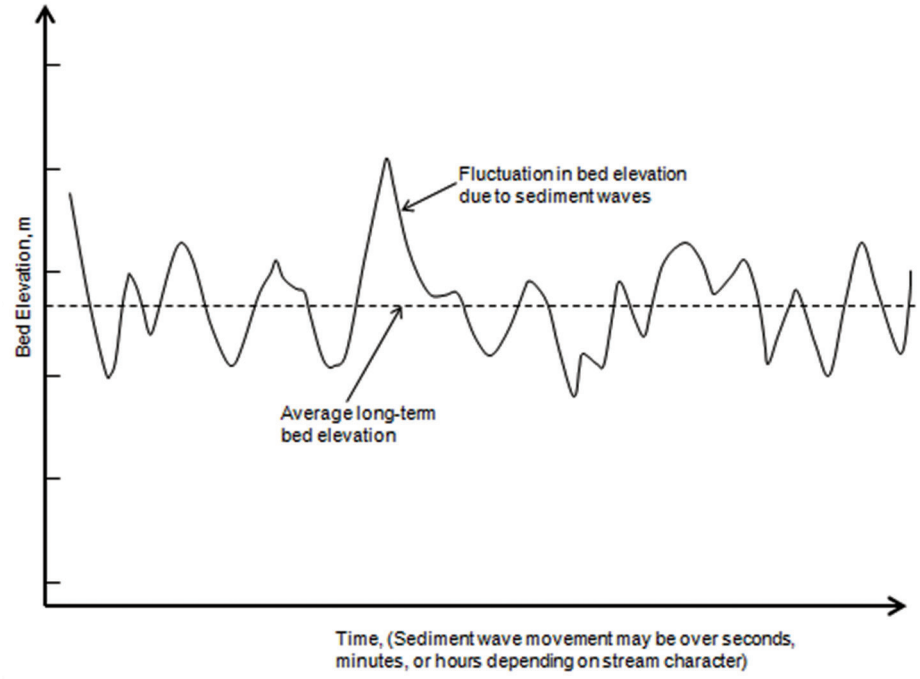

Figure 8.24 Development of additional depth due to sediment waves along river channel (Arneson, 2012)

Bed profiles typical of sand bed streams are commonly classified as flat bed, ripples, dunes, transition bed, antidunes, and chutes and pools (ASCE, 1966). The presence of coarser bed materials influences bed movement tendencies, generally suppressing the amplitude (height) of sediment waves as compared to beds composed entirely of sand. In rivers with gravel beds, bed form migration occurs primarily as the movement of gravel bars or waves down the stream. Bars are large depositional features that generally occur in meandering or braided channels. Bar migration can reduce channel waterway area and redirect flows, possibly resulting in increased scour owing to flows concentrating at the bank.

Sediment wave prediction is a two-stage process that requires estimating the type of bed form then its height. Available methods predict the types of bed profiles for sand bed streams based upon various combinations of flow strength and sediment characteristics. The topic is quite complex and the reader is referred to references for predictive equations and additional information (Simons and Richardson, 1966, van Rijn, 1984, Julien and Klaassen, 1995, Hey *et al*, 1982, Yalin, 1964 and 1992, Ikeda, 1984, Nordin and Algert, 1965, Shen *et al*, 1969, Raudkivi, 1990, Coleman, 1991, Coleman and Melville, 1994, Chang, 1988, and Williams and Cozakos, 1994). Although there are one or two exceptions, the empirically developed equations estimate average magnitude of bed forms at equilibrium conditions. There is significant scatter in the data used to develop the equations, and the principle source of concern is maximum bed form size as the sediment waves pass through the stream.

While average bed form height may be useful, the most significant issue for levee assessment and design is the maximum height, or the condition that yields the greatest scour depth. Yalin (1964) used experimental data and theory to project that the maximum dune height should not exceed one-sixth of the flow depth. Nordin and Algert (1965) suggested that $y/3$ is more appropriate for average maximum dune height, particularly where 3D bed profiles occur. Neill (1973) indicated that maximum dune heights for migrating dunes in natural alluvial streams can be up to half the flow depth. With respect to design of levee toe protection, Williams and Cozakos (1994) adopted $y/3$ as the design scour depth for bed form migration. Melville and Coleman (2000) suggest that peak flow depth due to bed form migration past a site, y_{ws}, can be estimated as:

$$y_{ws} = \max\left[1.5\,y\,;\; y + h_{ws}/2\right] \tag{8.65}$$

where y (m) is the flow depth without bed forms and h_{ws} (m) is the maximum bed form height determined from predictor equations. Melville and Coleman emphasise that judgement has to be exercised in using Equation 8.65 as the first equation (y_{ws}=1.5y) may produce unrealistically large scour depths.

Because of the complexity and interpretative nature of evaluating bed forms, predictor equations are not presented in this handbook. The reader should refer to Melville and Coleman (2000) or other references for details on the individual methods. Engineers with experience of river mechanics should be consulted for analysis required to estimate sediment wave characteristics needed to support analysis and design efforts for levees.

Melville and Coleman (2000) point out that Raudkivi (1990) observed that dunes formed when bed material consisted of a broad grading of sediment sizes were very different than when formed in uniformly graded sediment. They also state that the presence of a high concentration of colloidal materials in the flow affects bed forms by delaying their development, causing the transition to flatbed sooner than flows without suspended clays.

8.2.3.5 Confluence scour

Flow typically meets at the centreline of the junction, plunges toward the channel bed, and then returns to the surface towards the sides of the channel where two streams converge. This flow pattern results in helicoidal secondary currents that produce a deep scour hole with steep sides. Confluence scour can be of significant concern for levees located along braided channel systems. Braided systems can undergo rapid shifts in channel position resulting in the confluence of individual channels of a river rapidly moving towards a levee. The additional depth in the confluence increases total bank height, and slope stability analysis has to address the potential for exceeding a stable bank height. The addition of a levee in close proximity to a channel makes this situation more critical.

There is little agreement in the literature on principle parameters that influence confluence scour. In general, principle factors include confluence angle, flow rates, flow depths, channel slope, bed material size, bed-material transport rate, concentration of suspended sediments and type of channels involved. Melville and Coleman (2000) cite observations by Ashmore and Parker (1983) that indicate naturally occurring confluence angles are typically about 100°. Melville and Coleman used this angle to predict a maximum value of y_{cs}/y=5.34. Chow (1959), however, suggests that owing to the complexity of confluence scour there is no way to generalise the phenomenon and that model studies are the only feasible way to develop estimates of scour depth. The recommended approach for evaluating confluence scour is to develop numerical sediment transport models capable of simulating 2D development of the bed in the confluence region. For highly complex areas a physical model study may be warranted.

Good practice for levee design is to avoid placing levees in close proximity to confluences. In the case of braided channels, levees should be located well outside the zone of potential channel migration. Protective measures should be included in the levee project to guard against threats imposed by channel shifts and rapid changes in confluence locations where this is not feasible. Protection can be in the form of revetment along stream banks or other stream bank stabilisation measures. Melville and Coleman (2000) provide further details on contraction scour.

8.2.4 Scour of beaches in front of coastal levees

This section details scour of beaches in front of coastal levees following the approach shown graphically in Figure 8.25.

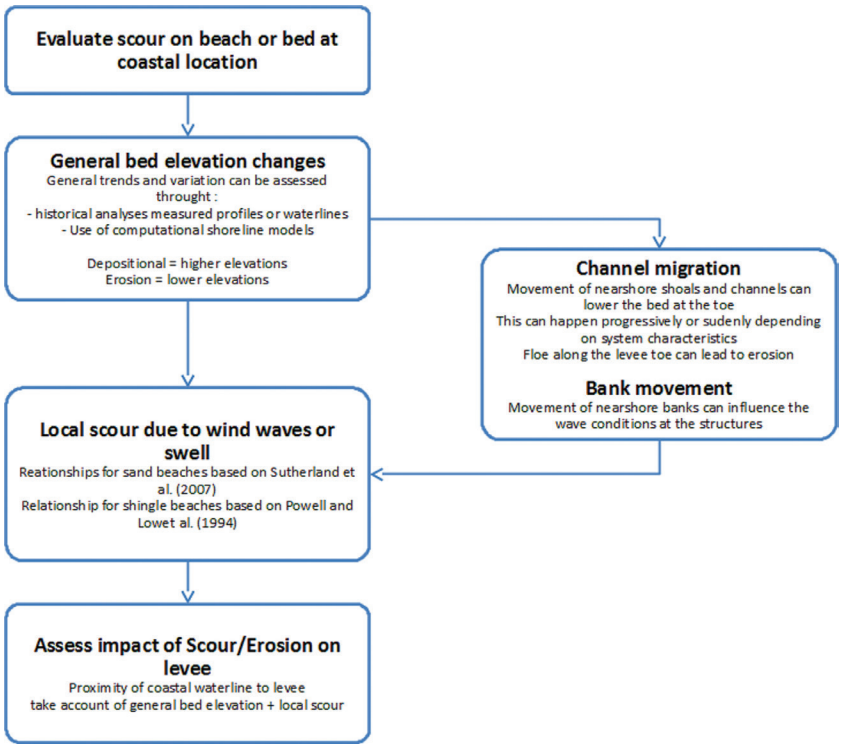

Figure 8.25 Basic approach to evaluating scour at the coast

8.2.4.1 General

The introduction of levees on an open coast will produce a system response where the toe of the structure is submerged. The degree of response will depend on characteristics of the structure including front face slope and roughness. The vulnerability to scour is governed by the water depth at the toe due to tidal variation, wave set-up at the shoreline, storm induced and possibly seasonal changes to normally occurring water levels. The nearshore and beach profile shape as well as sediment composition will also influence the response. The forcing of scour depends on the wave height and period of waves reaching the levee. The information in this section draws on results from laboratory research and field evidence at seawalls (Sutherland *et al*, 2006, Sutherland *et al*, 2007, and Wallis *et al*, 2009).

There are two sets of analyses that are required to evaluate the amount of vertical change that could be expected to occur in front of a levee at a coastal site. These are:

- predicting the lowering of beach levels
- predicting sediment scour at the toe of the wall. (Note localised sediment scour at the toe of the levee is a different physical process to beach lowering, although partly dependent upon that of broader scale beach lowering).

The approach that is adopted for the toe scour prediction is as detailed below. Methods are provided for scour on sand beaches and shingle beaches in front of vertical walls. Commentary is provided on how to relate the results to sloping walls as would be found on levees.

8.2.4.2 Predicting beach lowering

The performance of a beach largely depends on the volume of material present and the limits to its plan and profile changes – influenced particularly by sediment control structures within it (eg groynes, sills, breakwaters). Where there is a continuing net loss of sediment, then the lack of beach recovery is an issue. In general, pressure on the integrity of the structure can result from depletion in the volume of the beach through increased longshore and/or cross shore transport of beach sediment, or, a reduction in supply of sediment onto the beach front. Beach levels are constantly changing, and trends of depletion or

deposition are generally gradual (long-term), however significant erosion and lowering can occur during 'one-off' storm events.

The variations in beach levels occur in a range of timescales from one tide or storm to annual events, and are the accumulation of residual changes in level that occur during each tide or storm. It is common to find beach levels lower during the storm season (eg winter, monsoon, cyclone, and hurricane) due to the higher occurrence of increased levels of wave energy. It also follows that where there is a periodic signal of storm events the beach levels may show a greater variation about their seasonal mean during the storm season.

A range of advanced linear and nonlinear data analysis methods can be used to evaluate the long-term behaviour of beaches (Larson *et al*, 2003, and HR Wallingford 2008c). Data-based analysis will become more powerful as the amount of regularly sampled and accurate data collected, stored and managed by organised regional coastal observatories and other agencies increases. The evaluation of profile data may be supplemented by the results from process-based numerical models of cross-shore beach evolution (eg van Rijn *et al*, 2003).

One dilemma the engineer faces is what prediction 'horizon' can be expected when extrapolating beach level time series data. Analysis of beach monitoring data from Lincolnshire, UK (HR Wallingford, 2008a, and Sutherland *et al*, 2007) illustrates that the predictive ability of a straight line fit from more than 10 years of data are limited to a few years beyond the end of the dataset. However, this should be sufficient for the purposes of supporting annual inspection combined with predictive modelling. An indicative per annum allowance for beach lowering based on data provides a guide to potential beach lowering rates and informs the design and maintenance of coastal defences. The indicative allowances for beach lowering can be applied in the same way as, say, indicative allowances for sea level rise. Indeed, each site should be treated individually to determine the general context for the levee under consideration as this may also be influenced by nearshore banks and channels, which will affect waves and currents. Channels in open embayments, inlets and estuaries that move so as to run adjacent to the toes of levees can cause erosion.

8.2.4.3 Predicting sand bed scour due to waves

The development of toe scour is a dynamic process, highly dependent on the water level at the wall and the incident wave conditions. In areas of varying tidal range and wave climate, the development of a scour hole will be an episodic process with periods of erosion followed by infilling, and perhaps even general accretion of the bed (Powell and Lowe, 1994). So, the scour hole itself may be a short-lived feature with no obvious evidence of its extent, or perhaps even its existence after a storm has declined and infilling has taken place as the tide recedes. This means that the profile seen before and after the storm may be quite similar in consecutive beach profiles taken at low water. There is a need to be able to predict the maximum depth of the scour hole during storms, as well as the more widespread and longer-term processes that cause the lowering of beach/shore-platforms. This is an important factor to take into account at the design stage of a structure, and in its operational life to fully understand risks to integrity of the levee and plan for timely remedial action to be undertaken when required.

As storm event scour is frequently short-lived, a programme of annual or seasonal beach profile monitoring is unlikely to capture a major scour event but can indicate the way in which the beach is evolving and record seasonal variations at the seawall. Indeed, the evidence supplied by data from scour monitors (Sutherland *et al*, 2006) suggests that a significant amount of a scour hole can fill in within a few hours of the peak of a storm. So, even regular beach profiling with a spacing of a few weeks, supported by profiles collected within a day or two of each large storm may not capture the transient phenomenon of toe scour in the field. The combined evaluation of beach level trends and scour prediction is an appropriate way forward.

One rule of thumb for vertical seawalls has been that the maximum scour depth is equivalent to the (unbroken) significant wave height H_s. Whitehouse (1998) and CERC (1984) suggested the depth of scour may be equal to the maximum unbroken wave height H_{max} (ie $1.8H_s$). As an improvement on this

(Sutherland *et al*, 2007, and HR Wallingford, 2008b) recommended the use of a conservative predictor of scour depths, which may be used in the absence of site-specific information on beach slope. It is reproduced as Equation 8.66 with H_s as the commonly used scaling parameter for predicting scour depth:

$$\frac{S_{tmax}}{H_s} = 4.5\, e^{-8\pi(h_t/L_m+0.01)} \left[1 - e^{-6\pi(h_t/L_m+0.01)}\right] \tag{8.66}$$

for -0.013 ≤ H_t/L_m ≤ 0.18 and where:

S_{tmax} = maximum toe scour depth at a vertical wall (m)
H_s = the deep water (unbroken) significant wave height (m)
h_t = water depth above the sediment level at the toe of the wall (m)
L_m = $gT_m^2/2\pi$ the linear theory wavelength based on acceleration due to gravity g (default assumption of 9.81 m/s²) and mean wave period T_m (s)

The equation is plotted with data in Figure 8.26. When this equation was tested by validating laboratory tests with field data from two UK sites, Blackpool (vertical wall) and South Bourne (sloping wall), it was found that the field data generally had lower scour depths than the laboratory data. This is believed to have been caused by the fact that wave height, wave period and scour depth were only measured at a single tidal state in the laboratory. The field data was collected in situations with constantly varying water levels and wave heights. However, the upper limits of the field observations confirm the laboratory data and envelope curve of Equation 8.66 – even with a sloping wall.

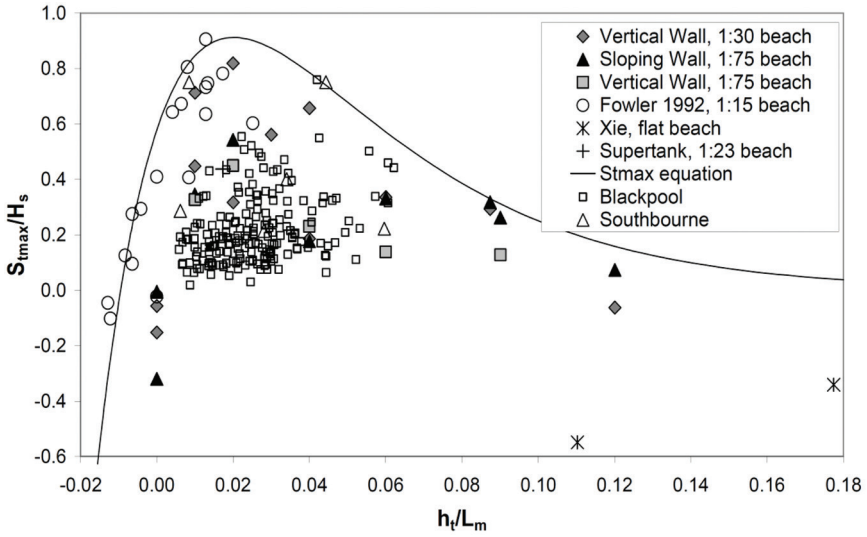

Figure 8.26 Envelope to scour predictor. Equation 8.66: laboratory data and field data (after Sutherland et al, 2007)

It can be seen from Figure 8.26 that the scour depth is always less than H_s, and that the peak scour depth occurs for relative water depths (H_t/L_m) of around 0.01 to 0.02 and that the scour depth reduces for shallower and deeper water.

In situations where the beach slope is known then an alternative empirical equation for the depth of scour at the toe of a vertical wall developed using the laboratory data in Figure 8.26 can be used (HR Wallingford, 2008b, and Sutherland *et al*, 2007). HR Wallingford (2008b) showed that the relative toe scour depth can be given with a beach slope dependency by Equation 8.67:

$$\frac{S_t}{H_s} = 6.8\,(0.207 \ln\alpha + 1.51)\, e^{-11.7\pi h_t^*/L_m} \left[1 - e^{-6\pi h_t^*/L_m}\right] - 0.137 \tag{8.67}$$

for -0.04 ≤ H_t/L_m ≤ 0.12 and where:

S_t = the scour depth at the toe of the structure (m)
H_s = the deep water (unbroken) significant wave height (m)
α = the beach slope (radians)
h_t^* = the water depth above the sediment level at the toe of the wall (m) including effect of wave set-up calculated using the equation of Holman and Sallenger (1985) where $h_t/L_m \leq 0$

Hollman and Sallenger's (1985) expression for the maximum set-up, η_{max}, that would occur on a natural beach is given in Equation 8.68, where both the wave height and wavelength (in the Iribarren number, *Ir* or ζ_m) are calculated in deep water but the beach slope is calculated at breaking:

$$\eta_{max} = 0.45\, H_s\, Ir = 0.45\, \tan\alpha \sqrt{H_s\, L_p} \qquad (8.68)$$

In the derivation of the scour predictor, Equation 8.68 was only applied for cases where $h_t/L_m \leq 0$ as the set-up is a maximum at the shoreline and decreases to the breaker line, where set-down will occur. In practice there will be an interaction between the incident and reflected waves so parameterisations of set-up derived for the open coast may not be particularly accurate in front of a structure.

Equation 8.66 was derived from tests with normally-incident irregular waves and beach slopes of 1:15, 1:30 and 1:75. The equation predicts maximum scour depth reducing with decreasing beach slope as seen in the laboratory data.

Equation 8.67 is plotted with the measured data in Figure 8.27, where 'O 1:N' and 'P 1:N' are the observed and predicted scour depths with a beach slope of 1:N (with N = 15, 30 or 75) respectively. The equation predicts the highest toe scour depths relatively well. There are relatively low errors for the high relative scour depths, which are likely to be the most important, while the largest errors in the predictions occur for negative observed scour depths (ie accretion at the toe of the structure). However, these cases may be relatively unimportant, at least as far as the stability of a structure is concerned.

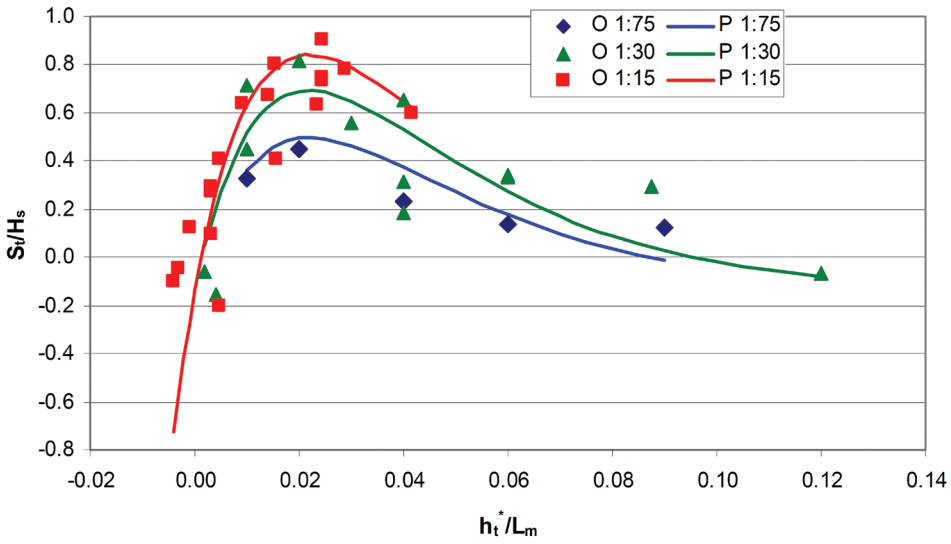

Figure 8.27 ***Measured and predicted (Equation 8.67) relative toe scour depths as a function of relative toe depth in sand (Sutherland et al, 2007)***

Both Equations 8.66 and 8.67 predict the scour after 3000 waves (ie 6.7 hours for an eight second period wave) and a correction has to be used to predict scour for time intervals other than 3000 waves.

8.2.4.4 Prediction of toe scour at vertical seawalls with shingle beaches

Scour depths in shingle beaches can be predicted using the parametric plot of Powell and Lowe (1994) reproduced as Figure 8.28. This was based on an extensive set of laboratory tests conducted with normally-incident irregular waves that broke on a 1:7 slope shingle beach, with a vertical impermeable seawall. The maximum scour predicted was $1.5H_s$. The method is valid for beach sediment in the range 5 mm $< d_{50} <$ 30 mm (modelled at 1:17 scale).

Figure 8.28 shows contours of S_{3000}/H_s plotted on a graph with axes of relative water depth, h_t/H_s and relative wave steepness, H_s/L_m, where:

h_t/H_s = the relative water depth

h_t = the initial water depth above the sediment level at the toe of the wall (m)

H_s = the extreme deep water (unbroken) wave height (m)
H_s/L_m = the wave steepness
L_m = the mean wavelength of the unbroken wave (using $T^2g/2\pi$) (m)
S_{3000} = the scour depth after 3000 waves.

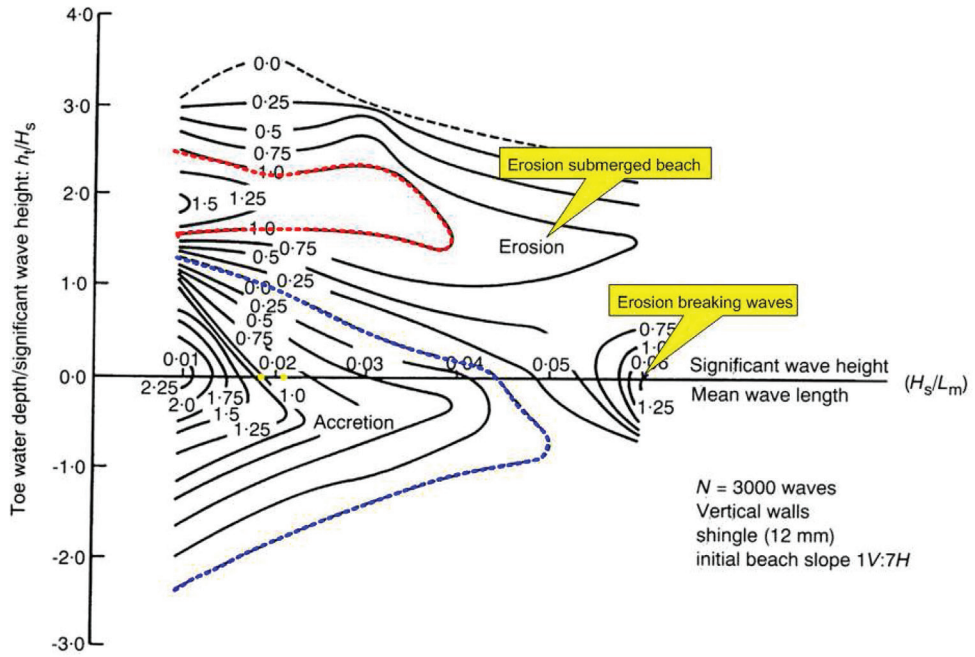

Figure 8.28 ***Prediction diagram for scour (erosion) and accretion at vertical seawalls with shingle beaches – contours of dimensionless scour depth S_{3000}/H_s (from Powell and Lowe, 1994)***

To select the worst possible scour, look at the dimensionless scour values for all h_t/H_s values below the maximum relative water depth, corresponding to the wave steepness, H_s/L_m and select the greatest relative scour height, which can exceed H_s. The plot gives the scour after 3000 waves, so a correction has to be used to predict scour for time intervals other than 3000 waves.

8.2.4.5 Effect of sloping front face on scour

The effect of a sloping wall on scour depths has been investigated by several authors, including:

- Sutherland *et al* (2006) compared the maximum scour depths and the toe scour depth at a 1:2 (27° above horizontal) sloping impermeable wall to those at a vertical impermeable wall for four different offshore wave conditions and water depths with H_{si}/h_t = 0.5 to 1.0, where H_{si} is the incident significant wave height and h_t the toe water depth. The results are shown in Figure 8.29 and show no systematic reduction in scour depth with wave height. In these cases the down-rush from the highest waves was reaching the seabed in some cases, which caused scour to occur.

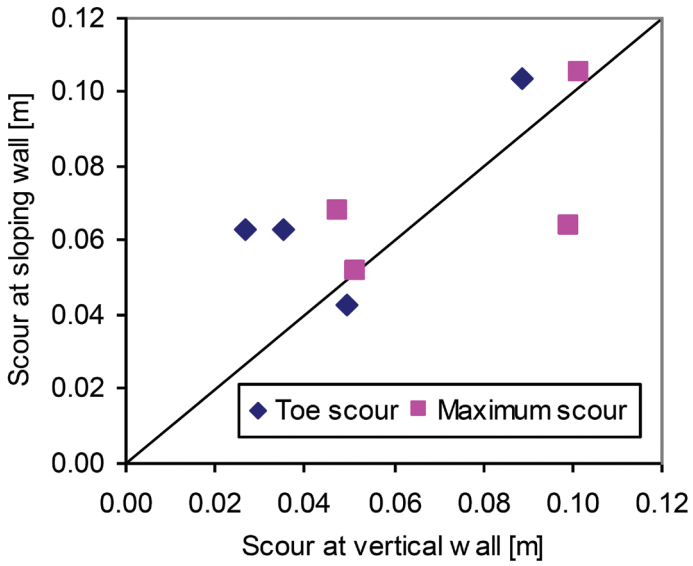

Figure 8.29 ***Comparison of laboratory measurements of scour depths in sand at a 1:2 sloping wall and at a vertical wall for the same offshore wave conditions (Sutherland et al, 2006)***

- Sumer and Fredsøe (2002) (Figure 7.17) quantified the effect of wall slope in the nonbreaking wave case ($0.05>d/L>0.2$) and showed that scour was reduced by about 80 per cent or 60 per cent for wall slopes of 30° and 40° respectively above horizontal (compared to the scour from a vertical wall). This is for the situation where the toe of the structure is always submerged and the bed in front of the structure is initially flat and horizontal
- Powell (1987) noted that for impermeable sloping structures of 1:1.5 to 1:2 there was no significant reduction in scour depth compared to that at a vertical wall. However, reducing the slope of an impermeable structure to 1:3 reduced the scour hole depth by 25 to 50 per cent. Powell also noted that rock armour revetments generally showed less susceptibility to local scour and may even show accretion
- Powell and Lowe (1994) showed a reduction in scour depth of almost 65 per cent in a shingle beach when a vertical wall was replaced by a sloping wall of 1:1.25. The scour depth was reduced by about 80 per cent for a 1:2 slope and there was accretion at the structure toe for a 1:3 slope. A rubble mound coastal defence showed no scour at its toe.

In shallow water the depth of scour is controlled by waves breaking on the wall and turbulence reaching the seabed. Under these circumstances the effect of reducing the seawall slope can be insignificant. It is only when water depths at the toe of the structure are sufficient to prevent turbulence reaching the seabed that a systematic reduction in scour depths with wave height can be expected. Moreover, for a sloping seawall, there is a phase shift on wave reflection (Sutherland and O'Donoghue, 1998) so the position of deepest scour may change to be away from the toe of the wall.

8.2.4.6 Storm duration

The duration of the wave/water level conditions is also an important control on toe scour development. Scour is not an instantaneous process – the trough deepens over a number of waves. Powell and Lowe (1994) demonstrated how scour in shingle develops until a quasi-equilibrium is obtained within about 3000 waves. It was noted that there was rapid initial scour that declined exponentially towards the equilibrium depth.

Similar trends are also apparent for sand beaches, though results from model studies (McDougal *et al*, 1996) suggest slower scour hole development, with equilibrium unlikely to be achieved within a realistic storm/water level duration. The experimental tests of Sutherland *et al* (2007) indicated that the average timescale of the scour was such that 95 per cent of the equilibrium scour depth would be reached after

about 2500 waves, although there was considerable scatter in the timescales derived. For typical storm mean wave periods of six to eight seconds, this would take between about four and 5.5 hours to achieve.

The use of Equation 8.69 is recommended for predicting potential scour depths in the field. If the environmental conditions are expected to last for less than 3000 wave periods, the expected scour depth may be reduced by a factor determined from Equation 8.69.

$$S(t) = S_e \left(1 - e^{-t/Ts}\right) \tag{8.69}$$

where:

$S(t)$ = scour depth at time t (m)
t = time since start of scour process (s)
S_e = equilibrium scour depth (m)
T_s = timescale for scour (s)

McDougal *et al* (1996) suggests $T_s = 3100T$, with T the wave period. Xie (1981) suggested that for fine sand in suspension the equilibrium scour depth would be reached in 6500 to 7500 wave periods for $H/L > 0.02$ and in 7500 to 10000 wave periods for $H/L < 0.02$.

8.3 INTERNAL HYDRAULIC PROCESSES

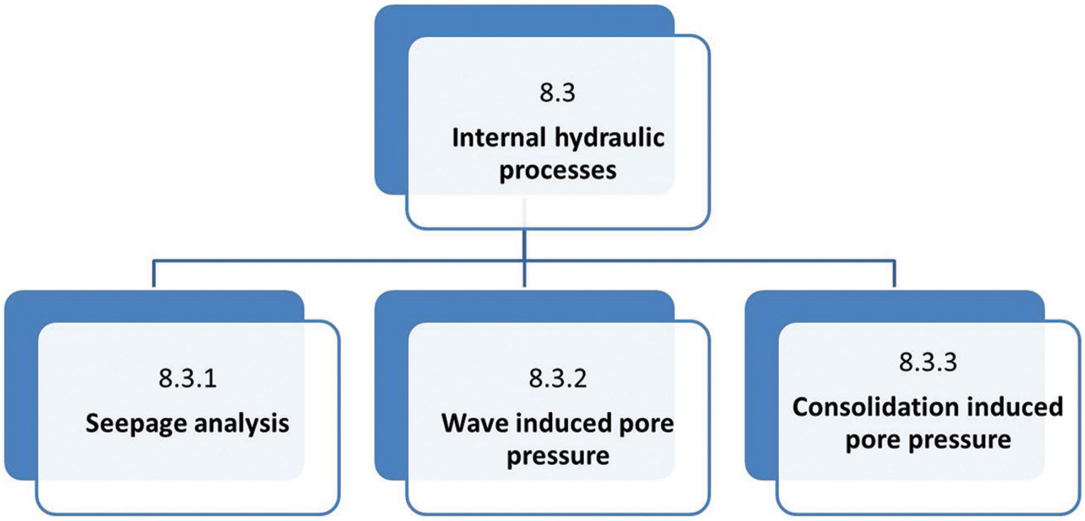

Hydraulic and mechanic actions may induce water flows and pore pressure fields within the levee and its foundation. Failure modes are influenced by the pore pressures and flow distributions and variation during time. All levees are subjected to internal flows as a result of either steady or transient external hydraulic conditions, and are a function of levee and foundation materials. Under hydraulic loading, seepage can occur either through the levee (through-seepage) or in its foundation (under-seepage). This phenomenon is accounted for in a levee stability assessment because pore water pressures and flows have a strong influence on deterioration and failure modes such as internal erosion (Section 8.5), slope stability (Section 8.6), and settlement (Section 8.7).

In this section, two main types of actions will be distinguished as shown in the section flow chart:

1 **Stationary hydraulic actions,** eg slow varying water level regarding the drainage characteristics of the soil

2 **Non-stationary hydraulic actions,** eg waves, which change rapidly regarding the drainage characteristics of the soil.

8.3.1 Stationary seepage analysis

8.3.1.1 Introduction

Seepage is governed by hydraulic laws initially developed for saturated soils. One difficulty for levees in opposition to dams is that materials (of levee body or foundation) are often totally or partially unsaturated when a flood event occurs and simple models or methods to study seepage are then not strictly applicable. However, they are often used in a first phase of studies because they are safer for stability analysis. Newer finite element programs include complex models to take into account unsaturated soil flow laws. These routines to perform partially saturated seepage analyses require additional inputs that are not very well known in practice.

The aim of a seepage study for levee design or analysis is to determine the following elements that could be used in stability analysis and for designing specific seepage control solutions:

- the phreatic line
- internal pore pressures that could occur in levee material or its foundation
- exit gradient
- seepage flow rate.

8.3.1.2 Basic hydraulic laws

Hydraulic head: Bernoulli's law and gradient

When a structure is subject to hydraulic head and for almost all geotechnical structures (and then for earthen levees and their foundations), flow of groundwater through a saturated soil is governed by Darcy's law:

$$q = A\,k\,i \tag{8.70}$$

where:

q = volumetric flow rate (m^3/s)
A = cross-sectional area of flow (m^2)
k = Darcy's coefficient of permeability or hydraulic (m/s)
i = hydraulic gradient in the direction of flow (-)

The hydraulic gradient i is defined as the rate of total hydraulic head dh (m) with distance dx (m) along the direction of flow, defined as follows.

$$\vec{i} = -\overrightarrow{grad}\,h \tag{8.71}$$

Box 8.6 gives a definition of hydraulic head, line of seepage and seepage surface.

Box 8.6 ***Definition of hydraulic head, line of seepage and seepage surface***

In saturated soil, Bernoulli's Equation 8.72 enables to have the total hydraulic head *h* in each point *M* of the levee:

$$h = z + \frac{u}{\rho_w g} + \frac{v^2}{2g} \tag{8.72}$$

The flow velocity *v* in soil is generally very slow (<1 m/s). So, the velocity head (quadratic term equivalent to kinematic energy) can be neglected in most cases and then the following simplified equation can be used:

$$u = z + \frac{u}{\rho_w g} \tag{8.73}$$

where:

h = hydraulic head (m)
z = altitude of considered point related to reference plan (m)
u = internal pore pressure (kN/m²)
v = flow velocity (m/s²)
ρ_w = water volumetric mass (kN/m³)
g = gravity acceleration (9.81 m/s²)

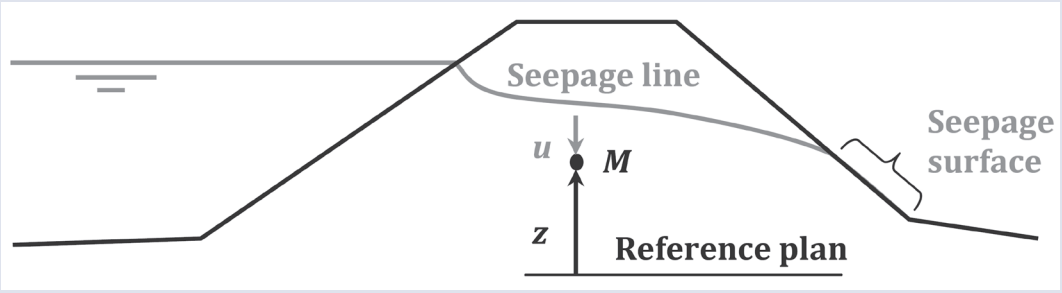

Figure 8.30 ***Phreatic line and surface of seepage in a levee cross-section with steady stage water level***

In saturated soils, Darcy's law is valid under certain conditions. Firstly, in very low permeability soil such as highly plastic clay, flow cannot occur under a high threshold hydraulic gradient. Soil is then considered to be impervious (range of permeability in 7.8.3). Secondly, at very high flow rate, it has been recognised that Darcy's Law does not hold because flow is turbulent and no longer laminar (Chugaev, 1971). Regarding average diameter of soil particles, boundary between laminar and turbulent flow can be determined using Reynolds number (Box 8.7).

Under conditions of partial saturation, the flow is in a transient state and is time dependent. Darcy's law can no longer be strictly applied. However, it can be useful to apply Darcy's law in conditions where it is not strictly valid, to have in a first step of levee design an approximation (often by excess) of flow rate, flow velocity etc.

Box 8.7 ***Boundary between laminar and turbulent flow using Reynolds number***

The Reynolds number R is a dimensionless number that expresses the ratio of internal flow force to viscous force:

$$R = \frac{v\,D\,\rho}{\mu} \tag{8.74}$$

where:

v = true flow velocity (m/s)
D = average diameter of soil particles (m)
ρ = fluid density (kN/m^3)
μ = kinematic viscosity of fluid (kN/m/s)

The critical value of R at which the flow in soil changes from laminar to turbulent has been determined to range from one to 12 (Chugaev, 1971). For a water temperature of 20°C, ρ = 9.982 kN/m^3 and $\mu = 1.002 \times 10^{-5}$ kN/m/s, Figure 8.31 shows the upper boundary of validity of Darcy's law (laminar flow). Then, depending on the discharge (flow) velocity v, it is assumed that Darcy's law is applicable for silts through medium sands.

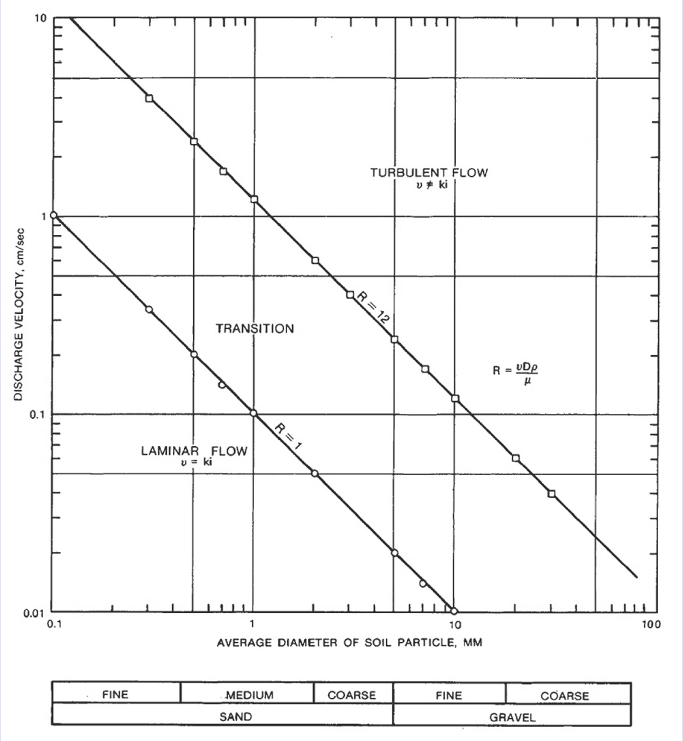

Figure 8.31 ***Boundary between laminar and turbulent flow in using Reynolds number and limit of Darcy (USACE, 1993)***

Flow velocity, seepage velocity and flow strength

For levees, if the duration of the flood is sufficiently long to impact the hydraulic conductivity of material (Case b, Figure 8.34), internal flow and seepage can occur. According to Darcy's law (Equation 8.70), the groundwater flow velocity (discharge flow velocity) is given by the following equation:

$$\overrightarrow{v_D} = k\,\overrightarrow{i} = -k\,\overrightarrow{grad}\,h \tag{8.75}$$

Equation 8.76 gives the relation between both velocities for a soil of porosity n ($0 < n < 1$, or a void index e):

Note

The discharge velocity is not the true velocity of the flow through the pores: the true seepage velocity v_t exceeds discharge velocity (which corresponds to an average laminar flow path through the soil as shown in Figure 8.32).

$$v_t = \frac{v_D}{n} = \frac{1+e}{e} v_D \tag{8.76}$$

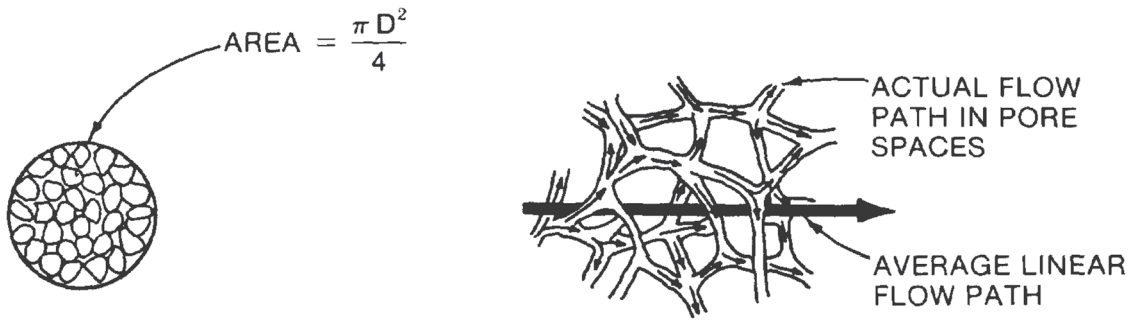

Figure 8.32 Concepts of flow paths through a soil column (USACE, 1993)

In a saturated soil, the flow velocity creates a flow density force on grains as presented in Figure 8.33. This force is given by Equation 8.77. This can initiate instabilities, primarily at the seepage exit point, like internal erosion of soil or shallow surface slope instabilities (Section 8.4) and then lead to important deteriorations or levee failure.

$$\vec{f} = \gamma_w \vec{i} \tag{8.77}$$

where:

γ_w = water volumetric mass (kN/m³)
i = hydraulic gradient (-)

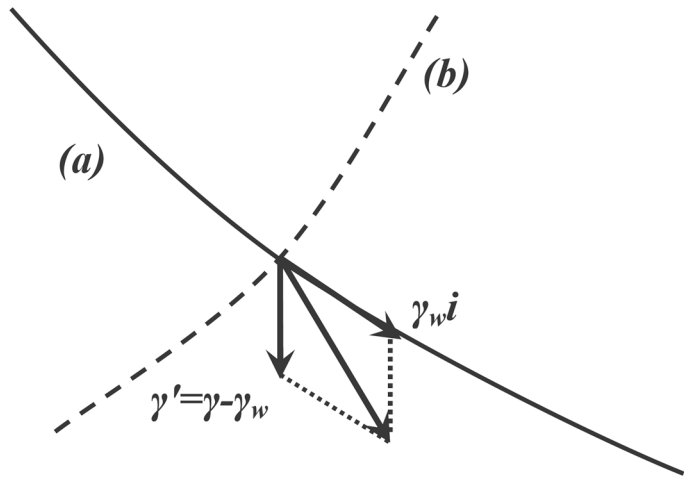

Figure 8.33 Hydraulic flow forces on grain in saturated soils due to flow gradient, current line (a) and equipotential line (b)

8.3.1.3 Permeability and anisotropic permeability effects on levee saturation

The permeability (also called hydraulic conductivity) is one of the main parameters influencing seepage. In natural soils or built earthen structures such as levees, this parameter is quite difficult to obtain and is not equivalent in all directions (anisotropy of permeability). The main parameters influencing permeability of soils are the nature of soils (deposition modes), sizes and forms of particles, contents of fine elements, properties of seepage fluids (viscosity regarding to temperatures) and degree of saturation of soils. More information can be found in USACE (1993) and CFBR (2010). *In situ* and laboratory devices and tests to measure permeability (k), anisotropy (i) are described in Chapter 7 (Section 7.8.3). Table 7.111 provides typical values of hydraulic conductivity (permeability) for different types of soils.

Figure 8.34 shows the influence of permeability on levee saturation during a flood event. In Case a, the permeability is low enough that the levee is only partially saturated and seepage will not occur during a flood event. In contrast, Case b, shows the permeability is large enough to lead to full levee saturation producing seepage during a flood event. Landward slope instabilities and internal erosion can then occur.

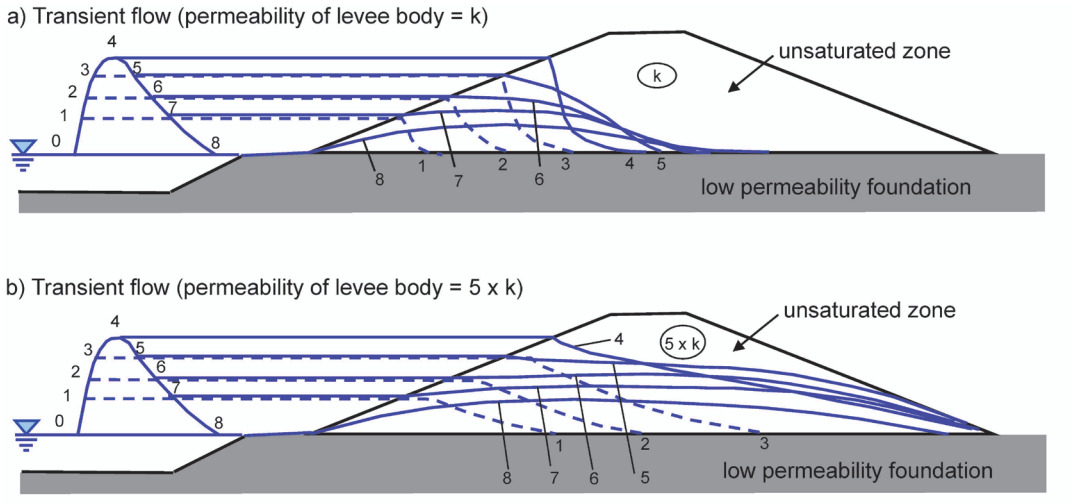

Figure 8.34 ***Effect of permeability on levee saturation during transient states of flooding situation (adapted from German guideline)***

Hydraulic conductivity is generally anisotropic, ie conductivity in vertical (k_v) and horizontal (k_h) directions are different. In natural soils, horizontal conductivity is generally greater than vertical conductivity (from 10 times in clay material to 100 times and more in fine layered soils), resulting from the deposition modes of soils. For built earthen structures as levees, this is often also the case because of construction of the levee by layers placed horizontally. Note that for the upper layer, cracks in silty or clayey soils can lead to a vertical permeability greater than the horizontal permeability. Figure 8.35 shows the effect of anisotropy on flow network. If the anisotropic rate is too large, seepage occurs on the landward slope.

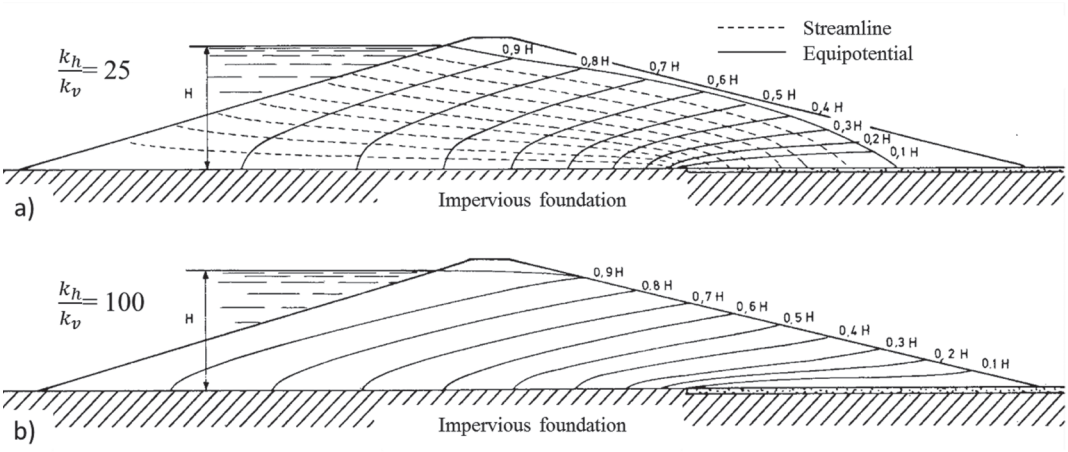

Figure 8.35 ***Impact of anisotropy of permeability on flow network for a permeable levee built on impervious foundation and for a steady state situation (after Josseaume, 1970)***

8.3.1.4 Determination of phreatic, flow and equipotential lines

For levee stability analysis and design, the flood event leads to several transient hydraulic situations. However, even in transient situations, it is easier and often safer to analyse the levee considering design water levels (Sections 7.3.5 to 7.3.9) in a permanent state (realising that these design situations do not strictly reflect reality). To do so, the determination of phreatic line is necessary and represents one of the first steps of modelling. Figure 8.36 gives an illustration of an approximation that can be done when considering permanent state instead of transient state. Note that for levee stability analysis (slope stability, internal erosion etc), considering permanent state water level (Case b, Figure 8.36) is often a safe approach because a higher internal phreatic line is taken into account in the design process.

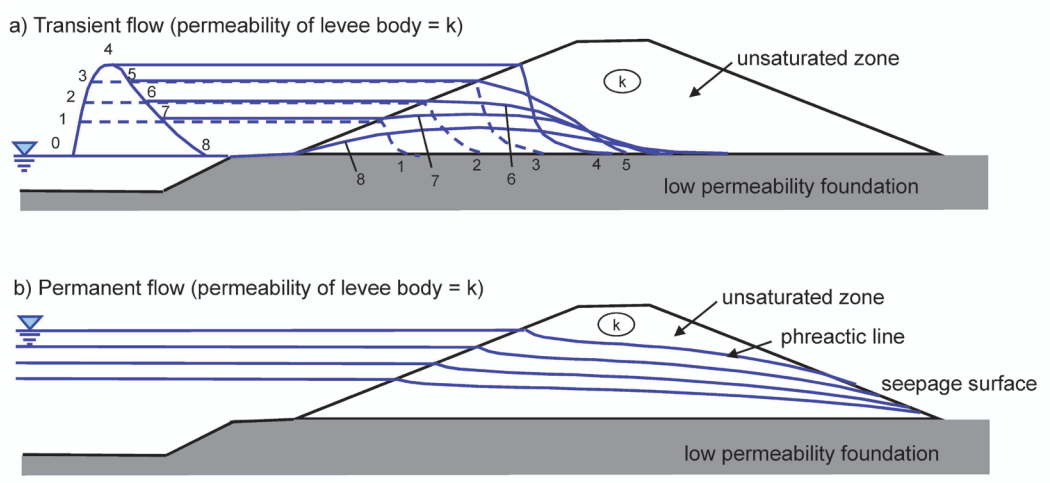

Figure 8.36 ***Comparison of saturation state during transient states of a flooding situation (a) and permanent state (b) considering same water level (after German guideline)***

The first step for a seepage analysis is to determine the position of the phreatic line, which is a hydraulic boundary condition for the flow network. Several methods are presently available to define the saturation line in an earthen structure including geometrical, analytical, and numerical methods. Simple methods such as the graphical methods determine this position with sufficient precision to perform initial calculations (Figure 8.37 in Box 8.8). Analytical methods, such as the segment method, are often empirical.

Box 8.8 ***Usual graphical methods for determining saturation line position***

Several authors proposed solutions to determine position of phreatic line and exit surface of seepage. These simplified methods are often used and give approximate but sufficient solutions. Kozeny shows that for a homogenous undrained earthen dam, the saturation line through the levee could be approximated with a parabolic line as defined on Figure 8.37 below. Several equations are proposed in Table 8.8.

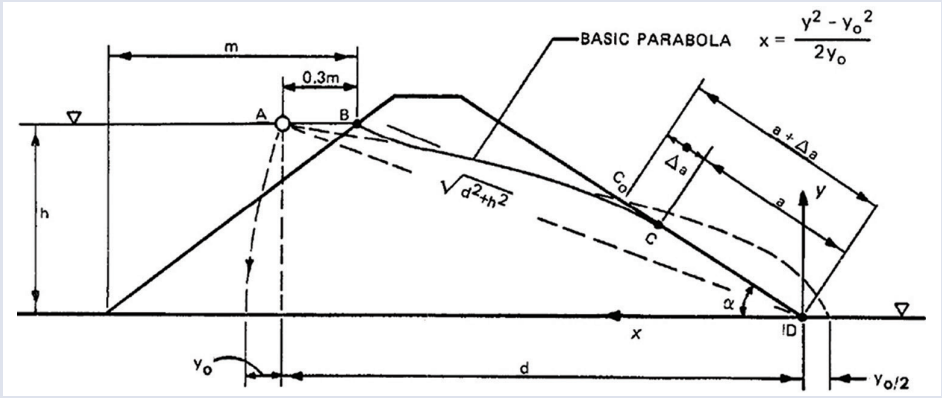

Figure 8.37 ***Phreatic line determination methods – terminology (USACE, 1993)***

Table 8.8 ***Equations for phreatic line determination (USACE, 1993)***

α (°)	Methods	Equations
< 30	Schaffernak	$a = \frac{d}{\cos\alpha} - \sqrt{\frac{d^2}{\cos^2\alpha} - \frac{h^2}{\sin^2\alpha}}$
	Van Iterson	$q = k\ a\ \sin\alpha \tan\alpha$

Box 8.8 *Usual graphical methods for determining saturation line position*

≤ 90	Casagrande	$a = s_0 - \sqrt{s_0^2 - \frac{h^2}{\sin^2\alpha}}$ with $s_0 = \sqrt{d^2 + h^2}$ if α ≤ 60° or $s_0 = (\widehat{AC} + \overline{CD})$ if 60° ≤ α ≤ 90
180	Kozeny	$a_0 = \frac{y_0}{2} = \frac{1}{2}\left(\sqrt{d^2 - h^2} - d\right)$ $q = 2\,k\,a_0 = k\,y_0$
30 to 180	Casagrande	Determine (a + Δa) as the intersection of the basic parabol a and levee slope. Then determine Δa from C value on figure (a) $q = k\,a\,\sin^2\alpha$ or $q = k\,y_0 = k\left(\sqrt{d^2 - h^2} - d\right)$

Numerical methods are commonly included in finite element software, but it is important for readers to appreciate that these methods use complex equations to resolve flow through porous material. Attention should be paid to the assumptions and limits for use of each software program, and the analyst should validate these complex methods even if the project is not complex. Readers can find more details on methods in USACE (1993).

When saturation line is determined, current and equipotential lines can be graphically obtained considering boundary conditions:

- river or sea face of levee is an equipotential line
- saturation line and contact line between impervious layer are both current lines
- equipotential line and current lines are perpendicular
- hydraulic pressure u along phreatic line is null so hydraulic head along this line is due to altitude.

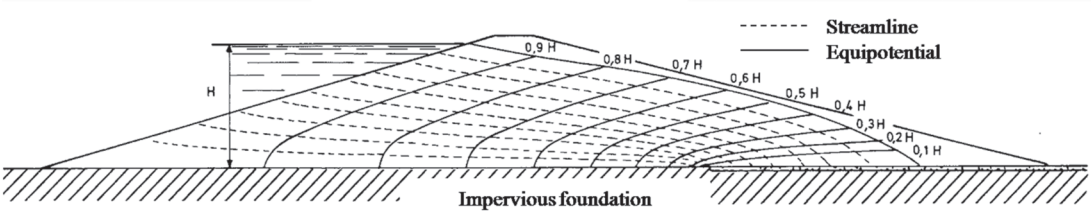

Figure 8.38 *Example of flow net construction in an earthen levee on impervious foundation (adapted from BLR, 1970)*

Then, flow net construction enables the estimation of total discharge q considering that, on each current line, Equation 8.70 can be applied.

8.3.1.5 Internal pore pressure

When the flow net is known and described, it is easy to determine internal pore pressure for each point as shown in Figure 8.39. Using terminology of this figure, M_0 and M_1 are on the same equipotential line so the internal pore pressure at M_0 expresses:

$$u\,(M_0) = \gamma_w\,[z\,(M_1) - z\,(M_0)] \tag{8.78}$$

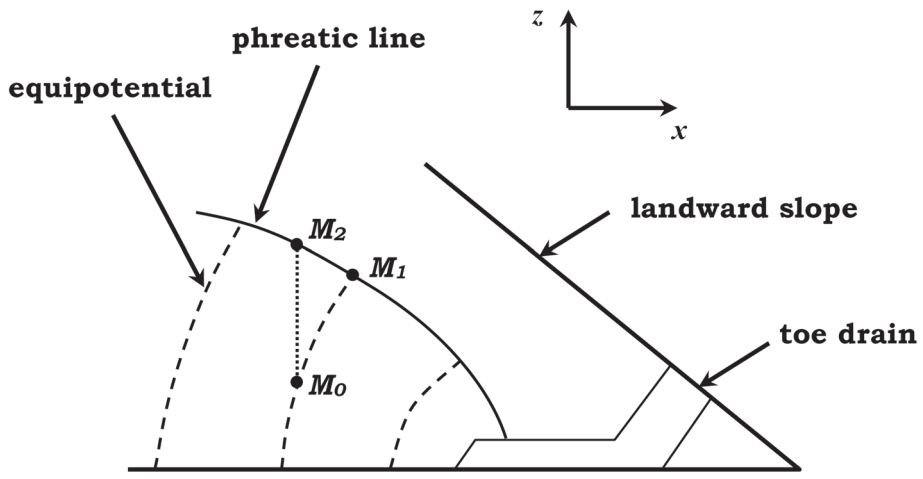

Figure 8.39 Example of internal pore pressure determination using flow net for a levee with toe drain (after Rolley et al, 1977)

For earthen levees, if the line of seepage is too high in the levee landward slope, it can initiate landward slope deterioration and instability. Design control systems are available (as toe drain etc) to control seepage. Description of such controls is given in Chapters 9 and 10. Such systems, designed to collect seepage flow passing through an embankment or its foundation has to follow criteria to be efficient for drainage but also to prevent material transport from one soil layer to another. These filter criteria are detailed in Chapter 9.

Hydraulic forces, excessive gradients or flow velocity through a levee or its foundation and the resulting excessive internal pore pressure are responsible for deterioration processes such as internal erosion (Section 8.5), and slope instabilities, hydraulic cracking, heave and uplift (Section 8.6).

8.3.1.6 Exit gradients

For levee diagnosis, specific design (interfaces with drainage systems) or complex structures (levees with embedded structures), it can be necessary to evaluate local exit gradients. For levee slope stability at the landward toe, most soil mechanics textbooks state that exit gradient should not be greater than one. However, considering earthen structures, factor of safety for critical exit gradient are recommended according to the soil's nature. Details on critical exit gradient are given in Section 8.5.

In flow-net and seepage analysis, if flow is unidirectional, the exit gradient $i_e = dh/dx$ (-) is determined between the last two successive equipotential lines at the landward toe. For a levee, the flow is generally not unidirectional (and vertical) but inclined with regard to the horizontal plane. Then, the exit gradient can be determined by Equation 8.79, knowing the exit velocity orientation as shown in Figure 8.40.

$$i_e = \frac{v}{k_s} = v\frac{k_h \sin^2\alpha + k_v \cos^2\alpha}{k_h k_v} \tag{8.79}$$

where:

k_s = is the soil conductivity in $\vec{v}$ direction (m/s)
α = the angle between $\vec{v}$ and the horizontal plane (°)
k_h = horizontal hydraulic conductivity (m/s)
k_v = vertical hydraulic conductivity (m/s)

It will be necessary to use a numerical program that enables the calculation of local velocities. Figure 8.40 shows an example of a levee flow network with local velocities.

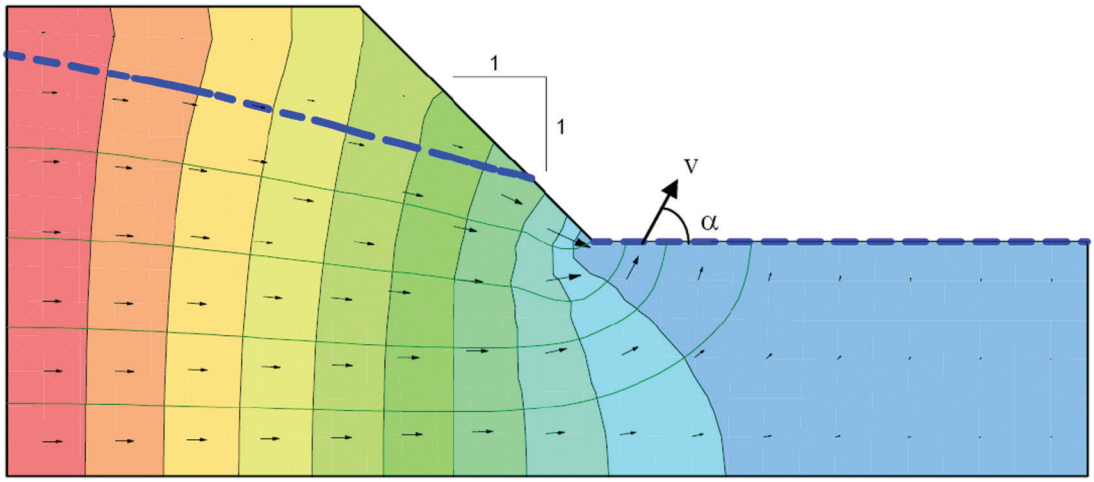

Figure 8.40 Example of levee flow network and local exit velocity orientation (after Mishraand Singh, 2005)

8.3.1.7 Numerical models for seepage analysis

For complex structures or for levee design in transient state, it is assumed that the use of 'piezometric lines' to determine pore water pressures can be incorrect (and unsafe) when there is a significant anisotropy of permeability and when vertical flows exist. Then, the use of numerical models, mostly based on FEM, is generally more rigorous and computations are rapid. However, they are more complex to use and require data based on additional sophisticated specific tests or specialised technical experience. Caution should be given that a result can always be obtained from the numerical models, which may not be based on valid data. It is then highly recommended to validate results with rapid simplified calculations to get an understanding of the order of magnitude of each parameter.

However, for complex levee design or critical analysis, it could be necessary to use specific geotechnical software that can take into account internal flow in porous media. Further points that should be noted (CFBR, 2010) are:

- elastic and perfectly plastic behaviour laws with Mohr-Coulomb criteria should be adopted
- construction stages to initiate effective stress in soil need to be modelled
- interstitial pore pressure, gradients, flows (saturated or unsaturated), and seepage should be taken into account
- interfaces between soil and rigid structures should be modelled
- for fine soil, consolidation should be taken into account.

Currently, several software programs (eg Seep/W, Plaxis and PlaxFlow, Cesar LCPC) enable engineers to study seepage using FEM of earthen structures. Each program has its own limits and the analyst should read the user manual to be familiar with these limitations. An example of FEM is shown in Box 8.9.

Note

For certain programs, the results defining material pore pressures during a flood event can be coupled with classical 2D stability programs, eg Talren V4 with Plaxis or Slope with Seep/W.

Box 8.9 ***Example of application of FEM for levee stability diagnosis and design***

On the River Loire, a general campaign of levee reinforcement began in the 1980s. Several techniques had been employed to ensure stability during flood events, but the most used was an enlargement of levee cross-section with embankment fill put on a drainage granular system (called 'drained carpet'). The geometry of the reinforcement enables lower slopes and containment of the phreatic line inside the levee, producing a better slope stability factor of safety.

At the same time, sandy and granular Loire sediments were extracted, external erosion occurred and the riverbed decreased by 2 m or 3 m locally. Instability then occurred on the riverside slopes and needed to be stabilised. For such design, an FEM was used to appreciate actual stability factor of safety and test different ways to reinforce the levees. Plaxis V8 and Plaxflow were used by the contractor to model the levee (Figures 8.41 and 8.42) during transient state of flood event.

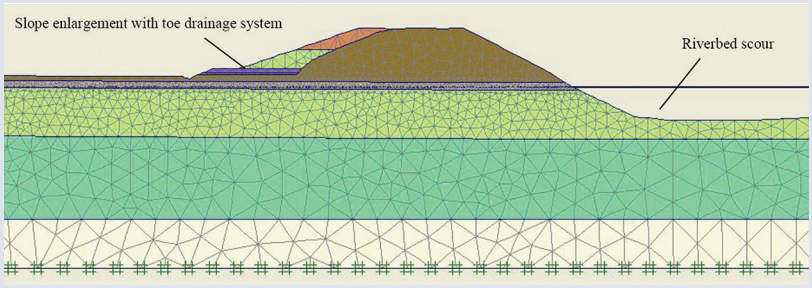

Figure 8.41 ***FEM of the River Loire's levee to study seepage and slope stability during permanent and transient state (flood event), Guilly, France***

Pore pressures, and flow velocities were considered at the landward toe to conduct stability analyses (slope stability, uplift, internal erosion etc) and design reinforcements.

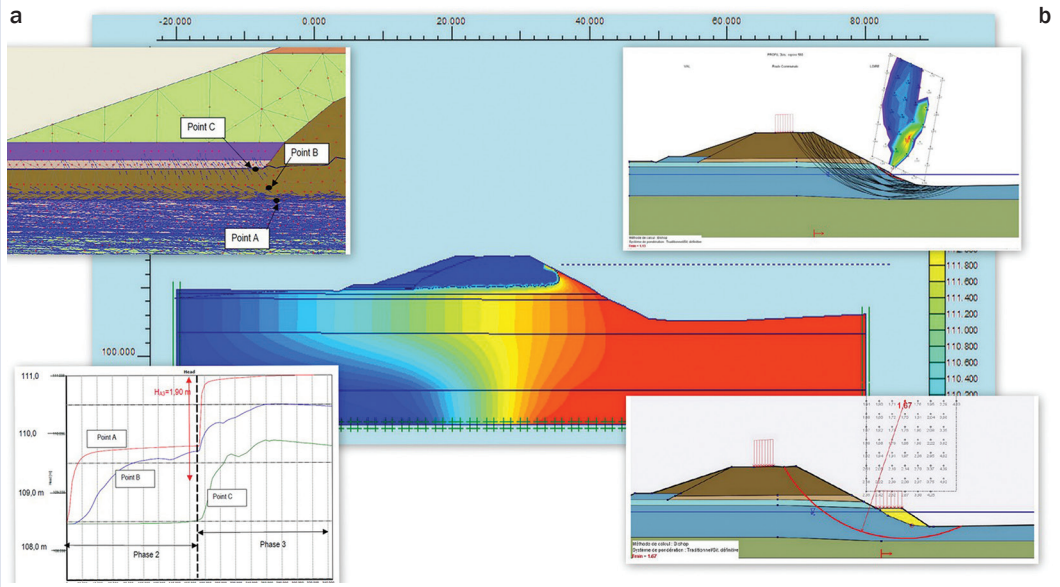

Figure 8.42 ***Example of a levee FEM used in transient state for appreciate saturation state (in the middle), pore pressures, active groundwater head and exit gradients during and after a 48 hours water elevation (flood event) (a) and slopes stability before and after reinforcement (b)***

8.3.2 Wave induced pore pressures

The specific effect of waves on internal pore water pressure lies in the fact that the hydraulic action varies quickly with time. The pore pressure response depends on the phreatic level imposed (Section 8.3.1), but also on two strain components of the soil under wave loading: elastic volume strain of soils skeleton and/or pore water and plastic volume strain of the soil skeleton (irreversible variation of the pore volume).

8.3.2.1 Pore pressure due to elastic strain

Variation of pore pressure results in effective stress variation and consequently variation of the pore volume due to the compression of the soil skeleton. This phenomenon produces water flow in and out at

a rate governed by the soil permeability. When the rate of pressure changes along the external boundary, the flow rate becomes too quick in relation to the soil permeability, so the soil is no longer fully drained and the pore water pressure may progressively increase. This mechanism is characterised by a phase lag in the propagation of the cyclic phenomenon. A simplified analysis (assuming the incompressibility of water) may be performed based on the determination of an elastic timescale T_{el} (s) defined as follows (CIRIA; CUR; CETMEF, 2007):

$$T_{el} = \pi L^2 \frac{\gamma_w m_{ve}}{k} \tag{8.80}$$

where:

L = is a distance of penetration through the soil (m)
k = the soil permeability (m/s^2)
m_{ve} = the elastic coefficient of volume change of the soil (-)

When considering the period of loading T (s), the ratio $T_{el}/T << 1$ corresponds to a negligible elastic storage and the load may be considered as quasi-stationary. However, if $T_{el}/T >> 1$, the elastic storage is important and the generated pore pressure increase has to be taken into account in the stability analyses.

8.3.2.2 Pore pressure due to plastic strain

Pore volume change may also be caused by dilatancy and contraction. Cyclic shear loading in loose soils may have a tendency to contract but in cases where the soil permeability is too small in relation to the period of external loading, the densification of the soil may be partly prevented by the pore fluid. The result of this phenomenon is a generation of excess pore water pressure within the soil, which increases at each load cycle (each wave). The characteristic timescale, T_{pl}, may be defined as follows (CIRIA; CUR; CETMEF, 2007):

$$T_{pl} = \frac{L^2}{N} \frac{\gamma_b m_{ve}}{k} \tag{8.81}$$

where:

L = the length over which the wave induced shear stress is important (m)
γ_b = the bulk unit weight of the dry soil (kN/m^3)
k = the soil permeability (m/s^2)

For example, the number of stress cycles for annulment of effective stress N may be determined in laboratory tests as a function of shear stress ratio and density index.

For practical application, 1D models are available (Ishihara and Yamazaki, 1984). The results of these models have to be taken into account in stability analyses.

An example of wave induced pore pressures that result in cyclic shear stresses in the soil is given in Box 8.10.

Box 8.10 *Wave-induced cyclic shear stresses (from Ishihara and Yamazaki, 1984)*

The differential loading on the floor caused by the pressure wave induces a cyclic shear stress loading in the underlying soil. These stresses may cause significant deformations and even failures due to liquefaction phenomenon. The most common method for wave-induced liquefaction assessment was developed by Ishihara and Yamazaki (1984) and may be summarised as follows.

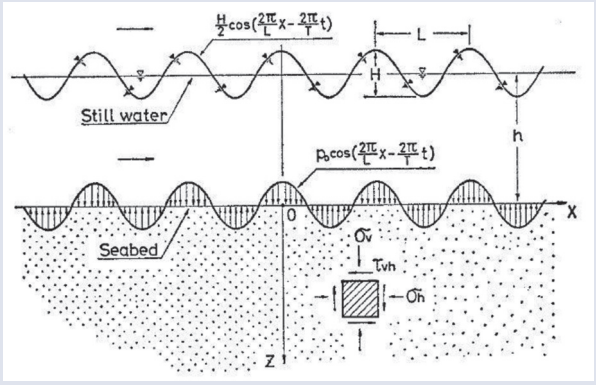

Figure 8.43 *Definition of notations for wave-induced shear stress (from Ishihara and Yamazaki, 1984)*

Water waves propagating are considered to consist of an infinite number of wave trains having a constant amplitude and wavelength. Passage of such waves creates harmonic pressure waves on the seafloor. The stresses induced in the seabed are therefore analysed applying a sinusoidal changing load on the infinite horizontal surface. It can be shown that the cyclic stress ratio equals to:

$$\frac{\tau_{vh}}{\sigma_{v\prime}} = \left(\frac{\tau_{vh}}{\sigma_{v\prime}}\right)_{z=0} e^{-2\pi z/L} \tag{8.82}$$

where:

τ_{vh} = amplitude of the shear stress (kPa)

σ_v' = vertical effective overburden pressure (kPa)

z = depth into the soil from the mud line (m)

The cyclic stress ratio at the mud line is expressed by:

$$\left(\frac{\tau_{vh}}{\sigma_{v\prime}}\right)_{z=0} = \frac{\pi\gamma_w H_0}{\gamma' L_0 \sin h\left(\frac{2\pi h}{L}\right)\sqrt{\tan h\left(\frac{2\pi h}{L}\right)\left(1+\frac{4\pi h/L}{\sin h(4\pi h/L)}\right)}} \leq \frac{\pi}{7}\frac{\gamma_w}{\gamma'}\frac{\sin h\left(\frac{2\pi h}{L}\right)}{\cos h^2\left(\frac{2\pi h}{L}\right)} \tag{8.83}$$

where:

γ' = submerged unit weight (kN/m^3)

h = water depth (m)

H_0 = wave height in deep water condition (m)

L_0 = wavelength in deep water condition (m)

L = wavelength of the wave train where the water depth is *h* (m)

Note that equation 8.83 constrains the wave steepness to a value below a critical value as expressed by the inequality at the end of the equation.

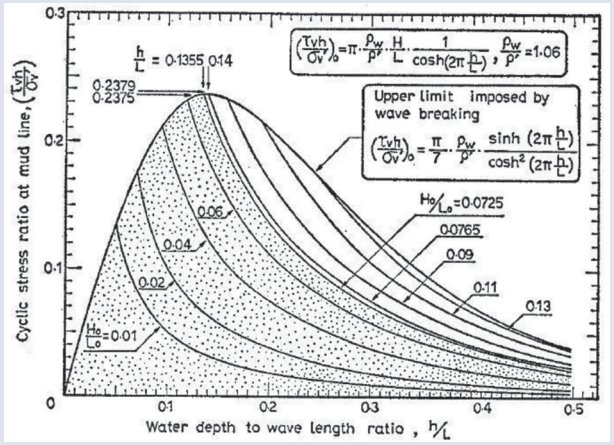

Figure 8.44 *Estimation of cyclic stress ratio at mud line (from Ishihara and Yamazaki, 1984)*

The cyclic stress ratio calculated is then compared to the cyclic stress ratio causing liquefaction and cyclic mobility in which the continuous rotation of principal stress directions is considered. The procedure is described in detail in Ishihara and Yamazaki (1984).

8.3.3 Consolidation induced pore pressure

It has been shown (Skempton and Bjerrum, 1957, and Henkel, 1959) that a relationship may be established between spherical and deviatoric consolidation stress increments according to Equation 8.84:

$$\triangle u\,(t) = B\,(\triangle \sigma_{oct} + A \triangle \tau_{oct})\,[1 - U\,(t)] \tag{8.84}$$

where B and A are pore pressure parameters (Section 7.8.3) depending on the degree of saturation and the compressibility of the soil skeleton, U(t) is the consolidation ratio at time t (Section 8.7.2). For normally saturated consolidated soils B is generally taken equal to one.

Except when the factor of safety of the slope is low, the part of the pore water pressure induced by shear deformations (coefficient A) is negligible and the horizontal earth pressure may be taken equal to the at-rest one K_0 (-). Under these assumptions, it is possible to express the pore pressure ratio r_u in terms of the incremental vertical load:

$$r_u\,(t) = \frac{\triangle u\,(t)}{\triangle \sigma_v} = \frac{1 + 2K_0}{3}\,[1 - U\,(t)] \tag{8.85}$$

This formula may be useful for determination of pore water pressure implementation in slope stability analyses (Section 8.6) during construction phases.

As illustrated in Figure 8.45, when a load is applied on a saturated low permeability soil, the pressure Δσ (total stress) is firstly supported by the soils interstitial water that is uncompressible. The excess pore pressure Δu becomes quasi instantaneously equal to load pressure. If that load is maintained constant, a time dependant compression phase begins known as the primary consolidation phase. It corresponds to a period where water goes out of the soil and excess pore pressure Δu decreases.

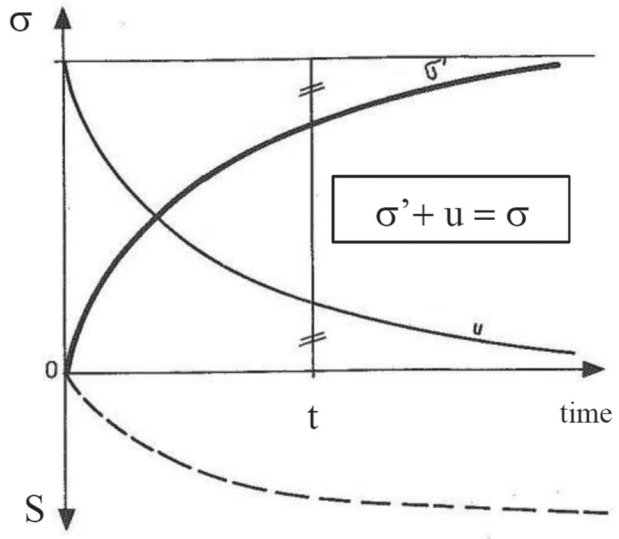

Notes

σ = total stress, σ' = effective stress (bold line), u = pore pressure, s = settlement (dotted line)

Figure 8.45 ***Soils primary consolidation phase. Settlement and excess pore pressure evolution (after Philipponnat and Hubert, 2003)***

8.4 EXTERNAL EROSION

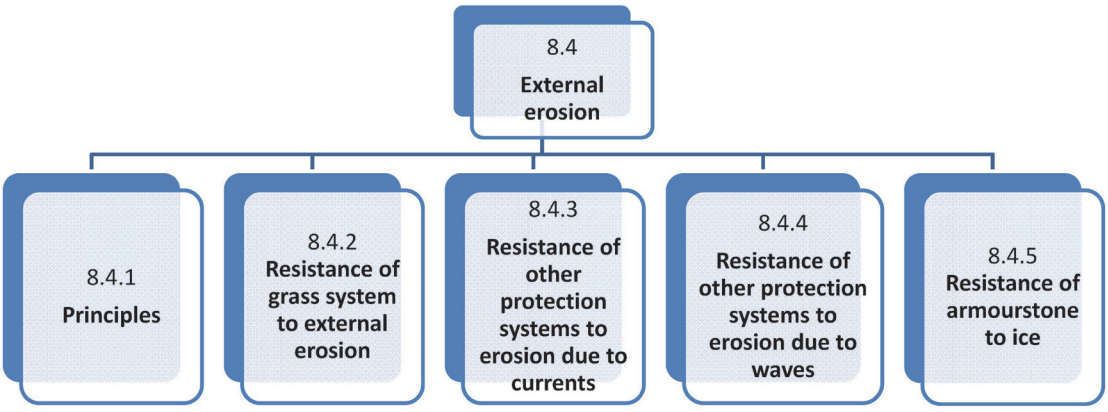

8.4.1 Principles

In addition to the hydrostatic and hydrodynamic forces that act on the levee structure, the movement of water over the surface of the levee has to be considered. Hydraulic interactions associated with wave and current action on levees have been previously described in Section 8.2. It is necessary to consider the influence of these interactions on the levee to ensure its integrity and long-term stability when exposed to various hydraulic loadings. This section describes methods for assessing the effect of currents and waves on the levee surface, and provides limited guidance for the design of measures to protect against those effects.

8.4.1.1 Currents

The importance of considering currents during levee design derives from the potential that exists for moving water to mobilise material on the levee surface or in locations that would impact levee stability. This section describes currents that should be considered during analysis or design of levees.

Currents in the main channel

Flow in the main channel interacts with and shapes the channel boundary. The continual change in channel boundary identified in the morphologic assessment described in Chapter 7 may indicate that protective measures are needed to prevent damage to the levee. Such protective measures may involve armouring the channel bank or installing features that redirect the current direction. Levee planning and design has to account for future changes in the channel to ensure acceptable system performance. Sediment transport studies done in site characterisation (Chapter 7) provide indication of long-term trends in channel erosion and deposition. So, it is necessary to expand those estimates to locations where there is potential threat to the levee. Specifically, local velocity at the exterior bank of bends and resulting scour depth has to be determined so that protection schemes can be designed. As described in Section 7.3, velocity distributions vary with cross-section shape and alignment. So, it is necessary to apply correction factors to mean channel velocity or to develop multi-dimensional numeric models to determine the near bank velocity in bends.

Currents on the levee surface

As flow moves across and along the surface of a levee it imposes not only static and dynamic forces that the levee has to resist, but also a drag on levee surface materials as it moves across the levee. The drag, caused by boundary shear stress (Section 7.3), can mobilise materials leading to erosion and eventual failure of the levee embankment. Currents induced by the stream flow during various levels of flood, including the maximum anticipated event, impose boundary shear stresses at different magnitudes. So, it is necessary to evaluate the shear stresses at various flow levels.

In steady flow, the current-induced shear stress acting on the bed may be calculated using Equation 7.45.

The first parameter to estimate is the cross-sectional averaged velocity for the portion of cross-section near the levee. This velocity is often available from numerical models developed during site characterisation (Section 7.3), or can be calculated from the model results. The Manning-Strickler or Chézy equations (Section 7.3.6.1) provide a simplified method for calculating the average cross-section velocity. The cross-section velocity gives some indication of velocities that may exist near the levee surface. The shear stress computed with average velocity acts at the stream bed. Evaluation of shear stress at locations other than at the bed requires adjustment in the values of average channel velocity. There are correction factors that can be used to adjust the mean velocity to better reflect local flow conditions (Section 8.4.1.2). An alternative approach is to use multi-dimensional models in local areas to calculate velocity magnitude and direction where excessive velocities are anticipated.

8.4.1.2 Basis of critical concepts for erosion

Analysis of the hydraulic stability of armourstone and sediments generally concerns individual stones and particles. By comparison, geotechnical stability analysis discussed elsewhere in Section 8.6 always concerns material in bulk. Movements of stones and sediment due to current and/or wave action are observed as 'displacements' of individual particles or as 'scour' holes when the bed consists of sand, small stones or gravel. This shows that the relative magnitudes of the movements of coarse and fine particles are of different order. Displacements of individual stones are of the order of several times the stone diameter, while scour depths/lengths in sediments are at least several orders of magnitude of the grain size.

Conventional design methods aim to prevent the initial movement of coarse and fine particles by defining 'threshold' conditions. These conditions are expressed in terms of critical values for shear stress, velocity, wave height, or discharge.

There is usually considerable experimental scatter around the point of initial movement, eg the critical shear stress parameter, ψ_{cr}, or the critical velocity, V_{cr}. The designer can take advantage of a probabilistic approach as described in CIRIA; CUR; CETMEF (2007) to account for uncertainties. In addition to the uncertainty in resistance or strength, certain damage may be accepted. This implies that some movement is allowed, but only up to predefined levels of displacement or scour. These threshold levels may be defined, for example, as the:

- maximum amount of displaced stones or concrete units (per unit time and area)
- critical scour depth
- maximum transport of material.

The concept of allowing some damage below a certain limit is the most common concept for the design of protective measures consisting of armourstone or structures armoured with concrete armour units.

The exceedance of the threshold conditions previously highlighted, leads to instability of loose materials. Waves, current velocities and differences in water levels, all acting through shear stresses, can be regarded as the principal hydraulic loadings. The principal stabilising or resistance forces are gravity and cohesion. Cohesion is only relevant to sediments in the clay and silt range ($D < 5\ \mu m$ and $D < 50\ \mu m$, respectively) or fine sand ($D < 250\ \mu m$) with appreciable silt content. In this regard it is convenient to classify material of erodible layers or subsoil as either:

- cohesive sediments — **silt**, $D < 50$ mm and **clay**, $D < 5\ \mu m$
- non-cohesive, fine sediment — **sand**, $50\ \mu m < D < 2$ mm
- non-cohesive, coarse sediment — **gravel**, $D > 2$ mm and **stone**, $D > 50$ mm

Box 8.11 contains information relating sediment material classification and material classification used in geotechnical engineering.

Box 8.11 Sediment classification

Sediment material characteristics relative to erosion and sediment mobility are defined differently than are soil material properties used in geotechnical soil classifications.

Sediment particle sizes for sediment mobility as stated in this manual refer to European designations. Sediment size classes in the US differ and can be found in Vanoni (1975), (Lane *et al*, 1947).

The structural response of particles can be practically described with one or more of the following hydraulic loading variables and parameters:

- specific discharge, q, across a structure ($m^3/s/m$)
- shear stress, τ (N/m^2), or non-dimensional, Shields parameter, ψ (-), or shear velocity, u^* (m/s)
- velocity, either depth-averaged, V, or local, u (m/s)
- water level, h, or head H or H–h (m).

The most prominent strength or resistance variables with regard to stability are:

- particle size, D (m) or nominal diameter, D_n (m) or mass, M (kg)
- relative buoyant density, $\Delta = (\rho_s - \rho_w)/\rho_w$, where ρ_s is the apparent mass density of the solid particle (kg/m^3) and ρ_w is the mass density of water (kg/m^3)
- mitigating factors that may bind individual particles together include inter particle cohesion or density of any grass root mass (kg/m^3).

Two basic concepts or methods exist to evaluate the hydraulic stability of a rock structure:

- the critical shear concept
- the critical velocity concept.

In practice, from these two methods other criteria can be derived in terms of mobility or stability numbers, Table 8.9.

Table 8.9 Stability concepts and the relation with structure types and stability formulae for design

Stability concept	Stability parameter	Structure type
Shear stress	ψ_{cr} (Shields parameter)	Bed and bank protection Spillways and outlets
Velocity	$U^2/(2g\Delta D)$ (Izbash number)	Bed and bank protection Near-bed structures Toe and scour protection
Discharge	$q/(g(\Delta D)^3)^{1/2}$	Sills Weirs (eg levee embankment)
Wave height	$H/(\Delta D)$ (stability number)	Rock armour layers Concrete armour layers Toe and scour protection
Hydraulic head	$H/(\Delta D)$	Sills Weirs (eg levee embankment)

The use of a velocity stability concept, although it is the simplest and most straightforward, may become difficult when a representative velocity has to be determined. It is often a local value that is required and not the depth-averaged value.

The bed shear stress concept incorporates the basic grain mechanics and so is most generally applicable. However, the vertical velocity profile has to be known first, and subsequently a reliable transfer should be performed from this velocity profile into shear stress. Some approaches are not purely based on grain mechanics, but rather on model tests and dimensional analysis.

In the cases of movement and erosion resistance of sediments under current attack, the method of critical shear stress and the method of permissible or critical velocity are most frequently used.

Critical velocity concept

According to the permissible velocity method, initiation of motion of material occurs when the critical or permissible velocity is exceeded. Selection of the proper velocity is essential to guarantee reliable application of these criteria. Usually, the depth-averaged flow velocity, V (m/s), is used and various corrective factors are added to adjust for local velocity conditions. Table 8.10 presents typical critical velocities, V (m/s) for non-cohesive materials where water depth, h, is 1.0 m. Critical velocities for water depths ranging from h = 0.3 to 3.0 m can be obtained by multiplying the values in Table 8.10 by the factors, K_1, given in Table 8.11.

To prevent damage due to erosion, calculated flow velocities have to be less than those given by this method. In addition to the ultimate hydraulic loading case, velocities for multiple flow conditions should be checked to verify that critical thresholds are not exceeded.

Table 8.10 Critical depth-averaged velocities, V, for loose granular material in water depth of 1 m

Material	Sieve size, *D* (mm)	Critical velocity *V* (m/s) for *h* = 1 m
Very coarse gravel	200–150	3.9–3.3
	150–100	3.3–2.7
Coarse gravel	100–75	2.7–2.4
	75–50	2.4–1.9
	50–25	1.9–1.4
	25–15	1.4–1.2
	15–10	1.2–1.0
	10–5	1.0–0.8
Gravel	5–2	0.8–0.6
Coarse sand	2–0.5	0.6–0.4
Fine sand	0.5–0.1	0.4–0.25
Very fine sand	0.1–0.02	0.25–0.20
Silt	0.02–0.002	0.20–0.15

Table 8.11 Velocity correction factors, K_i, for water depths ($h \neq 1.0$ m) in the range of 0.3 m < h < 3 m

Depth, *h* (m)	0.3	0.6	1.0	1.5	2.0	2.5	3.0
Ki (-)	0.8	0.9	1.0	1.1	1.15	1.2	1.25

Critical shear concept

The critical shear concept for unidirectional flow is based on the Shields criterion (Shields, 1936). The criterion expresses the critical value of the ratio of the de-stabilising fluid forces to the stabilising forces that act on a particle. The forces that tend to move the particle are related to the maximum shear stress exerted on the bed by the moving fluid, so the stabilising forces are related to the submerged weight of the particle. When the ratio of the two forces, represented by the Shields parameter, ψ, exceeds a critical value, ψ_{cr}, movement initiates. The Shields criterion for steady uniform flow is expressed in Equations 8.86 and 8.87. The Shields curve is given in Figure 8.46.

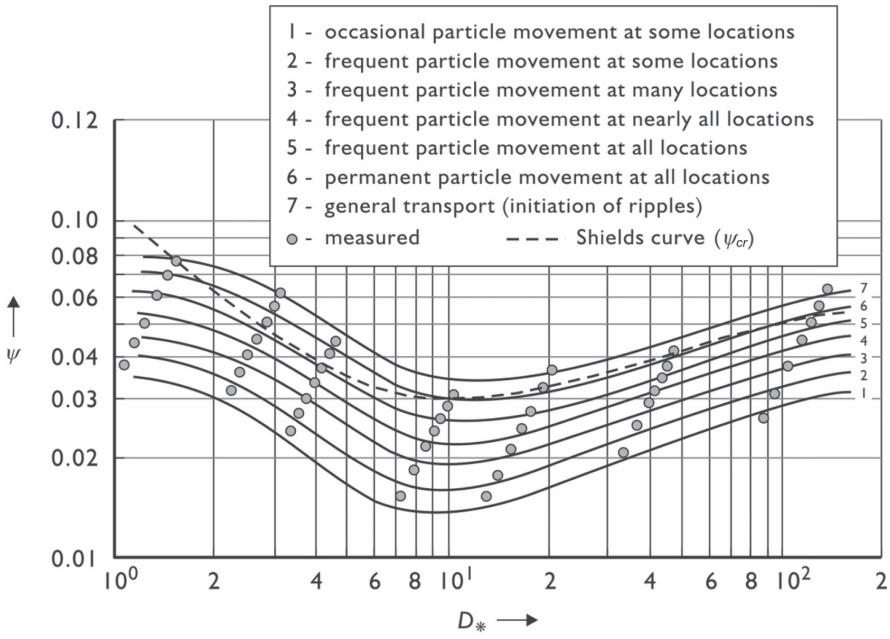

Figure 8.46 The modified Shields diagram for steady flow (CIRIA; CUR; CETMEF, 2007)

Equation 8.86 gives the Shields parameter, ψ_{Cr}, as a function of the critical value of the shear velocity, u^*_{cr} (m/s):

$$\psi_{cr} = \frac{\tau_{cr}}{(\rho_s - \rho_w)\, g\, D} = \frac{u^2_{*cr}}{\triangle g D} = f\,(Re) \tag{8.86}$$

Equation 8.87 gives the Shields parameter as a function of the depth-averaged critical velocity, V_{cr} (m/s):

$$\psi_{cr} = \frac{1}{C^2}\frac{V_{cr}}{\triangle D} \tag{8.87}$$

where:

τ_{cr} = $\rho_w g V_{Cr}/C^2$, critical value of bed shear stress induced by the fluid at which particles first begin to move (N/m^2)
ρ_s = apparent mass density of the particles (kg/m^3)
ρ_w = mass density of water (kg/m^3)
D = sieve size of material (m). The median size, D_{50}, is often as a characteristic value
D^* = $D_{50}(g\Delta/\nu^2)^{1/3}$, non-dimensional grain size (-)
u^*_{cr} = $(\tau/\rho_w)^{1/2}$, critical value of the shear velocity (m/s)
ν = kinematic fluid viscosity (m^2/s)
C = Chézy friction coefficient (m$^{1/2}$/s)
Re^* = u^*D/ν, Reynolds number, based on shear velocity (-)
Δ = relative buoyant density of the particles (-)

Following are approximate values of ψ , associated with state of particle mobility as indicated:

- ψ = 0.03 for initiation of movement
- ψ = 0.05 for limited movement
- ψ = 0.10 for general movement/transport.

For fluvial conditions, the average shear stress on the channel boundary across the entire cross-section of the river is calculated with Equation 8.88:

$$\tau = \gamma\, K_b\, R\, S_f \tag{8.88}$$

where:

K_b = bend coefficient (-)
γ = unit weight of water (kN/m^3)
R = hydraulic radius of river (area divided by wetted perimeter) (m)
S_f = slope of energy grade line (m/m)

Figure 8.47 presents a plot of critical shear stress as a function of mean grain size of particles. This diagram shows that the most erodible material is fine sands with a mean grain size range of 0.1 to 0.5 mm. It also shows that for fine grain size material with cohesion (silt, clay) erosion threshold does not correlate with mean particle size.

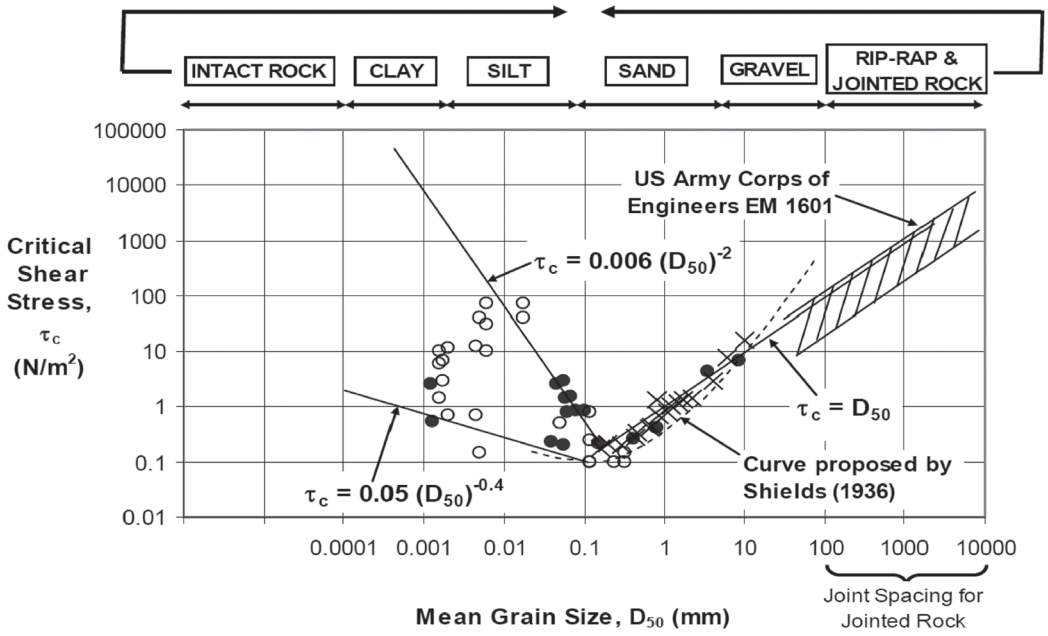

Figure 8.47 Critical shear stress vs. particle grain size (Briaud et al, 2001)

Both critical velocity and critical shear methods may use the depth-average velocity. This approach can be expanded to adjust for localised conditions if appropriate factors are included. These factors may be in the form of load amplification factors or strength reduction factors as shown in Table 8.12. A summary of equations used to calculate these factors is provided in Table 8.13. Further details of adjustment factors can be found in various literature eg CIRIA; CUR; CETMEF (2007).

Table 8.12 Amplification and reduction factors to adjust depth-averaged velocity

Loading	Factor type	Factor	Multiply with:
Additional waves	Amplification	k_w (≥ 1, limited to $\tau_w < 2.5\ \tau_c$)	u^2, ψ, τ, q^2, H
Excessive turbulence	Amplification	k_t (≥ 1)	u, $\psi^{1/2}$, $\sqrt{\psi}$, $\tau^{1/2}$ q, $H^{1/2}$
Depth or velocity profile (logarithmic distribution)	Amplification	Λ_{hf}	V
Slope	Reduction	k_{si} (≥ 1)	V

Table 8.13 Amplification and reduction factor formulae

Factor	Equation	Parameters
Wave amplification	$k_w = 1 + \frac{1}{2} f_w \frac{C^2}{2g} \left(\frac{u_0}{V}\right)^2$	f_w is the rough bed friction factor • f_w = 0.3 for $a_0/z_0 \leq 19.1$ • $f_w = 1.39(a_0/z_0)^{-0.52}$ for $a_0 > 19.1 z_0$. C is the Chézy coefficient u_0 is peak orbital velocity near the bed (m/s^2)
Turbulence	$k_t = \frac{1+3r}{1.3}$	r is the turbulence factor as described in Section 7.3.7.5
Depth or velocity profile	$\Lambda_h = \frac{1}{f_c} = \frac{C^2}{2g} = \frac{18^2}{2g} \log^2\left(\frac{12h}{k_s}\right)$	k_s is the bed roughness: • $k_s = 2(D_{90})$ or $\approx 4(D_{50})$ for sediments and gravel • k_s for armourstone depends on the situation • f_c is friction factor for currents.
Slope	$k_{sl} = \frac{\cos\psi \sin\beta + \sqrt{\cos^2\beta \tan^2\phi - \sin^2\psi \sin^2\beta}}{\tan\phi}$	ψ = angle made by flow to upslope direction (deg) β = angle of the sloping embankment with the horizontal (deg) ϕ = angle of repose of material

Combining the adjustment factors with the Shields parameter yields:

$$\frac{V^2}{2g} = k_{sl}\, k_t^{-2}\, k_w^{-1}\, \Lambda_h\, \psi_{cr} \triangle D \tag{8.89}$$

In Equation 8.89 ψ_{cr} can be used as a damage parameter with:

- $0.03 < \psi_{cr} < 0.035$ representing no damage or movement
- $0.05 < \psi_{cr} < 0.055$ representing some movement.

A variety of stability formulae can be derived from these concepts for special applications such as riverbanks. An example of stability criterion for stones is given in Box 8.12.

Box 8.12 Velocity-type stability criterion for stones on a sill

The well-known example of a velocity-type stability criterion was presented by Izbash and Khaldre (1970). Their empirically-derived formulae for exposed and embedded stones *on a sill* are given by:

Exposed stones:

$$\frac{v_b^2}{2g} = 0.7 \triangle D_{50} \tag{8.90}$$

Embedded stones:

$$\frac{v_b^2}{2g} = 1.4 \triangle D_{50} \tag{8.91}$$

where D_{50} is the median sieve size (m).

Range of validity: these equations, as developed by Izbash and Khaldre (1970), are valid for relative water depths, h/D, in the range of h/D = 5 to 10.

Note that Izbash and Khaldre (1970) defined v_b as the critical velocity for stone movement (m/s), which can be interpreted as the velocity near the stones and not as the depth-averaged flow velocity, V (m/s).

Cohesive soils

In the hydraulic resistance (erodibility) of cohesive sediments, the physical-chemical interaction between the particles plays a significant role. So, the determination of critical velocities relies heavily on empirical

data based on various experiments and *in situ* observations. The existing knowledge of the correlation of the Shields factor and/or the critical flow velocity U_{cr} with mechanical properties of the soil (silt content, plasticity index, shear stress etc) is still not sufficient to allow for a general approach. Cohesive materials such as clay generally have higher resistance to erosion than non-cohesive material. As an indication, the following values of critical velocities may be used:

- fairly compacted clay (e = 0.50) U_{cr} = 0.8 m/s
- stiff clay (e = 0.25) U_{cr} = 1.5 m/s.

While it is accepted that there is uncertainty in predicting the erosion of a soil because of the range of factors that can affect the state and the erodibility of a soil, as well as uncertainty in the performance of protection layers such as grass cover, methods are available to estimate performance as follows.

More detailed discussion of soil erodibility can be found in Section 8.10 as part of the discussion of breach processes.

8.4.2 Resistance of grass systems to external erosion

The potential for slopes to erode and scour can be determined by calculating current velocities and boundary shear stresses as outlined in Sections 8.4.1.1 and 8.4.1.2 and comparing these values to allowable limits for the materials. Soil movement (erosion) can be expected if calculated values exceed allowable limits for the embankment material. Once it has been determined that erosion and/or scour is a concern for levee safety, it is necessary to consider measures that can reduce or mitigate their resulting effects. Of these protection using grass systems is always worth considering as an option.

While there has been a lot of research into the effects of vegetation and grass on flow within channels, the degree of guidance available on the performance of grass cover for levees during overflow or wave overtopping conditions is more limited. Guidance divides into grass performance under overflow conditions (often misquoted as overtopping) and performance under wave overtopping conditions. A review of current research and guidance for both can be found in Morris *et al* (2012a).

Research and guidance often originates back to three sources:

- in the USA research by USDA at Stillwater, Oklahoma
- in the UK publications from CIRIA
- in the Netherlands ongoing research into grass performance on dikes during wave overtopping.

There are notable differences in approaches from each of these sources (Temple *et al*, 1987, Temple, 1997, Temple and Hanson, 1994, and Hanson and Temple, 2002). US guidance looks at the combination grass type and soil resistance to erosion, while UK guidance looks only at grass condition. Dutch guidance focuses upon wave overtopping, but applied to the performance of Dutch dikes, which are normally constructed from a grass covered clay layer sitting over a sand core. Performance analysis for the outer layer should be generically applicable though.

8.4.2.1 Grass resistance under overflow conditions

Existing guidance relates back to two sources:

1 In Europe, guidance often relates or refers to work by CIRIA during the 1970/1980s, drawing from Whitehead (1976) or Hewlett *et al* (1987).

2 In the US, guidance typically builds from Temple *et al* (1987).

CIRIA guidance provides design curves, which suggest acceptable limits for combinations of flow velocity and duration. The US approach estimates shear stress at the soil surface (as a function of vegetation type and impact) followed by acceptability in relation to the soil erodibility.

Figure 8.48 may be used as a first guide in designing the appropriate measure to protect embankments. Detailed calculations should follow use of Figure 8.49 to confirm adequate performance of the selected measure under site specific conditions. If Figure 8.48 indicates that more substantial revetment systems (such as mats and concrete blocks) are required, the more detailed guidance in Sections 8.4.4 should be followed. Where proprietary measures are to be used, manufacturer guidelines should be followed. Due to the inexact nature of defining erosion and scour and significant variation in various design formulae, it is advisable to use several methods to calculate a range of possible requirements.

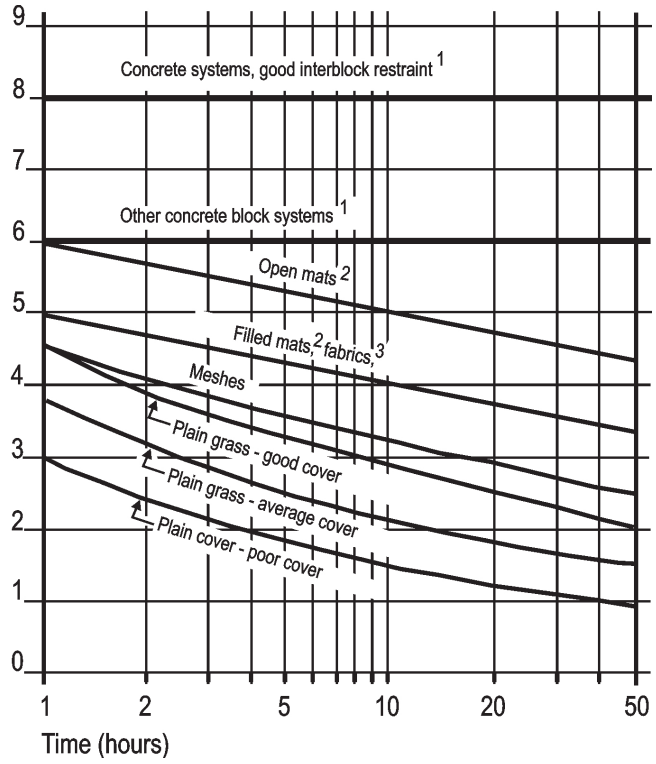

Notes

1 Minimum superficial mass 135 kg/m³.

2 Minimum nominal thickness 20mm.

3 Installed within 20 mm of soil surface, or in conjunction with a surface mesh.

4 These graphs should only be used for erosion resistance to unidirectional flow. Values are based on available experience and information contained in Hewlett *et al* (1987).

5 All reinforced grass values assume well-established, good grass cover.

6 Other criteria (such as short-term protection, ease of installation and management, and susceptibility to vandalism) have to be considered in choice of reinforcement.

Figure 8.48 Recommended limiting design values for erosion resistance of select erosion counter measures (Hewlett et al, 1987)

The design curves in Figure 8.48 appear to contain a factor of safety as compared to the performance curves presented in Whitehead *et al* (1976) (Figure 8.49). So, while these may be appropriate for use in design, the earlier curves (shown as dashed lines in Figure 8.49) should be used when undertaking a levee performance assessment.

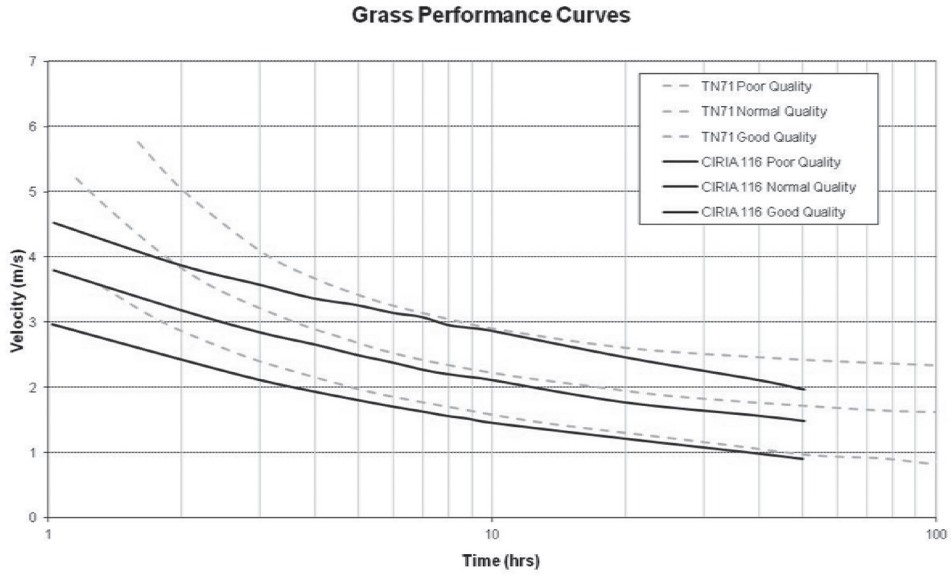

Figure 8.49 Comparison between R116 grass performance curves (Hewlett et al, 1987) and the original field test data (Whitehead et al, 1976)

8.4.2.2 Grass resistance under wave overtopping conditions

Early approaches to assessing wave overtopping resistance by grass cover used the same CIRIA performance curves but with an averaged rate of overflow arising from the periodic wave overtopping. This ignored the surges in flow that arise from wave action and might be assumed to under-predict the impact of wave action.

Recent (ie post 2000) and ongoing Dutch studies using a wave overtopping simulator (Figure 8.50) are allowing guidance on performance under wave overtopping conditions to be developed. Dutch dikes typically comprise a grass covered clay soil layer, covering an inner sand core (Figure 8.51). The analysis of grass performance relates to the grass cover, turf and top layer only. The top layer may be up to 0.2 m thick, including the turf that may be 0.05 m thick.

Figure 8.50 Recent Dutch studies into grass performance under wave overtopping, using the wave overtopping simulator (Morris et al, 2012a)

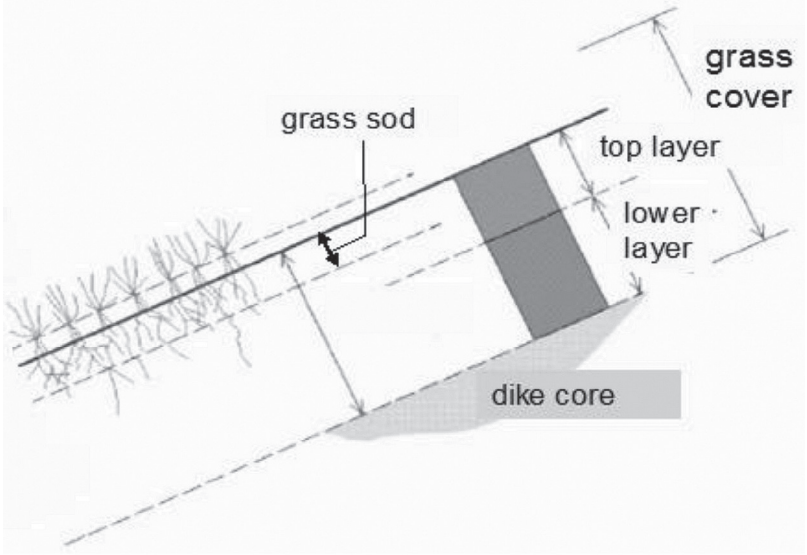

Figure 8.51 Recent Dutch studies into grass performance under wave overtopping, using the wave overtopping simulator (from TAW, 1997 and Rijkswaterstaat)

Three conditions of grass strength are described, being closed turf, open turf and fragmented turf. Damaged patches of less than 0.15 m square are not considered to significantly affect the performance of closed or open turf under wave overtopping. Fragmented turf is considered to offer little protection against erosion.

Four hydraulic load zones are identified (Figure 8.52) and failure mechanisms considered for zones 2 and 4.

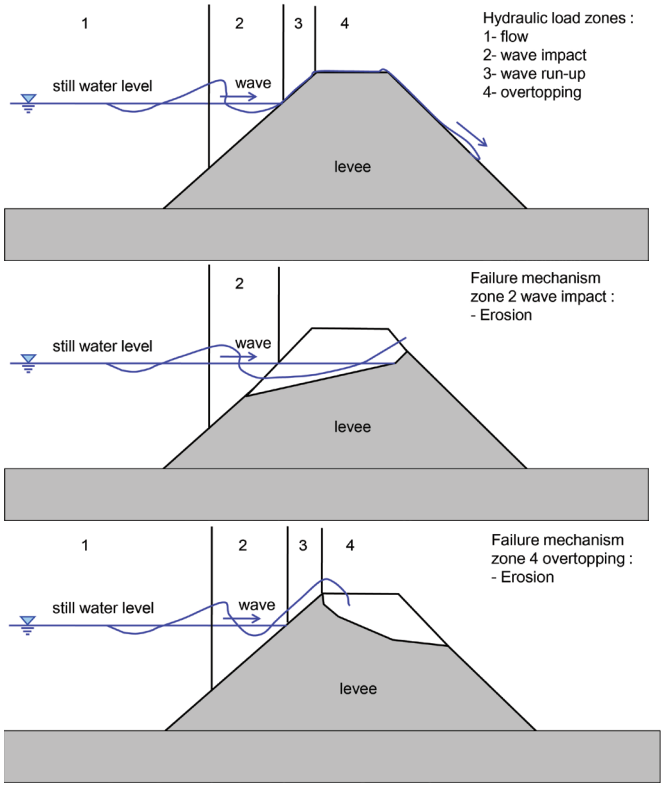

Note
The SBW is the overall research project of the Rijkswaterstaat (Morris *et al*, 2012a). Within the project, destructive testing has been undertaken using the Wave Overtopping Simulator on real dikes to give preliminary conclusions on strength of grassed inner slopes of dikes against wave overtopping.

Figure 8.52 Hydraulic load zones (1 to 4) and failure mechanisms addressed in the SBW research program (Morris et al, 2012a)

The failure model suggested for erosion in the wave impact zone (2) compares the wave impact load time t_i (hour) with the wave impact resisting time t_r (hour) for different wave height H_s (m) as given in Figure 8.53. The turf is sufficiently strong if $t_r > t_i$. The model does allow some minor damage to occur to the turf.

Model limitations concerning the slope angle are 1H:2.5V (or less steep) for $H_s \geq 0.5$ m and 1V:1.5H (or less steep) for $H_s < 0.5$ m. For a slope angle gentler than 1V:4H the resisting time t_r will increase, however, the model has no prediction capability on how much t_r will increase.

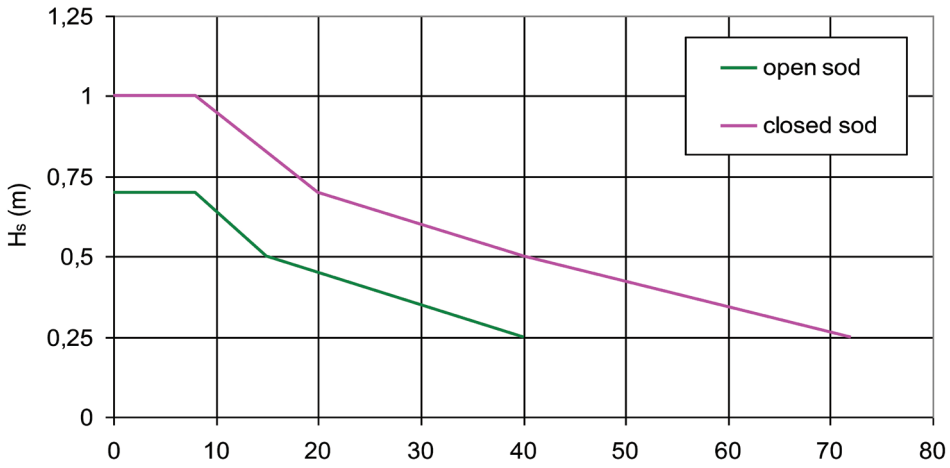

Figure 8.53 Wave impact resisting time t_r (hour) for different wave height H_s (m) and turf quality (open or closed) (Morris et al, 2012a)

No research within the SBW framework (Morris *et al*, 2012a) was aimed at erosion in the wave run-up zone (zone 3 in Figure 8.52), however, if the turf present in the wave impact zone (zone 2 in Figure 8.52) is sufficient, the turf in the run-up zone will also be sufficient. Pressure gradients in the turf and subsoil, causing erosion, are significantly larger in the wave impact zone than in the wave run-up zone. Grass cover will fail in the wave impact zone before it fails in the wave run-up zone if the grass cover is of equal quality in both zones.

The hydraulic load for erosion of the grass cover in the wave overtopping zone (crest and landward slope of the dike, zone 4 in Figure 8.52) consists of the overtopping wave volumes. Each of the overtopping volumes can be characterised by the maximum depth averaged flow velocity and maximum water layer thickness. As shown in Figure 8.54, each overtopping wave volume will result in a triangular shaped flow velocity development against time.

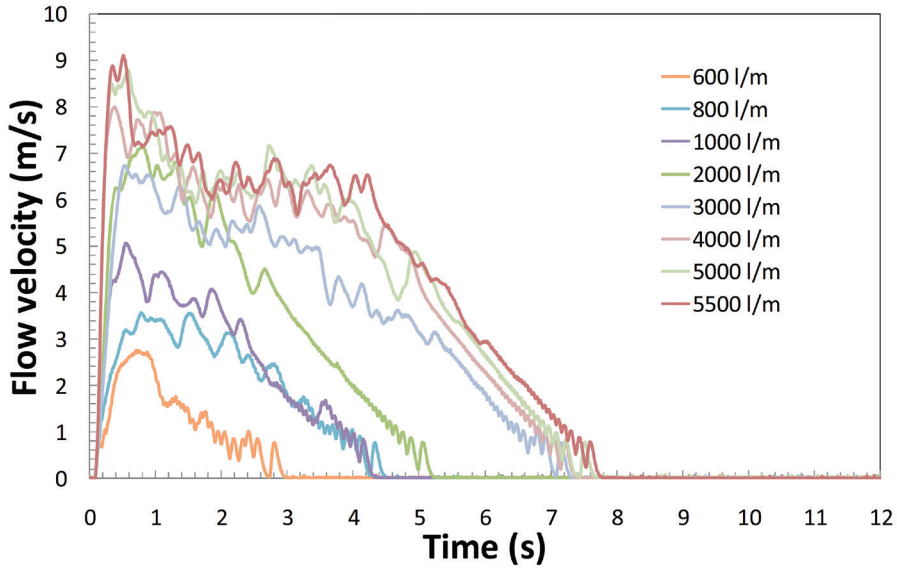

Figure 8.54 ***Velocity (m/s) against time (s) for different wave overtopping volumes (600–5500 l/m) measured at one wave-overtopping test sloped 1V:4.5H (van der Meer et al, 2010)***

The maximum depth averaged velocity U (m/s) in a wave overtopping event with a volume, V (m^3/m), can be estimated by the empirical formula $U = 5V^{0.34}$ (van der Meer *et al*, 2010). For example, a wave overtopping volume of 1000 l/m results in a maximum depth averaged velocity of 5 m/s and an overtopping volume of 5500 l/m in 8.9 m/s. Measurements at a relatively steep (1V:2.3H) and long slope showed an increase in velocity as the volume progressed down slope. Measurements at a relatively mild slope (1V:5H) showed a decreasing velocity. However, until further research gives conclusive insight in the development of the velocity depending on slope angle and slope length, the above estimate of the correlation between V and U is used for slopes of 1V:2.3H and more gentle. For steeper slopes the model presented in the following paragraphs is advised. Research to determine the velocity as a function of slope angle and slope length is in progress.

For steeper slopes, the distribution of wave overtopping volumes during a storm can be calculated using the formulae in Pullen *et al* (2007). Parameters involved are the storm duration and the average wave period, which determine the number of waves reaching the dike. The water level, slope geometry and roughness, wave height and period, determine the number of waves that reach the crest, and overtop, and the average overtopping discharge q (l/s per m).

In engineering practice the wave overtopping load is often described by the average wave overtopping discharge only. However, it is important to include consideration of the wave height as part of the erosion load. It is not enough to just use the average overtopping discharge when describing wave overtopping.

A fragmented turf does not have any strength that can be relied upon. If there is any significant wave overtopping to be expected (ie more than 0.1 l/s per m) a fragmented turf is not recommended. So, if the

risk of undermining can be excluded, and if a closed turf is present, the cumulative overload model is suggested (van der Meer *et al*, 2010):

$$\sum_{n=1}^{N_{ov}} \left(U_n^2 - U_c^2\right) < C \qquad (8.92)$$

With $U_n \geq U_c$, where:

N_{ov} = number of overtopping waves
U = maximum depth averaged flow velocity from an overtopping wave (m/s), for cases where $U > UC$
U_c = critical maximum depth averaged flow velocity depending on the top layer strength (m/s)
C = critical value (m²/s²) where:
- C = 500 (m²/s²) resembles a situation where initial damage occurs. A large scatter in the initial damage value is however observed
- C = 1000 (m²/s²) multiple spots with initial damage (not yet failure of the top layer)
- C = 3500 (m²/s²) failure of the top layer.

The cumulative overload depends mainly on U_c, the storm duration, and the combination of the average overtopping discharge and the wave height, H_s. From the wave overtopping tests, critical velocities were back-calculated and showed a range from U_c = 4 m/s (critical volume 500 l/m) up to 6.3 m/s (critical volume 2000 l/m), excluding tests with fragmented turf. The cumulative overload can be compressed in the graphs in Figure 8.55. The graph gives (on the vertical axis) the cumulative overload for a one hour storm condition (Figure 8.55).

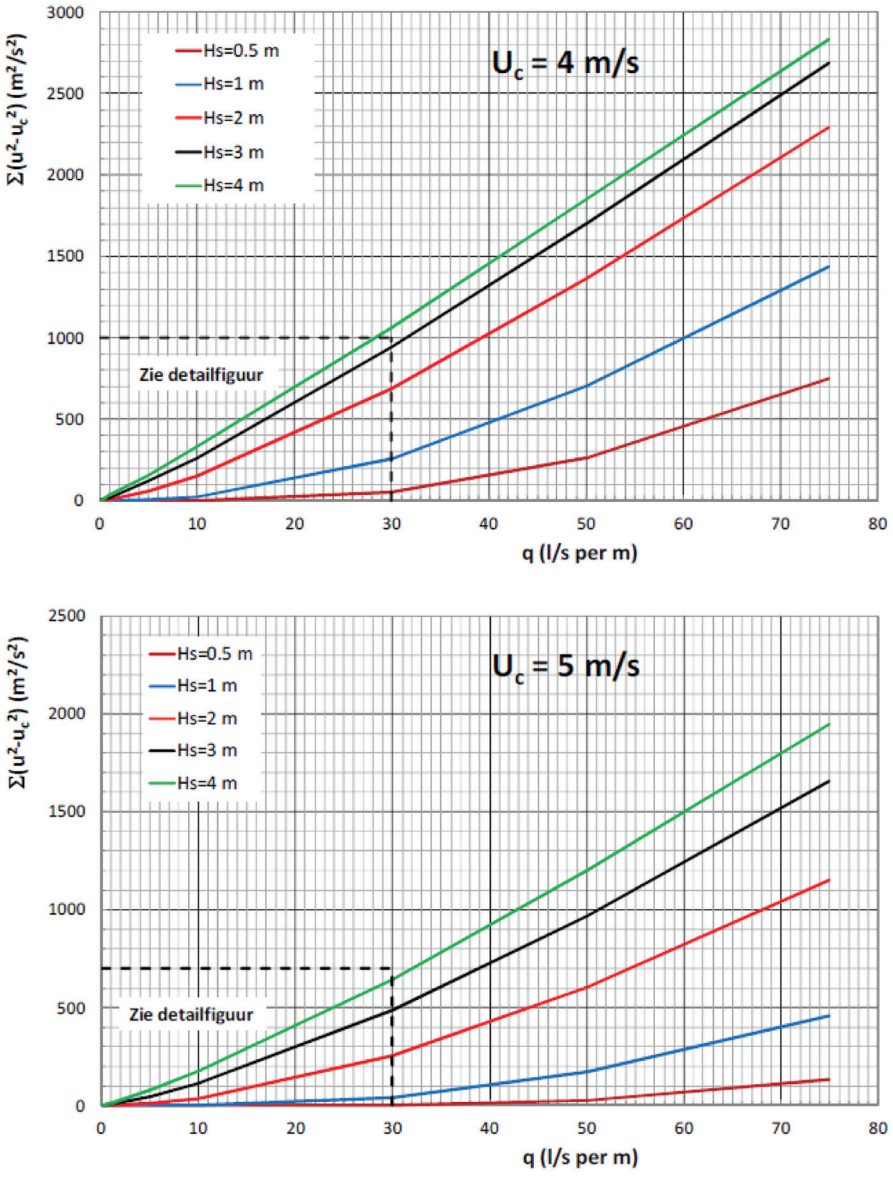

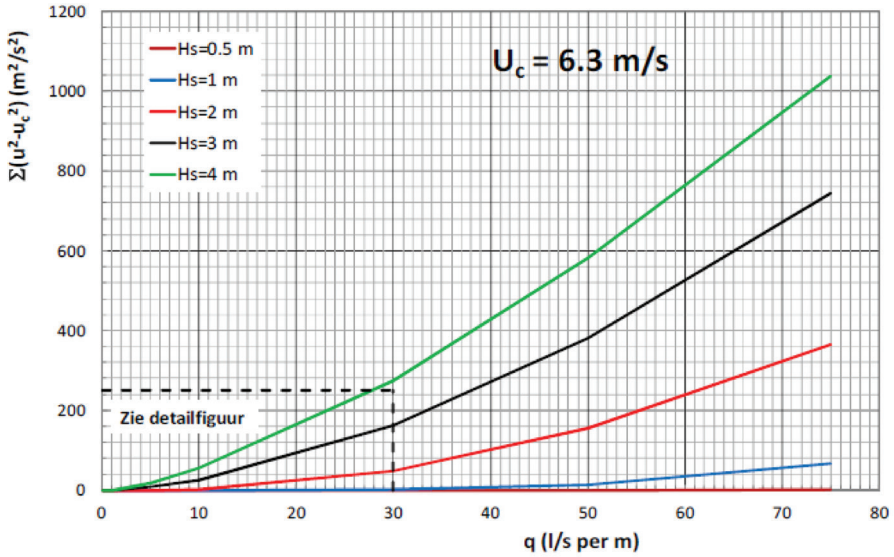

Figure 8.55 Cumulative overload (m^2/s^2) as a function of U_c (m/s), H_s (m) and q (l/s per m) for a one hour storm condition (Morris et al, 2012a)

The research within the SBW framework (Morris *et al*, 2012a) has not yet led to a reliable relation between U_c and field parameters. Based on the test results a value of U_c = 4 m/s and C = 1000 m^2/s^2 is advised for closed turf, and excluding cases too far beyond the range of wave overtopping tests, the most important being the slope angle of 1, 2, 3. For a closed turf it is likely that the critical velocity will be larger than 4 m/s, however, the research to predict U_c is still work in progress.

Example

For example, consider wave overtopping that lasts six hours, with Hs = 2 m. There are two hours of q = 10 l/s per m (water level rise and fall) and four hours of q = 25 l/s per m at the peak water level. Using the graph with U_c = 4 m/s for a closed turf, shows a cumulative overload of 150 m^2/s^2 per hour for 10 l/s per m and Hs = 2 m and 550 m^2/s^2 per hour for 25 l/s per m and Hs = 2 m. The total cumulative overload during the storm event will be 2 × 150 + 4 × 550 = 2500 m^2/s^2. This is larger than 1000 m^2/s^2, so the suggested criterion is not met.

If, in the same case U_c = 5 m/s than the graph shows a cumulative overload of 25 m^2/s^2 per hour for 10 l/s per m and Hs = 2 m and 200 m^2/s^2 per hour for 25 l/s per m and Hs = 2 m. The total cumulative overload during the storm event will be 2 × 25 + 4 × 200 = 950 m^2/s^2. This is smaller than 1000 m^2/s^2, so the suggested criterion is met.

8.4.3 Resistance of other protection systems to erosion due to currents

A large number of stability formulae for armourstone under current attack have been suggested by various authors, which tend to give quite different results in terms of the required stone size. CIRIA; CUR; CETMEF (2007) presents three methods selected from the range of formulae available in the literature. The three formulae addressed in CIRIA; CUR; CETMEF (2007) have been used extensively for current attack. Synopses of the methods follow.

Pilarczyk (1995) combined various design formulae to present a unified relationship between required armourstone size for stability and the hydraulic and structural parameters. Special factors and coefficients were added to the Shields (1936) formulations to derive Equation 8.93. Guidance related to parameters in the equation is presented in Table 8.14.

$$D = \frac{\phi_{sc}}{\triangle} \frac{0.035}{\psi_{cr}} k_h \, k_{sl}^{-1} \, k_t^2 \frac{U^2}{2\,g} \tag{8.93}$$

where:

D = characteristic size of the protection element (m), $D = D_{n50}$ for armourstone
ϕ_{sc} = stability correction factor (-)
Δ = relative buoyant density of the protection element (-)
ψ_{Cr} = critical mobility parameter of the protection element (-)
k_t = turbulence factor (-)
k_h = velocity profile factor (-)
k_{s1} = side slope factor (-)
U = depth averaged flow velocity (m/s)

Table 8.14 Design guidance for parameters in the Pilarczyk design formula

Characteristic size, D	Armourstone and rip-rap: Box gabions and gabion mattresses: Note that the armourstone size is also determined by the need to have at least two layers of armourstone inside the gabion.	$D = D_{n50} \cong 0.84\ D_{50}$ (m) D = thickness of element (m)
Relative buoyant density, Δ	Rip-rap and armourstone: Box gabions and gabion mattresses: where n_v = layer porosity Δ 0.4 (-), ρ_r = apparent mass density of rock (kg/m³) and ρ_w = mass density of water (kg/m³)	$\Delta = \rho_r/\rho_w - 1$ $\Delta = (1-n_v)\ (\rho_r/\rho_w - 1)$
Mobility parameter, ψ_{cr}	Rip-rap and armourstone: Box gabions and gabion mattresses: Rock fill in gabions:	$\psi_{cr} = 0.035$ $\psi_{cr} = 0.070$ $\psi_{cr} < 0.100$
Stability factor, φ_{sc}	Exposed edges of gabions/stone mattresses: Exposed edges of rip-rap and armourstone: Continuous rock protection: Interlocked blocks and cabled blockmats:	$\varphi_{sc} = 1.0$ $\varphi_{sc} = 1.5$ $\varphi_{sc} = 0.75$ $\varphi_{sc} = 0.5$
Turbulence factor, k_t	Normal turbulence level: Non-uniform flow, increased turbulence in outer bends: Non-uniform flow, sharp outer bends: Non-uniform flow, special cases:	$k_t^2 = 1.0$ $k_t^2 = 1.5$ $k_t^2 = 2.0$ $k_t^2 > 2.0$
Velocity profile factor, k_H	*Fully developed logarithmic velocity profile:* where h = water depth (m) and k_s = roughness height (m), k_s = 1 to 3D_n for rip-rap and armourstone, for shallow rough flow ($h/D_n < 5$), $k_h \approx 1$ can be applied *Not fully developed velocity profile:*	 $k_h = (1 + h/D_n)^{-0.2}$
Side slope factor, k_{sl}	The side slope factor is defined as the product of two terms, a side slope term, k_d, and a longitudinal slope term, k_l: where $k_d = (1-(\sin^2\alpha/\sin^2\varphi))^{0.5}$ and $k_l = \sin(\varphi-\beta)$, α is the side slope angle (°), φ is the angle of repose of the armourstone (°) and β is the slope angle in the longitudinal direction (°)	$k_{sl} = k_{dkl}$

Escarameia and May (1992) provide an equation that is a form of the Izbash equation. The Escarameia and May formulation (Equation 8.94) includes effects of turbulence and can be particularly useful in situations where turbulence levels are higher than normal (near river training structures, at bridge piers, downstream of hydraulic structures such as gates, weirs, spillways and culverts). Guidance for parameters used in Equation 8.94 is presented in Table 8.15 and Table 8.16.

$$D_{n50} = c_T \frac{u_b^2}{2g\Delta} \tag{8.94}$$

where C_T is the turbulence coefficient (-) and u_b is the near-bed velocity, defined at 10 per cent of the water depth above the bed (m/s).

Table 8.15 Design guidance for parameters in Escarameia and May formula

Median nominal diameter, D_{n50}	Armourstone: Gabion mattresses: Note that equations were developed from results of tests on gabion mattresses with a thickness of 300 mm	$D_{n50} = (M_{50}/\rho_r)^{1/3}$ (m) D_{n50} = stone size within gabion
Turbulence coefficient, c_r	Armourstone: (valid for r ≥ 0.05): Gabion mattresses: (valid for r ≥ 0.15): where r = turbulence intensity defined at 10% of the water depth above the bed (-), $r = u'_{rms}/u$	c_r = 12.3 r – 0.20 c_r = 12.3 r – 1.65
Near bed velocity, u_b	If data are not available an estimation can be made based on the depth-averaged velocity, *U* (m/s), as:	u_b = 0.74 to 0.90 U

Table 8.16 Typical turbulence levels for use in Escarameia and May formula

Situation	Turbulence level	
	Qualitative	*Turbulence intensity, r*
Straight river or channel reaches	Normal (low)	0.12
Edges of revetments in straight reaches	Normal (low)	0.20
Bridge piers, caissons and spur-dikes, and transitions	Medium to high	0.35–0.50
Downstream of hydraulic structures	Very high	0.60

Maynord (1993) developed the USACE design procedure based on an assumption that stability for rip-rap and armourstone should not be based on the threshold of movement criterion. Maynord instead based his formula on not allowing the underlying material to be exposed. As a result the layer thickness is included. Equation 8.95 gives the relationship between the characteristic stone sieve size, D_{50} (m) required to achieve stability subject to the imposed hydraulic and structural parameters. Guidance for parameters used in Equation 8.95 is given in Table 8.17.

$$D_{50} = f_g^{0.32} S_f \, C_{st} \, C_v \, C_T \, h \left(\frac{1}{\sqrt{\triangle}} \frac{V}{\sqrt{g \, h \, k_{sl}}} \right)^{2.5} \tag{8.95}$$

where:

f_g = gradation (factor = D_{85}/D_{15} (-))
S_f = safety factor (-)
C_{st} = stability coefficient (-)
C_v = velocity distribution coefficient (-)
C_T = blanket thickness coefficient (-)
h = local water depth (m)
Δ = relative buoyant density of stone (-)
V = depth-averaged flow velocity (m/s)
k_{sl} = side slope factor (-)

Maynord's blanket thickness coefficient, C_T, takes account of the increase in stability that occurs when stone is placed thicker than the minimum thickness ($1D_{100}$ or $1.5D_{50}$) for which $C_T = 1.0$.

Table 8.17 Design guidance for parameters in Maynord (1993)

Safety factor, S_f	Minimum value	S_f = 1.1
Stability coefficient, C_{st}	Angular armourstone: Rounded armourstone:	C_{st} = 0.3 C_{st} = 0.375
Velocity distribution coefficient, C_v	Straight channels, inner bends: Outer bends: where r_r = centre radius of bend (m) and B = water surface width just upstream of the bend (m) Downstream of concrete structures or at the end of dikes	C_v = 1.0 C_v = 1.283–0.2 log(r_b/B) C_v = 1.25
Blanket thickness coefficient, C_T	Standard design: Otherwise see Maynord (1993)	C_T = 1.0
Side slope factor, k_{sl}	$k_{sl} = {}^{-}0.67 + 1.49\cot\alpha + 0.045\cot\alpha$	

Note

The methods presented in this section are indicative methods. Other design methods can be found in CIRIA; CUR; CETMEF (2007). In view of the differing results, it is advisable in most instances to try more than one design formula for the evaluation of the required armourstone size and to use engineering judgement for the final selection.

These methods can be used to calculate the nominal size of rock required based on site hydraulic data, namely velocity. It is recommended that at least these three methods be used in selecting the size material to use. In order to achieve adequate protection armour, void spaces within the layer thickness must not be excessive and there should be good interlocking between the individual armourstones. This requires that a variety of rock sizes be included in the final placement. Once nominal stone size is determined the full gradation of the armour layer has to be specified to achieve this. Typically this involves defining a D_{15}, D_{85}, and/or D_{100} sizes. The approach to defining the required gradation varies by nation. In Europe, the gradation approach set out in BS EN13383-1:2002 should be followed. Further details can be found in CIRIA; CUR; CETMEF (2007).

These methods can also be used to size individual concrete armour blocks. Where blocks have interlocking features or external anchoring, the appropriate size should be based on manufacturer recommendations. Current recommendations for design of concrete block armour units on levee embankments is to determine sizing based on individual units without the benefit of anchoring.

8.4.4 Resistance of other protection systems to erosion due to waves

The principal requirement of an armouring system is dissipation of wave energy, and protection of the finer materials in the core. The armour has to remain stable under wave attack, and should dissipate energy over and within the voids in the armour and under layer(s), thus limiting wave run-up and overtopping, and reflections. In resisting severe wave action, armoured structures may suffer damage or failure in many different ways. The main failure modes for which functional relationships have been established may be defined as:

1 **Armour movement on the front face:** deemed to include rocking, displacement, and breakage of armour units.

2 **Armour movement on the rear face:** caused by wave overtopping.

3 **Crown wall movement:** principally sliding backwards or tilting under wave forces, horizontal and uplift.

4 **Toe erosion:** localised erosion of the foundation material at the toe of the breakwater.

Only mechanism (1) is discussed here as the others are discussed in detail in CIRIA; CUR; CETMEF (2007). Also, note that the advice of a coastal engineering specialist should be sought. The front face armour has to limit wave run-up and/or overtopping, and restrict reflections from the structure. Both of these are assisted by breaking the waves on the sloping face of the structure, and by dissipating wave energy in flow over/within rough and permeable armour layers. The seaward slope angle and crest

freeboard generally have the most significant influence on the hydraulic performance. Armour porosity and permeability are particularly important in determining the potential for wave energy dissipation, with both influencing the armour stability.

The main parameters used to describe wave attack, and to calculate the principal hydraulic responses may be summarised as:

Significant wave height (inshore or offshore):	H_s, H_{si}, H_{so}
Mean or peak wave periods:	T_m, T_p
Mean or peak offshore wave length:	$L_m = gT_m^2/2\pi$, $L_p = gT_p^2/2\pi$
Mean or peak wave steepness:	$s_m = H_s/L_m$, $s_p = H_s/L_p$

The main parameters describing the structure geometry are summarised in CIRIA; CUR; CETMEF (2007). Some frequently used terms are listed here:

Nominal unit dimension:	$D_n = (M/\rho_r)^{1/3}$, generally D_{n50}
Unit mass:	M, (eg M_{50})
Material density:	ρ_p or ρ_c (usually in kg/m^3)
Depth of water:	h, or h_s at the structure
Armour crest or structure freeboard:	A_c, R_c
Front armour slope:	α or α_f

8.4.4.1 Armourstone design formulae

Simple approaches to the design of rock armour to such structures have often concentrated on extraction of individual armour units, generally termed 'damage'. The armour size required was derived from formulae using a regular wave height and value of a stability coefficient derived from model tests at a 'no damage' limit (often zero to five per cent extractions). The influences of many other parameters were ignored. Most design methods for rock or concrete armour calculate the median unit mass, M_{50}, or the nominal median stone diameter, D_{n50}, defined as: $D_{n50} = (M_{50}/\rho_r)^{1/3}$.

The two most commonly used methods are:

1 The Hudson formula, as used in USACE (2006a).
2 Van der Meer's equations, as used in CIRIA; CUR; CETMEF (2007).

In each instance, the design method is used to determine the limiting value of the armour size for given wave conditions, and structure geometry.

Hudson's formulae

Hudson developed a simple expression for the minimum armour weight required to resist a (regular) wave height, H, which may be re-written:

$$M_{50} = \rho_r H^3 / K_D \cot\alpha \triangle \tag{8.96}$$

where:

ρ_r, ρ_w = density of armour/water (kg/m^3)
Δ = buoyant density of rock = $(\rho_r/\rho_w)-1$
α = slope angle of the structure face
K_D = is a stability coefficient to take account of the other variables.

For wide graded rock armour, or rip-rap, values of a coefficient K_{RR} are substituted for K_D. Values of K_D were initially derived from model tests using regular waves with permeable cross-sections subject

to no overtopping. A range of wave heights and periods were studied. In each case the value of K_D corresponded to the wave condition giving the worst stability condition. Some rearrangement of the armour was expected, and values of K_D suggested for design correspond to a 'no damage' condition where up to five per cent of the armour units may be displaced.

The Hudson equation has many limitations, which include:

- potential scale effects from the tests used to generate the data
- the use of regular waves only
- no account taken of wave period or storm duration
- insufficient definition of the damage level
- the use of non-overtopped and permeable core structures only.

Before turning to other methods, however, it is convenient to consider another way of looking at Equation 8.96. The use of ($K_D$cotα) does not always best describe the effect of the slope angle, and it is often convenient to substitute a single stability number for ($K_D$cotα), and to work in terms of the nominal armour unit diameter $D_{n50} = (M_{50}/\rho_r)^{1/3}$. The Hudson equation may be re-arranged in terms of the stability number N_s:

$$N_s = \frac{H_s}{\triangle D_{n50}} = (K_D \cot\alpha)^{1/3} \tag{8.97}$$

The Hudson formula does not itself give any information on the level of damage. However, information is available in USACE (2006a) that allows the derivation of a similar equation relating a damage parameter,$N_{d\%}$, to the relative wave height. Taking $S_d = 0.8N_{d\%}$, a damage formula based on Equation 8.97 may be written:

$$\frac{H_s}{\triangle D_{n50}} = a\ (K_D \cot\alpha)^{1/3} S_d^b \tag{8.98}$$

where for rock armour = 0.67, b = 0.16, for Tetrapods or cubes = 0.69, b = 0.14 and S_d, design damage number = A_e/D_{n50}^2 (below for definitions and critical values).

Van der Meer's formulae

Van der Meer (1988) derived formulae to include the effects on armour size:

- of random waves
- of a wide range of core/underlayer permeabilities
- of the chosen level of damage
- and to distinguish between plunging and surging wave conditions.

For plunging waves:

$$\frac{H_s}{\triangle D_{n50}} = 6.2\, P^{0.18} \left(\frac{S_d}{\sqrt{N_z}}\right)^{0.2} \frac{1}{\sqrt{\xi_m}} \tag{8.99}$$

For surging waves:

$$\frac{H_s}{\triangle D_{n50}} = 1.0\, P^{-0.13} \left(\frac{S_d}{\sqrt{N_z}}\right)^{0.2} \sqrt{\cot\alpha}\, \xi_m^P \tag{8.100}$$

where parameters not previously defined are:

P = notional permeability factor, see Figure 8.56a
S_d = design damage number = A_e/D_{n50}, see Table 8.18
A_e = erosion area from profile
N_z = number of zero-crossing waves
ζ_m = Iribarren number = $\tan\alpha/s_m^{1/2}$

s_m = wave steepness for mean period = $2\pi H_s/gT_m^2$
T_m = mean wave period

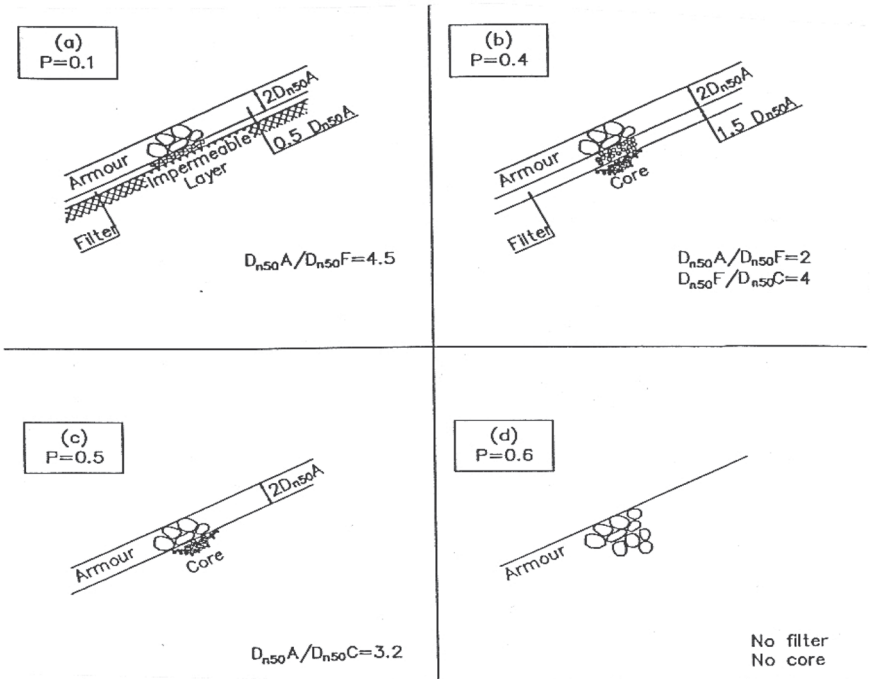

Figure 8.56 Permeability factors used in van der Meer's stability formulae for rock armour

The transition from plunging to surging waves is calculated using a critical value of $\xi_m = \xi_{mcr}$:

$$\xi_{mcr} = \left[6.2\, P^{0.31} \sqrt{\tan\alpha}\right]^{1/(P+0.5)} \tag{8.101}$$

The recommended values of the design damage number, S_d, equivalent to the number of D_{n50} sized stones extracted from a D_{n50} wide strip of the structure, are given in Table 8.18, for initial damage, intermediate damage, and failure. Failure is assumed when the filter layer is first exposed.

A range of core/underlayer configurations were used in the test programme, each with an armour layer thickness, $t_a = 2.2D_{n50}$. To each of these a value of the permeability factor, P, was assigned. In most cases for levee design the conservative value of $P = 0.1$ should be assumed, comparable to the value given by van der Meer (1988) for armour on an underlayer over an impermeable embankment. Other values for P are given by van der Meer (1988) for more permeable situations, but these should only be adopted after referring to detailed guidance available, for example CIRIA; CUR; CETMEF (2007).

Table 8.18 Suggested levels of damage, S_d, of armourstone protection systems

Slope	Damage, S_d		
	Initial	*Intermediate*	*Failure*
1:1.5	2	–	8
1:2	2	5	8
1:3	2	8	12
1:4–6	3	8	17

8.4.4.2 Design formulae for other revetment systems, slabs and blocks

Alternative forms of armouring for slopes shallower than 1:2 use concrete slabs, concrete blocks, pitched stone grouted by bitumen or concrete, or asphaltic materials. The stability of this type of armouring requires that the net uplift pressures acting across the concrete are balanced by the net weight force.

Simple stability formulae have been suggested for the preliminary analysis or design of blockwork or stone pitching on revetment slopes. The formula may be used to determine the block thickness, t_a:

$$\frac{H_s}{\triangle t_a} = \frac{S_b}{\xi_{op}^{0.67}} \tag{8.102}$$

where:

ζ_{op} = $\tan\alpha / s_{op}^{1/2}$
s_{op} = H_s / L_{op}

Ranges of values of the stability parameter S_b for different block types and underlayer materials are given in Table 8.19.

Table 8.19 ***Values of block stability parameter, S_b for different block and underlayer materials***

Block type	Underlayer	$S_{b,min}$	$S_{b,max}$
Loose	Granular	2.6	5.6
Loose	Geotex. + sand	3.7	8.0
Loose	Clay	5.1	11.0
Linked	Granular	3.7	8.0
Linked	Geotex. + sand	5.1	11.0

Using the highest value of S_b will give the slab thickness beyond which the structure will be unstable. Using the lowest value of S_b will give the slab thickness that will be stable under the design conditions. In practice, as little guidance is available on performance of the structure between these two limits, the designer will be likely to use the more conservative value of the two.

Yarde *et al* (1996) gave particular consideration to the case of reservoir dams, and to wave conditions generated over limited fetch lengths such as those occurring on inland bodies of water, where wave periods are short and wave steepness is large. They extended the general method of Klein Breteler and Bezuijen (1991) for short wave periods and for larger slabs, and suggested the following modified equation:

$$\frac{H_s}{\triangle t_a} = \frac{S_c}{\xi_{op}} \tag{8.103}$$

Yarde *et al* (1996) quantified the stability coefficient, S_c, as a function of the dimensions and permeabilities of the cover layer and underlayer:

$$S_c = 3.3 \ln \left[\frac{\sqrt{A_s}}{t_f} \left(\frac{w}{D_{f15}} \right)^{0.1} \right] + 4.0 \tag{8.104}$$

where:

A_s = slab area (m^2)
t_f = thickness of the filter layer (m)
w = gap between slabs representing drainage area or cover layer permeability (m)
D_{f15} = 15 per cent non-exceedance diameter of the filter layer material, obtained from the grading curve (m), and is taken as indicating the relative permeability of the filter layer

A comparison between the outputs of the alternative design formulae is given in Figure 8.57.

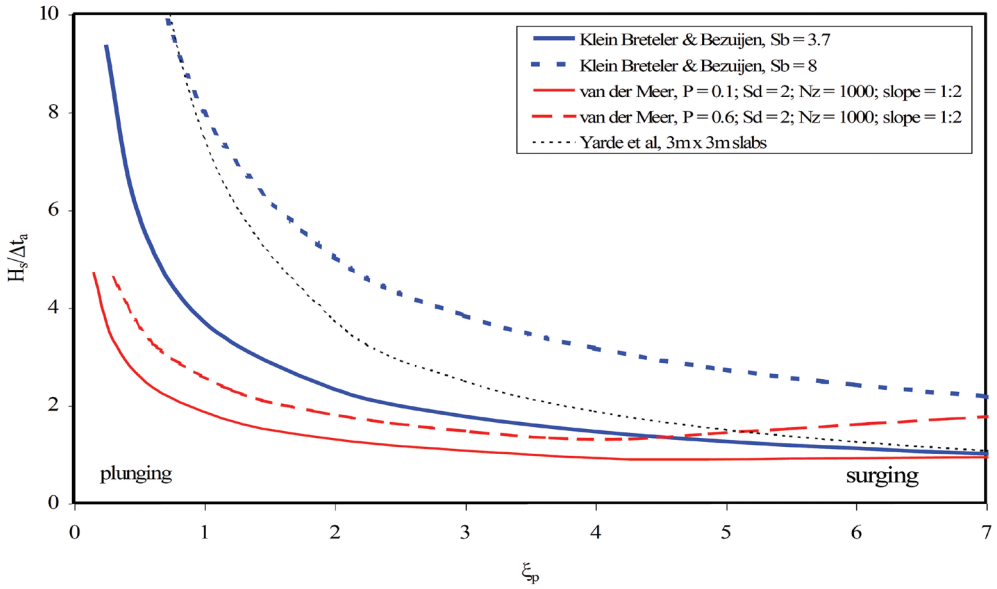

Figure 8.57 Comparisons between stable revetment thickness predictions for rock armour, blockwork and slabbing (from McConnell and Allsop, 1999)

8.4.5 Resistance of armourstone to ice

Brown and Clyde (1989) identified that ice (Section 7.3.13) can affect surface protection systems in a number of ways:

- moving surface ice can cause crushing and bending forces and large impact loadings
- the tangential flow of ice along a protected levee can cause high lateral shearing forces
- the thawing of upstream ice jams can cause a rapid release of water and blocks of ice leading to flooding and possible overtopping of water and ice.

Ice forces should be evaluated on a case-by-case basis using past experience and local codes of practice. In most instances, ice flows will not be of sufficient magnitude to warrant detailed analysis. For example, historic observations of ice flows in rivers in New England, USA indicate that rip-rap sized to resist design fluvial flow events will also resist ice forces (Brown and Clyde, 1989, and Colorado Department of Transportation, 2004).

Where ice flows have historically caused problems, the diameter of armourstone calculated using procedures such as those set out in Sections 8.4.4, should be multiplied by an additional stability factor based on local experience. Table 8.20 provides an initial guide to the magnitude of this stability factor developed by Brown and Clyde (1989).

Table 8.20 Guidelines for the selection of stability factors for rip-rap design (Brown and Clyde, 1989)

Condition	Stability factor* range
Uniform flow, straight or mildly curving reach (curve radius/channel width > 30), impact from wave action and floating debris is minimal, little or no uncertainty in design parameters	1.0–1.2
Gradually varying flow, moderate bend curvature (30 > curve radius/channel width > 10), impact from waves or floating debris moderate	1.3–1.6
Approaching rapidly varying flow, sharp bend curvature (10 > curve radius/channel width), *significant potential impact from floating debris and/or ice*, significant wind and/or boat generated waves (0.30 m to 0.61 m), high flow turbulence, turbulently mixing flow at bridge abutments, significant uncertainty in design parameters	1.6–2.0

Note

* Testability factor is the number by which the design rock diameter for hydraulic design should be multiplied to take account of ice effects.

Vaughan *et al* (2002) carried out independent assessments and calculations to investigate the appropriateness of the Brown and Clyde (1989) recommendations in five relatively severe ice related scenarios:

1 Anchor ice rafting and rip-rap specific gravity reduction.
2 Raft ice impact damage.
3 Raft ice push-up onto shore.
4 Ice jams causing velocity increase.
5 Increased longitudinal effective tractive force imposed by stream ice cover.

They concluded that, for the scenarios investigated, the higher stability factors in Table 8.20 (ie in the range 1.6 to 2.0) were still relevant.

Note

Consideration of the stability formulae in Sections 8.4.3 and 8.4.4 shows that as an alternative to increasing the size of the armourstone, flatter levee slopes may be adopted to deliver the same increase in size of the stability factor. This is reflected by the practice described in Box 8.13.

Box 8.13 USA practice for levee slopes prone to ice action

General practice in the Midwestern USA is to keep slopes at 1V:4H or flatter. If use of a 1V:4H slope is not an option, the size of the armourstone is increased.

Extension of rip-rap protection up to the 10 per cent event ice water surface profile should also be considered (a practice adopted by the Omaha District Corps of Engineers). If required, numerical modelling may be used to estimate the 10 per cent event ice water surface profile.

When considering the design methodologies available for blockwork, it became apparent the methodologies are mainly based on loose or interlocking blocks of low permeability. Many proprietary cellular block systems are available that have much higher permeabilities. Consideration of model test data from Lindenberg (1983) suggested that the method of Klein Breteler and Bezuijen (1991) could be applied with careful choice of the stability coefficient S_b.

Often concrete blockwork may be cable-tied with nylon or steel cables being used to create blockwork mats which facilitate placement of the blocks. While it is generally agreed that the cables should not be considered to provide additional strength in the structure allowing thinner blocks to be used, they may help to provide a restraining force in the event that sliding failure of the revetment occurs.

Model studies by Lindenberg (1983) and practical experience suggest that gravel blinding of blockwork may help provide an increase in the stability of concrete blocks. This enhancement would, however, only work if both the concrete blocks and the binding material were sufficiently robust/durable to resist crushing over the life of the revetment. There is much debate as to whether this stability increase can be relied upon and McConnell (1998) recommends that this improvement be ignored in performing ultimate stability calculations.

8.4.5.1 Design formulae for asphaltic revetments

Many coastal levees are protected from erosion of their core by an asphalt revetment, typically between 15 cm and 30 cm in thickness. The thickness is larger in the lower part of the revetment in order to avoid uplift when the sea level drops. The discussion in this section is an introduction, focusing mainly on impermeable asphaltic revetments. For such revetments, three failure mechanisms are normally considered detailed as follows:

Uplift

The failure of an asphalt revetment layer by uplift forces can be described by a simplified analytical solution, in which the maximum water head difference is related to the thickness of the revetment. This solution can be applied to an impermeable asphalt revetment on a sand bed with an open toe construction (Figure 8.58).

The driving load is expressed in terms of a head difference H_{max}.

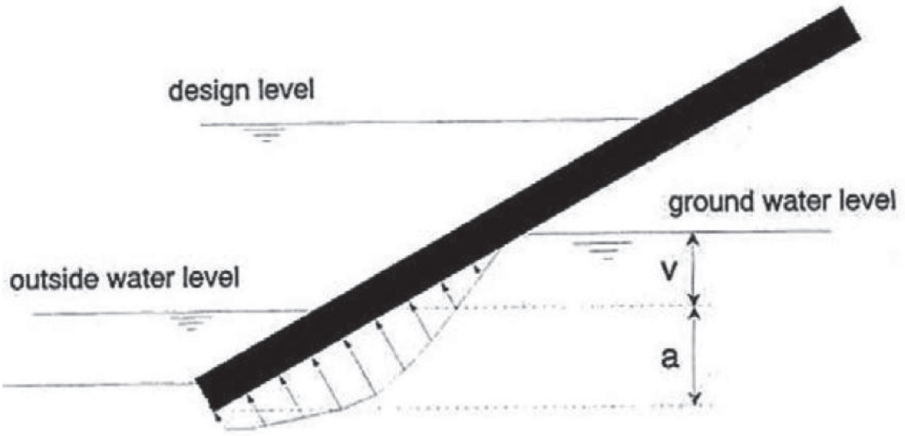

Figure 8.58 Uplift sketch for asphaltic revetment (from FLOODsite, 2007)

The layer thickness h can be derived from the equilibrium equation for uplift:

$$h = H_{max} \triangle / \cos \alpha \tag{8.105}$$

where:

Δ = relative buoyant density of the asphalt = $(\gamma_\rho - \gamma_w)/\gamma_w$, where γ_r for asphalt = 23 kN/m^3
h = thickness of asphalt layer (m)
α = slope angle (°)

Two situations need to be considered:

1 Where the outside water level at which the maximum uplift pressure occurs is higher than the average outside water level, Equation 8.106 should be used (Van Herpen, 1998):

$$H_{max} = \frac{v}{\pi} \arccos \left(2 \left[\frac{v + h \cos \alpha}{a + v} \right]^{\pi/\theta} - 1 \right) \tag{8.106}$$

with $\theta = \arctan(n) + \pi/2$, and a and v as shown in Figure 8.58.

For a given groundwater level and a variable outside water level Equation 8.106 can be maximised to $v/(a + v)$. For slopes between 1:1 and 1:8 this gives $v/(v + a) = 0.53$. This can be inserted in Equation 8.106 in order to obtain an equation for $H_{max\ critical}$ depending on h and α at the critical outside water level. This equation for $H_{max\ critical}$ can be inserted into Equation 8.105. The resulting equation can be solved numerically to find $h/(a + v)$ and where the groundwater level $(a + v)$ is known this calculation results in a value for the layer thickness h.

In the case of a slope angle 1:4, the numerical results have been fitted by means of the function Q_n, which results in the following formula for the layer thickness h:

$$h = 0.21\, Q_n\, (a + v) / \triangle \tag{8.107}$$

where:

Q_n = $0.96/(\cos \alpha)^{1.4}$

2 Where the critical outside water level at which the maximum uplift pressure occurs is lower than the average outside water level, $a/(a + v)$ is defined with reference to the average outside water level. This means that a correction factor R_w is needed in Equation 8.107. R_w varies with $v/(a + v)$ as shown in Figure 8.59.

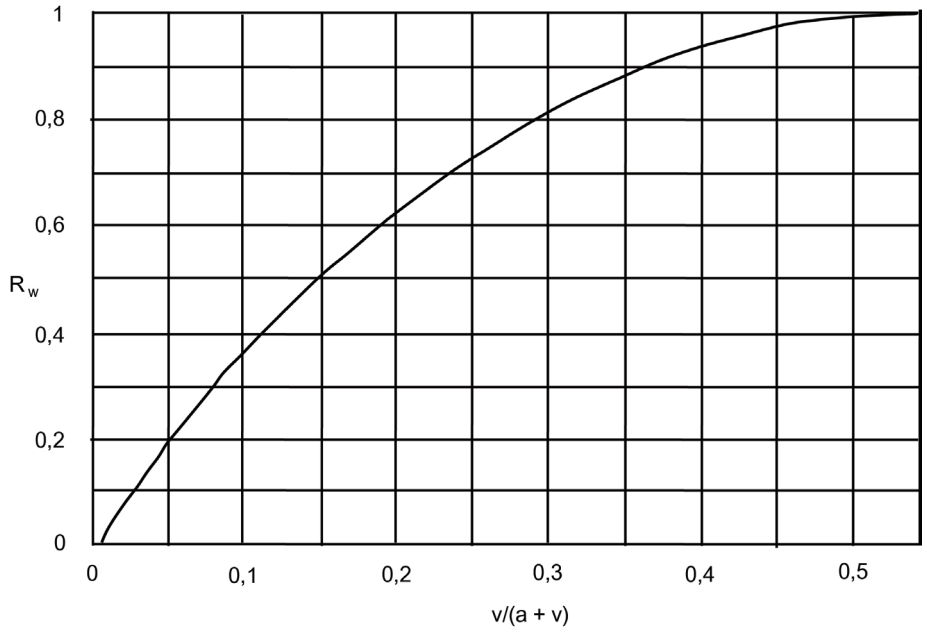

Figure 8.59 *Reduction factor R_w for h where the outside water level at which the maximum uplift pressure occurs is lower than the average outside water level (Morris et al, 2012a)*

Resistance against wave loading

Asphaltic revetments may be able to resist repeated waves with significant heights of up to 4.5 m. However, the asphalt layer can fail as a result of fatigue due to repeated loading under storm conditions. Indeed, in the event of very high wave loads, the asphalt can fail after just a few large waves. So, in conditions of severe wave attack, calculations should be carried out to ensure that the asphalt has sufficient fatigue strength to resist the impact forces of wave loading, which cause bending in the asphalt due to limited support from the underlying materials. Appropriate fatigue calculations can be facilitated (de Looff *et al*, 2006) by suitable software such as 'Golfklap' (wave attack in English).

Sliding

Sliding is avoided when:

$$H_{max} =\leq h \cos\alpha \left[\frac{\gamma_w}{\gamma_r}\left(1 - \frac{\tan\alpha}{f}\right) - 1\right] \qquad (8.108)$$

where:

h = thickness of revetment (m)

f = coefficient for friction (-), for $\theta < \varphi$: $f = \tan\theta$, for $\theta \geq \varphi$: $f = \tan\varphi$

8.5 INTERNAL EROSION

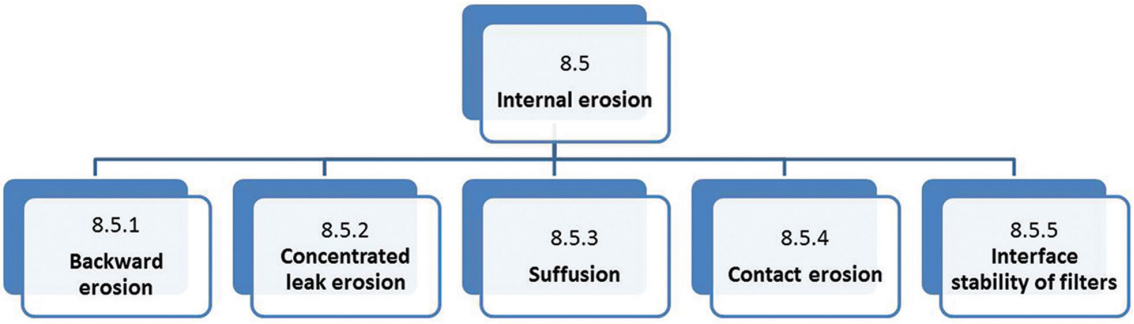

Internal erosion is related to all processes that involve soil particles detachment and transport by seepage flow within the dam or levee, or its foundation. Such processes can ultimately lead to the instability of the levee. Failure by internal erosion is categorised into three general modes:

- internal erosion through the embankment
- internal erosion through the foundation
- internal erosion at the levee foundation contact.

Basic mechanisms of internal erosion

Four different mechanisms may be identified ICOLD (2012). These mechanisms form the basis for information presented in this section and shown in the section flow chart.

1 **Backward erosion:** detachment of soil particles when the seepage exits to an unfiltered surface, leading to worm-holes and sand boils.

2 **Concentrated leak erosion:** detachment of soil particles through a pre-existing path in the embankment or foundation.

3 **Suffusion:** selective erosion of the fine particles from the matrix of coarse particles.

4 **Contact erosion:** selective erosion of the fine particles from the contact with a coarser layer.

General conditions for occurrence of internal erosion

Two conditions should be fulfilled for internal erosion to occur described as follows, and shown in Figure 8.60:

1 The first condition is that particles can be detached, ie that hydraulic shear stresses are larger than resistant contact forces. To reach this hydro-mechanical criterion, water seeping through the flood defence should have sufficient velocity to provide the energy needed to detach particles from the soil structure.

2 The second condition is that detached particles can be transported through the soil. Two criteria should be fulfilled:

   a A hydro-mechanical criterion, where flow is sufficient to carry the eroded particles.

   b A geometric criterion (which is specific to internal erosion), where voids exist in the soils within the flood defence that are large enough for detached particles to pass through. This void is either a pipe inside the soil, as in backward erosion or concentrated leak erosion, or pore space within the grains of a coarse layer, as observed in suffusion and contact erosion.

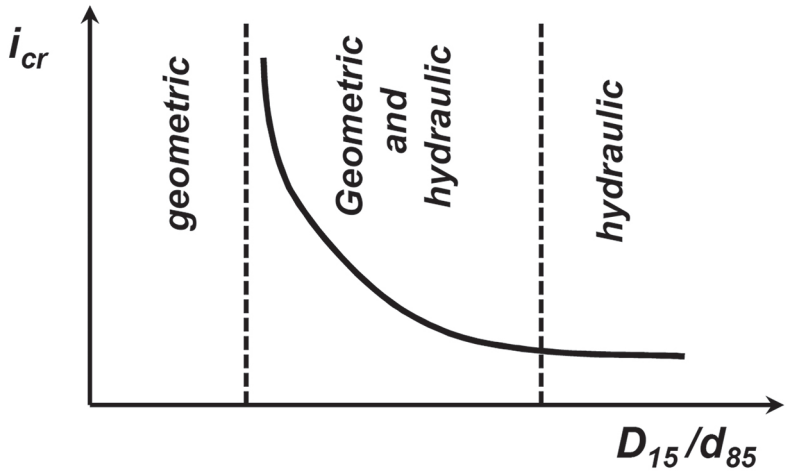

Figure 8.60 Interaction of geometric and hydraulic influence on internal erosion mechanisms

The nature of the soil in the embankment determines its vulnerability to erosion. Two main classes have to be distinguished.

1 **Granular non-cohesive soils:** erosion resistance is related to particle buoyant weight and friction. Hydro-mechanical transport criterion is linked to rolling and sliding resistance of the grains.

2 **Cohesive soils:** erosion resistance is mainly related to attractive contact forces in between the soil particles. The main transport mode is suspension flow.

Successive phases of internal erosion

From ICOLD (2012), the process of internal erosion of embankment dams or levees and their foundations can be represented by four phases.

1 **Initiation:** first phase of internal erosion, when one of the phenomenon of detachment of particles occurs.

2 **Continuation:** phase where the relationship of the particle size distribution between the base (core) material and the filter controls whether or not erosion will continue.

3 **Progression:** phase of internal erosion, where hydraulic shear stresses within the eroding soil may or may not lead to the erosion process being ongoing and, in the case of backward and concentrated leak erosion, to formation of a pipe. The main issues are whether the pipe will collapse, or whether upstream zones may control the erosion process by flow limitation.

4 **Breach:** final phase of internal erosion (Section 8.10).

8.5.1 Backward erosion

Backward erosion involves the detachment of soil particles when the seepage exits to a free unfiltered surface. The seepage flow erodes particles upwards and backwards below the embankment through erosion pipes, sometimes called worm-holes, and sand boils form on the surface. In critical circumstances, such as floods, the head difference increases, these pipes may grow progressively from the area with a lower hydraulic head towards the higher head.

The erosion shortens the seepage path and increases the gradient leading to higher flow velocities causing further backward erosion, increasing the length of the worm-hole, and causing failure when the worm-hole extends backwards to greater than half the width of the embankment base. Two configurations are identified:

- backward erosion in a sandy layer below an impermeable roof (clay layer, horizontal structure). This configuration involves the development of retrogressively growing pipes in the sand layer below the levee due to groundwater flow

- backward erosion in a cohesive soil. In this configuration, erosion is initiated by a leakage at the exit of a cohesive core to the foundation. The formation of a hole in the core increases erosion rate and hence leads to progressive backward extension of a pipe.

Criteria for initiation and progression of backward erosion may be related to local hydraulic conditions (exit gradients) or global hydraulic conditions averaged along the flow path.

8.5.1.1 Local criteria

Since erosion primarily involves removal of granular material, backward erosion is only possible if there is a prior destabilisation of the surface of the soil in the exit flow zone. When the exit zone is constituted by a pervious top soil layer, the destabilisation process of the near surface may exist depending on the flow direction and hydraulic gradient. In the special case of horizontal layer with vertical upward flow, this mechanism is called heave (or fluidisation). When the exit zone is composed of an impervious soil layer, the destabilisation process develops at the layer scale (development of cracks within the top layer) and is called uplift.

Heave (fluidisation)

In pervious (granular) soils, movement of soil at the downstream seepage exit may not occur as flotation followed by particle-by-particle movement. A mass of soil may be lifted, followed by piping. This phenomenon is called heave (or fluidisation) and occurs when the upward seepage force due to differential head equals the overlying buoyant weight of soil. Slope stability condition for purely frictional soils (Box 8.14) may be expressed in terms of slope angle:

$$\beta \leq \varphi' - \sin^{-1}\left\{\frac{i}{i_{cr}}\sin\left(\varphi' + \lambda\right)\right\} \tag{8.109}$$

where:

i_{cr} = γ'/γ_w is the Terzaghi critical gradient

As mentioned by Philippe and Richard (2008), the ratio i/i_{Cr} can be interpreted as a Shields' number, which enables making the link with sand erosion framework. The stability condition may also be expressed in terms of gradient:

$$i \leq i_{cr}\frac{\sin\left(\varphi' - \beta\right)}{\sin\left(\varphi' + \lambda\right)} \tag{8.110}$$

In the special case of a horizontal pervious (granular) soil layer ($\beta = 0$) and vertical upward flow ($\lambda = 0$), the stability condition may be written in terms of hydraulic gradient, $i_v \leq i_{Cr}$. The critical gradient may also be written in terms of intrinsic parameters of the soil, $i_{Cr} = (\rho_s - 1)/(1 + e)$, where ρ_s is the specific density of soil grains ($\rho_s \approx 2.7$) and e the void ratio (-).

Uplift

When seepage occurs beneath an impervious soil layer, the layer at its base is subject to a hydraulic force, which tends to lift the soil upward. The stability of soil against heave may be checked by verifying vertical equilibrium of a soil column. This condition may be expressed by:

$$\sigma_v > u \tag{8.111}$$

where σ_v is the stabilising vertical stress (kPa), and u the destabilising pore water pressure (kPa) beneath the imperious layer.

Box 8.14 Slope stability under water flow

Shallow sliding of slopes under-seepage conditions depends on the flow direction and hydraulic gradient, particularly near the ground surface. In the case of homogeneous slopes, analytical solutions based on the infinite slope model may be used. In the infinite slope stability model, the slip surface is assumed to be a plane parallel to the ground surface and the end effects are neglected. This analysis is valid if the ratio of depth to length of the sliding mass is small (a ratio of 1: 20 is commonly used). The slope element is subjected to both seepage and gravitational forces, in a block stability approach.

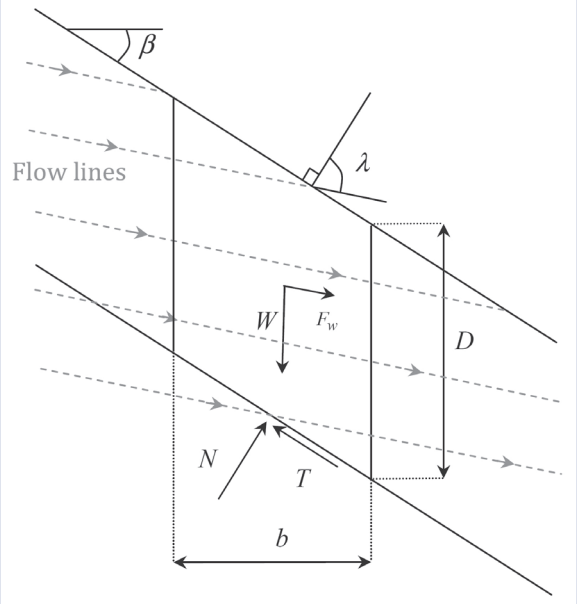

Figure 8.61 Infinite slope model with parallel flow lines

From geometrical considerations, the gradient can be derived as a function of seepage direction (λ) and slope angle (β). This exit gradient, corresponding to a locally uniform seepage, may be expressed as:

$$i = \frac{\sin\beta}{\sin\lambda} \tag{8.112}$$

It can be shown (Delinger and Iverson, 1990, and Ghiassian and Ghareh, 2008) that equilibrium condition of the sliding mass may be expressed in terms of slope geometry parameters and effective shear strength parameters of the soil:

$$\sin\beta + i\frac{\gamma_w}{\gamma'}\sin\lambda \leq \frac{c'}{\gamma' D\cos\beta} + \left(\cos\beta - i\frac{\gamma_w}{\gamma'}\cos\lambda\right)\tan\varphi' \tag{8.113}$$

where:

D = vertical soil depth (m)
β = inclination of the slope from the horizontal (°)
C' = soil effective cohesion (kPa)
φ' = soil effective internal friction angle (°)
γ' = unit weight of submerged soil (kN/m³)
γ_w = unit weight of water (kN/m³)

8.5.1.2 Global criteria

Global criteria models apply only in the configuration of backward erosion in a sandy layer below an impermeable roof, which is considered as perfectly rigid (not erodible). They introduce the concept of the length of the path travelled by seeping water and lead to the development of creep ratios or creep coefficients. Figure 8.62 shows the basic parameters required for the analysis.

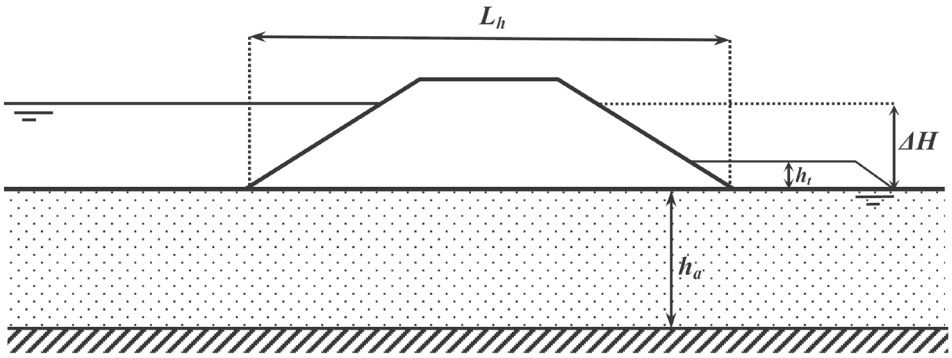

Figure 8.62 Definition of geometrical parameters

Bligh model

The rule of Bligh (1927) states that failure from backward erosion occurs if:

$$\triangle H - 0.3\, h_t > \frac{L_h}{C_{Bligh}} \tag{8.114}$$

where:

ΔH = hydraulic head over the levee (m)
h_t = thickness of the top layer (m)
L_H = horizontal seepage length (m)
C_{Bligh} = creep factor of Bligh (-)

Lane model

The presence of a structure, such as a cut-off wall, causes an extra barrier for the seepage path. Lane (1935) introduced a vertical seepage length L_v so that the rule of Lane states that backward erosion occurs if:

$$\triangle H - 0.3\, h_t > \frac{L_h/3 + L_v}{C_{Lane}} \tag{8.115}$$

where:

L_v = vertical seepage length (m)
C_{Lane} = creep factor of Lane (m)

The creep factors depending on the type of soil are given in Table 8.21.

Table 8.21 Value of creep coefficient

Type of soil	C_k (Lane)	C_k (Bligh)
Very fine sand or silt	8.5	18
Fine sand	7	15
Medium size sand	6	–
Coarse sand	5	12
Fine gravel or sand and gravel	–	9
Medium size gravel	3.5	–
Coarse gravel	3	–
Boulders, gravel and sand	–	4 to 6
Clay	2 to 3	–

Sellmeijer model

Large research programs were performed in the 1970s and 1980s to create a better understanding of the piping mechanism. More recently, scale effects have been studied with small, medium and full-scale experiments. Recent advances (van Beek *et al*, 2011, and Sellmeijer *et al*, 2011) in understanding the process has led to the improvement of a theoretical model, in which the equilibrium of grains in the bed of the pipe is used as criterion for development of the pipe. The critical gradient can be calculated by combining groundwater flow with the flow conditions in the pipe. Curve-fitting resulted in a formula relating sand characteristics to the geometric properties of the sand bed. This model takes into account scale effect (ratio between grain size and gradient $\Delta H/L$). According to the model of Sellmeijer (for horizontal retrogressive erosion in a sand layer below a clay dike) backward erosion is prevented if (Sellmeijer and Koenders, 1991):

$$\triangle H - 0.3\, h_t < F_{resistance}\, F_{scale}\, F_{geometry}\, L_h \tag{8.116}$$

with:

$$F_{resistance} = \frac{\gamma_p'}{\gamma_w}\, \eta\, \tan\theta \left(\frac{D_R}{D_{Rm}}\right)^{0.35} \left(\frac{C_U}{C_{Um}}\right)^{0.13} \left(\frac{R}{R_m}\right)^{-0.02} \tag{8.117}$$

$$F_{scale} = \frac{d_{70}}{\sqrt[3]{\kappa L_h}} \left(\frac{d_{70m}}{d_{70}}\right)^{0.6} \tag{8.118}$$

$$F_{geometry} = 0.91 \left(\frac{h_a}{L_h}\right)^{\frac{0.28}{(h_a/L_h)^{2.8}-1}+0.04} \tag{8.119}$$

where the m index refers to the characteristics of the small scale tests and:

ΔH = actual hydraulic head over the flood defence (m)
L_h = horizontal seepage length (m)
h_a = thickness of the aquifer (uppermost sand layer sensitive for retrogressive erosion) (m)
h_t = thickness of top layer (m)
γ_s' = unit weight of sand grains under water (16.5 kN/m^3)
γ_w = unit weight of water (10 kN/m^3)
θ = bedding angle of sand grains (°)
η = White's constant (0.25)
κ = intrinsic permeability of aquifer (m^2)
d_{70} = d_{70} of aquifer (m), (d_{70} = 208μm)
D_R = relative density (%)
R = roundness of the particles (%)

The parameters κ and d_{70} may be determined from grain size distribution analyses. The bedding angle determines how a grain is disposed on the other grains. It is only related to the weight and geometry since the model assumes that the grain rolls over the others without friction. Experimental data show that $\theta = 37°$ is a good estimation from current cases.

It should be noted that the above set of equation does not include a margin of safety and that for design purposes, a factor of safety may be necessary.

Hoffman's method

Another approach has been developed by Hoffmans (2012) to determine the critical gradient. Considering that progression of backward erosion needs transport of the detached particles through the piping channel, the critical gradient is decomposed in a critical Shields gradient and a critical Darcy's gradient. The most important variables of this model are hydraulic conductivity, particle sizes d_{50} and d_{15} and some coefficients determined experimentally. This approach enables capturing the influence of permeability on the magnitude of the critical gradient. This model does not account for all physical processes but secondary effects are included by calibration of some parameters of the model.

Schmertmann's method

Based on several laboratory tests on fairly uniform soils ($1.0 < C_u < 6$) ranging from fine to medium sands, Schmertmann (2000) proposed the following linear expression of the critical gradient:

$$i_{cr} = 0.05 + 0.183\,(C_U - 1) \tag{8.120}$$

This approach has the advantage of simplicity however this correlation was not confirmed for different types of soils.

An example of the use of a simplified method for under-seepage analysis is given in Box 8.15.

Box 8.15 ***Simplified method for under-seepage analysis***

In fluvial environments, levees are often placed on alluvial floodplains covered with silty or clayey soils that form impervious foundations. These impervious layers are frequently founded on a sandy soil stratum (aquifer), generally anisotropic, with permeability that is much greater, enabling horizontal flows. So, the simplified model (USACE, 1993) based on the following basic assumptions may be used:

- flow through the blanket is vertical
- flow through the pervious foundation is horizontal
- all flows are laminar and steady state
- the levee material (or its core) is impervious
- aquifer has a constant thickness and is horizontal.

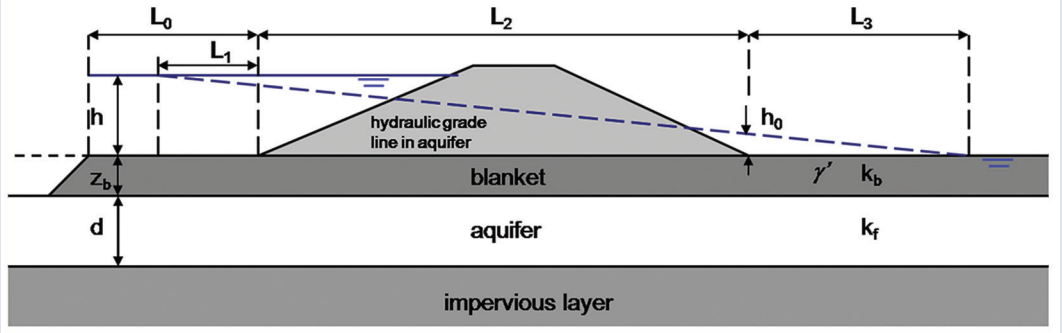

Figure 8.63 *Geometric notations for under-seepage analysis (after USACE, 1993)*

When the upstream impervious blanket is not continuous, its upstream effective length, L_1 (m), has to be defined as

$$L_1 = \sqrt{\frac{k_f}{k_{bu}} Z_{bu}\, d} \tag{8.121}$$

Box 8.15 *Simplified method for under-seepage analysis*

where:

k_f = horizontal permeability of the pervious foundation (m/s)

k_{bu} = vertical permeability of the upstream blanket (m/s)

Z_{bu} = thickness of the upstream blanket (m)

d = thickness of the pervious aquifer (m)

The effective length of the downstream blanket, L_3 (m), is:

$$L_3 = \sqrt{\frac{k_f}{k_{bd}} Z_{bd}\, d} \tag{8.122}$$

where:

k_{bd} = vertical permeability of the downstream blanket (m/s)

Z_{bd} = thickness of the downstream blanket (m)

The pressure head under the blanket at the downstream toe of the levee is estimated as follows:

$$h_0 = \frac{h\, L_3}{L_1 + L_2 + L_3} \tag{8.123}$$

where:

L_2 = length of impervious core or levee base (m)

This pressure head is then compared to the critical pressure head $h_b = Z_{bd}\, \gamma'/\gamma_w$, so that the factor of safety against uplift at the downstream toe of the levee is:

$$F = \frac{h_0}{h_c} = \frac{Z_{bd}}{h} \frac{\gamma'}{\gamma_w} \frac{L_1 + L_2 + L_3}{L_3} \tag{8.124}$$

8.5.2 Concentrated leak erosion

Concentrated leak erosion appears in a preferential path such as crack openings or pre-existing holes. Along this path, water flow is sufficient to initiate soil particle detachment from lateral surfaces and transport away inducing enlargement of the path. In the presence of cohesive materials able to 'hold a roof', theses openings result in the formation of a continuous tunnel called a 'pipe' between the upstream and the downstream side of the embankment or its foundation.

8.5.2.1 Model for concentrated leak erosion

The first model to interpret concentrated leak erosion was proposed by Wan and Fell (2002, and 2004a and b) for a specific type of tests, called the hole erosion test (HET) (Box 8.16 or Section 7.8.3). This test reproduces concentrated leak erosion in a pre-existing cylindrical pipe. More recently, a model combining hydrodynamic equations for a turbulent pipe flow and tangential erosion law was able to interpret more accurately experimental HET results (Bonelli *et al*, 2006, Bonelli and Brivois, 2008, Bonelli, 2012, and Benahmed and Bonelli, 2012). These models use a local erosion law, which is often written in the form of a threshold law:

$$\varepsilon = C_e \left(\tau - \tau_c\right) \tag{8.125}$$

where:

ε = eroded mass rate per unit surface (kg/m^{2}s)

τ = hydraulic shear stress applied to the surface of the hole (Pa)

τ_c = critical shear stress (Pa)

C_e = coefficient of erosion (s/m)

Critical shear stress and coefficient of erosion characterise the 'erodibility' of the soil. The critical shear stress is the minimum hydraulic shear stress required to initiate the detachment of soil particles. Below this value, no erosion is observed. The coefficient of erosion reflects the rate of the detachment of soil particles when the stress is maintained constant above the critical shear-stress. Piping occurs if $P_0 > \tau_c$ where P_0 is the driving pressure, equal to the tangential shear stress exerted by the piping flow on the

soil, and τ_c is the critical stress. The evolution of pipe radius during erosion with constant pressure drop obeys an exponential scaling law:

$$R(t) = R_0 \left[\frac{\tau_c}{P_0} + \left(1 - \frac{\tau_c}{P_0} \right) e^{+\frac{t}{t_{er}}} \right] \tag{8.126}$$

with

$$P_0 = R_0 \frac{\triangle p}{2\,L} \tag{8.127}$$

and

$$t_{er} = \frac{2\,\rho_{dry}\,L}{C_e\,\triangle p} \tag{8.128}$$

where:

P_0 = driving pressure (Pa)
τ_{er} = characteristic piping erosion time (s)
R_0 = initial radius (m)
Δp = pressure drop in the hole (Pa)
L = hole length (m)
ρ_{dry} = dry soil density (-)
C_e = Fell coefficient of soil erosion (s/m)

The Fell coefficient of soil erosion is related to the Fell erosion index by $I_e = -\log (C_e/C_{ref})$ with $C_{ref} = 1$ s/m.

Box 8.16 Hole erosion test (HET)

Concentrated leak erosion resistance of soils can be tested in laboratory using a HET apparatus (Figure 8.64).

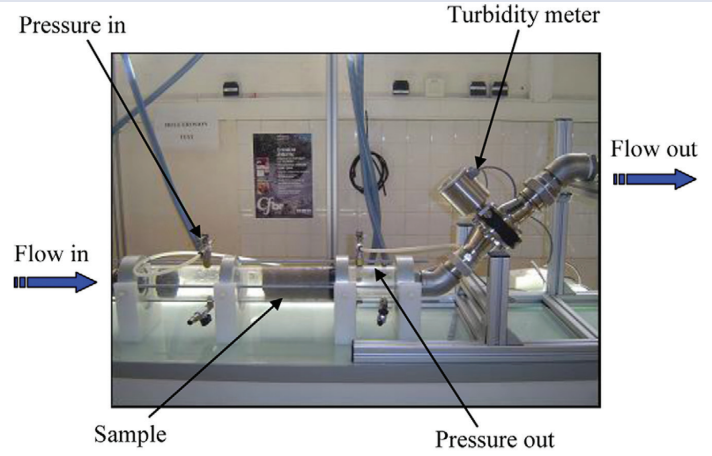

Figure 8.64 Hole erosion test (HET) apparatus at Irstea

A typical experimental result of a HET is shown in Figure 8.65. The experimental data are expressed in terms of pressure gradient and turbidity versus time.

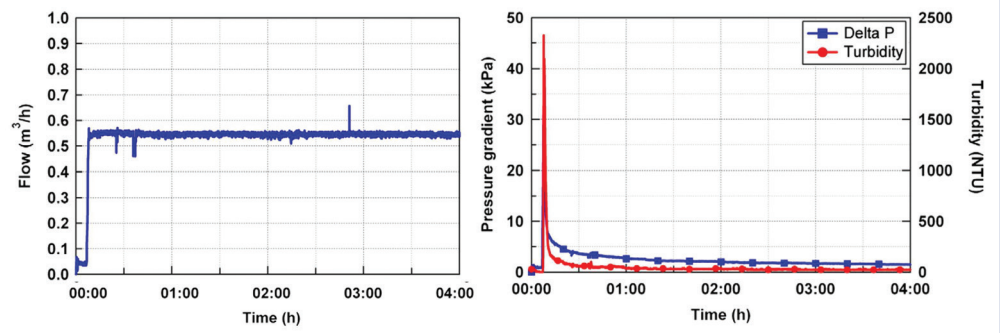

Figure 8.65 Example of evolution of turbidity and pressure gradient during a hole erosion test (Benahmed and Bonelli, 2012)

Box 8.16 *Hole erosion test (HET)*

An example of an eroded sample is shown in Figure 8.66. The longitudinal section of the sample cut at the end of the test clearly shows the enlargement of the initial hole after the erosion process. It can also be seen that the shape of the enlargement is fairly uniform.

Figure 8.66 *Example of enlargement of initial hole by erosion on white kaolinite sample, sample before the test (a), sample after the test (b), and longitudinal section of the sample after the test (c) (Benahmed and Bonelli, 2012)*

The same model as presented in Section 8.5.2.1 is used to interpret a HET and provides the values of the erodibility parameters of the soil sample, namely the critical shear stress, τ_c, and the coefficient of erosion, C_e.

8.5.2.2 Factors affecting time to failure

Consider the case of a straight and circular pipe of current radius R(t), in an embankment of height and base width (Figure 8.67) (Bonelli and Benahmed, 2011, and Bonelli *et al*, 2012).

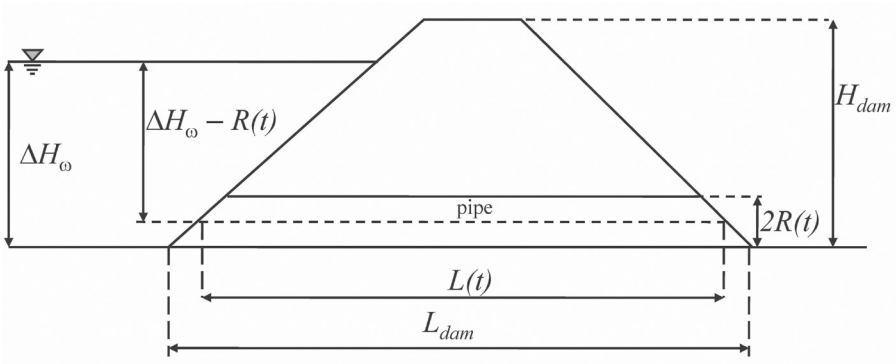

Figure 8.67 *Sketch of a pipe flow with erosion*

The rate of pipe enlargement is highly dependent on the erodibility of the soil as measured by the erosion coefficient and the critical shear stress. The enlargement of the pipe ultimately causes roof collapse and creates a breach. The scaling law of the piping erosion process with a constant hydraulic gradient is given in Equation 8.129. An expression for the time remaining to breaching can then be proposed. The piping process begins at time, t_0, with the initial radius R_0, both of which are unknown.

Visual inspection defines the initial time $t_d > t_0$ for detection and can provide an estimation of the output flow rate, and so an estimation of the radius $R_d > R_0$. R_u and t_u can be used to denote the maximum radius of the pipe before roof collapse and the collapse time, respectively. For $t > t_u$, piping failure continues to cause erosion in a way similar to that of an overtopping failure (Section 8.4.2). So, the remaining time before breaching may be estimated as follows:

$$\triangle t_u \approx t_{er} \ln\left(\frac{R_u}{R_d}\right) \propto \frac{1}{C_e} \tag{8.129}$$

This significant result means that erosion coefficient C_e can serve as an indicator of the time remaining to breaching unlike the critical shear stress τ_c. The peak flow is assumed to correspond to the maximum radius of the pipe. Consequently, the time before breaching is also the time from detection (eg eyewitness

observations) to peak discharge, and visual detection of the piping event as well as reporting are required. The following orders of magnitude (Bonelli and Benahmed, 2011) are found: if the erosion index I_e is of the order of magnitude of 2 ($C_e \approx 10^{-2}$ s/m), an d the levee failure will take place very quickly, within a few minutes. If the erosion index I_e is of the order of magnitude of 3 ($C_e \approx 10^{-3}$ s/m), the levee failure will take place within several hours. If it is greater than 4 ($C_e < 10^{-4}$ s/m), then the levee failure will not occur until several days, allowing time to take appropriate action. This coefficient can be obtained with the HET. However, the change of scale (from the laboratory to the structure) could affect the coefficient of erosion, which remains to be addressed.

8.5.3 Suffusion

Both geometric and hydraulic conditions must be fulfilled for suffusion to occur. Many granulometric criteria exist in various literature. However, one of the most commonly used is the standard proposed by Kenney and Lau (1985), which combines grain size distribution and filtration rules. More recently, Fannin and Li (2006) have compared this criterion with another proposed by Kezdi (1979) while Wan and Fell (2008) have shown that the previous commonly used methods are conservative for silt-sand-gravel or clay-silt-sand-gravel soils.

8.5.3.1 Kenney and Lau model

This model considers that grains smaller than a given diameter d can be detached if there are not enough grains in the interval (d to $4d$) to keep them trapped (Figure 8.68). They proposed the following criterion:

$$\min_{F_d<X} \left(\frac{F_{4d}}{F_d} - 1 \right) \geq 1 \tag{8.130}$$

where:

d = diameter of grains (m)

F_d = cumulative mass percentage of grains smaller than the diameter d (-)

For coefficient of uniformity of the soil (C_u, defined as the ratio d_{60}/d_{10}) smaller than 3, the parameter X is taken equal to 0.3. For $C_u \geq 3$, it may be taken equal to $X = 0.2$.

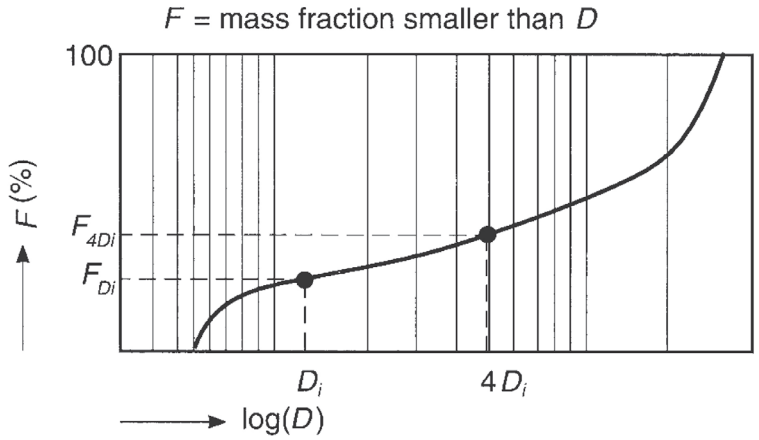

Figure 8.68 Definition of cumulative mass percentage criterion (from CIRIA; CUR; CETMEF, 2007)

8.5.3.2 Model of Kezdi

This model proposes a simpler criterion:

$$\min_{d} (F_{4d} - F_d) \leq 0.15 \tag{8.131}$$

This criterion is more conservative than the Kenney and Lau model for $F_d < 0.15$.

8.5.3.3 Li and Fannin approach

Using some new experiments and those existing in various literature, Li and Fannin (2008) have recently proposed to use Kezdi criterion for gap-graded size distribution whereas Kenney and Lau criterion is suited for widely-graded soils as shown in Figure 8.69.

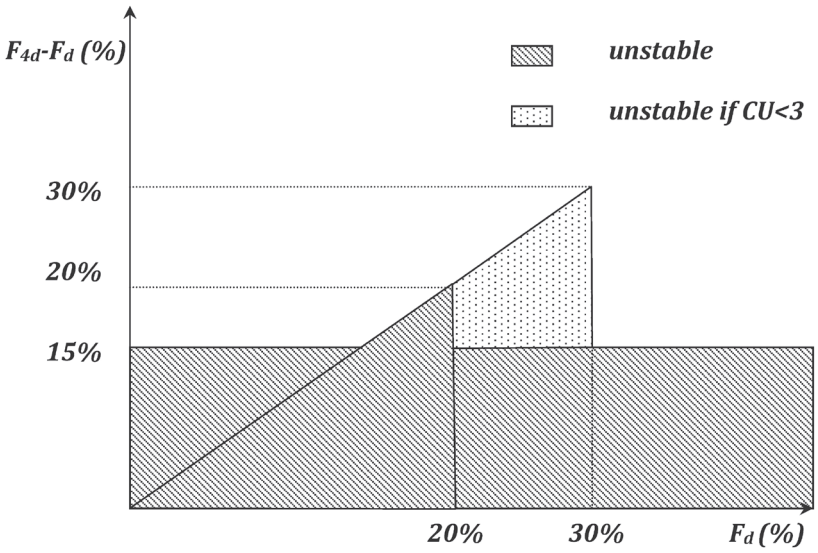

Figure 8.69 Graphical synthesis of Kenney and Lau and Kezdi approaches

Li (2008) proposed also a hydro-mechanical criterion in terms of threshold hydraulic gradient, validated for experiments on unstable soils, which is simply a fraction of the critical gradient i_{Cr} first introduced by Terzaghi:

$$i_{suf} = \chi\, i_{cr} = \chi\, \frac{\gamma'}{\gamma_w} \tag{8.132}$$

with:

$$\chi = 3.85\, \frac{d'_{85}}{O_{50}} - 0.616 \tag{8.133}$$

where:

i_{suf} = threshold hydraulic gradient initiating suffusion (-)
i_{Cr} = critical hydraulic gradient initiating heave (-)
d'_{85} = d_{85} of the fine fraction of soil (m)
O_{50} = effective constriction size of the coarse fraction (m)

The χ parameter generally falls between one-fifth and one-third. Other methods may be used in the case of well-graded soils (Burenkova, 1993, and Lubockov, 1965).

8.5.4 Contact erosion

As in suffusion, both geometric and hydraulic conditions must be fulfilled. But unlike suffusion, which concerns a unique material with a broad graded grain size distribution, contact erosion appears at the interface between two different materials having distinct grain size distributions. Consequently, the geometric condition for contact erosion to occur is simply fulfilled when the classical filter rules are not satisfied and the studies related to contact erosion have mainly focused on hydraulic threshold.

Most of the models proposed for contact erosion are dedicated to the first configuration, ie underlying fine material layer with non-cohesive soils (sand). They result from an adaptation of Shields criterion (Shields, 1936) with an empirical coefficient that accounts for the specific geometry of the coarse layer (Brauns, 1985, and Bezuijen *et al*, 1987). Darcy velocity has been chosen by the majority of the models' authors as a good indicator of the hydraulic loading. This threshold reads:

$$U_{cr} = \alpha\, n_D \sqrt{\frac{\gamma'}{\gamma_w} g\, d_{50}} \tag{8.134}$$

where:

α = empirical coefficient (-)
n_D = porosity of the coarse layer (-)
γ' = buoyant specific weight (kN/m^3)
γ_w = unit weight of the water (10 kN/m^3)
d_{50} = median diameter of sand grading curve (m)

The empirical coefficient α is equal to 0.65 as proposed by Brauns (1985), or depends on the type of fine soil and flow characteristics (Bezuijen *et al*, 1987). More precisely, Béguin *et al* (2013) showed that α may be explained by the existence of a hydrodynamic transition zone just above the layer of the fine soil.

The inverse configuration as well as cohesive soils have been studied recently (Schmitz, 2007, Guidoux *et al*, 2010, and Beguin, 2011). Based on experimental results of contact erosion tests with silts and clays, Guidoux *et al* (2010) adapted empirically Brauns' expression to take into account the adhesive forces. Beguin (2011) proposed to use the same threshold erosion law as for concentrated leak erosion (Section 8.4.3). This requires a relation between shear stress and hydraulic gradient (or equivalently Darcy velocity) as the ones proposed by Reddi *et al* (2000) or Wörman and Olafsdottir (1992). Note that for cohesive soils, Béguin (2011) also successfully used the excess shear stress erosion law proposed for concentrated leak erosion. Information from all of these sources is summarised in Figure 8.70.

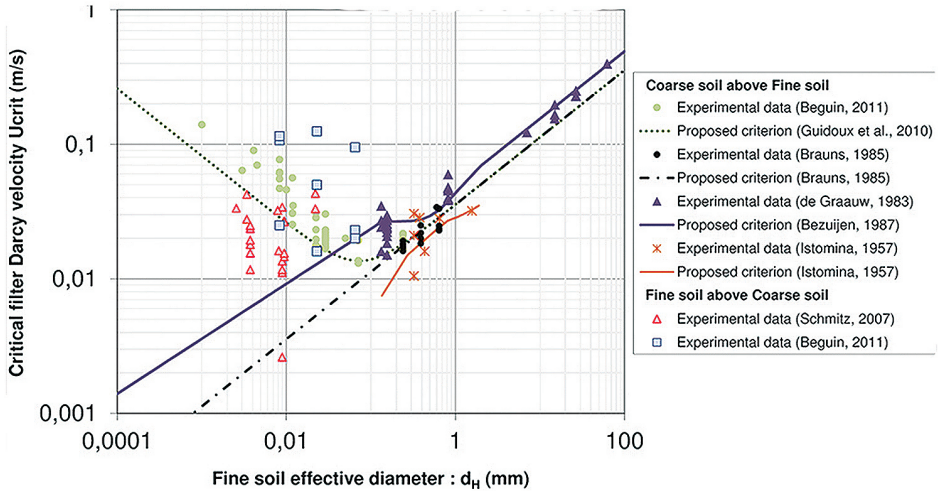

Figure 8.70 ***Summary of experimental data and models for the critical Darcy velocity at the initiation of contact in the configuration with a coarse material over a layer of fine soil (Béguin, 2011)***

8.5.5 Interface stability of filters

8.5.5.1 Granular filters

Granular filters have to fulfil five requirements:

- soil retention
- drainage
- self-filtering
- not crushable
- not cohesive.

The crushability of the filter depends on the nature of soil particles. For silicate soil particles, it may be assumed that this criterion is intrinsically met as long as no shear failure develops within the drain. The

non-cohesiveness is generally met when the fine content FC < 5 per cent, and self-filtering is guaranteed when the filter is not subjected to suffusion (Section 8.5.3). The following paragraphs will focus on the first two requirements.

The filter stability at the interface of two different granular materials is called interface stability. The finer of the two materials is called the 'base' (index *b*) and the coarser the 'filter' (index *f*).

Terzaghi retention criterion

For a matrix consisting of grains of diameter D, a particle of diameter d is prevented from being transported through the matrix, based on geometrical considerations, using criterion developed by Terzaghi (1940):

$$\frac{D_{15}}{d_{85}} < 4 \text{ to } 5 \tag{8.135}$$

where:

D_{15} = particle size diameter for 15 per cent passing of the filter (mm)
d_{85} = particle size diameter for 85 per cent passing of the base soil (mm)

This purely geometric retention criterion has been shown to be generally quite conservative and applicable for truncated $d < 4.75$ mm fraction of the soil.

When the soil has relatively few particles in a certain size range, the soil may be considered as 'gap-graded' and the grading curve may be characterised by a concave shape with a relatively flat curve in the intermediate range. The criteria mentioned here may still be relevant provided that it is considered as a mixture of two subgradings with quite different particle size ranges. When the base is gap-graded, the d_{85base} value may be replaced by the sieve size d'_{85base} (mm) of the smaller of the two subgradings. Mlynarek *et al* (1993) suggest that this size may more or less correspond to the D_{30base} of the overall base material. So, the Terzaghi criterion would become:

$$\frac{d_{15f}}{d_{30b}} < 5 \tag{8.136}$$

Criteria for design purposes

Based on extensive laboratory research, Sherard and Dunnigan (1985 and 1989) proposed filter design criteria for drains based on the distinction of four soil classes. These criteria, presented in Table 8.22, are generally well accepted by practitioners for design purposes of new structures.

Table 8.22 Filtering criteria of Sherard and Dunnigan (1989)

FC	Soil class	Filter condition
< 15 %	Sand, gravel	$d_{15f} < 4d_{85b}$
15–40%	Silty and clayey sands	$d_{15f} < 0.7 + (40–FC)\,(4d_{85b}–0.7)/25$
40–85 %	Sands, silts, clays	$d_{15f} < 0.7$ mm
> 85 %	Fine silts, clays	$d_{15f} < 9d_{85b}$
FC: percentage of fines passing 75µm (%)		

Criteria for assessment purposes

Based on an extensive investigation of existing dams, Foster and Fell (2001) showed that the criteria previously defined include some built-in factors of safety. They proposed less conservative criteria adapted to the assessment of filter performance of existing hydraulic structures. Although it has been shown that other factors such as clay content influence the erosion behaviour of the filter, the D_{15}/d_{85} ratio is so dominant that these new criteria only use this ratio (Table 8.23).

Table 8.23 Filtering criteria of Foster and Fell (2001)

Base soil	Filter condition	
d_{95b} < 0.3 mm		$d_{15f} < 9\ d_{95b}$
0.3 mm < d_{95b} < 2 mm		$d_{15f} < 9\ d_{95b}$
d_{95b} > 2 mm	FC < 15%	$d_{15f} < 7\ d_{85b}$
	15% < FC < 35	$d_{15f} < 1.6\ (0.7 + (35–FC)\ (4\ d_{85b}–0.7)/20)$
	35% < FC < 85	$d_{15f} < 0.7$ mm
	FC > 85	$d_{15f} < 9\ d_{85b}$
FC = percentage of fines passing 75μm (%). Criteria are applicable if d_{95b} < 4.75 mm. Otherwise, passing has to be determined on the 0 mm to 4.75 mm fraction.		

Giroud's approach

Giroud (2003) suggested that the approach used for geotextile filters could also be used for granular filters. This approach leads to the graph shown in Figure 8.71 for the proposed retention criterion for granular filters in the case of a dense soil. The retention criteria proposed by Terzaghi, is represented by the horizontal dashed line in the graph. For large coefficients of uniformity, greater than five, Terzaghi's retention criteria may be unconservative. It is for this reason that truncation of the particle size distribution curve is traditionally employed in the design of granular filters. Truncation artificially decreases the coefficient of uniformity of the soil to compensate for this potential unconservatism in the case of high coefficients of uniformity. The graph shown in Figure 8.71, as proposed by Giroud (2003), is applicable regardless of the maximum particle size and is not limited to particles smaller than 4.75 mm.

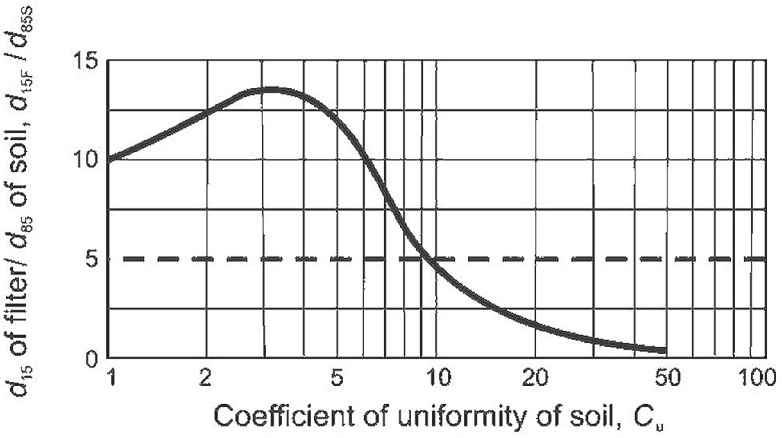

Figure 8.71 Retention criterion for granular filters for the case of dense soils (after Giroud, 2003)

Permeability requirements

The general requirements relative to permeability are $k_f > 3.5\ 10^{-5}$ m/s and $k_f/k_b > 25$. Considering the Vaughan and Soares' formula, this condition is equivalent to the following geometrical criteria:

$$d_{15f} > 0.1\,\text{mm} \tag{8.137}$$

and

$$\frac{d_{15f}}{d_{15b}} > 5 \tag{8.138}$$

8.5.5.2 Geotextile filters

Geotextile filters have to be designed and installed carefully as defined in Chapter 9.

Soil retention requirements

The criterion for interface stability of a geotextile filter is generally formulated according to a geometrically tight principle. The filtration opening size of the geotextile filter O_{95} (Figure 8.72) should meet the following:

$$D_{min} \leq O_{95} \leq D_I \tag{8.139}$$

where:

D_{min} = largest fine particle being transported in suspension (mm)
D_I = indicative diameter of the soil particle to be filtered (mm)

Giroud *et al* (1998) estimated the minimum value D_m in ≈ 50 μm. The diameter of the particles to be filtered may be estimated (AFNOR, 1993):

$$D_I = C\, d_{85b} \tag{8.140}$$

where C is a coefficient depending on the state of the soil. For example, for a uniform soil ($C_u < 5$), the coefficient may be taken as $C = 0.4$ if the soil is in a loose state and $C = 0.6$ for a soil in a dense state. In the case of non-cohesive soils with uniformity coefficient $C_u > 5$, criteria proposed by Giroud (1988) may be used. If the soil is dense ($I_D > 50$ per cent) then:

$$D_1 = 18 C_u^{-1.7} d_{85b} \tag{8.141}$$

If the soil is loose ($I_D < 50$ per cent), then:

$$D_1 = 9 C_u^{-1.7} d_{85b} \tag{8.142}$$

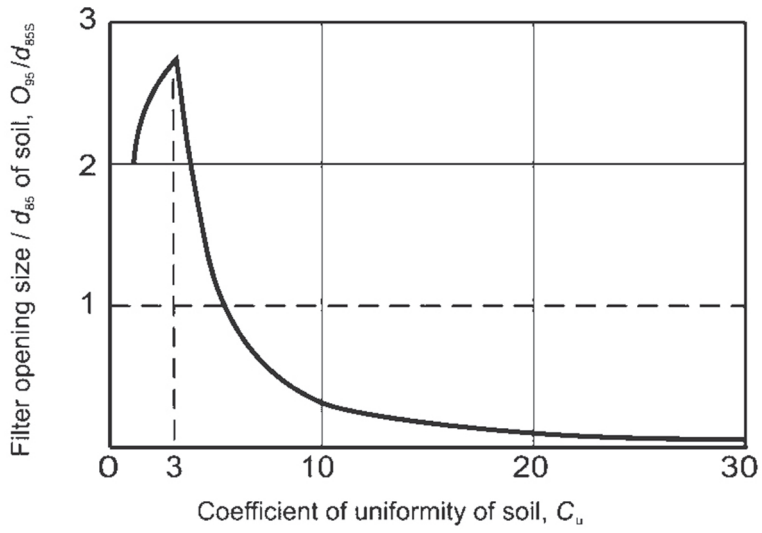

Figure 8.72 Retention criterion for geotextile filters for the case of dense soils (from Giroud, 1982)

Permeability requirements

Because the geotextile permeability may be reduced considerably during its lifetime (blocking, clogging etc) the target values of permeability are generally much higher than those required for granular filters. The permeability requirements are defined in terms of a permeability ratio as shown in Table 8.24.

Table 8.24 Permeability requirements for geotextile filters

Type of structure	k_f/k_b
Coastal protection structures	≥ 100
Hydraulic structures	≥ 100
Standard dewatering trench	≥ 10

It is important to mention that the minimum values correspond to long-term reduced values.

8.6 SLOPE STABILITY

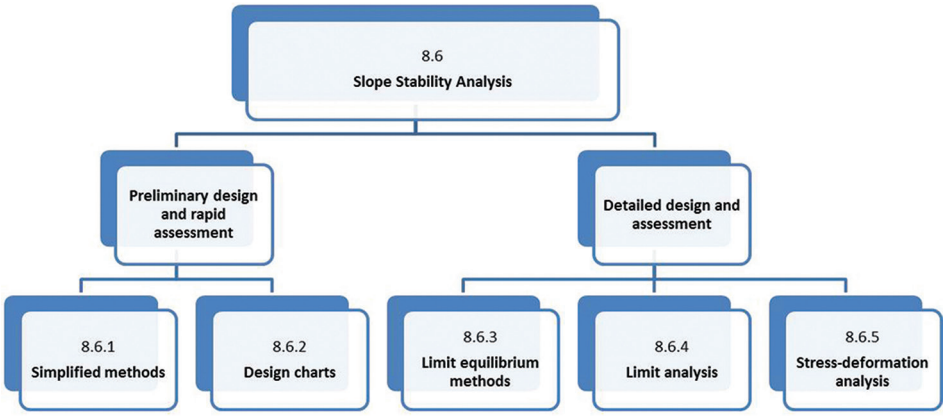

Slope sliding is one of the prevalent forms of instability encountered in levees and will be detailed in this section according to the flowchart. It is a 3D phenomenon in which a certain volume of soil moves down the slope under the influence of gravity and/or external actions. The sliding mass is bounded above by the surface of the slope and bellow by a surface of sliding (Figure 8.73) characterised by a discontinuity in strain and velocity field (it is in fact a transitional zone generally sufficiently thin to be considered as a surface as regards to the sling soil volume).

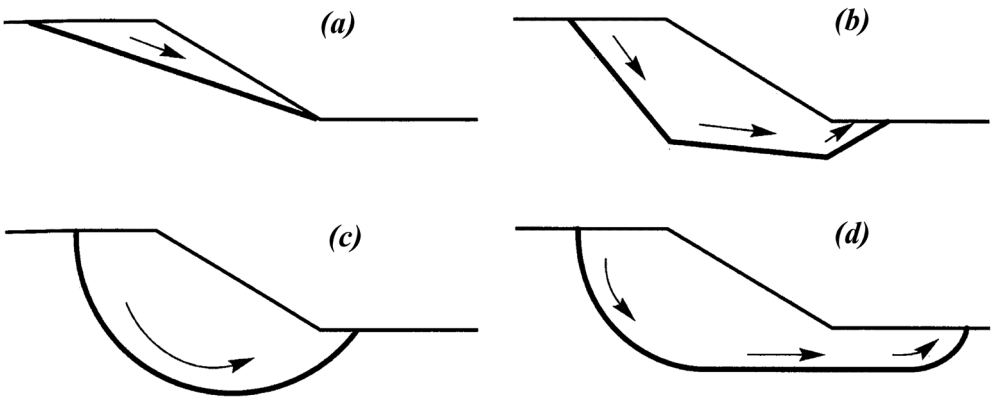

Figure 8.73 Common failure surface geometries: planar (a), multiplanar (b), circular (c), and noncircular (d)

Theoretical analysis of homogeneous slope stability (Baker and Garber, 1978) leads to the determination of two families of possible critical slip surfaces. The first is a straight line, the second a logarithmic spiral. In reality, the homogeneous case is marginal and the failure surfaces often have different shapes, which mostly depend on the geometrical model, the geological context and the hydro-geological condition.

Slope stability analysis methods

The procedures for analysis of slope stability under static conditions are well-established. Currently, the most used methods of static slope stability analysis are:

- limit equilibrium analyses
- stress-deformation analyses.

Theoretical and practical comparison of some approaches has been provided in the literature (Jiang and Magnan, 1997, Yu *et al*, 1998, and Duncan, 1996). These approaches share some common features, and different theoretical backgrounds, which should be understood by engineers applying these methods.

2D versus 3D analysis

Most of the slope stability methods have been developed in the 2D plane strain context, but have also been extended to 3D. 3D analysis may be a more accurate representation of the critical failure surface, however, there are valid arguments to continue the use of 2D models in practice.

From a theoretical point of view, it has been proven that for a given slope the 3D factor of safety always exceeds the 2D factor of safety (Cavounidis, 1987). From a practical point of view, Duncan (1996) showed that this theoretical result was generally verified on actual cases and that in publications showing otherwise, significant inaccuracies and simplifying assumptions led to neglect of important aspects of the problem. In particular, it is noted that a 2D factor of safety is calculated for the most critical 2D section. Here, the use of any rule of thumb, such as a 10 per cent increase to compensate for the neglect of 3D effects, is not advisable in all cases because the ratio between the two may vary within a range of 1.0 to as high as 1.4 (Morgenstern, 1992, and Hungr *et al*, 1989).

Moreover, the validity of 2D slope stability methods has been demonstrated by back analysis of actual cases and models, as well as by extensive practical applications. From a numerical point of view, this generalisation to 3D models are still quite consuming in terms of resources and implies complementary assumptions (except for numerical methods), which may be difficult to calibrate and pose additional problems of numerical convergence.

Therefore, for all these reasons, the slope stability problem is generally simplified in a 2D problem in plane strain state. In this handbook, guidance and technical references have been developed for the 2D plane strain formulation. However, 2D analysis may need attention when estimating the strength of certain materials through back analysis (for example, in the diagnosis of an existing levee). Neglecting a strong 3D effect in the back analysis may result in a serious over-estimation of the back-calculated strength.

Effective versus total stress analysis

For given loading and drainage conditions the response of the soil may be considered as drained or undrained. In the undrained case, the analysis has to be performed in total stress, considering undrained shear strength parameters, whereas in the drained case, an effective stress analysis considering effective shear strength parameters is relevant. Given that the slope stability analysis methods do not presume the type of analysis performed, the shear strength parameters involved in their description may be either effective or undrained shear strengths (Duncan 1996).

Accuracy of the methods

The accuracy of a slope stability method depends on:

- governing parameters estimation, ie the accuracy with which the geological model, strength properties, pore water pressure and geometric conditions can be defined
- the inherent accuracy of the method of analysis
- the degree of understanding of the program by the engineer and ability to evaluate the results to avoid mistakes and misuse.

In most cases, the uncertainties related to definition of geometry, pore water pressures and soil properties are greater than those that arise from the approximations involved in the analytical technique. In this section, it is considered that the most accurate evaluation of the geometrical

and geological model has been made and that the characteristic values of each soil layer have been determined (Chapter 7). The stability analysis conditions and the choice of the shear strength parameters to be used are also assumed to have been appropriately determined (Chapter 9). The tools concerning the determination of pore water pressure issues are addressed in different sections: pore water pressure build-up related to consolidation processes is treated in Section 8.7 concerning settlement analysis, and wave-induced pore water pressure is discussed in Section 8.3.2.

In the following sections, focus is given to the presentation of the methods of analysis in terms of their inherent accuracy to provide guidance for choosing an appropriate slope stability analysis method according to the need and the tools the engineer can mobilise. The presentation follows a tiered approach presenting the different alternatives from the simplest (stability charts and simplified methods) to the most complex (numerical analysis).

8.6.1 Simplified methods

The simplified methods may be used as preliminary verification in the case of levees resting on soft soils. They should be completed by limit equilibrium or stress-deformation methods according to the relevant geotechnical standards.

8.6.1.1 At-rest pressure approach

The at-rest earth pressure method is used to estimate the potential for lateral spreading and horizontal sliding of an embankment, as shown in Figure 8.74.

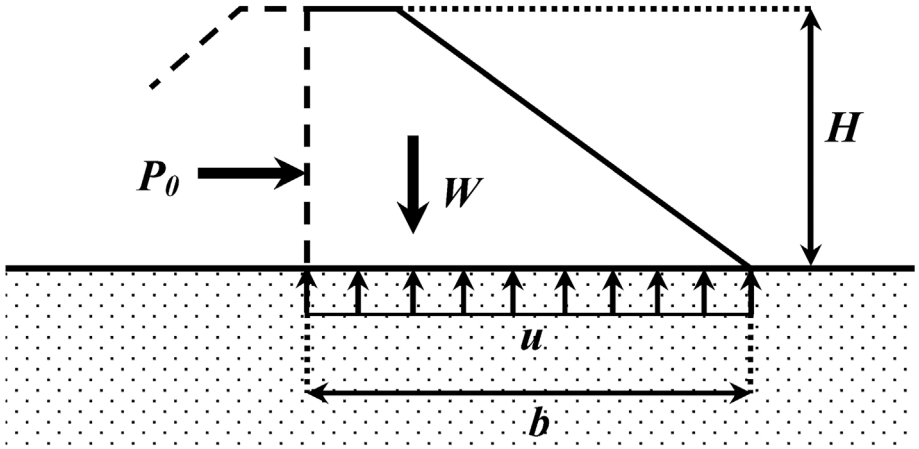

Figure 8.74 At rest pressure approach for stability analysis

The method compares the at-rest earth pressure, P_0, on a vertical plane through the embankment to the shear resistance along the base of the embankment. The method is only partly a limit equilibrium method, because the at-rest earth pressures are calculated independently of any equilibrium conditions and then compared to the limiting shear resistance. The safety factor is expressed as:

$$F_s = 2\frac{cb + (W - ub)\tan\varphi}{K_0 \gamma H^2} \tag{8.143}$$

where:

c = cohesion along the embankment-foundation contact (kPa)
φ = friction angle along the embankment-foundation contact (°)
u = average pore water pressure along embankment-foundation contact (kPa)
K_0 = at-rest earth pressure coefficient (-)
γ = unit weight of embankment (kN/m^3)
d = half width of the levee (m)
H = height of the levee above foundation (m)

Ensuring that an embankment has an adequate factor of safety by this analysis will assist in limiting deformation where two or more materials with significantly different stress-strain behaviour are present. A common example application is a zoned levee with a clay core.

8.6.1.2 Bearing capacity approach

The concept of bearing capacity of the foundation refers to a criterion of shear failure of the foundation for punching failures. These are failures of the foundation soil characterised by the fact that the embankment collapses while undergoing traction. The failure of the foundation is general because it concerns the entire width of the embankment. The failure pattern of the foundation soil is similar to that which occurs under a shallow foundation, and can be studied as such.

The bearing capacity methods are limited to homogeneous foundations where simple bearing capacity equations are applicable. These methods are also used primarily for evaluating short-term, undrained stability of embankments resting on soft, saturated clay foundations. These methods are intended only for preliminary analyses and for use as an approximate check of more rigorous and thorough analyses.

This simple bearing capacity approach ignores the shear strength of the embankment fill and is conservative in this respect. Because the shear strength of the embankment material is ignored, questions about incompatibility between the stress-strain behaviour of the embankment and the foundation do not arise. Although more sophisticated approximations can be made, bearing capacity analyses should not be considered to be a substitute for detailed slope stability analyses.

When new levees or projects of heightening of existing levees are concerned, the worst case is generally the end of construction (short-term situation). So, the stability check should assume the embankment being built instantly, without dissipation of pore pressures in the foundation: the short-term undrained characteristics have to be considered.

The bearing capacity limit state is defined by the same methodology as the one concerning rigid footings stability, considering the design vertical stress $q = \gamma H$. The limit pressure on a soil with undrained cohesion C_u can be written:

$$q_f = N_c c_u \tag{8.144}$$

where:

N_c = a factor function of b/t
b = is the half-width of the embankment
t = the thickness of soft cohesive foundation

Several authors have established bearing capacity factors (Prandtl, Terzaghi, Meyerhof, Hansen, Vesic, Mandel and Salençon etc) in function of unit weight, cohesion and friction angle of a uniform semi-infinite soil layer, but generally in the case of a rigid footing. Michalowski (1993) proposed a solution taking into account a finite thickness of soft cohesive foundation t. The boundary condition at the contact with the soft soil embankment is characterised by the parameter χ defined as:

$$\chi = \frac{\tau_m}{c_u} \tag{8.145}$$

where τ_m is the mean shear stress at the base of the embankment, and the roughness of the contact soft soil-substratum is characterised by the parameter κ defined as:

$$\kappa = \frac{c_0}{c_u} \tag{8.146}$$

where c_0 is the shear resistance at the base interface.

The bearing capacity factor N_c may then be determined from Figure 8.75. This figure shows that for a perfect contact interface between the embankment and its foundation ($\chi = 0$) and a semi-infinite foundation layer (b/t = 0), the N_c factor takes the classical value of $\pi + 2$.

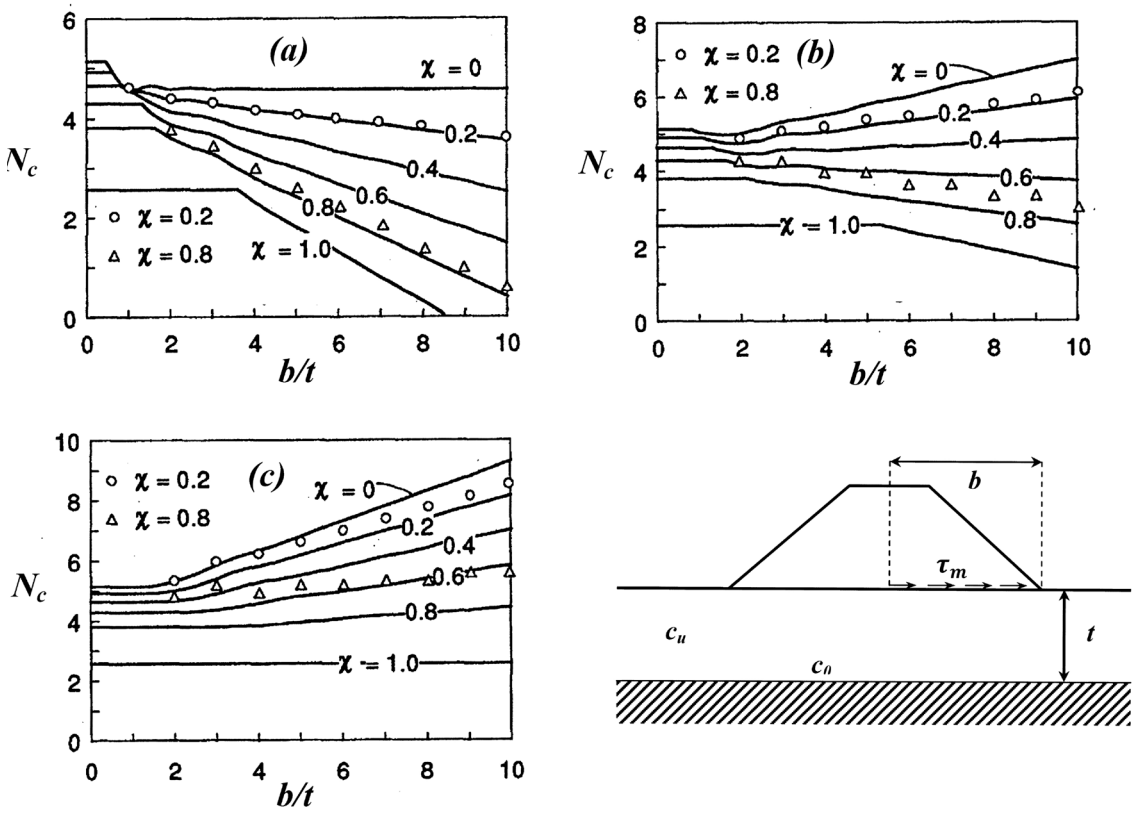

Figure 8.75 *Dimensionless limit load q/c for outward horizontal loads on the foundation layer, homogeneous soil: smooth base (a), base interface strength equal to half of the shear strength of the soil (b), perfectly rough base (c). Solid lines indicate the numerical solution and bullets mark the closed-form solution (from Michalowski, 1993)*

8.6.2 Design charts

Slope stability charts provide a means for rapid analysis of slope stability. They can be used for preliminary analyses, for checking detailed analyses, or for complete analyses. They are especially useful for making comparisons between design alternatives, because they provide answers so quickly. The accuracy of slope stability charts is usually as good as the accuracy with which shear strengths can be evaluated.

In this section, chart solutions are presented for four types of slopes:

- slopes in soils with $\varphi = 0$ and uniform strength throughout the depth of the soil layer
- slopes in soils with $\varphi > 0$ and $c > 0$ and uniform strength throughout the depth of the soil layer
- infinite slopes in soils with $\varphi > 0$ and $c = 0$ and soils with and $\varphi > 0$ and $c > 0$
- slopes in soils with $\varphi = 0$ and strength increasing linearly with depth.

Using approximations in slope geometry and carefully selected soil properties, these chart solutions can be applied to a wide range of nonhomogeneous slopes.

Averaging procedure

For simplicity, charts are developed for homogenous soil conditions with simplified slopes. To apply these to complex conditions, it is necessary to approximate the real conditions with an equivalent simplified slope. The most effective method of developing a simple slope profile for chart analysis is to begin with a cross-section of the slope drawn to scale. On this cross-section, using judgment, draw a geometrically simple slope that approximates the real slope as closely as possible.

Shear strength averaging

To average the shear strengths for chart analysis, it is useful to know the location of the critical slip surface. The charts contained in the following parts of this section provide a means of estimating the position of the critical circle. Average strength values are calculated by drawing the critical circle, determined from the charts, on the slope. Then the central angle of arc subtended within each layer or zone of soil is measured with a protractor. The central angles are used as weighting factors to calculate weighted average strength parameters, c^* and φ^* as follows:

$$c^* = \frac{\sum \theta_i c_i}{\sum \theta_i} \tag{8.147}$$

$$\varphi^* = \frac{\sum \theta_i \varphi_i}{\sum \theta_i} \tag{8.148}$$

where:

c^* = average cohesion (kPa)
φ^* = average angle of internal friction (°)
θ_i = central angle of arc, measured around the centre of the estimated critical circle, within zone i (°)
c_i = cohesion in zone i (kPa)
φ_i = angle of internal friction in zone i (°)

To average the unit weights for use in chart analyses, it is usually sufficient to use layer thickness as a weighting factor, as indicated by the following expression:

$$\gamma^* = \frac{\sum h_i \gamma_i}{\sum h_i} \tag{8.149}$$

where:

γ^* = average unit weight (kN/m^3)
γ_i = unit weight of layer i (kN/m^3)
h_i = thickness of layer i (m)

Unit weights should be averaged only to the depth of the bottom of the critical circle. If the material below the toe of the slope is a $\varphi = 0$ material, the unit weight should be averaged only down to the toe of the slope, since the unit weight of the material below the toe has no effect on stability in this case.

Use of the charts

The slope stability charts were developed by Janbu (1973)as described following:

- for purely cohesive soils refer to Figure 8.76
- for $\varphi > 0$ soils refer to Figure 8.77
- for frictional soils refer to charts providing adjustment factors for surcharge loading at the top of the slope as shown in Figure 8.78
- charts providing adjustment factors for submergence and seepage are shown in Figure 8.79
- charts providing adjustment factors to account for tension cracks are shown in Figure 8.80.

First, the engineer has to decide which cases should be investigated. For uniform soil conditions, the critical circle passes through the toe of the slope if the slope is steeper than about 1H/1V. For flatter slopes, the critical circle usually extends below the toe, and is tangent to some deep firm layer. The chart in Figure 8.76 can be used to compute factors of safety for circles extending to any depth. Multiple possibilities should be analysed, to be sure that the overall critical circle and overall minimum factor of safety have been found. The following criteria can be used to determine which possibilities should be examined:

- if a soil layer is weaker than the one above it, the critical circle may be tangent to the base of the lower (weaker) layer. This applies to layers both above and below the toe
- if a soil layer is stronger than the one above it, the critical circle may be tangent to the base of either layer, and both possibilities should be examined. This applies to layers both above and below the toe.

The following steps are performed for each circle:

- calculate the depth factor $d = D/H$ where D is the depth from the toe of the slope to the lowest point on the slip circle and H the slope height above the toe of the slope. The value of d is 0 if the circle does not pass below the toe of the slope. If the circle being analysed is entirely above the toe, its point of interaction with the slope should be taken as an 'adjusted toe', and all dimensions like D, H, and Hw has to be adjusted accordingly in the calculations
- find the centre of the critical circle using the charts at the bottom of Figure 8.76
- determine the average value of the strength for the circle considered, using the previously developed averaging procedure
- calculate the quantity P_d using the formula:

$$P_d = \frac{\gamma H + q + \gamma_w H_w}{\mu_q \mu_w \mu_t} \tag{8.150}$$

where:

γ	=	average unit weight of homogenous soil (kN/m^3)
H	=	slope height above toe (m)
q	=	surcharge (kPa)
γ_w	=	unit weight of water (kN/m^3)
H_w	=	height of external water level above toe (m)
μ_q	=	surcharge adjustment factor (-), see Figure 8.78
μ_w	=	submergence adjustment factor (-), see Figure 8.79
μ_t	=	tension crack adjustment factor (-), see Figure 8.80

- use the chart at the top of Figure 8.76, determine the value of the stability number, N_0, which depends on the slope angle, β, and the value of d. The factor of safety can be estimated following the formula:

$$F_s = N_0 \frac{c}{P_d} \tag{8.151}$$

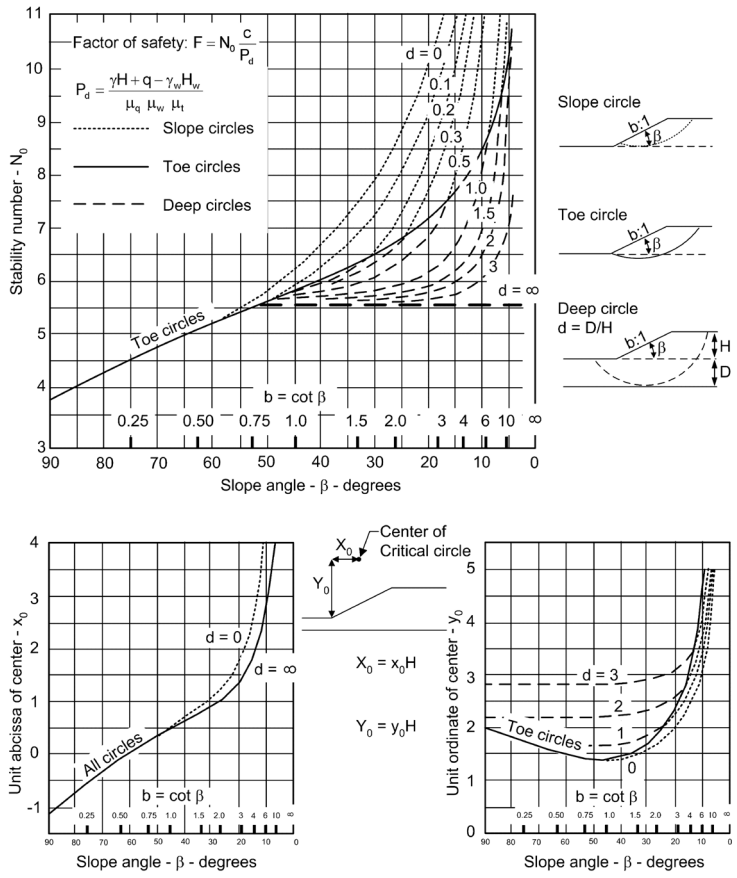

Figure 8.76 Slope stability chart for purely cohesive soils (from USACE, 2003)

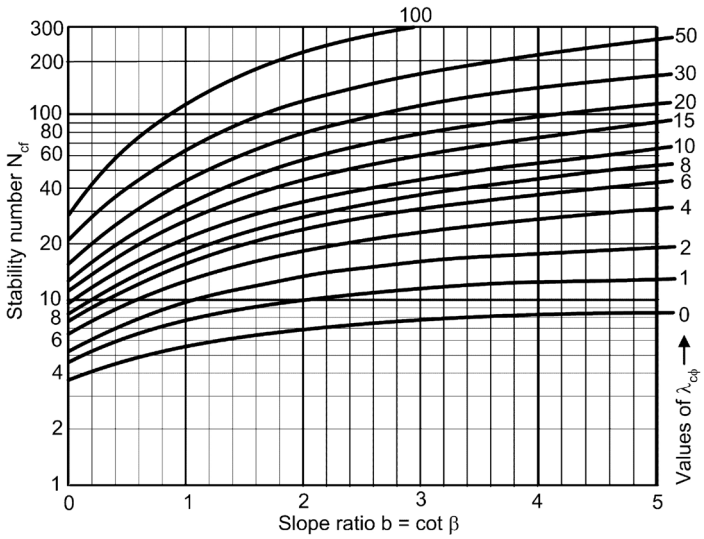

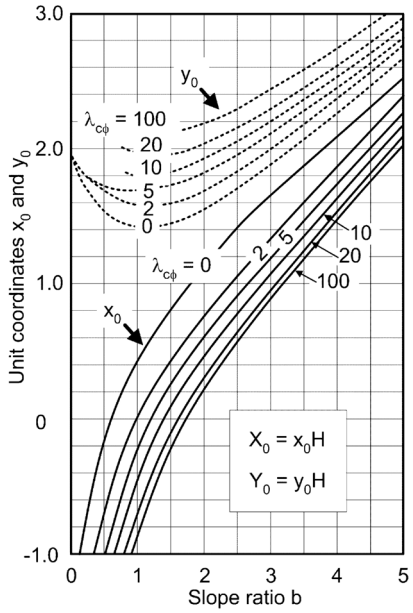

$$F = N_{cf}\frac{c}{P_d} \qquad P_d = \frac{\gamma H + q - \gamma_w H_w}{\mu_q \mu_w \mu_t}$$

$$\lambda_{c\phi} = \frac{P_e \tan\phi}{c} \qquad P_e = \frac{\gamma H + q - \gamma_w H'_w}{\mu_q \mu_w}$$

Stability numbers and center coordinates for circles passing through the toe of the slope.

Figure 8.77 Slope stability chart for $\varphi > 0$ soils (from USACE, 2003)

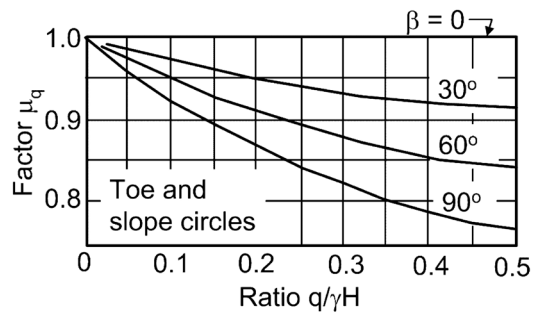

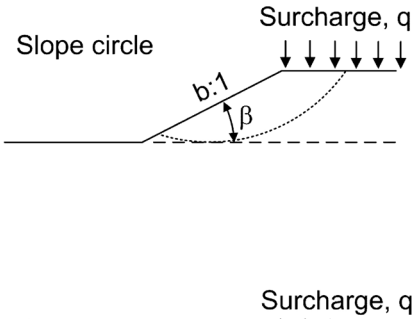

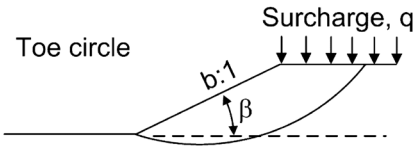

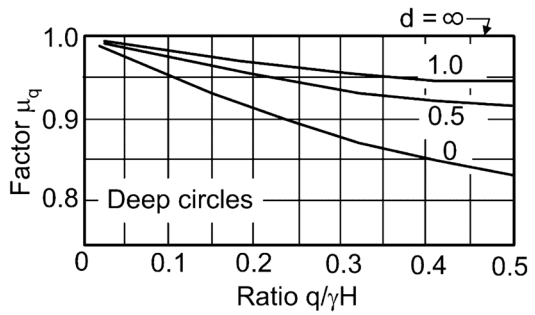

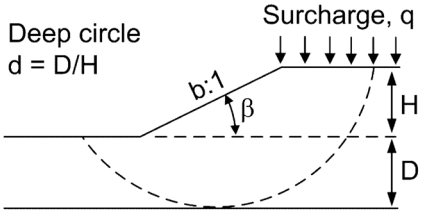

Figure 8.78 Surcharge adjustment factors (from USACE, 2003)

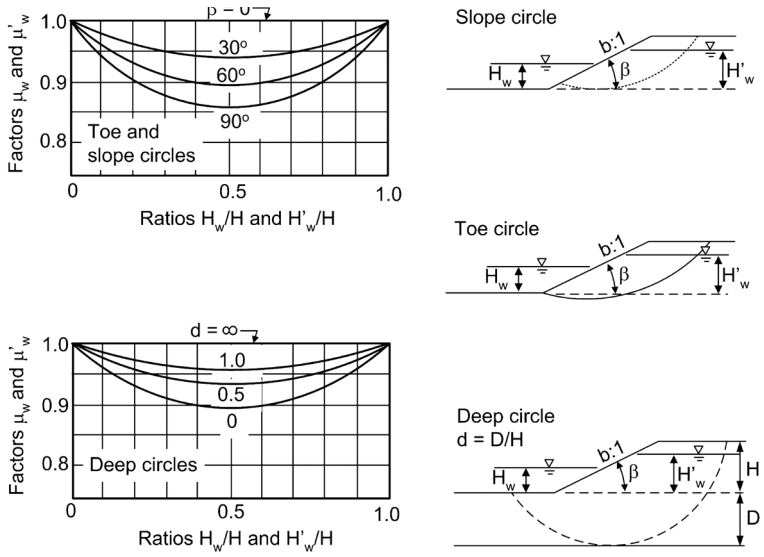

Figure 8.79 Submergence and seepage adjustment factors (from USACE, 2003)

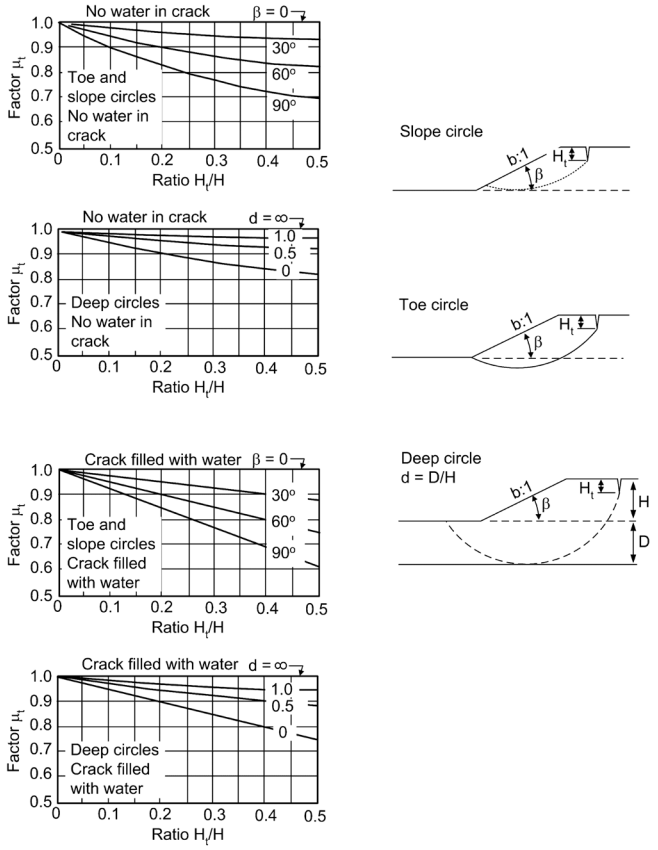

Figure 8.80 Tension crack adjustment factors (from USACE, 2003)

For frictional soils, one has to calculate the P_d parameter and then calculate the parameter P_e using the formula:

$$P_e = \frac{\gamma H + q + \gamma_w H'_w}{\mu_q \mu'_w} \tag{8.152}$$

where:

H_w' = height of water within slope (m)

μ_w' = seepage correction factor (-)

H_w' = the average level of the piezometric surface within the slope. For steady seepage conditions this is related to the position of the phreatic surface beneath the crest of the slope as shown in Figure 8.81. If the circle being studied passes above the toe of the slope, H_w' is measured relative to the adjusted toe.

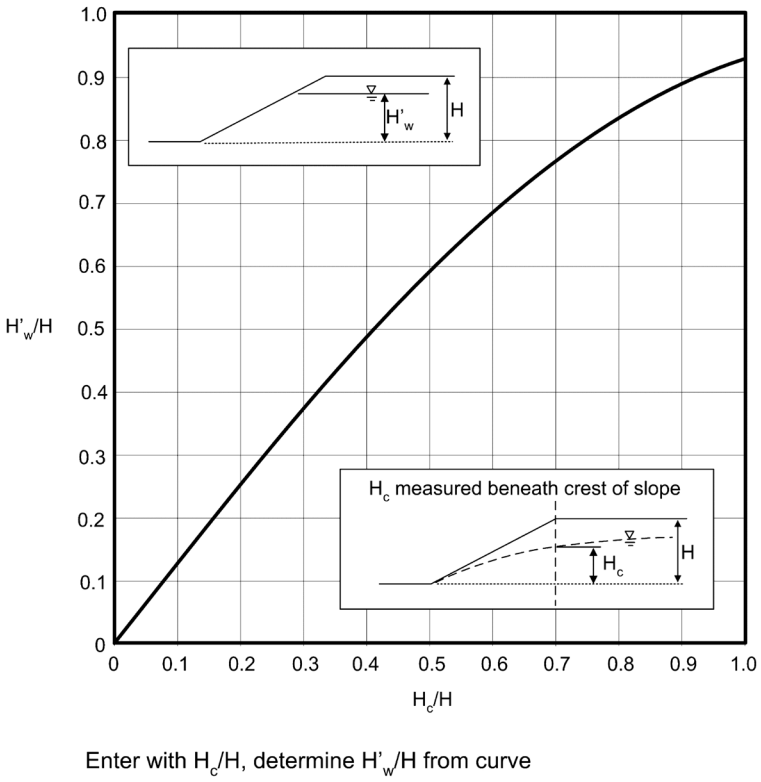

Figure 8.81 Steady seepage adjustment factor for $\varphi > 0$ soils (after Duncan et al, 1987)

The default values of adjustment factors are $\mu_w' = 1$ if there is no seepage and $\mu_q = 1$ if there is no surcharge. In a total stress analysis, internal pore water pressure is not considered, so $H_w' = 0$ and $\mu_w' = 1$ in the formula for P_e. Calculate the dimensionless parameter P_c using the formula:

$$\lambda_{c\varphi} = P_e \frac{\tan\varphi}{c} \tag{8.153}$$

where:

φ = average value of φ (°)
c = average value of c (kPa)

Then, it is possible to estimate the factor of safety, F_s, using the formula:

$$F_s = N_{cf} \frac{c}{P_d} \tag{8.154}$$

8.6.3 Limit equilibrium methods

Limit equilibrium analysis method has been the most popular method for slope stability calculations. A major advantage of this approach is that complex soil profiles, seepage and a variety of loading conditions can be easily handled. Using a global equilibrium condition, the limit equilibrium approach is purely static and neglects the plastic flow rule of the soil. In the limit equilibrium approach, it is postulated that the slope might fail by mass of soil sliding on a failure surface. These methods have been widely used for assessing the stability of natural or man-made slopes. These methods were successively developed in order to deal with circular or arbitrary shaped slip surfaces. The common features of limit equilibrium methods are as follows:

- the problem is considered as 2D in plane strain formulation
- the Mohr-Coulomb failure criterion is assumed
- the factor of safety is defined in reference to a given slip surface as a ratio between the shear strength of soil and the shear stress required for equilibrium of the sliding body

- the strength of the slip surface is mobilised to the same degree to bring the sliding body into a limiting state. The overall slope and each part of it are in static equilibrium
- the factor of safety estimation is based on force and/or moment equilibrium equations.

If the soil at failure is assumed to be a rigid, perfectly plastic material obeying an associated flow rule, then collapse mechanisms selected by the limit equilibrium method are usually kinematically inadmissible. In addition, the static admissibility of the stress field is not satisfied because some arbitrary assumptions are made to remove the static indeterminacy and, in some methods, only a global equilibrium condition (rather than equilibrium conditions at every point in the soil) is satisfied. The different limit equilibrium methods may be merged into three groups:

1 **Analytical and graphical methods:** explicitly solved (even manually) methods based on the hypothesis of a simple shape of slip surface. These are the simplest methods and are useful for first approximation calculations.

2 **Slices and blocks methods:** iteratively solved methods based on the decomposition of the sliding mass into slices or blocks and requiring assumptions regarding interslice forces to solve the non-linear implicit problem.

3 **Perturbations methods:** explicitly solved methods based on assumptions regarding the normal stress distribution along the slip surface.

Although some of the methods presented (Table 8.25) in this section are not widely used in engineering practice, they are given to cover most of the methods implemented in commercial software, in order to provide a wide range of users useful tools for slope stability analyses.

Table 8.25 Characteristics of limit equilibrium procedures

Procedures		Equilibrium conditions satisfied			Shape of slip surface
		V	*H*	*M*	
Analytical and graphical methods	Infinite slope	x	x		planar
	Culmann	x	x		planar
	Swedish			x	circular
	Wedge method	x	x		three segments
Slice methods	Fellenius	x		x	circular
	Bishop simplified	x		x	circular
	Van's method	x	x	x	one segment and two arcs of circle
	Carter	x	x		any
	Janbu simplified	x	x		any
	USACE	x	x		any
	Lowe-Karafiath	x	x		any
	Spencer	x	x	x	any
	Morgenstern-Price	x	x	x	any
	Janbu rigorous	x	x	x*	any
Multi-block method	Sarma	x	x	x	any
Perturbation methods	Bell, Faure, Zhu	x	x	x	any non-planar

Notes

V = vertical equilibrium, *H* = horizontal equilibrium, *M* = global moment equilibrium

* moment equilibrium satisfied for each individual slice

Some slope stability analysis methods were developed based on variational calculus. However, in view of the fact that both practical results and theoretical basis are questionable (Duncan, 1996) it appears that these types of approaches have not resulted in significant advancement to the practical state of art for slope stability analysis. Also, this technique is mathematically complex and very few calculation tools exist using this type of approach. So, this handbook does not explain the theoretical details of this approach.

Because of the approximate and somewhat arbitrary nature of limit equilibrium analysis, there is often concern about how accurate these types of solutions are. However, limit equilibrium methods have shown great accuracy in geotechnical engineering with justification procedures and guidelines largely making reference to required factors of safety calibrated as regards to this approach (USACE, 2003).

8.6.3.1 Analytical and graphical methods

- **Infinite slope model**

  This method assumes that the slope is of infinite lateral extent and that sliding occurs along a plane surface parallel to the surface of the slope. Solving the problem requires vertical and horizontal equilibrium of the vertical block as shown in Figure 8.82. The factor of safety may be expressed as:

$$F_s(z) = \frac{c + \gamma z\,(1 - k\tan\beta)\cos^2\beta\tan\varphi}{\gamma z\cos\beta\,(\sin\beta + k\cos\beta)} \tag{8.155}$$

where:

z = vertical soil depth (m)
β = inclination of the slope from the horizontal (°)
c = soil cohesion (kPa)
φ = soil internal friction angle (°)
γ = unit weight of soil (kN/m³)

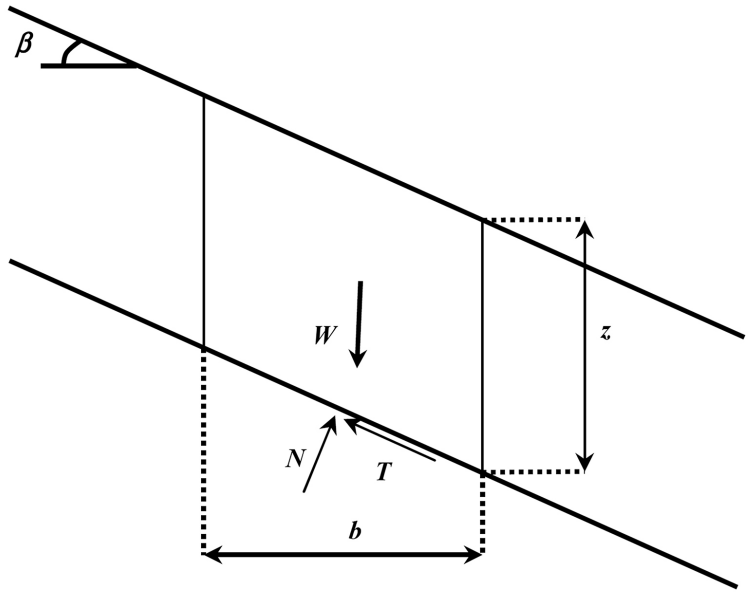

Figure 8.82 Infinite slope model

Real slopes are not infinite up and down. When the thickness of the sliding mass is not negligible as regards to its length, active and passive wedges may be introduced.

Culmann method

Culmann analysis is based on the assumption that the failure of a slope occurs along a plane when the average shearing stress tending to cause the slip is more than the shear strength of the soil, Figure 8.83. Consider a failure surface defined by an angle θ with the horizontal plane, the plane of length l elimiting

a sliding mass and the associated linear weight W are dependent on the θ angle and the factor of safety may be expressed as:

$$F_s(\theta) = \frac{cl(\theta) + (W(\theta)\cos\theta - U(\theta))\tan\varphi}{W(\theta)\sin\theta} \tag{8.156}$$

where U is the water pressure applied on the failure surface.

The minimum factor of safety is obtained when the derivative of the safety factor function becomes null. This null criterion defines the optimum angle θ^* giving the minimum factor of safety $F_s(\theta^*)$.

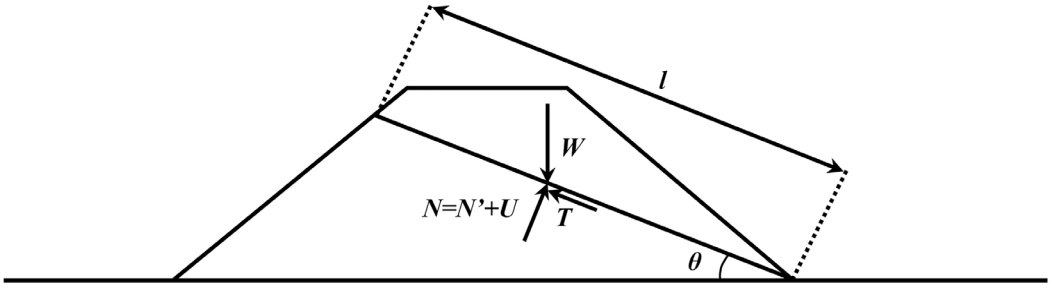

Figure 8.83 Culmann model for planar sliding surface

Swedish method

This method is the simplest circular analysis used to analyse the short-term stability for both homogeneous and non-homogeneous slopes. It assumes that a rigid cylindrical block fails by rotation about its centre (x_0, y_0) and the soil is assumed to be purely cohesive ($\varphi = 0$) (Figure 8.84).

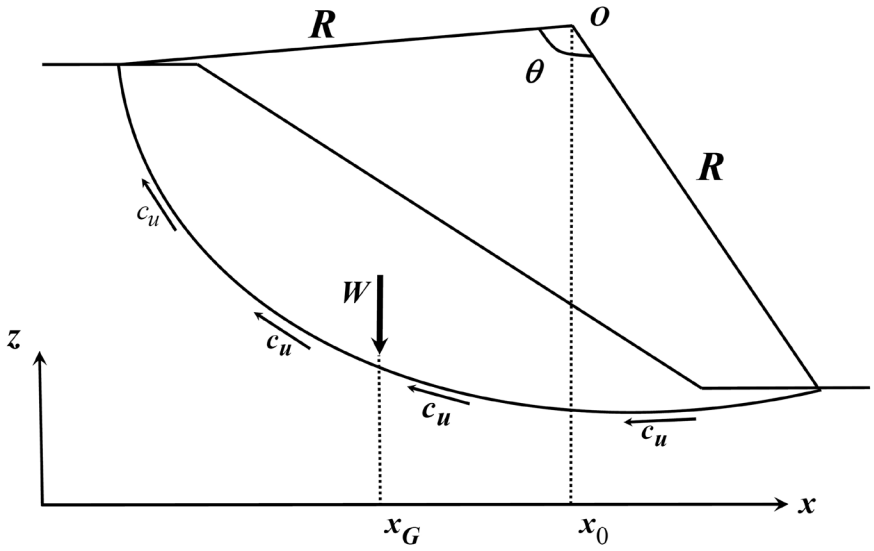

Figure 8.84 Swedish circle method model (φ = 0)

The factor of safety is defined in terms of moment equilibrium:

$$F_s = \frac{c_u R^2 \theta}{W(x_G - x_0)} \tag{8.157}$$

where:

c_u = undrained shear strength (kPa)
R = radius if circular slip surface (m)
θ = angle between entry and exit of slip surface (°)
W = weight of soil mass above sliding surface (kN)
x_G = abscissa of centre of gravity of soil mass (m)

Wedge method

The Wedge method assumes that the sliding mass is composed of three regions, the active wedge, the central block, and the passive wedge (Figure 8.85). The inclination angles of the forces on the vertical boundaries between the zones are assumed. The Wedge method is actually a special case of the force equilibrium procedure. The Wedge method fully satisfies equilibrium of forces in the vertical and horizontal directions and ignores moment equilibrium.

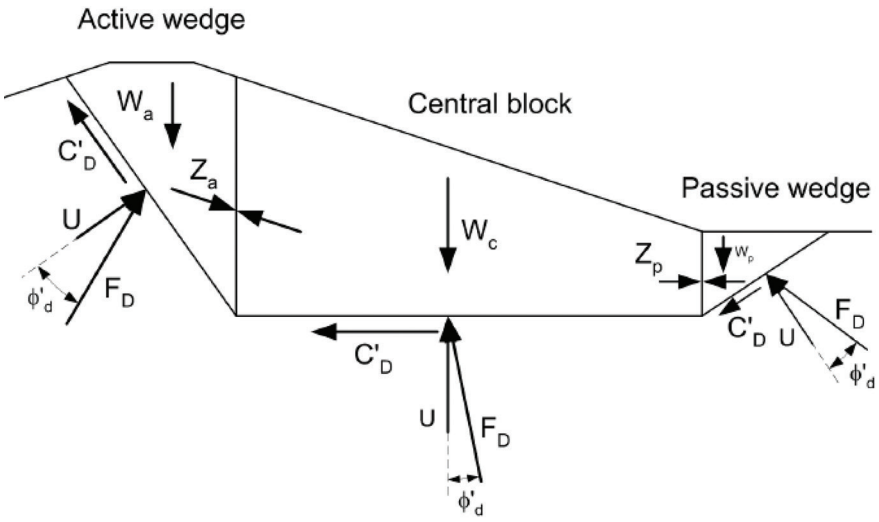

Figure 8.85 Block decomposition of the Wedge method

The Wedge method has the same limitations as other force equilibrium procedures. In addition, the specific 'wedge' shape of the slip surface restricts use of the procedure to slopes where slip surfaces of this shape are likely to be critical. Factors of safety calculated using the Wedge method are sensitive to the assumed inclinations of the side forces. The Wedge method may be used to check Spencer's solutions for three-part noncircular shear surfaces. In this case, the side force inclination is taken as the same side force inclination found in Spencer's approach.

8.6.3.2 Slice methods

The conventional methods of slices involve division of the sliding body into n vertical slices. Figure 8.86 shows the different notations used in the methodology.

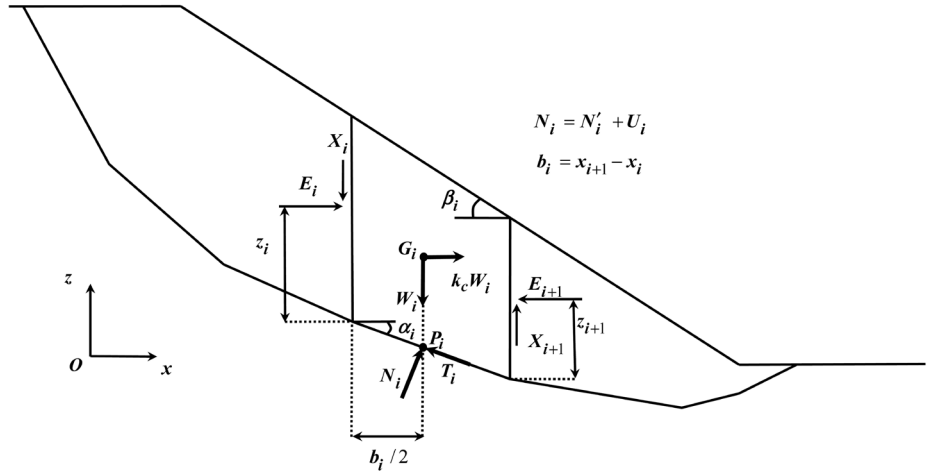

Figure 8.86 General slice method model

Problem determination

The verification of vertical, horizontal and moment equilibrium for all slices gives $3n$ equations. The unknowns are:

- n values of the normal reaction on the slice base N_i
- n values of the location of l_i
- n-1 values of vertical interslice forces X_i
- n-1 values of horizontal interslice forces E_i
- n-1 locations of interslice forces z_i
- *1* value of safety factor F_s.

However, following the limit equilibrium principle, the values of tangential reaction T_i must also be accounted for in the slice at limit equilibrium. In total, there are $5n–2$ unknowns. So, for more than one slice or block, the number of unknowns exceeds the number of equations by $2n–2$. In conventional slice methods, the number of unknowns is reduced by considering that the normal reaction on the slice base acts at the centre of the base ($l_i = b_i/2$), assuming that it introduces very little uncertainty, which is often the case when the slices are narrow. In the same manner, the horizontal gravity centre is often assumed to be vertical to the centre of the slice. These assumptions leave $n–2$ non trivial assumptions required to make the number of equations balance the number of unknowns.

Solving the problem consists of making as many assumptions as the equilibrium conditions chosen to verify. The slice methods differ in:

- the static equations employed in deriving the factor of safety equation
- the assumptions used to render the problem determinate.

The methods of slices have become the most common methods due to their ability to accommodate complex geometries and variable soil and water pressure conditions. Also, their implementation in commercial codes contributed greatly to their popularity among the geotechnical community.

General framework

From the general slice model represented on the Figure 8.86, the following equations concerning vertical and horizontal equilibrium of each slice can be written:

$$N_i \cos\alpha_i + T_i \sin\alpha_i = W_i - (X_{i+1} - X_i) \tag{8.158}$$

$$N_i \sin\alpha_i - T_i \cos\alpha_i = k_c W_i - (E_{i+1} - E_i) \tag{8.159}$$

The relation between the normal and tangential reaction forces is given by the limit equilibrium condition so that according to the definition of the factor of safety:

$$T_i = \frac{1}{F_s}\{c_i b_i + (N_i - U_i)\tan\varphi_i\} \tag{8.160}$$

The normal reaction equation may be expressed as:

$$N_i = \frac{W_i + \frac{1}{F_s}(U_i \sin\alpha_i \tan\varphi_i - c_i b_i) + (X_{i+1} - X_i)}{\cos\alpha_i + \frac{\sin\alpha_i \tan\varphi_i}{F_s}} \tag{8.161}$$

The limit equilibrium condition may be written from a global horizontal force point of view:

$$F_s = \frac{\sum_{i=1}^{n} \cos\alpha_i \{c_i b_i + (N_i - U_i)\tan\varphi_i\}}{\sum_{i=1}^{n} \{k_c W_i + N_i \sin\alpha_i\}} \tag{8.162}$$

or from a global moment point of view:

$$F_s = \frac{\sum_{i=1}^{n} (y_{Pi}\cos\alpha_i + x_{Pi}\sin\alpha_i)\{c_i b_i + (N_i - U_i)\tan\varphi_i\}}{\sum_{i=1}^{n} \{W_i (x_{Gi} + k_c y_{Gi}) + N_i (x_{Pi}\cos\alpha_i - y_{Pi}\sin\alpha_i)\}} \tag{8.163}$$

Note

The interslice assumptions do not appear explicitly in the global equilibrium conditions. However, determination of the normal reaction, N_i, depends on the assumptions made on the interslice forces. The limit equilibrium methods differ on the assumptions made concerning interslice forces.

Given that these assumptions have n-1 interslice force relationships, the problem becomes over-determinate. Some methods render the problem determinate by only verifying one of the global equilibrium conditions (force or moment). But more rigorous methods introduce one more degree of freedom into the relationship between the vertical and horizontal components of the interslice forces by assuming the general pattern:

$$X_i = (\lambda f_i + g_i)\, E_i \tag{8.164}$$

where $f_i = f(x_i)$and $g_i = g(x_i)$ are assumed functions of x and λ a coefficient to be determined (Chen and Morgenstern, 1983). The prescribed functions that were proposed in the literature are constant (Spencer, 1967), half-sine (Morgenstern and Price, 1965), extended half-sine (Zhu *et al*, 2006), clipped sine, trapezoid, data-point specified, and others.

Some authors have developed methods using other relationships defining directly a shear interslice force function $X_i = \lambda f_i$ (Pan, 1980, Madej, 1984, and Correia, 1988). These methods will not be detailed because theoretically there is no guarantee that the failure criterion is not violated along the interslice boundary, and these methods are not implemented in commercial codes. Finally, there is need to mention Sarma's method (Sarma, 1973), which considers all equilibrium equations and assumes that every interslice boundary is also at limiting equilibrium. The resolution procedure may be analogous to the Morgenstern and Price method. The resolution of the problem consists in determining the λ value for which the factors of safety given by the force equilibrium and the moment equilibrium are equal. The search of the λ parameter can be a trial and error one (Fredlund and Krahn, 1977) or guided by moment equilibrium of each individual slice (Zhu *et al*, 2005).

Assumptions that are made for each of the slice methods are presented in Table 8.26. Examples of selected methods are presented in Boxes 8.17 to 8.20.

Table 8.26 ***Assumptions referring to the different slice methods***

Slice method procedures	Assumptions
Fellenius	Interslice forces neglected
Bishop simplified	Resultant of interslice forces horizontal
Carter	Resultant of interslice forces horizontal
Janbu simplified	Resultant of interslice forces horizontal and correction factor to account interslice shear force
USACE	Direction of resultant interslice forces parallel to the ground surface
Lowe-Karafiath	Direction of resultant interslice forces equal to the average of the ground surface and slope of the base of the slip surface
Spencer	Resultant interslice forces are of constant slope throughout the sliding mass
Morgenstern-Price	Direction of the interslice forces defined using an arbitrary function
Janbu rigorous	Location of the horizontal interslice force is defined by an assumed line of thrust
General multi-block	The shear strength is mobilised on the sides of all inclined slices

Box 8.17 Ordinary slice method

This method, first developed by Fellenius (1936) is applicable to circular slip surfaces. The method assumes that the interslice forces can be neglected because they are thought to be parallel to the base of each slice. So, the normal reaction at the base of each slice may be written as:

$$N_i = W_i \left(\cos \alpha_i - k_c \sin \alpha_i\right) \tag{8.165}$$

The factor of safety is then simply derived from summation of moments about a common point (either a fictitious or real centre of rotation of the sliding mass). Given that the slip surface is circular, the moment produced by the normal force equals zero. So, the explicit expression of the factor of safety is obtained:

$$F_s = \frac{\sum_{i=1}^{n} \{c_i b_i + (N_i - U_i) \tan \varphi_i\}}{\sum_{i=1}^{n} W_i \left(\sin \alpha_i + k_c \cos \alpha_i\right)} \tag{8.166}$$

It is important to see that under these assumptions, Newton's principle of 'action equals reaction' is not satisfied between the slices. The indiscriminate change in direction from one slice to the next result in factor of safety errors, which may be as much as 60 per cent (Whitman and Bailey, 1967).

Also, from the tangential reaction expression, note that there are situations where the shear reaction may be negative (when r_u is close to 1). This implies that there is a negative shear stress on the base of the slice, which is physically impossible. In order to complete the calculation, one may set the shear stress to zero for all such slices, but this may result in substantial errors. As shown by Bishop (1955), the computed factor of safety is generally too small and errors may be as much as 20 per cent.

Box 8.18 Bishop's simplified method

In this method (Bishop, 1955), the slip surface is also assumed to be an arc of circle and the normal force is assumed to be at the centre of the base of each slice. So, *n–2* additional assumptions are required to make the problem determinate. Bishop proposed to neglect the shear interslice terms (X_{i+1}–X_i = 0), considering that the discrepancy introduced by this assumption is usually much less than the probable error in measured values of shear strength characteristics. Then, the vertical force equilibrium equation leads directly to the normal force by:

$$N_i = \frac{W_i + \frac{1}{F_s}\left(U_i \sin \alpha_i \tan \varphi_i - c_i b_i\right)}{\cos \alpha_i + \frac{\sin \alpha_i \tan \varphi_i}{F_s}} \tag{8.167}$$

Considering a circular slip failure, the factor of safety can be calculated using equation 8.166 with the normal force, N_i, as determined in equation 8.167. However, this relation is no longer explicit (F_s appears on both sides of the equation) so that the calculation has to be performed iteratively.

Carter method

The Carter method has been developed to generalise the Bishop's method to a general form of slip surfaces. Carter (1971) noticed that the global momentum equilibrium tends to equate to the global horizontal equilibrium when the centre of rotation is taken high enough. In this method, the factor of safety is determined from the global horizontal equilibrium of the sliding mass and applied to any slip surface.

Box 8.19 Van's method (from Van, 2001)

For many embankments built on soft deposits with a relatively rigid, permeable sand layer underneath, failure may be induced by the uplift mechanism. A high water level in the river or estuary in front of the embankment may generate high pore pressures in the sand layer under and behind the embankment. Consequently, the shear stresses at the interface between the sand layer and the soft deposits are reduced, eventually to zero, in case of actual uplift of the soft deposits, and failure along a relatively deep sliding plane may occur as indicated in Figure 8.87.

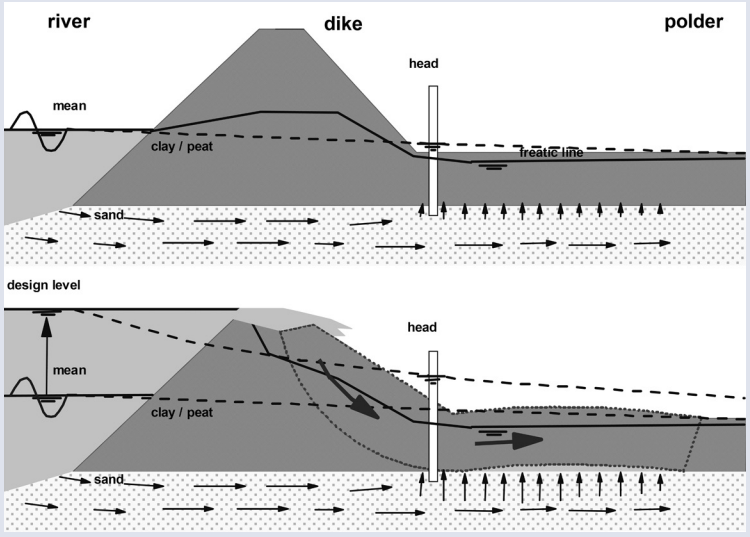

Figure 8.87 Uplift induced embankment failure

In the lower parts of the Netherlands, the uplift phenomenon turns out to be the dominant failure mechanism for the majority of the embankments if the rather high design water levels are applied. The standard approach in the Netherlands for checking stability is a circular slip surface (Bishop method). But in the case of uplift, the zone in which the shear stresses are reduced most significantly is hardly included in a circular analysis.

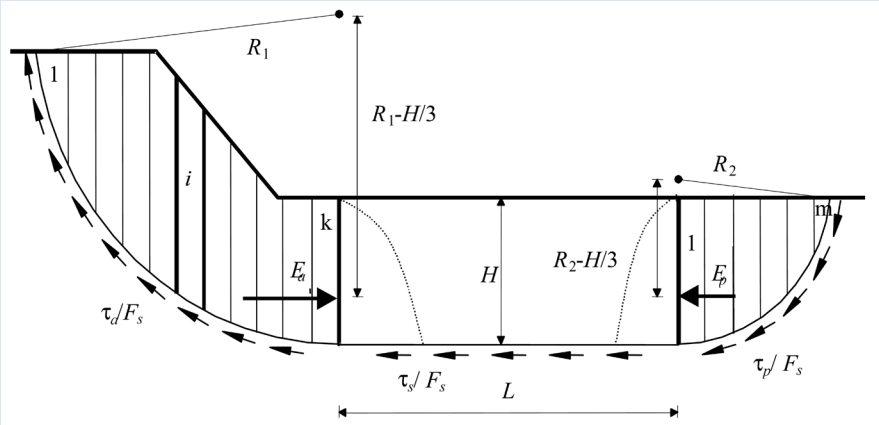

Figure 8.88 Van's slip surface model

In the method presented by Van (2001) the principles of Bishop's simplified method are applied to determine the stability factor of the slip plane shown in Figure 8.88. In accordance with Bishop's method, the safety criterion applies to the stability factor being the lowest denominator of the shear stress τ along the sliding plane, which results in equilibrium. The inter-slice horizontal forces E_a and E_p are supposed to act at one-third of the beam segment height above the sliding plane, which is a safe assumption. The horizontal and momentum equilibrium conditions lead to the following expression of the factor of safety (Van *et al*, 2005):

$$F_s = \frac{\dfrac{\sum_{i=1}^{k}\left\{\tau_i \dfrac{b_i}{\cos\alpha_i}\right\}}{1-\dfrac{H}{3R_1}} + \dfrac{\sum_{j=1}^{m}\left\{\tau_j \dfrac{b_j}{\cos\alpha_j}\right\}}{1-\dfrac{H}{3R_2}} + \tau_s L}{\sum_{i=1}^{k}\gamma_i h_i b_i \sin\alpha_i + \sum_{j=1}^{m}\gamma_j h_j b_j \sin\alpha_j} \qquad (8.168)$$

For $R_1 = R_2$ and $L = 0$ the method is equal to Bishop's method. In the more general case, some of the geometrical limitations of Bishop's method are relaxed, as required for an accurate description of the uplift mechanism, while the approach is consistent with a model that has turned out to be accurate in practice in cases where the slip surface is indeed more or less circular. In both the Bishop and Van methods the stability factor needs to be calculated by iteration. Fortunately, in both methods, convergence proceeds without any complications.

Box 8.20 *Janbu rigorous procedure (from Janbu, 1973)*

This method considers all the force and moment equilibrium conditions by assuming the location of the thrust line $z(x)$ (generally about one-third of the slice height). In order to solve the factor of safety, the interslice forces have to be evaluated. For the first iteration, the shear forces are set to zero ($X_i = 0$). For subsequent iterations the interslice forces are computed from the moment equilibrium of individual slice about the centre of the slice base, which is assumed to be the point of application of the normal force N_i. As the width of the slice is assumed to be infinitesimal, some terms are becoming negligible and a recurrence relationship can be exhibited on the X_i values. The horizontal interslice forces, E_i, are obtained by combining horizontal equilibrium equation and vertical equilibrium and the moment equilibrium of each slice being satisfied, so the force equilibrium given by Equation 8.162 should be considered.

Generalisation to multi-block failure analysis

Sarma (1973) was the first to generalise the approach of slices to inclined slice interfaces. The inclinations of slices are chosen so that a kinematic slip mechanism can develop. Since these inclinations are not known in advance, one may start with assumed inclined planes where sliding can take place inside the mass and later iterate to find a critical set. This approach may be seen as a generalisation of the Wedge method presented earlier.

Even if the mass contained within the slip surface is in a state of limiting equilibrium, the mass will not be able to move unless shear surfaces are formed within the body (Figure 8.89). To fulfil the kinematic compatibility condition, the inclinations of slices may be chosen so that a reasonable kinematic slip mechanism can develop.

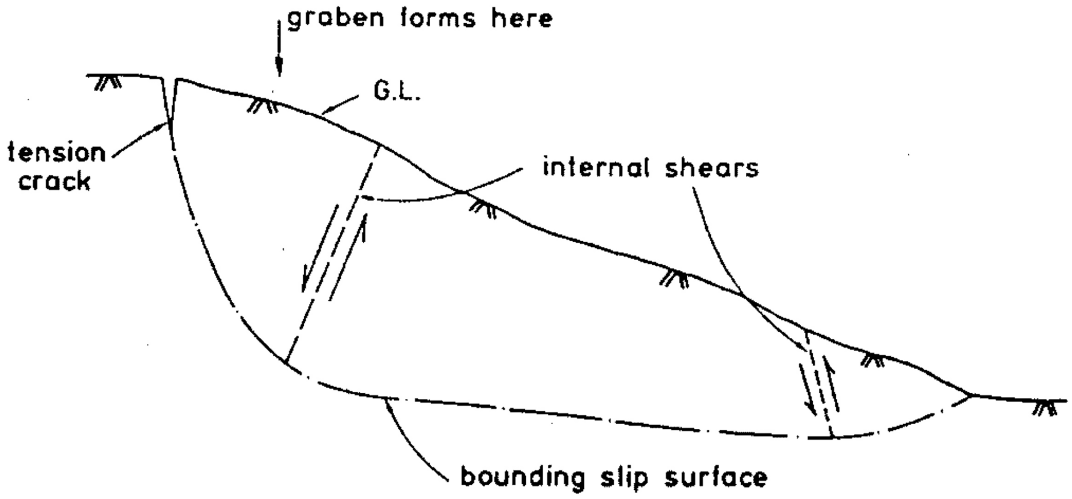

Figure 8.89 *Typical internal shear required to permit movement in a non-circular slide (from Hutchinson, 1987)*

Since inclinations of sliding interfaces within the sliding mass are not known in advance, one may start with assumed inclined planes and later iterate to find a critical set. Once a decomposition of the sliding mass is done, assume that the body forces X and E on the slice boundaries are such that they are in a state of limit equilibrium. It is then possible to write, for each i^{th} interslice boundary:

$$X_i = \frac{1}{F_s}\left\{(E_i - P_{w,i})\tan\widetilde{\varphi}_i + \widetilde{c}_i b_i\right\} \tag{8.169}$$

where d is the length of the inclined interslice boundary and P_w the force due to water pressure on the plane and the 'tilde' shear strength parameters are those averaged along the blocks interfaces. In this analysis, there are $n-1$ assumptions regarding the X_i and E_i relationship. In order to make the problem completely determinate, additional assumptions need to be made about the point of applications of all but one N_i normal force. Or, alternatively, points of applications of N_i can be determined by assuming the line of thrust of interslice forces. A suitable assumption may be to consider the point of application at the middle of the block base or vertical to the gravity centre.

As in the methods of slices, the solution obtained should satisfy the criterion of acceptability, ie all the N_i and T_i values should be positive. The values of z_i should lie within the slice, preferably in the middle

third. Since the moment equilibrium equation does not play any part in the determination of the k_c, the slices can be as large as possible and in fact should be controlled by the change of inclination of the slip surface. The solution k_c depends on the assumed block decomposition of the sliding mass. The technique for finding the optimal sliding mass decomposition is a trial and error procedure.

Numerical difficulties

Computational difficulties may occasionally be encountered in solving the factor of safety equations. Three of the most common problems, which have been discussed in the literature (Ching and Fredlund, 1983) are:

- unreasonably large and/or negative magnitude of the normal force on the base of the slice calculated as a result of the denominator term of N_i (Equations 8.162 and 8.163)approaching zero and/or going negative
- computation of a negative normal force on the base of a slice if the soil slope is highly cohesive
- convergence difficulties encountered when unreasonable side force function is assumed. For example, when the inter-slice force assumptions depend directly on the geometry of the problem (eg USACE, Lowe and Karafiath, 1960, and rigorous Janbu methods, 1973), some numerical difficulties may arise when the ground surface, the slip surface or the thrust line are not smooth, resulting in unreasonable discontinuity of interslice force distribution. To overcome this numerical difficulty smoothing techniques may be used (eg Zhu *et al*, 2003).

Several authors presented suggestions to resolve these difficulties (eg Ching and Fredlund, 1983). It is beyond the scope of this handbook to treat these questions. In cases of complex geometry, it is recommended to use two different methods to detect the potential numerical difficulties.

Accuracy comparison of slice methods

It should be noted that the limit equilibrium solutions are neither upper nor lower bound for the actual solutions. However, the solutions calculated within a rigorous context provide a rather narrow range for possible solutions. It has been pointed out in different studies (Fredlund and Krahn, 1997, Duncan, 1996, and Zhu *et al*, 2003) that the differences between factors of safety calculated by rigorous methods generally do not exceed ± six per cent. This limit is represented by the dotted line in Figure 8.90. This is certainly close enough for practical purposes, because slope geometry, water pressures, unit weights and shear strength can seldom be defined with accuracy as good as ± six per cent.

Thus, if an engineer performs slope stability analyses using methods satisfying all conditions of equilibrium of the sliding mass, it is justified in virtually every case to conclude that the accuracy of the analyses is as good as, or better than, the accuracy with which the analysis conditions are defined. The engineer can then devote his or her attention to the most important and most difficult issues involved in analyses of slope stability: those of defining geometry, shear strengths, unit weights and water pressures, and of determining the possible uncertainties in these quantities.

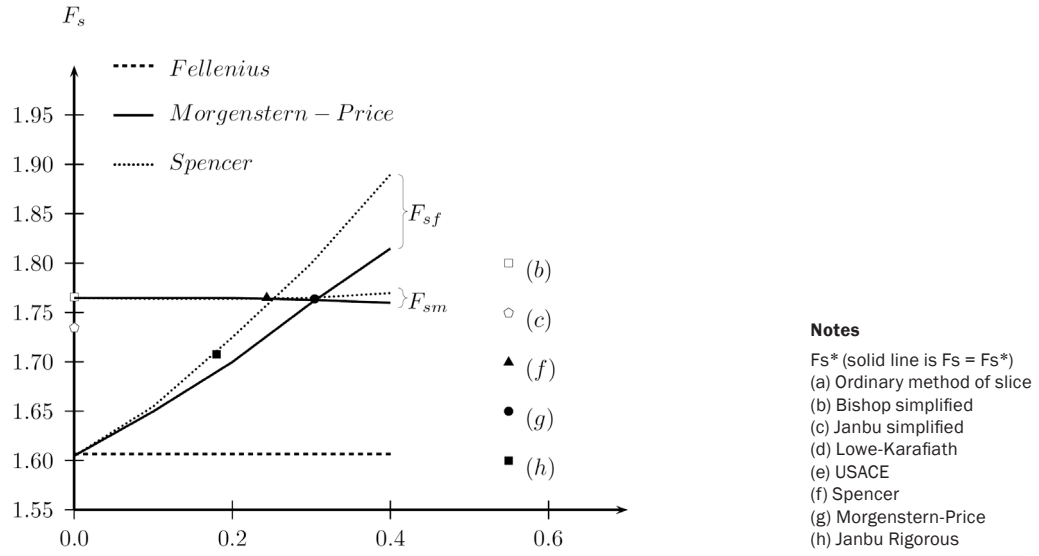

Figure 8.90 *Comparison of factors of safety obtained by different methods as regards to the mean factor of safety for rigorous methods (from Fredlund and Krahn, 1977, Zhu and Jiang, 2003, Yuang and Yamasaki, 1993, and Sinha, 2008)*

To understand the differences between the factors of safety determined from various methods, some authors have drawn plots of F_{sf} and F_{sm} as functions of λ values. Figure 8.91 shows the influence of interslice force assumptions on the computed factor of safety on the base of one example taken from Fredlund and Krahn (1977).

It is important to note that the factor of safety calculated using the ordinary method of slices (ie Fellenius method, 1936) is almost equal to the one calculated using the uncorrected simplified Janbu method (without the f_0 correction factor). The Janbu generalised method does not use an explicit λ factor, but given that this method is based on the force equilibrium equations, the Janbu rigorous method has been placed along the force equilibrium line to give an indication on the equivalent λ value.

The main observation to make is that the factor of safety obtained by the Spencer, Morgenstern-Price and Bishop methods are generally similar, ie the factor of safety based on the moment equilibrium has a small influence on the interslice forces assumptions. However, the factors of safety based on overall force equilibrium are far more sensitive to the side force assumptions (Figure 8.91).

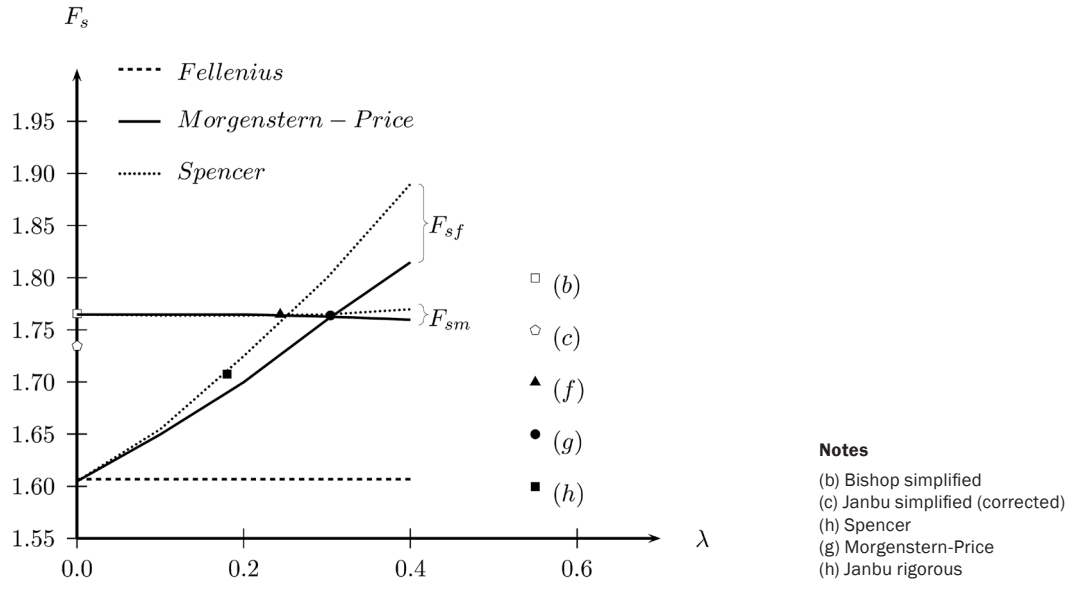

Figure 8.91 *Example of influence of interslice forces assumptions on the factor of safety*

Limitations and recommendations

The general remarks formulated on the different approaches are as follows:

- ordinary method of slices may be highly inaccurate for effective stress analyses of slopes with high pore pressures – the computed factor of safety is too low. The method is more accurate for purely cohesive soils in total stress analyses using circular slip surfaces. The method does not have numerical problems
- Bishop's simplified method is accurate for all conditions. Its limitations are that it is applicable only to circular slip surfaces and that numerical problems can be encountered under some conditions. If a factor of safety calculated using Bishop's method is smaller than the factor of safety for the same circle calculated using the ordinary method of slices, then it can be concluded that there are numerical problems with the Bishop's modified method analysis
- methods considering only force equilibrium conditions (eg Janbu simplified, USACE, Lowe-Karafiath) are sensitive to the assumed inclinations of side forces between slices. A poor assumption regarding side force inclination can result in a serious error in the computed factor of safety. These methods are inclined to have numerical problems
- methods satisfying all conditions of equilibrium of the sliding mass (eg Janbu rigorous, Spencer, Morgenstren-Price, Sarma) are generally accurate for any condition and slip surface forms. However, all of these methods have numerical problems under some conditions.

8.6.3.3 Perturbation methods

Other approaches consist of trying to estimate directly the normal stress distribution along the slip surface. That is the aim of the perturbation methods. A typical slope profile with a general-shaped slip surface is presented in Figure 8.92. In this 2D, the cross-section of the slope is visualised as having a unit length. The sliding body is bounded by the ground surface $y = g(x)$ and the slip surface $y = s(x)$.

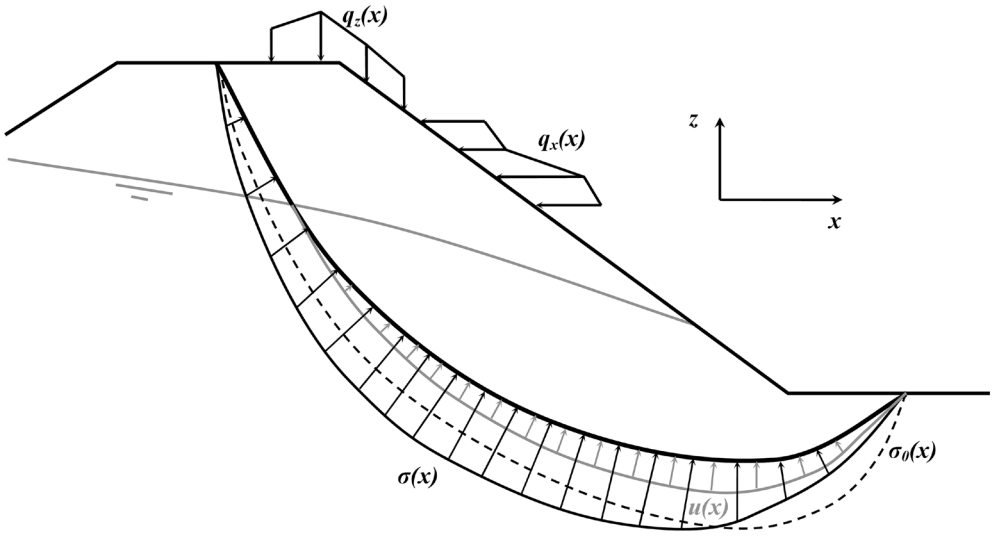

Figure 8.92 Geometry of slope stability model – sliding mass

By assigning a constant factor of safety, F_s, to the whole failure surface the sliding body is brought into a limiting state under the combined action of:

- $w(x)$: unit weight of the soil
- $k_c\, w(x)$: horizontal seismic force
- $u(x)$: pore water pressure along the slip surface
- $q_x(x)$, $q_z(x)$: horizontal and vertical surcharges or reinforced pressures.

The normal and tangential stresses on the slip surface are $\sigma(x)$ *and* $\sigma(x)$ respectively. In terms of effective stresses, the Mohr-Coulomb failure criterion is given by:

$$\tau = \frac{1}{F_s}\{c + (\sigma - u)\tan\varphi\} \tag{8.170}$$

where σ and c are friction angle and cohesion respectively, u is the pore water pressure.

When the sliding body is in an equilibrium state, three equations have to be verified: horizontal force equilibrium, vertical force equilibrium and overall moment equilibrium about a selected centre (x_c, y_c).

Solving the problem consists of determining the couple $(s(x),\sigma(x))$ that minimise the safety factor F_s. In limit equilibrium methods, assume the shape of the slip surface $s(x)$ and look for stress distribution $\sigma(x)$ and F_s parameter consistent with the equilibrium equations. The minimum value of the factor of safety is obtained by exploration of kinematically admissible slip surfaces. In the perturbation method, statically admissible normal stress distribution is determined by assuming an *a priori* normal stress distribution $\sigma_0(x)$ and 'perturb' it to satisfy the required equations of equilibrium. It can be shown (Baker and Garber, 1978) that every $\sigma(x)$ function that has at least two degrees of freedom can satisfy the three equilibrium equations. The modifying function should then involve two auxiliary unknowns (λ, μ) to make the problem determinate. The general normal stress function is put in the form:

$$\sigma = \lambda\sigma_\lambda + \mu\sigma_\mu + \sigma_\delta \tag{8.171}$$

where σ_λ, σ_μ and σ_Δ are determinate functions depending on x. The verification of equilibrium equations leads to a 3D linear system in terms of λ, μ and F_s. The condition of existence of the solution leads to a polynomial cubic equation in terms of F_s, which can be analytically solved in the simplest cases. In the more complex cases the resolution is made based on the discretisation of the slip surface and linear interpolation of integrals. The accuracy of the result depends on the assumed functions σ_λ, σ_μ and σ_δ. Different functions have been proposed in the literature. The most commonly used methods consider the reference functions:

$$\sigma_\lambda = \frac{w(1 - k_c s') + q_z - s' q_x}{1 + s'^2} \tag{8.172}$$

and

$$\sigma_\delta = 0 \tag{8.173}$$

In Bell's method (Bell, 1966), the function σ_μ is defined as a sin function:

$$\sigma_\mu = \sin\left(2\pi\frac{x - a}{b - a}\right) \tag{8.174}$$

Whereas in the method proposed by Faure (1985) the function σ_μ depends on the reference function.

$$\sigma_\mu = s'\sigma_\lambda \tag{8.175}$$

There is also a method proposed by Zhu and Lee (2002), for which the components are expressed as cubic polynomial functions.

Equivalence with slice methods

The direct approach presented here is related to the slice procedures developed earlier in the case of infinitesimal width slices. To check the reasonableness of the normal stress distribution, some verification may be useful. When the factor of safety has been obtained, the λ and μ parameters and the normal stress distribution are known. So, the horizontal and vertical forces, $E(x)$ and $T(x)$ respectively, may be obtained by considering horizontal and vertical force equilibrium conditions of the sliding slice from a to x, while the moment of forces acting on the same part of the sliding mass about a centre of rotation (x_0, y_0) gives the position of the point of action of the internal force. If the point of action lies within the interslice boundary the solution is statically reasonable.

8.6.3.4 Shape of the slip surface

All of the limit equilibrium methods require that a potential slip surface be assumed in order to calculate the factor of safety. In practice, calculations are repeated for a sufficient number of trial slip surfaces to ensure that the minimum factor of safety has been calculated. For computational simplicity the candidate slip surface is often assumed to be circular or composed of a few straight lines. However, the slip surface will need to have a more complicated shape in complex stratigraphy. The assumed shape is dependent on the problem geometry and stratigraphy, material characteristics (especially anisotropy), and the capabilities of the analysis procedure used. Commonly assumed shapes are as follows:

Planar: failures occurring along a planar surface are generally relevant for very steep slopes or specific geological contexts (thin weak layers).

Circular: observed failures in relatively homogeneous materials often occur along curved failure surfaces. A circular slip surface is often used because it is convenient to sum moments about the centre of the circle, and because using a circle simplifies the calculations. A circular slip surface should be used in the ordinary method of slices and Bishop simplified method. Circular slip surfaces are almost always useful for starting an analysis. Also, circular slip surfaces are generally sufficient for analysing relatively homogeneous embankments, or slopes and embankments on foundations with relatively thick soil layers.

Wedge: 'wedge' failure mechanisms are defined by three straight line segments defining an active wedge, a central block, and a passive wedge. This type of slip surface may be appropriate for slopes where the critical potential slip surface includes a relatively long linear segment through a weak material bounded by stronger material. A common example is a relatively strong levee embankment founded on weaker, stratified alluvial soils. Wedge methods, including methods for defining or calculating the inclination of the base of the wedges, are discussed in the following section.

General, non-circular shape: slope failure may occur by sliding along surfaces that do not correspond to either the wedge or circular shapes. The term general slip surface refers to a slip surface composed of a number of linear segments that may each be of any length and inclined at any angle. The term noncircular is also used to describe such general-shaped slip surfaces. Recently improved search techniques and computer software have increased the capability to analyse such slip surfaces. Stability analyses based on general slip surfaces are now much more common and are useful as a design check of critical slip surfaces of traditional shapes (circular, wedge) and where complicated geometry and material conditions exist. It is especially important to investigate stability with noncircular slip surfaces when soil shear strengths are anisotropic.

8.6.3.5 Location of the critical slip surface

A full slope stability analysis generally comprises evaluation of the critical slip surface for which the factor of safety is minimal. Because different analysis procedures employ different assumptions, the location of the critical slip surface may vary among different methods of analysis. The critical slip surface for a given problem analysed by a given method is found by a systematic procedure of generating trial slip surfaces until the one with the minimum factor of safety is found. Searching schemes vary with the assumed shape of the slip surface and the computer program used. Common schemes are discussed as follows.

Circular slip surfaces: a circular surface, Figure 8.93, is defined by three parameters that may be:

- centre co-ordinates (X_c, Y_c) and radius (R). The trial is generated on a grid of centre points and eventually on radii
- centre co-ordinates (X_c, Y_c) and a point through which the circle must pass (X_p, Y_p). The trial relies on the definition of a grid of centre points, the radius being given by the definition of the anchor point
- centre co-ordinates (X_c, Y_c) and a plane to which the circle should be tangent. The trial also relies on the definition of a proper grid of centre points, the radius being given by the tangent line.

In the case of homogeneous slopes and circular slip surfaces, Jiang *et al* (2003) provided a chart for critical slip surface location. Depending on the shear strength parameters, he defined ranges of values for which shallow toe circles (which exit directly through the toe of the slope), deep toe circles (which pass below the toe of the slope before exit at the toe of the slope) or deep base circles (DB), are the most critical (which pass below the toe of the slope and exit down the slope). This kind of analysis could be useful for a qualitative verification of the credibility of the critical slip surface location.

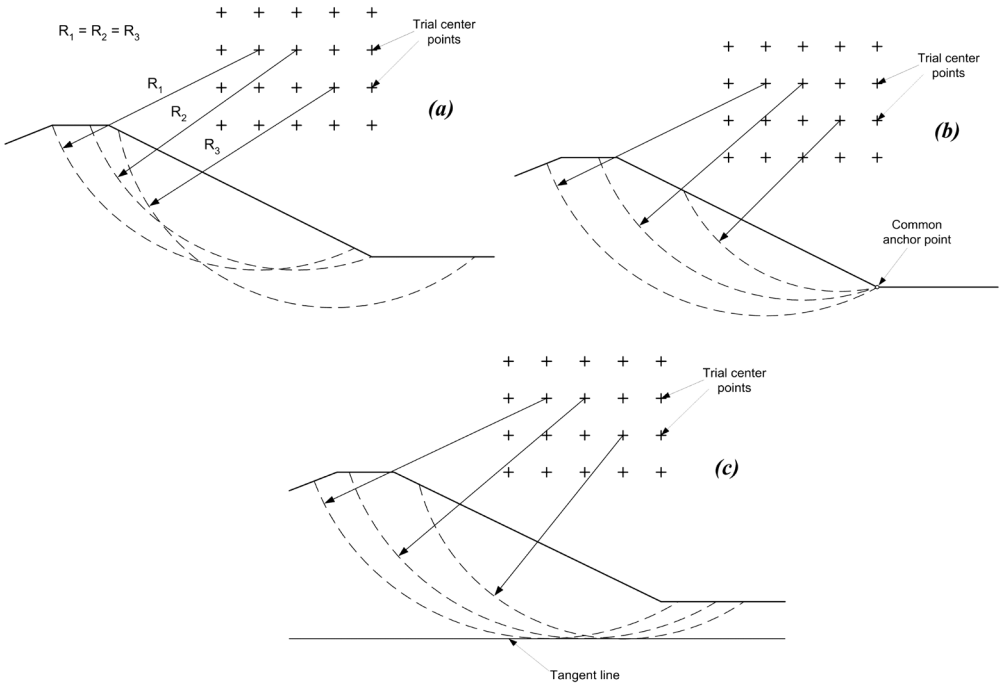

Figure 8.93 Different types of searching patterns for circular slip surfaces

Wedge-shaped slip surfaces: wedge-shaped slip surfaces require searching for the critical location of the central block and for the critical inclination of the bases of the active and passive wedges. Searching for the critical location of the central block involves varying systematically horizontal and vertical co-ordinates of the two ends of the base of the central block, until the central block corresponding to the minimum factor of safety is found. For each trial position of the central block, the bases of inclinations of the active and passive wedge segments should be set based on searching critical inclinations (Figure 8.94).

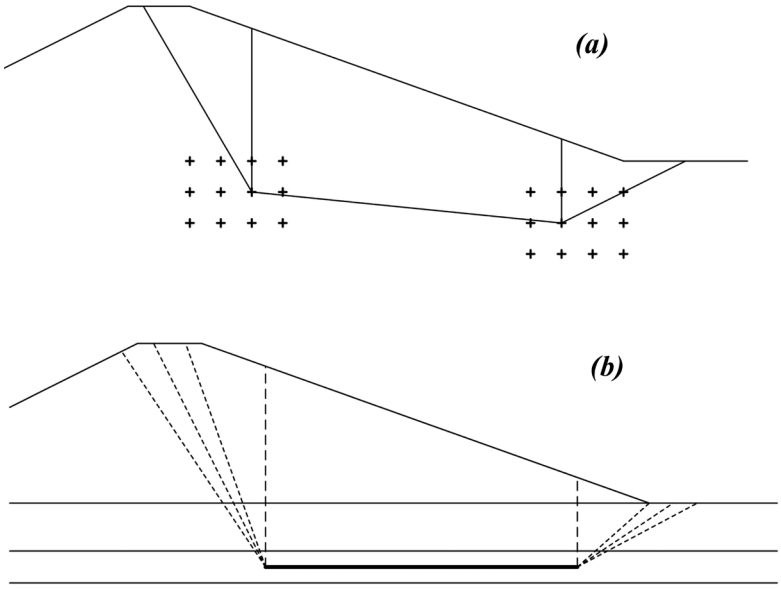

Figure 8.94 Different types of searching patterns for wedge slip surfaces: search scheme for critical central block (a), and search scheme for wedge inclinations (b) (from USACE, 2003)

General shapes: a number of techniques have been proposed and used to locate the most critical general-shaped slip surface. One of the most robust is the one developed by Celestino and Duncan (1981), shown in Figure 8.95. In this iterative method, an initial slip surface is assumed and represented by a series of points that are connected by straight lines. The factor of safety is first calculated for the assumed slip surface. Next, all points except one are held fixed, and the 'floating' point is shifted a small distance in two directions. The directions might be vertically up and down, horizontally left and right, or above and below the slip surface in some assumed direction. The factor of safety is calculated for the slip surface with each point shifted as described. This process is repeated for each point on the slip surface.. Once all points have been shifted in both directions and the factor of safety has been computed for each shift, a new location is estimated for the slip surface based on the computed factors of safety. The slip surface is then moved to the estimated location and the process of shifting points is repeated. This process is continued until no further reduction in factor of safety is noted and the distance that the shear surface is moved on successive approximations becomes minimal.

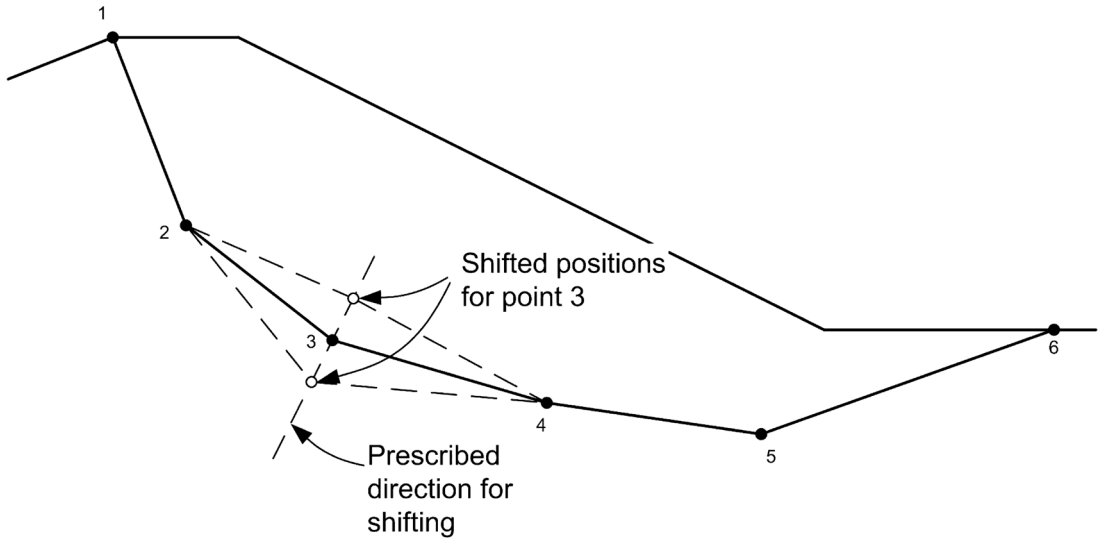

Figure 8.95 Search scheme for non-circular slip surfaces (Duncan and Celestino, 1981)

Genetic algorithms: in cases of complex geotechnical conditions, the minimisation solution may have several local minimum. Some authors proposed to use genetic algorithms to locate the global critical slip surface under general conditions with general constraints (eg Zolfaghari *et al*, 2005, Sun *et al*, 2008, Sengupta and Upadhayay, 2009, van de Meij, 2010, and Li *et al*, 2010). The advantage of this approach is that convergence to any prescribed degree of precision can be achieved and the algorithm has been demonstrated to be computationally superior to most of the optimisation routines, like the Monte-Carlo method and grid-points approaches. The disadvantage is that this kind of approach is rarely implemented in commercial codes.

Limitations considering slip surface assessment

Any search scheme employed in computer programs is restricted to investigating a finite number of slip surfaces. In addition, most of these schemes are designed to locate one slip surface with a minimum factor of safety. The schemes may not be able to locate more than one local minimum. The results of automatic searches are dependent on the starting location for the search and any constraints that are imposed on how the slip surface is moved. Automatic searches are controlled largely by the data that the user inputs into the software. The first thing to ensure is that the critical surface found is located inside the exploration domain and not on its borders. Regardless of the software used, a number of separate searches should be conducted to confirm that the lowest factor of safety has been calculated.

These limitations come from the fact that the problem of locating the critical slip surface can be viewed as a form of nonlinear, non-smooth, global optimisation and the objective function to be minimised is the factor of safety function. Some of the difficulties in the location of the critical slip surfaces are:

- the objective function of the factor of safety is non-smooth and can be non-convex in nature. The constraints, which include kinematically acceptable shapes of failure surfaces, rock and soil profile etc, may also be non-smooth, non-convex functions
- the existence of multiple minima is a fundamental feature of a slope stability problem
- a good trial for general ground conditions with arbitrary loadings can be difficult to develop for optimisation analysis.

Despite the fact that some modern heuristic optimisation methods (genetic algorithms, artificial networks etc) have been employed with success in the research field, most engineers still rely on their experience at present.

8.6.3.6 Cracking assessment

When soils at the crest of the slope have cohesion, the calculated values for the normal forces and side forces in this area are often negative. Negative forces are consistent with what would be calculated by classical earth pressure theories for the active condition. The negative stresses result from the tensile strength that is implicit for any soil having a Mohr-Coulomb failure envelope with a cohesion intercept. This type of shear strength envelope implies that the soil has tensile strength. Because few soils have tensile strength that can be relied on for slope stability, tensile stresses should be eliminated before an analysis is considered acceptable. Tensile stresses can be eliminated from an analysis by introducing a vertical tension crack near the upper end of the slip surface. The slip surface is terminated at the point where it reaches the bottom of crack elevation (Figure 8.96). The appropriate crack depth can be determined in either of the following ways:

- a range of crack depths can be assumed and the factor of safety calculated for each depth. The crack depth producing the minimum factor of safety is used for final analyses. The depth yielding the minimum factor of safety will correspond closely to the depth where tensile stresses are eliminated, but positive (driving) stresses are not
- the crack depth can be estimated as the depth over which the active Rankine earth pressures are negative. For total stresses and homogeneous soil the depth is given by:

$$d_{crack} = \frac{2c}{\gamma \tan(\pi/4 - \varphi/2)} \tag{8.176}$$

where C and φ represent the developed cohesion (kPa) and friction angle (°) respectively, γ the soil unit weight (kN/m^3). Similar expressions can be developed for the depth of tension for effective stresses and/or non-homogeneous soil profiles.

In some cases the depth of crack computed using Equation 8.176 will be greater than the height of the slope. This is likely to be the case for low embankments of well-compacted clay. For embankments on weak foundations, where the crack depth computed using Equation 8.176 is greater than the height of the embankment, the crack depth used in the stability analyses should be equal to the height of the embankment, so the crack should not extend into the weak foundation. In this case, the engineer must take great care concerning the validity of the limit equilibrium assumptions and the definition of the slip surface. Stress-deformation may be necessary.

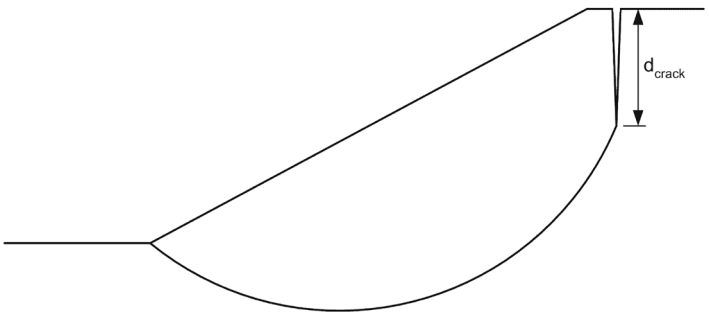

Figure 8.96 Vertical crack modelling

8.6.4 Limit analysis approaches

Limit analysis (Chen, 2007) approaches consist in modelling the soil as a perfectly plastic material obeying an associated flow rule. Two approaches were developed in this theoretical framework, static and kinematic. The general procedure is to assume a statically admissible stress field or a kinematically admissible failure mechanism and then optimise the objective function with respect to a very limited number of variable parameters. In this way, an upper or lower bound value of the limit load can be respectively found and the theoretically true collapse load is bracketed from above and below. This feature is particularly valuable in cases for which an exact solution cannot be determined, because it provides a built-in error check on the accuracy of the approximate collapse load.

The limit analysis framework can be used considering the upper bound solutions based on kinematically admissible rigid-block velocity fields (associated with the Mohr-Coulomb criterion) with the same practical advantages of limit equilibrium methods. In this case, it was shown (Michalowski, 1989) that the global force equilibrium was satisfied so that an upper bound limit analysis solution may be regarded as a special limit equilibrium solution, but not vice versa. Limit analysis approaches may also be implemented in finite element codes as a lower (Yu *et al*, 1998) or upper bound (Jiang and Magnan, 1997) formulation.

Limit analysis applied to rigid block assumption offers the advantage of simplicity. Just as for limit equilibrium methods, it requires the definition of the shear parameters (cohesion and friction angle) and of the slip surface. The rigorous elasto-plasticity formulation need no other assumptions related to interslice forces and give an upper bound of the factor of safety.

The disadvantage of this approach is that it requires that the materials modelled obey the associative flow rule. In effect this requires that all shearing resistance is modelled as dilation rather than a combination of dilation and friction as occurs with real soils. This is accurate for undrained problems where the angle of shearing resistance is zero, however for drained problems it typically leads to a small overestimate of load capacity. In extreme cases it can lead to volumetric locking and no collapse. Experience has shown that for moderately unconstrained problems, the increase in load estimate is minor. Manzari and Nour (2000), indicate, for example, that non-associative results for cohesive-frictional slope stability problems typically give values three to 10 per cent lower than for the associated flow rule case. To put this into context, this corresponds to using an angle of shearing resistance in an associated flow model approximately three per cent lower than the actual angle, which is of the order of 1°. However, it is not possible to give guidance on its effect on all problems.

8.6.5 Stress-deformation analysis

Stress-deformation may be performed by finite element or finite difference codes. This approach enables the estimation of stresses within the soil and the magnitude of the induced displacements. It is possible to model irregular geometries, complex soil behaviour, complex boundary conditions and a variety of construction phases.

For static slope stability analysis, stress-deformation approaches offer the advantages of being able to identify the most likely failure mode by determining the slope deformation, locating the most critically stressed zones within a slope and predicting the effect of slope failure on the adjacent or supported structures. These advantages come at the cost of increased engineering time for problem formulation, characterisation of material properties, interpretation of results and increased computational efforts.

8.6.5.1 Sources of inaccuracy

Duncan (1996) provided a very comprehensive review of the experience of using finite element methods to estimate stresses and deformations in slopes and embankments. Most of those conclusions are still valid and are summarised as follows. The sources of uncertainty in the results of the stress-deformation analyses are related primarily to the difficulties in predicting the actual densities and water contents of soils in the field, and with being able to anticipate the sequence of operations that will be followed during construction.

According to Kramer (1996), the accuracy of stress-deformation analyses is strongly influenced by the accuracy of the stress-strain model of the soil. Many behaviour laws have been developed in the past 30 years, each of them having advantages and limitations. It is beyond the scope of this handbook to discuss stress-deformation analysis tools in detail. It is important to emphasise that the accuracy of simple models is usually limited to certain ranges of strain and/or certain stress paths. Models that can be applied to more general stress and strain conditions are often quite complex and may require a large number of input parameters that may be difficult to determine experimentally.

There are generally three types of behaviour laws used for slope stability analyses:

1 **Linear elastic laws:** they have the advantage of simplicity and the limitation that they only model the behaviour of real soils at low stress levels and small strains, which is not the domain pertinent for slope stability analyses.
2 **Hyperbolic laws:** they have the advantage of simplicity, they model nonlinear behaviour, the parameters involved have physical significance and that they can easily be determined by conventional triaxial tests. They have the limitation that they are inherently elastic and do not model plastic deformations in a fully logical way.
3 **Elasto-plastic laws:** they have the advantage that they can model more realistically the behaviour of soils close to failure, at failure and after failure. They have the limitation that they are more complex to calibrate and some parameters have no real physical significance.

Comparisons of the results of FEM with field measurements have shown that the calculated deformations have a tendency to be larger than the measured deformations. According to Duncan (1996), the reasons for differences may be significantly influenced by the approximation of field parameters from laboratory testing procedures on intact or reconstituted samples (Chapter 7).

8.6.5.2 Factor of safety evaluation

The concept of factor of safety is not pertinent in the context of deformation analysis. But, given that most of the standards and recommendations express the requirement in terms of factors of safety, it may be a necessary output of the analysis.

Strength reserving approach

The definition of the factor of safety given by Duncan (1996) is particularly efficient in the framework of limit equilibrium methods. However, in a FEM, there are some difficulties related to the determination of the critical slip surface. In this approach, the factor of safety is generally obtained through the strength reduction technique as the value for which division of the shear strength parameters by F_s would onset a slope failure. So far, there has been no generally accepted failure criterion. The definition of the critical equilibrium state as the moment at which the plastic zones that enclose the critical sliding surface are linked together and pass through the slope from the toe to the top is much more preferable than the 'non-convergence of resolution algorithm' criterion.

Also, determination of the critical sliding surface requires some technical measures to visualise the shear bands, for example, the adaptive mesh refinement procedure (Zienkiewicz and Taylor, 1991), the technique of enhanced visualising failure mechanism (Griffiths and Kidger, 1995) etc. When this definition is used in finite element or finite difference analysis, some precautions should be taken.

Overloading approach

For all the reasons previously discussed, some authors have proposed another definition. The factor of safety is then defined as the ratio of total resisting forces to total driving forces along a certain slip line. The critical sliding surface is then regarded as the passage along which the ratio is a minimum. As compared with the previous definition, there are some advantages using this definition:

- only one model is needed in finding factor of safety associated with the loading definition
- this approach considers the effect of different stress paths on the degree of safety of the slope.

Choice of approach

When the FEM is used for slope stability analysis, the results from the overloading definition might be significantly different from both results from the strength reduction technique and the results from the limit equilibrium methods, particularly in terms of the position of the critical slip surface. Usually, the critical slip line associated with the overloading definition of the factor of safety is for the most part shallower than that associated with the strength reserving definition. Some authors (Zheng *et al*, 2006) recommend that the results from the strength reduction technique be taken as the standards in design and safety assessment of slopes, but when considering man-made slopes, the factor of safety associated with the overloading definition could be used to compare the effect of different construction procedures.

8.7 SETTLEMENT

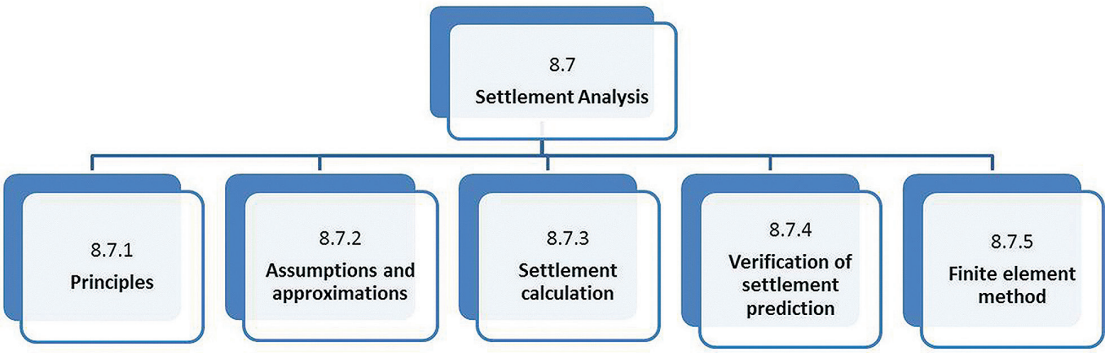

8.7.1 Principles

When a structure is built on soil, the stress state in soil is modified not only in the loaded area but also widely in an influence zone. The vertical displacement of soil due to this modification is called settlement. For sandy foundations, settlements appear in the short-term (during construction phases). For clay soils and specifically for soft soils or peats, this modification leads to consolidation of soils and then to displacements (horizontal and vertical). For a new levee construction or enlargement of an existing levee, the prediction of total settlements and differential settlements is an important issue for the project because it is directly linked to the capacity of reaching the design level of protection of the levee. The design process has to take into account a sufficient overbuild of the levee to accommodate predicting settlements, and to find building solutions to limit settlement or to accelerate them.

For linear structures such as levees, the problem can be considered as 2D with quite good accuracy. The methods presented rely on a pertinent definition of the geotechnical model consistent with the models used for other analyses (eg slope stability analysis). When the 2D assumption is no longer valid, ie when drainage, deformations, applied loads and geometry cannot be considered as 2D, a 3D model may be necessary.

Simple to complex methods are commonly used to estimate settlements but it is assumed that a 1D method or oedometer method is often sufficient to predict settlements. This section will detail conventional methods and introduce control methods and numerical methods as shown in the flow chart.

8.7.2 Assumptions and approximations

This section presents the most commonly used method to evaluate the settlement of a compressible foundation layer.

Unidimensional consolidation

As it is quite difficult to determine the load-induced stress field within the foundation layer (other than with a linear elastic model), the stress is first estimated vertical to the axis of the levee. In this central

zone, provided that the compressible foundation layer is thin in regards to the levee width ($b/H > 1$), assume that the drainage path is vertical and that horizontal deformations are negligible. Under these assumptions, consider that the conditions for application of unidimensional consolidation theory are met. These concepts are shown in Figure 8.97.

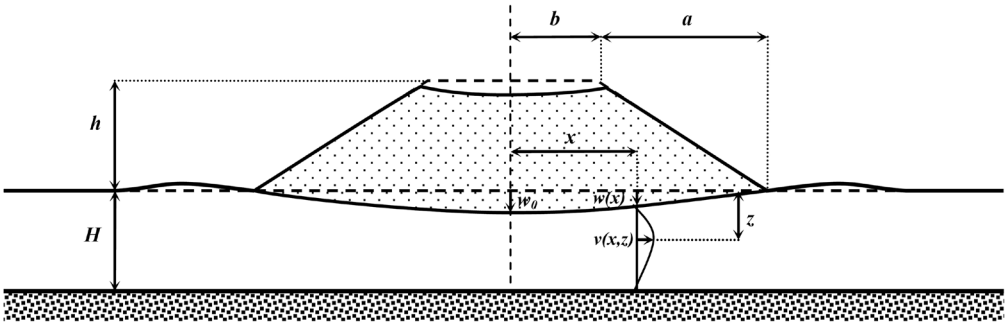

Figure 8.97 Definition of the geometrical parameters

Lateral deformations

At the toe of the slope, drainage conditions and deformations are much more complex (Figure 8.98). On one hand, there is an additional horizontal drainage component, while on the other hand, lateral deformations may occur as well as shear deformations along potential sliding surfaces. The smaller the factor of safety, the larger the shear deformations will be. Regarding the pore water pressure dissipation process, two concurrent phenomena may occur:

- primary consolidation processes due to the embankment loading, which tend to dissipate pore water pressure with time
- pore water pressure build-up due to contractive behaviour of the soil under shear stress.

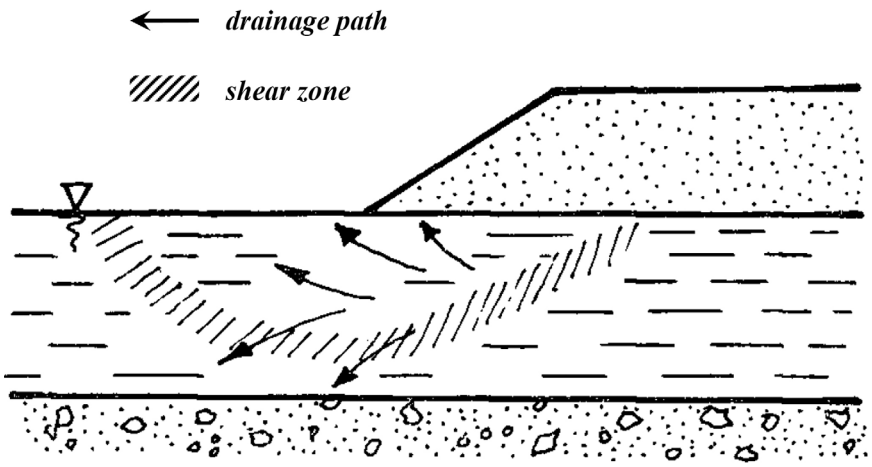

Figure 8.98 Drainage and deformation under the toe of the embankment

So, the determination of settlement under the embankment becomes a function of several parameters expressed as:

$$w\left(x\right) = w_0\, \mathcal{F}\left(\frac{x}{H}, F_s, \frac{x}{b}\right) \tag{8.177}$$

where w_0 is the settlement at the centre of the embankment, F_s is the factor of safety deduced from slope analysis, H the height of the embankment, b the half width of the crest of the embankment and x, the distance from central axis.

8.7.3 Settlement calculation

According to consolidation theory, total settlement w_t is the sum of the following components:

w_i = instantaneous settlement occurring under undrained condition
w_c = consolidation settlement (or primary settlement)
w_s = secondary settlement (or creep settlement)
w_l = settlement due to irreversible lateral movement (deduced from w_i).

Then total settlement w_t is given by:

$$w_t = w_i + \mu w_c + w_s + w_l \tag{8.178}$$

where μ is a correction factor, introduced by Skempton and Bjerrum (1957), which takes into account the 2D aspect of the consolidation process. The different components of settlement, w_t, are shown in Figure 8.99.

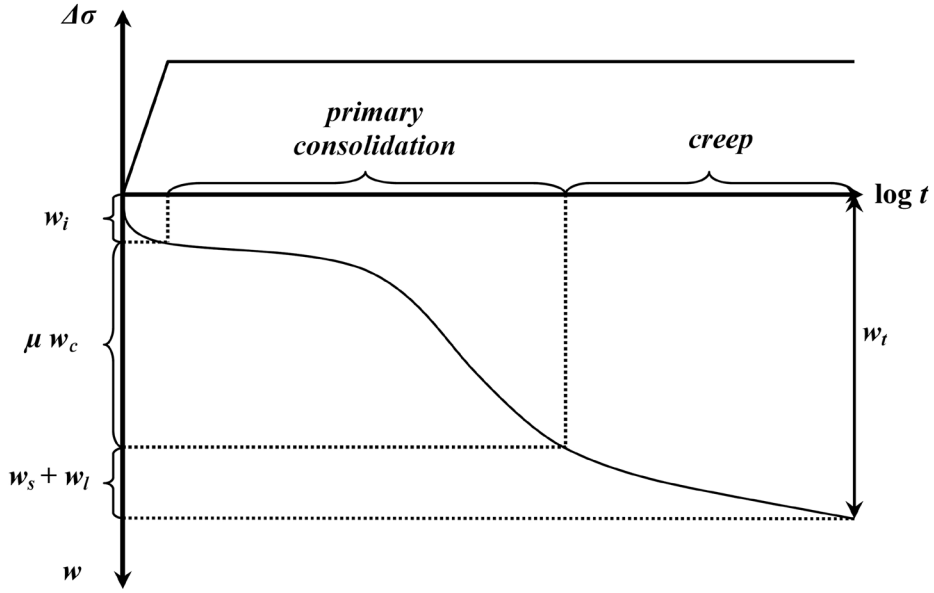

Figure 8.99 Different components of the settlement w_t (negative ordinate) as function of load $\Delta\sigma$ (positive ordinate), and time (t)

Determination of vertical stress

When an embankment is constructed, applying a uniform pressure to the soil surface, the increase of total vertical stress depends on height and geometry of the embankment. Since maximum vertical stress is situated at the centreline of the levee, some authors have developed practical graphs to obtain the vertical stress increase in foundation due to surface loads.

Considering the geometrical definition of the embankment (Figure 8.97), the vertical stress increment at depth $\Delta\sigma_v(z)$ along the axis of the embankment may be estimated from the chart proposed by Osterberg (1957) to obtain vertical stress increment from the following equation:

$$\Delta\sigma_v(z) = 2\, I(z)\, \Delta\sigma \tag{8.179}$$

where I (-) is the coefficient of influence and $\Delta\sigma$ (kPa) the vertical stress increment at the surface of the soil foundation. In Figure 8.100, a (m) is the width of slope's base, b (m) is the half width of the levee crest and z (m) represents the depth.

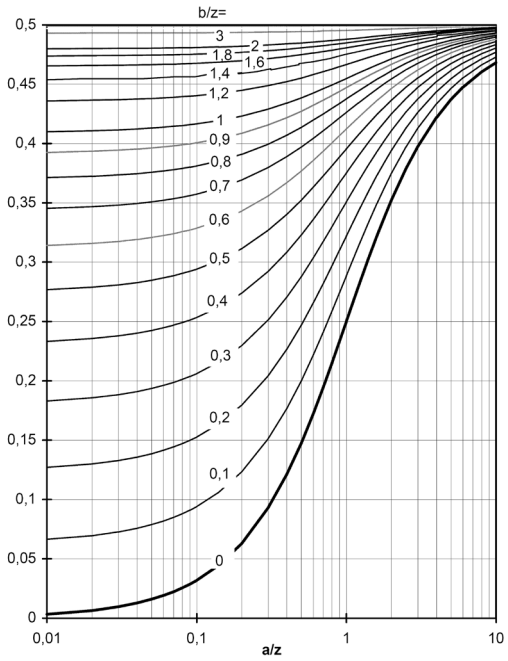

Figure 8.100 Graph giving vertical stress under half an embankment (after Osterberg, 1957)

8.7.3.1 Instantaneous settlement

Soil strains contributing to instantaneous settlement are caused during initial loading for undrained conditions. Loading for levee construction is not applied instantaneously and the soil is generally in a partly saturated state. So, the strict separation between w_i and w_c is not exact. However, some simple methods and charts are available to determine instantaneous settlements, w_i, according to elasticity theory by the following equation:

$$w_i = \frac{\Delta\sigma}{E_u} I \tag{8.180}$$

where:

$\Delta\sigma_v$ = incremental load (kPa)
E_u = elastic modulus of compressible soil for undrained condition (kPa)
I = influence factor (see Figure 8.101)

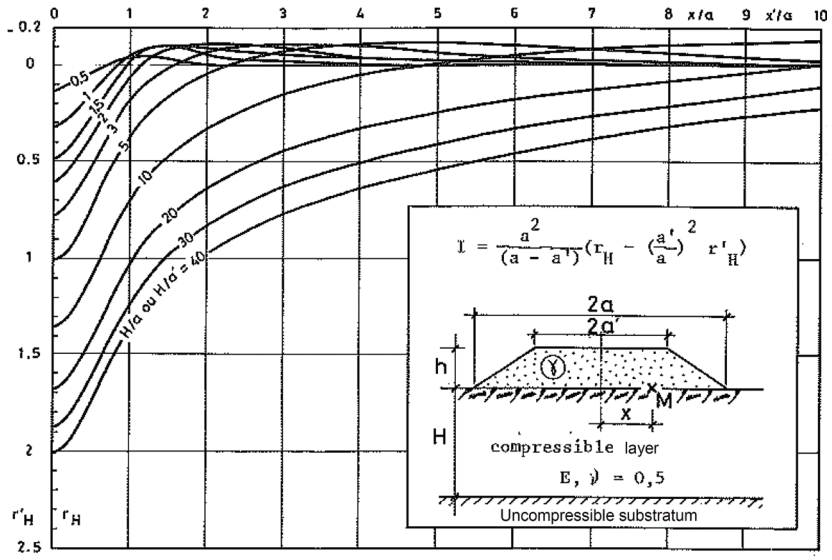

Figure 8.101 Elastic instantaneous settlement charts (Giroud, 1973)

8.7.3.2 Primary consolidation

This method was developed by Terzaghi and proposes to individualise soil into homogeneous layers with thickness H_0, characterised by oedometer test. This test yields the consolidation state of the soil and the vertical preconsolidation stress σ'_p that will govern the soil behaviour, based on an increase of vertical load $\Delta\sigma_v$, such as due to an embankment. The value, σ'_p, indicates if the soil has been previously loaded to a stress exceeding the actual stress σ_{v0}. From this test (Section 7.8.3), oedometric settlements can be defined by Equations 8.181 or 8.182 depending on the soil consolidation state and position of final stress $\sigma'_{v0} + \Delta\sigma$. In the common case of normally consolidated soils, the final primary settlement may be calculated as:

$$w_{c\infty} = \frac{H_0}{1+e_0} C_c \log \frac{\sigma'_{v0} + \triangle\sigma}{\sigma'_{v0}} \tag{8.181}$$

where:

e_0 = initial void ratio of soil (-)
C_c = consolidation coefficient (-)
H_0 = initial height of the compressible soil layer (-).

This relationship may be extended at any time during primary consolidation considering a consolidation ratio U(t) (Figure 8.102) defined as:

$$w_c(t) = U(t)\, w_{c\infty} \tag{8.182}$$

with:

$$t = \frac{H^2}{C_v} T_v(U) \tag{8.183}$$

where:

C_v = consolidation coefficient (m²/s)
T_v = non-dimensional time parameter (-)
H_d = drainage path length (m)

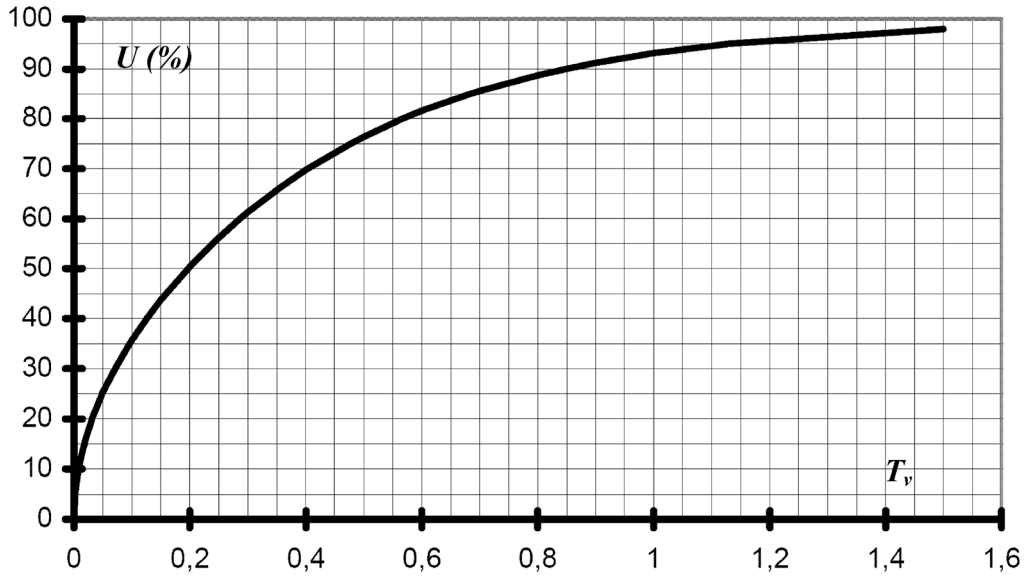

Figure 8.102 Consolidation ratio (U) as a function of the non-dimensional time (T_v)

Because compressible soils have relatively poor geomechanical characteristics (defined by undrained cohesion C_u), their bearing capacities are often limited and embankment works need to be phased into several steps. For each phase, settlement values and time of consolidation are designed but the accuracy of the prediction is insufficient and necessitates controls during construction. Construction techniques to

anticipate and measure settlements during construction phases are given in Section 10.5.4. Controls are very important for construction works on compressible soils because predictions are highly dependent on the soils character and drainage potential, while geotechnical investigations during design phases are often insufficient to properly capture the soils heterogeneity. Settlement control programs also contain soil pore pressure measurement devices to track drainage of the soil and anticipate possible soil failure (loss of bearing capacity of soil due to excessive pore pressure) and embankment failures.

Methods to estimate total settlements during construction regarding settlement evolution are given at the end of this section. Section 7.7.5 details some observational methods useful for determination of base settlement.

8.7.3.3 Secondary compression

After primary compression, for clayey and particularly organic soils such as peats, a second compression phase takes place (secondary or creep consolidation) corresponding to soil grain reorganisation without lateral displacement. For very soft soils and peats, the secondary settlement phase could be important regarding the life time of the structure and should be taken into account earlier in the project.

Different methods (field or laboratory devices) exist to determine consolidation characteristics of soils. Classically, consolidation behaviour of soils can be appreciated by laboratory oedometer compression tests (developed in Section 7.8.3). The secondary settlement is given by:

$$w_s(t) = \frac{H_{ref}}{1 + e_{ref}} C_\alpha \log \frac{t}{t_{ref}} = H_{ref} C_{\alpha e} \log \frac{t}{t_{ref}} \tag{8.184}$$

where:

C_{ae} = creep index (determined with long-term oedometer test)
t_{ref} = reference time from which the creep settlement is calculated (eg at 90 per cent of consolidation)
H_{ref} = corresponding thickness of compressible layer
e_{ref} = corresponding reference void index

Settlement due to lateral creep deformations

For compressible soils, the displacement of soil during earthen construction is not only vertical (settlement) but also horizontal. Note that this phenomenon can cause deteriorations to existing structures placed in the influence zone and has to be take into account during design (eg for choice of levee location) and controlled during construction (Section 10.5.4).

Settlement due to lateral displacement is difficult to obtain. The order of magnitude may be appreciated from the empirical relationship (**to use with extreme caution as a rule of thumb**):

$$w_l = 0.11 \frac{H}{a + b} w_s \tag{8.185}$$

where H is the thickness of compressible layer, and $a + b$ the half equivalent width of the embankment.

Other 1D methods are available (such as stress path method initiated by Skempton and Bjerrum (1957) and developed by Lambe, 1964). As lateral displacements can be expressed as a function of settlement along the embankment axis, different methods to avoid failure (eg observational methods) and to verify predicted total settlements (eg construction monitoring controls) should be employed.

8.7.4 Verification of settlement prediction

Asaoka method based on settlement measurement

To verify final settlement predictions during construction and react if necessary, Asaoka (1978) proposed a simple method based on measurement of soil settlements at regular time intervals. The method

consists of measuring settlements, (S_{i-1}, S_i), at constant time intervals,Δt, and plotting them such as shown in Figure 8.103. In this method, S_i is the settlement measurement at t_{i-1} and S_i is the settlement measurement at $t_i = t_{i-1} + \Delta t$.

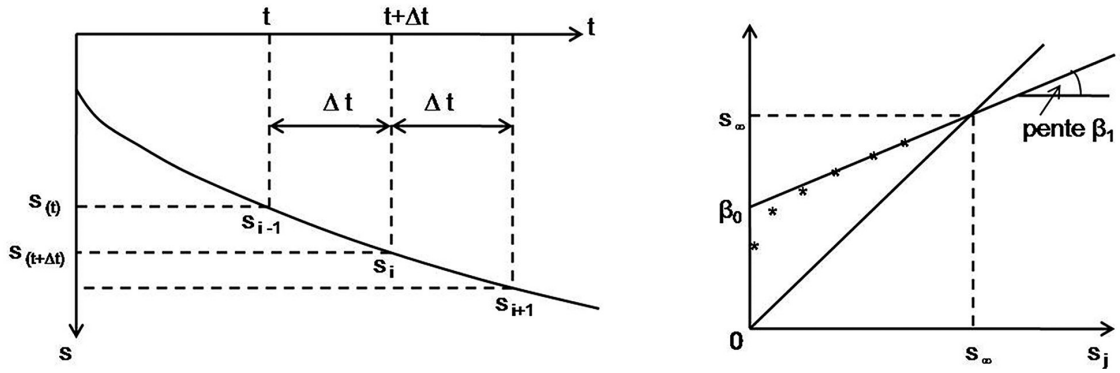

Figure 8.103 Total settlement curve of compressible layer (a), and Asaoka's construction curve (b) (Asaoka, 1978)

Steps for using the Asaoka method are:

- construct a time-settlement curve (as shown in Figure 8.103a) and select a series of settlement values at increasing time intervals
- plot the settlement values (S_{i-1} versus S_i) as shown in Figure 8.103b
- the plotted values will form a straight line as shown in Figure 8.103b as the β_0 line
- the estimated total settlement is where the β_0 line crosses the 45° line ($S_i = S_{i-1}$).

This method also enables adjustment to the time consolidation prediction by knowing the average vertical coefficient of consolidation, *Cv*, of the compressible layer given by equation of the β_0 line:

$$C_v = -\frac{5H^2}{12\Delta t}\ln\beta \tag{8.186}$$

Other methods are based on lateral displacement measurements or interstitial pressure measurements in clay soils. The reader is referred to any soil mechanics text book for further information.

8.7.5 Finite element method (FEM)

Numerical calculations are available for settlement predictions and some software proposes models for nonhomogeneous soil, anisotropic soil etc. Such models require complex input data, which are not easy to obtain from classical laboratory tests. Generally it is often more accurate for a levee project to predict settlements with 1D methods such as oedometer testing than with complex numerical methods.

8.8 SEISMIC ANALYSIS

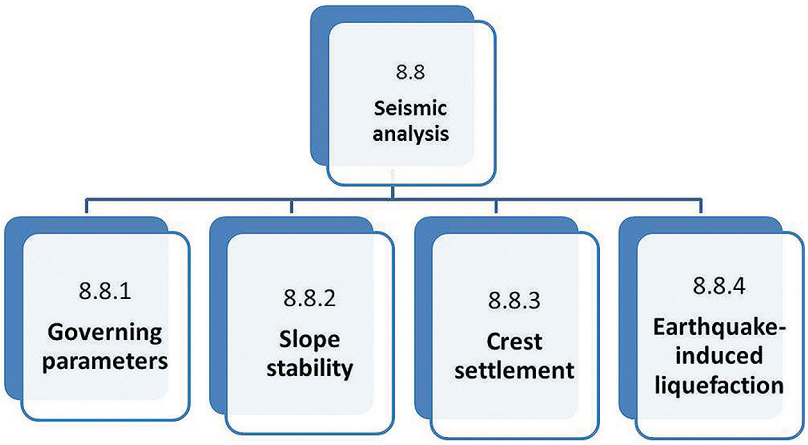

Two critical design issues must be addressed when evaluating the seismic performance of a levee:

- loss of significant strength of the material within or below the levee as a result of cyclic loading (eg soil liquefaction, water pressure build up in sands and silts, or post-peak reduction in sensitive clays)
- significant deformations that may jeopardise satisfactory performance.

Methods for stability analysis and evaluation of seismically induced permanent displacements attributed to deviatoric shear deformation are developed below as shown graphically above.

In addition to deformation of the embankment from slipping in response to earthquake shaking, the levee may settle in response to the stresses developed in each soil element. This generalised settlement can be estimated by using soil mechanics consolidation, empirical, and/or finite element procedures. Post seismic settlement in the foundation due to pore pressure dissipation is also a key issue under the scope of this section (Tokimatsu and Seed, 1987, Ishihara and Yoshimine, 1992, and Tsukamoto and Ishihara, 2010).

Other factors that may play a role in determining the acceptability of the performance of the levee following an earthquake are:

- the occurrence of flooding
- the ability or lack thereof to quickly repair a damaged structure.

8.8.1 Governing parameters

8.8.1.1 Seismic action

The seismic action to be considered for design purposes should be based on the estimation of the ground motion expected at each location in the future, ie it should be based on the hazard assessment (deterministic seismic hazard analysis or probabilistic seismic hazard analysis).

Probabilistic seismic hazard analysis gives hazard curves that depict the exceedance probability of a certain seismologic parameter (eg the peak ground acceleration, velocity or displacement) for a given period of exposure, at a certain location (normally assuming a rock ground condition).

For most countries, the seismic hazard is described by a zonation map defined by the national authorities.

Elastic response spectra represent maximum responses of a series of single-degree-of-freedom systems of different natural periods to a given ground-motion excitation. The response spectrum amplifications vary with the value of damping.

The standard response spectra are commonly used. The spectra is developed using the peak or effective ground motion parameters in conjunction with a standard spectral shape. It incorporates soil property effects, but ignores the influence of earthquake magnitude and distance on the shape of the spectra (Figure 8.104).

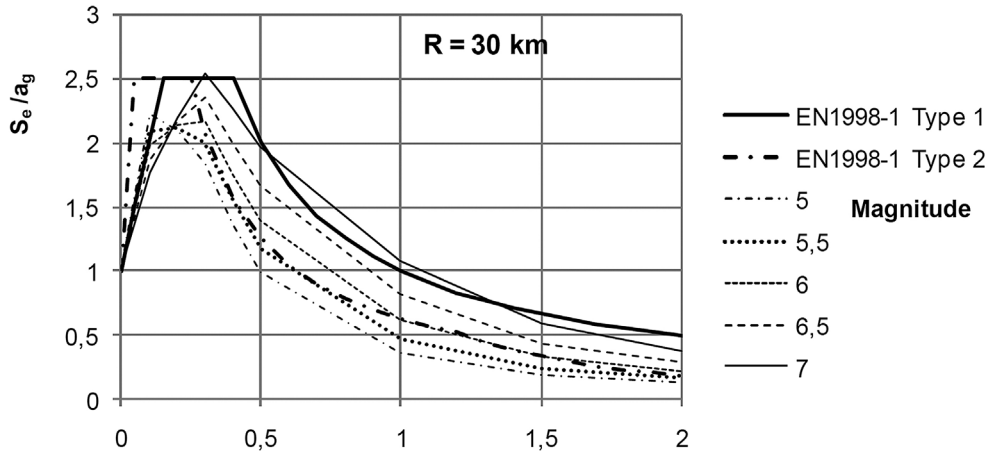

Figure 8.104 Recommended spectral shapes for Type 1 and Type 2 seismic action in EN1998-1 and illustration of the effect of magnitude (from Bisch et al, 2011)

Site-specific procedures are used to produce response spectra that correspond closely with those expected, based on the seismological and geological conditions at the site. These procedures use either the deterministic or probabilistic method to develop site-specific spectra.

The earthquake vibration at the surface is strongly influenced by the underlying ground conditions and correspondingly the ground characteristics very much influence the seismic response of structures. EN 1998-1 provides for example five ground profiles (A to E) and corresponding site coefficient of amplification (S).

Guidance in the choice of selecting seismic parameters can be found in ICOLD (2010).

8.8.1.2 Soil properties

Strength properties

For cohesive soils the relevant strength characteristic is the undrained shear strength (C_u). For most materials this value can be taken equal to the conventional 'static' shear strength. Some plastic clays may be subject to cyclic degradation with a loss of strength. Consequently most investigators recommend that the static undrained strength of soft clay be reduced by 20 per cent to account for strength loss during strong earthquake shaking. However, some clays may exhibit a shear strength increase with the rate of loading. These phenomena should ideally be given due consideration in the choice of the relevant undrained shear strength.

For pulverulent (powdery) soils the relevant properties are the drained friction angle ϕ' and the drained cohesion c'. These parameters are directly usable for dry or partially saturated soil. For saturated soils they would require the knowledge of the pore water pressure variation, u, during cyclic loading, which directly governs the shear strength (Section 7.8.3.3). EN1998-5 suggest an alternative approach, which consists of using the undrained shear strength under cyclic loading, $\tau_{cy,u}$. This undrained shear strength may be determined from laboratory tests or experimental relationships with, for example, the soil relative density or any other index parameter like blow counts, N, measured in standard penetration tests (SPT).

Note

Those considerations serve for assessing the characteristic value of the relevant strength characteristic in the sense of Eurocode 7 Part 1 and also its design value (for example, by applying the partial factor γ M 'material factor' in approach 3, see Section 7.5.4).

Deformation characteristic

The soil stiffness is defined by the soil shear modulus G:

$$G = \frac{\Delta\tau}{\Delta\gamma} \tag{8.187}$$

where$\Delta\tau$ and $\Delta\gamma$ are respectively the shear stress and shear strain variations. The small strain value may be estimated equal to $G_{max} = \rho V_s^2$ where ρ is the unit mass and V_s is the shear wave propagation velocity of the ground (Section 7.9.5). The relevant values to use in most of the calculation models are not the elastic ones but secant values compatible with the average shear strain induced by the earthquake. EN1998-5 proposes a set of reduction factors correlated to the peak ground surface. Soil internal damping $\eta(\gamma)$, generally taken between five and 20 per cent, shall be considered in some analysis.

8.8.2 Slope stability

The seismic stability of slopes has been a topic of considerable interest in geotechnical engineering practice for the past 40 years. During that period, the state of practice has moved from simple pseudostatic analyses to more complicated permanent displacement analyses. A variety of analytical tools ranging from sliding block analyses to multidimensional nonlinear dynamic response analyses are now available for prediction of permanent displacements. These tools represent the mechanics of the seismic slope stability problem with different levels of rigor, and require different levels of information on material behaviour. The most useful are those that can represent the important physical mechanisms of a particular seismic stability problem using material information that can be obtained practically and economically (Kramer and Smith, 1997).

8.8.2.1 Pseudostatic approach

Among the methods of analysis of the seismic stability of slopes, the pseudostatic methods are the oldest and the most widely used in engineering practice. Pseudostatic analysis represent the transient effects of an actual earthquake motion by applying constant unidirectional accelerations (horizontal and vertical) to a mass of potentially unstable material. The resulting inertial forces are taken to act in directions that destabilise the slope. The magnitudes of the horizontal and vertical pseudostatic loads are usually expressed in terms of seismic coefficients, k_h and k_v, numerically equal to the ratios of the inertial forces to the weight of the potentially unstable material. By solving force and/or moment equilibrium of the potentially unstable soil, a pseudostatic factor of safety can be computed. The pseudostatic factor of safety provides an index of stability under seismic conditions in a form familiar to geotechnical engineers. Selection of an appropriate seismic coefficient, however, is a crucial and complicated matter (Kramer and Smith, 1997).

The seismic inertia forces F_H and F_V acting on the soil sliding mass (Figure 8.105), for the horizontal and vertical directions respectively, in pseudostatic analyses shall be taken as:

$$F_H = k_H\, W \tag{8.188}$$

$$F_V = k_V\, W \tag{8.189}$$

where:

k_H = pseudostatic horizontal seismic coefficient (-)
k_V = pseudostatic vertical seismic coefficient (-)
W = total weight of the sliding mass (kN)

Vertical seismic coefficient is usually not taken into account. Simplifications made in using the pseudostatic approach to evaluate seismic slope stability include:

- replacing the transient earthquake motion by a constant horizontal acceleration equal to $k_H g$ (where g is acceleration of gravity)

- simplify amplification in the embankments using peak horizontal average acceleration of the failure mass.

Slope stability methods

Most of the slope stability methods developed in Section 8.6 may be used by adjusting the weight, *W*, of each slice to accommodate the seismic inertia forces F_H and F_V.

Soils properties

Static undrained strength should be used in the analysis. Most investigators recommend that the static undrained strength of soft clay be reduced by 20 per cent to account for strength loss during strong earthquake shaking.

Selection of the seismic coefficient

Recommendations for selecting an appropriate pseudostatic seismic coefficient were provided by different authors. The first recommendations were developed for embankment dams and were based on a level of acceptable deformation that would not compromise the integrity of the embankment. Using a limit of 1 m as a criterion, for acceptable performance, Seed (1979) recommended using seismic coefficients of 0.1 and 0.15 (together with a factor of safety of 1.15) for earthquake magnitude 6.5 and 8.25 respectively (crest acceleration less than 0.75 g).

The general expressions for seismic coefficients are given by the following equations:

$$k_H = \pm \alpha S \frac{a_g}{g} \tag{8.190}$$

$$k_V = \pm \beta S \frac{a_{vg}}{g} \tag{8.191}$$

where:

a_g = horizontal peak ground acceleration at bedrock (m/s²)
a_{vg} = vertical peak ground acceleration at bedrock (m/s²)
S = site amplification factor (-)
g = acceleration of gravity (m/s²)

The parameters α and β define the average peak horizontal acceleration of the potential failure mass (including amplification in the embankment) from the ground acceleration. It needs to be emphasised that choosing $\alpha < 1.0$ implies that if there are sliding surfaces for which the condition $F_s < 1$ is met, permanent displacements will occur during the earthquake.

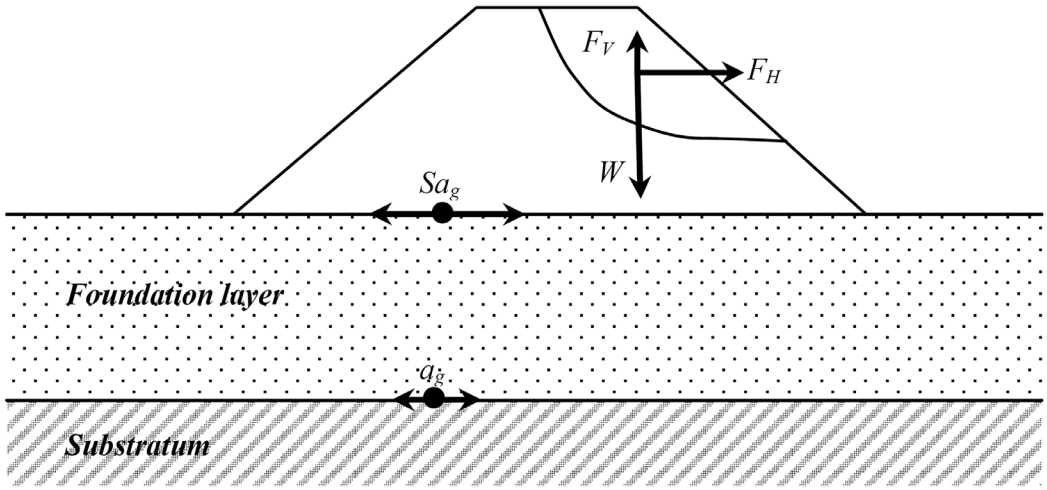

Figure 8.105 Definition of pseudo-static approach terms

The values generally accepted in engineering practice are α = 2/3 and β= 0. However, for slope design, BS EN 1998-5: 2004 proposes using horizontal seismic coefficient α = 0.5 and β = 0.17–0.25 depending on a_{vg}/a_g ratio. This value of the α coefficient has been selected based on empirical analysis, observed performance of slopes and embankments during earthquakes, and back-calculations. In the case of the design of a sensitive structure, implying the decision of limiting the induced permanent displacements, higher values of seismic coefficient may be chosen, possibly equal to or greater than the peak ground acceleration at the base of the levee ($\alpha \geq 1$) if amplification is expected in the levee. For example, the practice of dam engineering in Switzerland is to consider amplification α = 1.5 (OFEG, 2003).

Pseudostatic slope analysis conservatively evaluates the potential for occurrence of a slope failure due to earthquake loading. If the results of the pseudostatic analysis indicate a factor of safety less than one, then the potential for slope movement exists (not necessary failure) and a deformation analysis may be appropriate to quantify the permanent seismic deformations.

8.8.2.2 Pseudo-dynamic approaches

Sliding block analysis

This approach is based on the analogy of a rigid block resting on an inclined plane representing a potential sliding mass of soil (Figure 8.106). A simple procedure for estimating displacement of slopes during earthquake shaking is based on the concept of critical (or yield) acceleration (a_c) originally proposed by Newmark (1965). The yield acceleration is the minimum pseudostatic acceleration required to produce a displacement of the block (factor of safety F_s = 1). When equivalent acceleration applied to the block, corresponding to the inertial forces due to the earthquake, which exceeds the critical acceleration, a displacement of the block occurs.

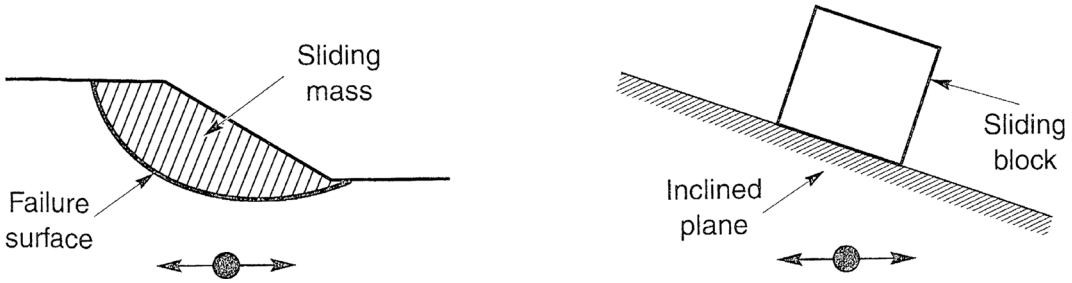

Figure 8.106 Analogy between potential sliding mass and rigid block resting on an inclined plane (from Kramer, 1996)

With the soil mass being rigid, the permanent displacement is obtained by a simple double integration of the excess acceleration (Figure 8.107). Given that an earthquake motion can exceed the yield acceleration many times, it may produce a number of increments of displacement. So, the total displacement is influenced by strong-motion duration as well as amplitude and frequency content of the earthquake spectra.

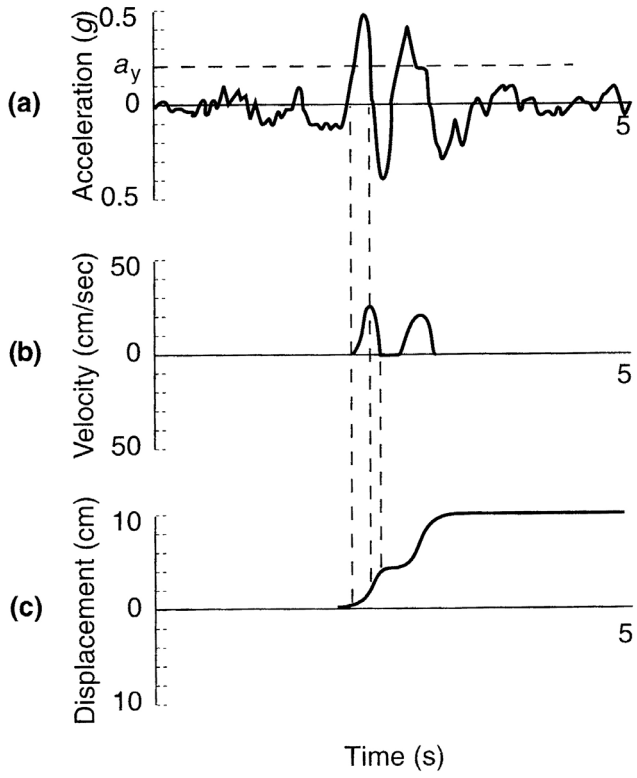

Figure 8.107 Newmark integration scheme (from Wilson and Keefer, 1985)

Different approaches were developed to refine the Newmark method by using a variety of acceleration pulses as well as large collections of actual strong motion records.

Ambraseys and Menu formula (1988)

Ambraseys and Menu (1988) proposed various regression equations to estimate Newmark displacement as a function of the critical acceleration ratio based on analysis of 50 strong-motion records from 11 earthquakes. They concluded that the following equation best characterised the results of their study:

$$\ln(D) = 0.90 + \ln\left[\left(1 - \frac{k_c}{k_{max}}\right)^{2.53}\left(\frac{k_c}{k_{max}}\right)^{-1.09}\right] \pm 0.30 \qquad (8.192)$$

where D is the expected displacement of the sliding mass of soil (cm), $k_c = a_c/g$ the critical seismic factor (-) and $k_{max} = a_{max}/g$ the maximum averaged seismic factor (-).

Jibson formula (2007)

Jibson (1993) suggested using Arias intensity (I_a) rather than peak ground acceleration to characterise the strong shaking. Arias (1970) defined this measure of the shaking content of a strong-motion record as:

$$I_a = \frac{\pi}{2}\int_0^T [k(t)]^2\, dt \qquad (8.193)$$

where:

g = the acceleration of gravity (m/s^{-2})
T = the duration of the significant shaking (s)
$k(t)$ = $a(t)/g$, the seismic coefficient history

Because Arias intensity measures the total acceleration content of the record rather than just the peak value, it provides a more complete characterisation of the shaking content of a strong-motion record than the peak ground acceleration. Jibson (2007) proposed an equation based on a rigorous analysis on hundreds of strong-motion records to generate the following regression equation:

$$\ln(D) = 0.561 \ln I_a - 3.833 \ln\left(\frac{k_c}{k_{max}}\right) - 1.474 \pm 0.616 \tag{8.194}$$

Validity domain

The accuracy of a sliding block analysis depends on the accuracy of the input motion applied to the inclined plane (Figure 8.108). The sliding block method assumes the potential sliding mass of soil to be rigid, in which case the appropriate input motion would be the ground motion at the level of the failure surface. However, actual levee slopes deform during the earthquake shaking. Their dynamic response depends on their geometry, stiffness and spectral content of the underlying ground motion. For levees composed of stiff soils and/or subjected to low frequency motion, lateral displacement throughout the potential sliding mass may be nearly in phase and the rigid block assumption is a good approximation. In the case of softer soils and/or higher frequency motion, the displacement field throughout the potential sliding mass may not be in phase. When this occurs, the inertial forces acting on the sliding mass have different directions and the resultant inertial force may be significantly smaller than that by the rigid block assumption.

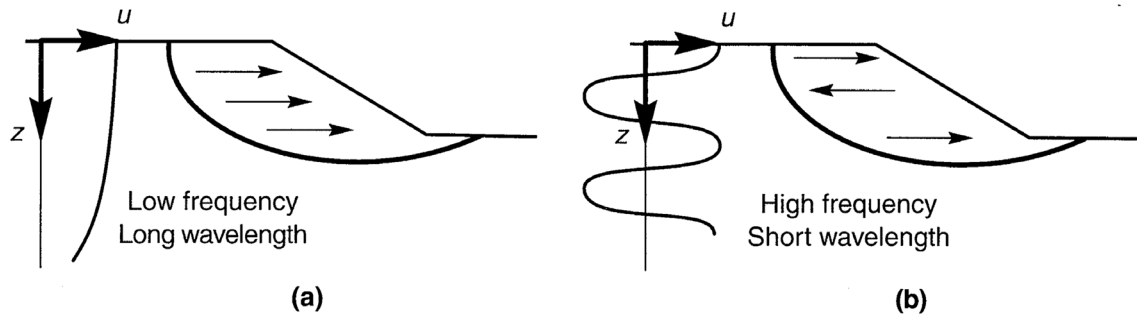

Figure 8.108 Influence of frequency on earthquake-induced displacements, soil motion in phase (a), and soil motion in opposite directions (b) (from Kramer, 1996)

Makdisi and Seed approach

Makdisi and Seed (1978) used dynamic finite element analysis to determine the horizontal component of the dynamic stresses acting on a potential failure surface. The resultant inertial force was divided by the mass of soil above the failure surface to produce the average acceleration of the potential sliding mass. Then they performed a sliding block analysis to estimate the permanent earthquake-induced displacement of earth dams and embankments. By making simplifying assumptions about the results of the numerical analyses, a simplified procedure was developed.

Critical seismic coefficient, k_c

In the simplified procedure, the critical acceleration ($k_c g$) for a particular potential failure surface is computed using dynamic yield strength of the soil (assuming a 20 per cent reduction of the undrained strength). The critical yield acceleration, k_c, may be determined using slope stability analysis and limiting equilibrium methods. To this purpose, it has to be noted that the Sarma method explicitly produces a critical (yield) seismic coefficient.

Seismic coefficient at the crest, $k_{0,max}$

The next step of the method consists in determining the maximum seismic coefficient at the crest of the levee ($k_{0,max}$). It may be done by the following equation:

$$k_{0,max} = \frac{1}{g}\sqrt{(1.6\, S_{a,1})^2 + (1.06\, S_{a,2})^2 + (0.86\, S_{a,3})^2} \tag{8.195}$$

where S_a, n is the spectral acceleration for the nth mode corresponding to the T_n period. The first three natural periods may be determined by:

$$T_1 = 2.62\,\frac{h}{V_s} \quad , \quad T_2 = 1.14\,\frac{h}{V_s} \quad , \quad T_3 = 0.73\,\frac{h}{V_s} \tag{8.196}$$

where h is the height of the levee and V_s the average strain-dependent shear wave velocity of soil.

Averaged seismic coefficient of the sliding mass, k_{max}

The dynamic response of the embankment is accounted for by an acceleration ratio that varies with the depth of the potential sliding surface (z) relative to the height of the embankment (H). The relation between these parameters is represented on Figure 8.109.

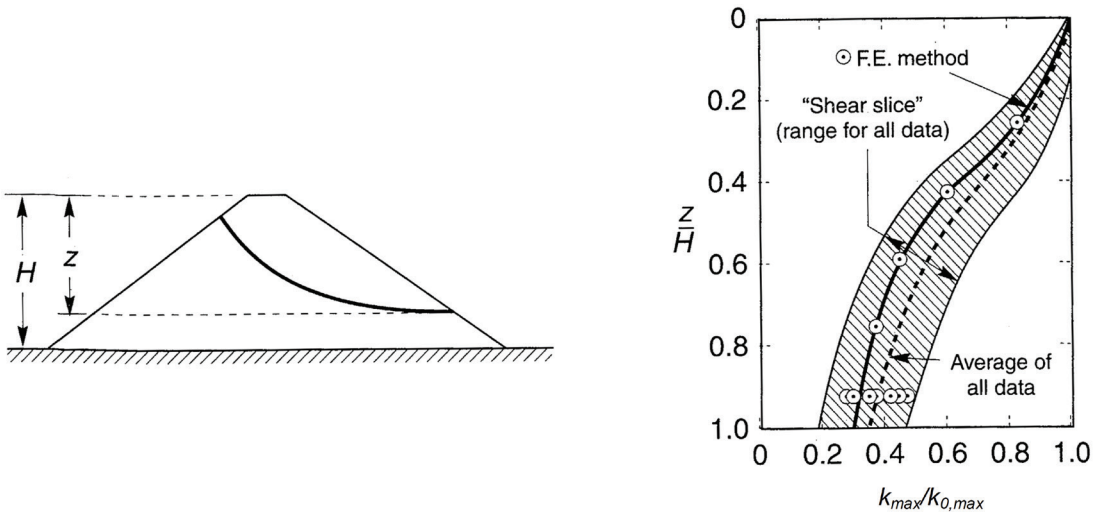

Figure 8.109 Influence of the depth of the failure surface on the average maximum acceleration of the potential sliding mass (from Makdisi and Seed, 1978)

Validity domain

This is one of the greatest limitations of this method. As shown in Figure 8.109, which presents results based on linear equivalent method analyses of columns of waste placed on top of a firm foundation for a number of ground motions, the maximum seismic coefficient at the top of the levee $k_{0,max}$ varies significantly. There is great uncertainty regarding what value of $k_{0,max}$ to use. So, the uncertainty in the estimate of k_{max} is high, because the uncertainty in estimating the crest maximum acceleration is high. Even with advanced analyses, estimating the maximum seismic coefficient at the crest is difficult, and the need to perform any level of dynamic analysis to estimate the crest acceleration conflicts with the intent of a simplified method that should not require more advanced analysis.

Also, the bounds shown on the Makdisi and Seed (1978) plot of $k_{max}/k_{0,max}$ vs z/H (Figure 8.109) are not true upper or lower bounds. Stiff earth structures undergoing ground motions with mean periods near the degraded period of the earth structure can have k_{max} values exceeding 50 per cent of the crest maximum acceleration for the base sliding case (ie, $z/h = 1.0$), and flexible earth structures undergoing ground motions with low mean periods can have k_{max} values less than 20 per cent of the maximum acceleration of the crest for base sliding (Kramer, 1996).

The variation of normalised permanent displacement with the critical seismic coefficient for different magnitude earthquakes is shown in Figure 8.110.

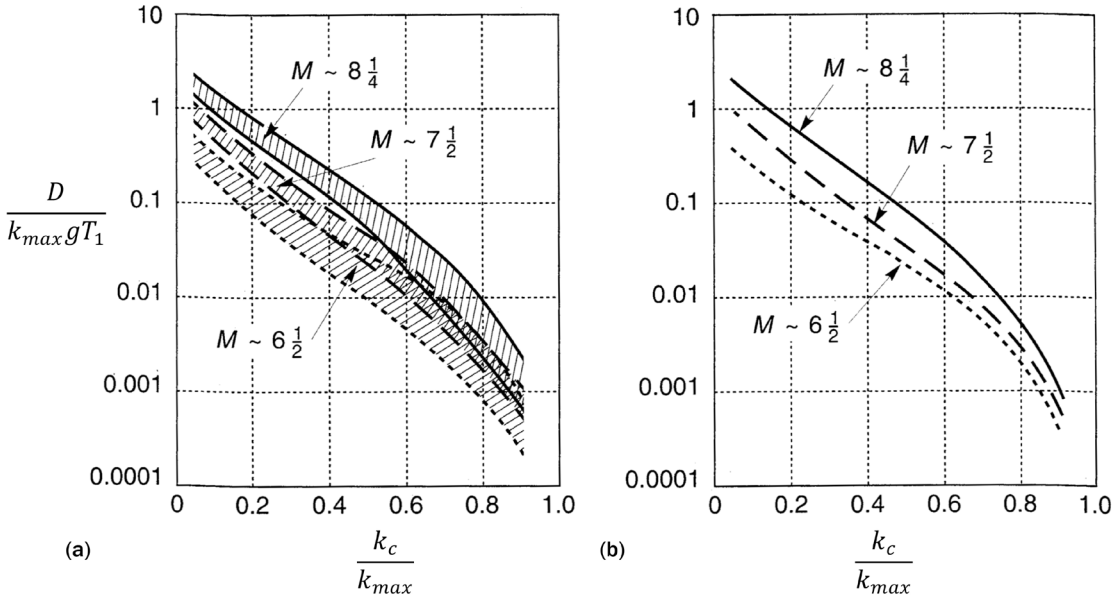

Figure 8.110 Variation of the normalised permanent displacement (D) with the critical seismic coefficient for different magnitudes, summary of several earthquakes (a), and average values (b) (from Makdisi and Seed, 1978)

Bray and Travasarou method (2007)

The earthquake ground motion is one of the most important components of a seismic displacement analysis in terms of its contribution to the calculation of the amount of seismic displacement. Yet, currently available simplified slope displacement estimation procedures are largely based on a relatively limited number of earthquake records or simulations. Bray and Travasarou (2007) tried to overcome this limitation working on a large database of case studies.

Spectral acceleration has been commonly employed in earthquake engineering to characterise an equivalent seismic loading on a structure from the earthquake ground motion. Similarly, Bray and Travasarou (2007) found that the five per cent damped elastic spectral acceleration at the degraded fundamental period of the potential sliding mass, equal to 1.5 times the initial fundamental period, was the optimal ground motion intensity measurement in terms of efficiency and sufficiency.

Contrary to the previously developed methods, Bray and Travasarou (2007) use a fully coupled model taking into account the vibratory behaviour of the structure, and deviatoric and volumetric behaviour of the soil constitutive of the embankments. As uncoupled models are not always conservative, the approach eliminates this. The first step is to determine critical acceleration, k_c, using slope stability analysis (limiting equilibrium methods). Then the model for estimating seismic displacement, D, consists of two discrete computations of:

- the probability of negligible ('zero') displacement (typically $D \leq \delta = 1$ cm)
- the likely amount of 'non-zero' displacement.

The probability of negligible displacement is calculated by the following equation:

$$P(D \leq \delta) = 1 - \Phi(-1.76 - [3.22 + 0.484T_s]\ln(k_c) + 3.52\ln(S_a(1.5T_s))) \quad (8.197)$$

where:

D = seismic displacement (cm)
Φ = the standard normal cumulative distribution function
k_c = yield coefficient (-)
T_s = fundamental period of the sliding mass (s) (Figure 8.111)
S_a = spectral acceleration of the input ground motion at a period of $1.5T_s$(g)

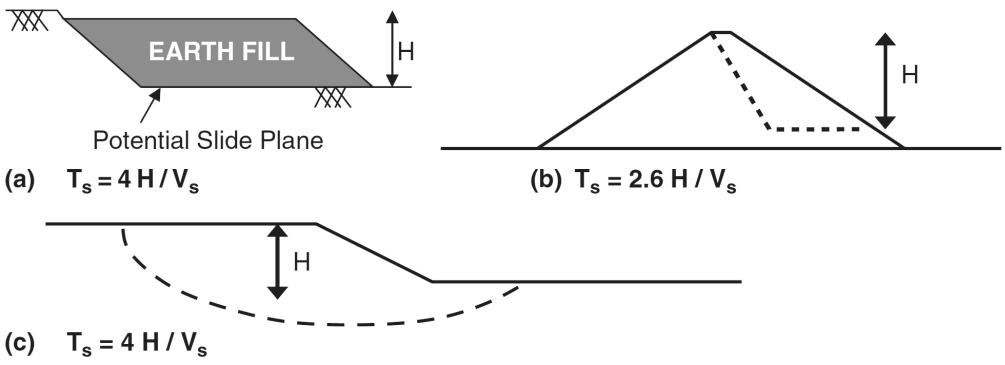

Figure 8.111 Initial fundamental period of potential sliding mass (from Bray, 2007)

If there is not a high probability of negligible displacement, the amount of 'non-zero' displacement, D, can be estimated by the following equation:

$$\ln(D) = -1.10 - 2.83\ln(k_c) - 0.333\left[\ln(k_c)\right]^2 + 0.566\ln(k_c)\ln(S_a(1.5\,T_s)) \\ +3.04\ln(S_a(1.5\,T_s)) - 0.244\left[\ln(S_a(1.5\,T_s))\right]^2 + 1.50\,T_s + 0.278\,(M-7) \pm \varepsilon \quad (8.198)$$

where:

M = magnitude of the earthquake (-)

ε = normally distributed random variable with zero mean and standard deviation σ = 0.66

To eliminate the bias in the model when $T_s \approx 0$ s, the first term of equation should be replaced with -0.22 when $T_s < 0.05$ s. The median minus one standard deviation to median plus one standard deviation range of seismic displacement can be approximated as half the median estimate to twice the median estimate of seismic displacement. So, the median seismic displacement calculated using equation with ε = 0 can be halved and doubled to develop approximately the 16 to 84 per cent exceedance seismic displacement range estimate.

Validity domain

The Bray and Travasarou method was originally developed for the analysis of embankments (dams and waste dumps) and natural slopes (soil and rock). It was developed to study the maximum deviatoric component of the movement of the embankments on their bases. This approach does not intend to deal with soils susceptible to pore water pressure increase during an earthquake and the related soil softening regime. The statistical model was constructed from 688 recorded accelerograms from 41 earthquakes with magnitudes between 5.5 and 7.6 at an epicentral distance less than 100 km on broad soil foundation types. Calculations concern embankments of height between 12 m and 100 m, shear wave velocities ranging from 200 m/s to 425 m/s, critical seismic coefficient ranging between 0.02 and 0.4, and fundamental periods varying from 0 to 2 seconds. The method takes into account that gravity is constant and equal to 17.6 kN/m^3, with a single curve of shear modulus and damping. They justify this choice by a low incidence of these curves on the results of a sensitivity analysis.

Validation of the method over 16 dams showed good predictions for structures having undergone the lowest seismic displacements (< 5 cm). The model gives the order of magnitude for the largest seismic displacements (5 cm to 50 cm), and generally offers a better prediction than previous methods. The interpretation of this validation test suggests that the estimated displacement would be zero when the method predicts a probability of negligible displacement greater than or equal to 50 per cent. However, a probability of zero per cent of negligible displacements corresponds to measured displacements higher than 15 cm.

8.8.3 Crest settlement

Swaisgood (2003) has carried out an extensive study of case histories of embankment dam behaviour during earthquakes, particularly those that are not susceptible to liquefaction problems. The objectives of the study were to determine if there is a 'normal' trend of seismic deformation that can be predicted and if there are certain factors that consistently have an effect on the amount of damage and deformation incurred during earthquakes. Nearly 70 case histories have been reviewed, compared and statistically analysed in this effort. The results of this empirical study have shown that the most

important factors that appear to affect embankment crest settlement during earthquake include the:

- peak ground acceleration at the site
- earthquake magnitude.

The relationship between the magnitude of measured settlement and the peak ground accelerations during earthquake are plotted in Figure 8.112.

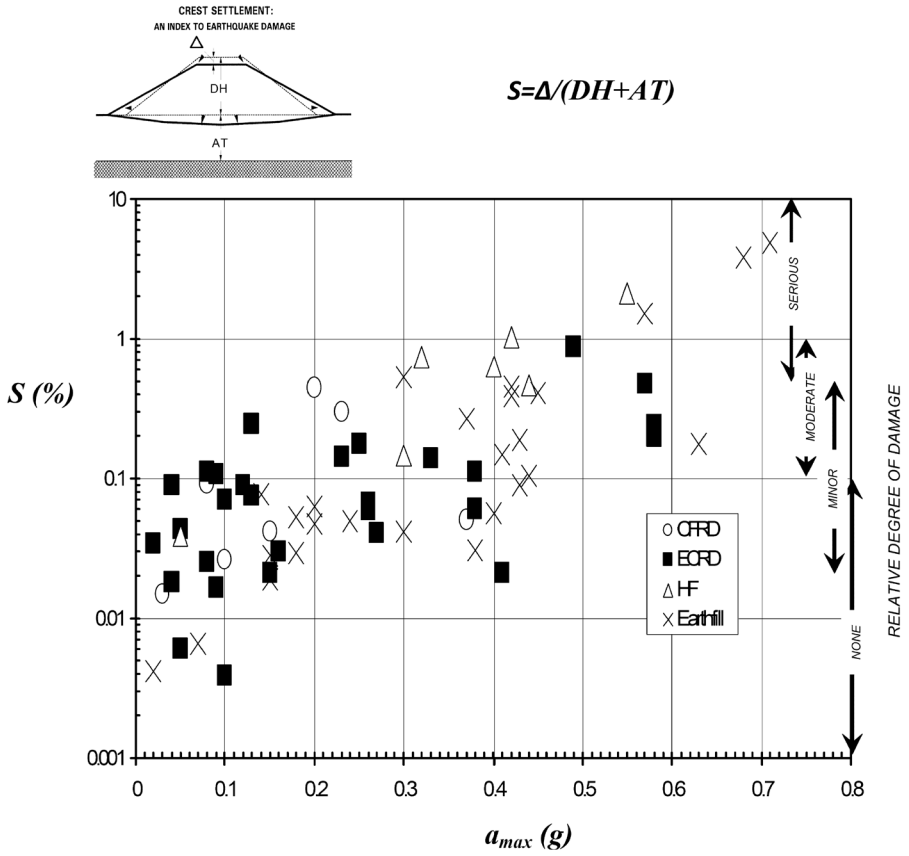

Figure 8.112 Empirical relationship between the peak ground acceleration and crest settlement (Swaisgood, 2003)

An empirical equation was formulated as an aid in estimating the amount of embankment crest settlement as follows:

$$S = \exp\left(6.07 a_{max} + 0.57M - 8.00\right) \tag{8.199}$$

where:

S = crest settlement in per cent (%)

a_{max} = peak ground acceleration (g) at the foundation rock

M = earthquake magnitude (-)

Validity domain

As reliability of this kind of method depends on the database where it has been established, this approach only gives an order of the magnitude of the crest settlement. Differences between calculated and measured settlements ranging from one to six are possible. Due to its exponential trend, this formula may be limited to moderately seismic zones. This method may only be used as a rule of thumb in early phases of the project or rapid assessment.

8.8.4 Earthquake-induced liquefaction

Liquefaction designates the generic term for the loss of strength of cohesionless soils due to excess

pore water pressure caused by cyclic loading. In many strong earthquakes, liquefaction was observed and caused significant damage to infrastructure and buildings. The mechanism of liquefaction has been studied in detail since the 1960s, starting with the Niigata and Alaska earthquakes in 1964. The knowledge of this mechanism has been gradually improved, allowing a better prediction of its occurrence during earthquakes.

8.8.4.1 Physical processes

The term liquefaction is used to describe phenomena in which the generation of excess pore pressure leads to reduction of effective stress and to softening and/or a significant weakening of effective soil strength (Kramer and Elgamal, 2001). The increase in pore pressure in the soil mass (related to the contractive behaviour of the soil under undrained loading) may be the result of applying quasi-static or dynamic loading, monotonic or cyclic stresses, shock or water transfers between layers. The term liquefaction covers several different physical phenomena such as flow liquefaction and cyclic mobility, which are defined as follows:

- **flow liquefaction** is a phenomenon that occurs when the liquefaction is initiated in a soil whose residual strength is smaller than the resistance necessary for static equilibrium of the environment. This type of failure occurs only in loose soils of low residual strength. It is the consequence of instability, which when triggered causes this movement. It can lead to extremely large deformations (slip-type flow). However, these strains are actually caused by the static shear stresses still present. The cases of flow liquefaction are relatively rare in practice, but they can cause immense damage.
- **cyclic mobility** is a phenomenon in which the shear stresses produce cyclic pore pressures in soil with residual strength greater than that which is necessary for static equilibrium of the medium. This mechanism is often manifested *in situ* in the form of lateral movement (lateral spreading), the process of accumulation of permanent displacements under the effect of static stresses during an earthquake. These deformations can occur in both relatively dense and loose soil with amplitudes more or less pronounced.

The contrasting views on the definition of soil liquefaction are due to the different approaches considered, depending on whether one prefers sites (and structures) or actions, or behavioural aspects of sandy soils in terms of description by laboratory tests or in terms of modelling. However, these definitions separate the effects of movement within the soil mass from the mechanism that drives the movement. Often, it is difficult or impossible to differentiate in the field in many cases. Note that the term residual strength seems a misnomer to sand if referring to the ultimate shear strength, but it is has become customary.

Finally, it is necessary to distinguish the concept of susceptibility to liquefaction and the liquefaction potential. According to Youd and Perkins (1978), the susceptibility to liquefaction of the soil corresponds to the fact that the soil is unable to withstand cyclic shear stresses. It depends on the particle properties, soil structure (texture), void ratio, and initial conditions. The liquefaction potential of a mass of soil concerns the risk of liquefaction of the soil for given seismic conditions. The potential for liquefaction depends on the seismic excitation and susceptibility of the soil to liquefaction as a behaviour.

8.8.4.2 Governing parameters

In the field, liquefaction generally concerns cohesionless soils and particularly fine to coarse sands, especially when such materials have a uniform size. But this view, oriented towards the behaviour of an elementary volume of soil (laboratory test), is not sufficient to characterise liquefaction phenomenon at the scale of a soil layer, because many additional factors are involved in this process.

The soil liquefaction susceptibility is the inability of soil to resist shear stress and monotonic or cyclic loading. It does not only depend on the physical and mechanical properties of soil. Liquefaction potential of a soil mass concerns the risk of liquefaction of the mass in the considered loading conditions, monotonic or cyclic. Liquefaction potential of a soil layer depends on several factors, which are not always easy to distinguish in the field (Prakash, 1981). These factors may be listed as follows:

- parameters related to the site:
  - thickness and depth of the layer
  - morphology of the site
  - profile of the underlying soils, the depth of substratum, surface layer (and all their physical, mechanical and hydraulic properties)
  - saturation and drainage conditions (hydraulic boundary conditions)
  - degrees of freedom of ground motion in the kinematic conditions of the site
  - structures built on the site, including soil reinforcement
- parameters related to the load:
  - type of load applied to the soil from its original state, static (monotonic) or dynamic (cyclic)
  - in static mode, the load and speed
  - dynamic mode, intensity, frequency and duration of loading and, in terms of earthquakes, the intensity and duration of seismic motion, the distance to the source etc
- parameters related to the soil:
  - history and age of the deposit
  - the soil physical properties (particle size, specific gravity etc), Its structure, its homogeneity, cementing
  - mechanical properties (undrained strength, deformability), hydraulic (permeability), and its anisotropy
  - the initial state mechanical, with the depth and variable depending on the history of the soil.

Density

The mechanical behaviour of sandy soils depends on two main factors, their physical nature and state. The physical nature of the soil corresponds to the mineralogical composition of grains, their size distribution, shape and angularity, fines content etc. Soil state refers to conditions under which the soil occurs. This state is described by variables such as relative density (represented by the density index, I_D. See Section 7.8.3), soil texture, and effective stress in the field.

In general, the cyclic strength of sands depends strongly on density. Loose sands are collapsible under drained conditions and have a higher susceptibility to liquefaction under undrained conditions.

Age effect

The resistance of sandy soils to liquefaction is not only influenced by the relative density and grain size distribution, including the presence of fines, but also by the age of the formation, which affects the soil structure. The precise mechanism of aging of soils is still not well understood. However, these changes are related to mechanical processes such as sedimentation, over-consolidation or rearrangement of particles in configurations more stable and/or physicochemical processes of cementation by creating links to soil particle contacts.

Youd and Perkins (1978) noted that the most recent soils, ie younger than 500 years, have a susceptibility to liquefaction of high to very high. The oldest soils of Holocene age (500 to 10000 years) have moderate to high susceptibility and soils of Pleistocene age (10000 to 1.8 million years) a very low to low susceptibility.

Initial stress conditions

The stress states encountered *in situ* are not isotropic and there are many situations in practice where the soil foundation supports a non-zero initial shear stress on a horizontal plane (on a slope or at the foot of a foundation or earth structure). In the simplest situations, the initial stress states are defined by a coefficient of earth pressure at rest K_0 different from unity, which is the ratio of effective horizontal stress σ'_{h0} and effective vertical stress σ'_{v0} to the depth z ($K_0 = \sigma'_{h0}/\sigma'_{v0}$). During the earthquake, the soil element

is subjected to additional shear stresses (cyclic) due to wave propagation in the soil mass. The presence of initial static stress plays an important role on the cyclic response of the soil.

Work dedicated to evaluate the effect of initial stresses on cyclic resistance lead to contradictory conclusions. It appears that the cyclic strength of sands can both increase or decrease in the presence of anisotropic initial stress, according to the relative density of sand (as it is expanding or contracting), the level of static shear stresses, and amplitude of cyclic shear, Δq_{SA} (alternating cycles or not).

Loading mode

In the laboratory, the cyclic strength of sands depends on the mode of loading (triaxial, simple shear, torsion or other). Correction factors have been proposed to standardise the measurements of resistance from different sources. More generally, the resistance also depends on the nature of the unidirectional or multidirectional seismic signals.

Soil structure

The cyclic resistance of reconstituted sands in the laboratory depend strongly on the method of specimen preparation (pluviation, moist tamping, compaction). This shows the importance of structural effects.

Many other factors have been studied experimentally concerning the nature of the sands, their structure (given by the method of preparation for the soil reconstituted), shape and grain size, grain crushability etc. These factors often appear to have significant influence, at least in small deformations until the outbreak of a possible instability of the sand, and seem to have less influence during the regime of steady flow.

8.8.4.3 Liquefaction criteria for sands

From a phenomenological point of view, the definition of liquefaction of sands based on monotonic and cyclic undrained laboratory tests expresses:

- two successive stages in the process, a step of triggering (or not) of the instability of sand, followed by a step of flowing (or not)
- trigger thresholds, which can be defined by different criteria formulated in terms of deformations, stresses, or pore pressures or another combination of the previous parameters.

All definitions given in the literature are not equivalent and all thresholds are not interchangeable because they often depend on the conditions under which they were defined (including loading modes, the initial state, and the structure of sand etc). So, it is important to distinguish the triggering criteria of liquefaction of sands and its potential effects.

In terms of cyclic loading, failure is defined by a threshold axial strain reached for a given number of cycles of uniform shear stress. This definition of liquefaction corresponds to the point where a sudden loss of resistance is observed followed by unlimited deformation (steady-state deformation). Other definitions are based on the ratio of pore pressure $r_u = \sigma_v/u$ and liquefaction initiation defined as the moment when r_u = 100 per cent.

In practice, the definition of criteria for liquefaction is quite arbitrary. Indeed, the thresholds are defined in the range of small and medium deformations. One great difficulty is that the state conditions strongly affect the behaviour of sands in this deformation range and that the criteria are highly dependent on, among others, the loading modes. So, it is difficult to define criteria for liquefaction triggering in general and applicable to *in situ* (unknown) conditions prevailing at the sites.

In situ state of sands

Studies of the behaviour of natural sand cannot be undertaken without an effective means of collecting

these materials *in situ*. Various techniques are used including large diameter sampling or freezing before sampling and transportation to the laboratory. Testing has shown that the cyclic resistance of natural sands is generally larger than their equivalent reconstituted samples at the same density. These additional resistances were probably acquired at the time of their deposition and subsequent aging.

8.8.4.4 Clayey soils liquefaction potential

It is difficult to determine the susceptibility to liquefaction of silty and clayey soils and, where they are susceptible, how to characterise this. In other words, "are the test methods and criteria for sands transferable and applicable to clayey and/or silty soils?" These questions arise primarily for recent unconsolidated deposits, in which these materials are generally soft, not very resistant and very deformable.

Boulanger and Idriss (2006) propose new criteria to qualify the "liquefaction susceptibility" of saturated silts and clays. The term liquefaction is used incorrectly in this case, even if these materials can exhibit high levels of strain during monotonic or cyclic loads. Also, considering the fine soils as a whole, the authors advocate using the term liquefaction to describe the large deformation or loss of strength that appear in sandy soils (sand-like) and the term of cyclic softening to describe similar mechanisms that appear in clayey soils (clay-like).

Recent poorly consolidated clayey soils are soft and deformable. They have a very low resistance, undrained shear strength, c_u, in terms of total stress, with low deformation moduli. In natural homogeneous normally consolidated deposits, c_u increases approximately linearly with depth. The relationship between c_u and effective vertical stress σ'_{v0} is of the order of 0.2 ($c_u/\sigma'_{v0} \approx 0.2$). But the undrained cohesion also depends on the degree of over-consolidation of the clay. Undrained cohesion is used to normalise the mechanical properties of clays, as the ratio τ_{cyc}/C_u for example, where τ_{cyc} is the cyclic shear strength. Undrained strength of clays also increases with the speed of loading, five to 15 per cent per log cycle of the shear rate.

Undrained cyclic tests generally show a progressive amplification of deformations, associated with a gradual increase in pore pressure, showing no signs of instability, unless a particular case of sensitive clays. The state of zero effective stress is not reached during cycles ($r_u < 100$ per cent).

8.8.4.5 Silty soils liquefaction potential

Silts can be considered intermediate between sands and clays in terms of undrained behaviour. Many authors have emphasised their liquefiable character in support of *in situ* observations from different earthquakes. As for the sandy soils, many experimental studies focus on laboratory tests on reconstituted soils by mixing sand with silt particles, or even clay particles. As for reconstituted sands, the representativeness of these mixtures is often discussed.

Intact silt samples under undrained conditions show a behaviour under cyclic leading intermediate between natural unconsolidated clays and sands. By filiation with the sands, their dilatancy helps limit deformations. But dilatancy cannot be exacerbated as well as in clean sands because the voids are filled by fine particles. However, according to several studies, it appears that silts or silty clayed sands with low to medium plasticity behave differently from the sands during cyclic loading under undrained conditions, in terms of progression of the deformations and pore pressure generation in particular. The data available to date does not reveal any instability mechanism in intact silts.

There is a degree of confusion in the engineering profession about the liquefaction susceptibility of silty soils (Andrews and Martin, 2000). Because the grain size of silt falls between that of sand and clay, it is often assumed that the liquefaction susceptibility of silts must also fall somewhere between the high susceptibility of sands and the non-susceptibility of clays. Confusion about the liquefaction susceptibility of silty soils is further exacerbated whenever silts and clays are coupled under the one heading 'fines'.

8.8.4.6 Physical properties of soils criteria

Procedures to identify potentially liquefiable soils have been developed around the consistency limits, particle size distribution and the water content, or combinations of these properties. These procedures are based on a proposal by Wang (1979), later developed by Seed and Idriss (1982) as the Chinese criteria (Figure 8.113).

These criteria are used to identify suspicious soils with respect to the risk of liquefaction and non-susceptible soils, considering the site conditions and the seismic level. However, authors such as Boulanger and Idriss (2006) and others believe that these criteria are often misinterpreted as evidence of liquefaction risk exclusion, and should be abandoned in practice.

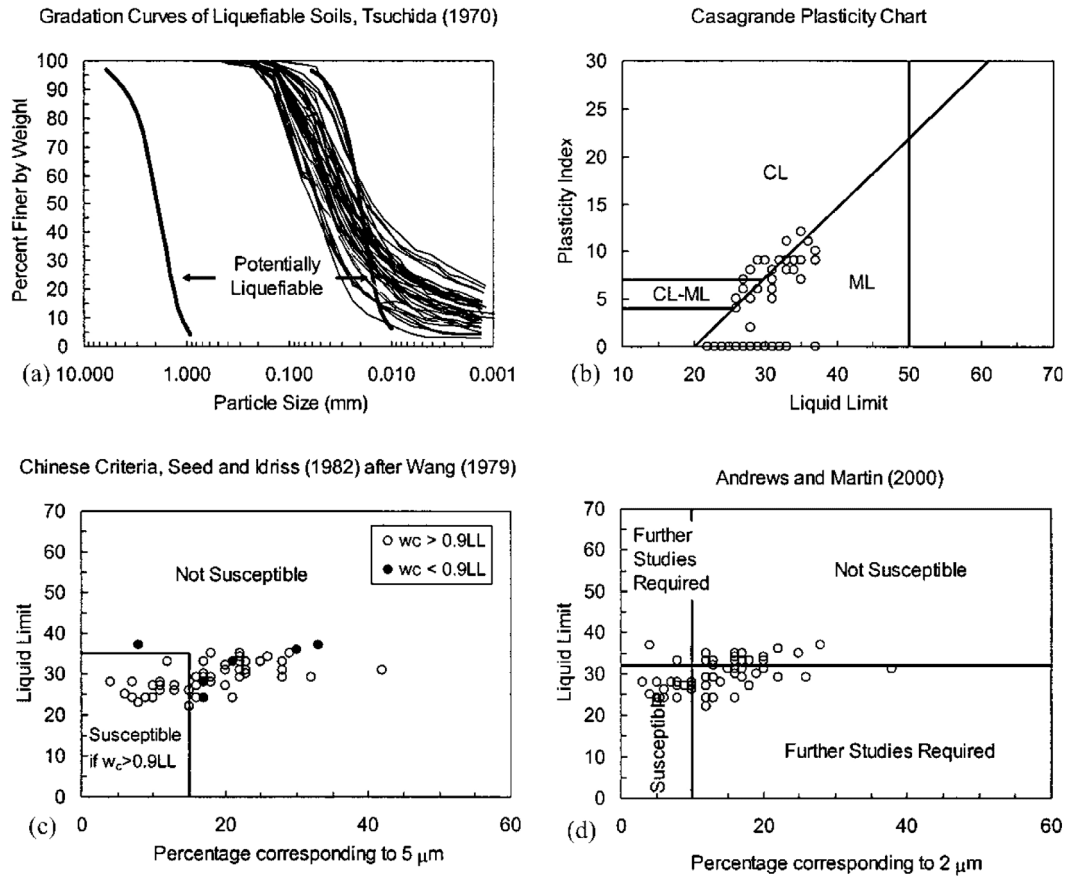

Figure 8.113 Different criteria for determining liquefaction susceptibility of fine-grained soils (from Seed and Idriss, 2004)

However, the physical properties of fine soils may still constitute a guide to a soils' susceptibility to liquefaction. These properties can provide useful clues to distinguish soils with sand-like behaviour from those with clay-like behaviour, as advocated by Boulanger and Idriss (2004). Based on a large number of references to undrained monotonic and cyclic tests compiled in various literature, these authors propose to classify soils into these two families of behaviour. These classifications are associated with consistency limits, which allow display of an intermediate class between sandy type soils and clay type soils. The transition is on a very narrow range of the plasticity index ranging from three to seven (Figure 8.114).

The authors then propose rules for practical applications. Soils with plasticity index greater than 7 (PI $\geq$ 7) can be considered as clay-like. This includes clay of low plasticity (CL). For soils classified as silt and clay of low plasticity (ML-CL), the criterion may be reduced to PI $\geq$ 5. Soils that do not meet this criterion should be considered sand-like and eventually liquefiable, unless specific laboratory or *in situ* tests show otherwise. These soils are those for which the correlations with field tests are most appropriate to assess their cyclic strength (CPT, SPT). For soils whose behaviour is intermediate and PI whose indices range from three to six, it is recommended to perform laboratory tests in conjunction with field tests, which are not considered totally reliable in this case. In the absence of laboratory tests, the threshold remains at PI = 7.

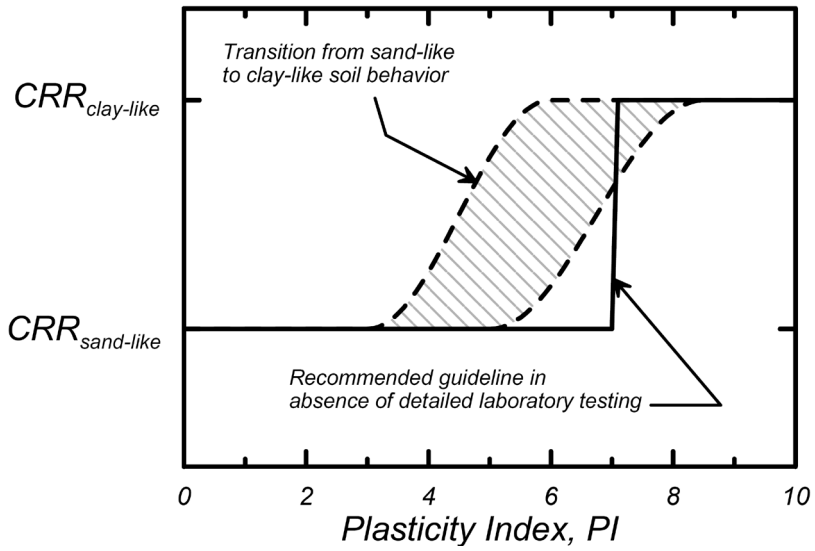

Figure 8.114 Schematic illustration of the transition from sand-like to clay-like behaviour for fine-grained soils with increasing PI, CRR = cyclic resistance ratio (from Seed and Idriss, 2004)

8.8.4.7 Simplified methods

A simplified procedure for the evaluation of soil resistance to liquefaction was proposed by Seed and Idriss (1971). The liquefaction resistance is expressed by means of the cyclic resistance ratio (CRR), while the cyclic loading imposed on the ground by the earthquake is expressed by the cyclic stress ratio (CSR). Soil liquefaction is possible if CSR ≥ CRR.

Two hypotheses form the basis of the simplified methods. The first hypothesis assumes that the shear stresses act on a horizontal plane in the soil mass. This assumption is based on an approximation that the shear waves propagate vertically from the bottom to the top of the soil column. The second hypothesis is to assume that irregular seismic signals can be converted into equivalent signals whose amplitude is uniform and in relation with the peak acceleration surface.

Determination of cyclic stress ratio

Under these hypotheses, seismic induced stresses into the soil mass reduce to a shear stress where the maximum value at depth, z, is given by:

$$\tau_{max} = \sigma_{v0} \frac{a_{max}}{g} r_d \tag{8.200}$$

where a_{max} is the maximum surface acceleration (m/s²), g the gravitational constant (9.81 m/s²), σ_{v0} the total vertical stress and r_d a stress reduction coefficient that accounts for the flexibility of the soil column (ie r_d = 1 corresponds to rigid body behaviour), which decrease from one at the surface to approximately 0.9 at 12 m depth. Equivalent uniform cyclic stress produced by the seismic loading, τ_{sis}, at the considered depth may be expressed as:

$$\tau_{sis} = 0.65\, \tau_{max} \tag{8.201}$$

The coefficient 0.65 defines a value of cycles more representative of loading experienced by the soil mass during the earthquake. Other close values have been proposed in the literature (0.67 or 0.66). In this approach, the cyclic stress ratio is defined by:

$$CSR = \frac{\tau_{sis}}{\sigma'_{v0}} \tag{8.202}$$

where σ'_v is the effective vertical stress at the considered depth. The method also introduces a magnitude scaling factor (MSF) to provide an approximate representation of the effects of shaking duration or the

equivalent number of stress cycles. The cyclic stress ratio is defined as a normalising factor to enable the comparison of different magnitude earthquakes:

$$MSF = \frac{CSR_M}{CSR_{7.5}} \tag{8.203}$$

Finally, normalised cyclic stress ratio is calculated by:

$$CSR_{7.5} = 0.65\, a_{max} \frac{\sigma_{v0}}{\sigma'_{v0}} \frac{r_d}{MSF} \tag{8.204}$$

Determination of MSF

The relation proposed by Idriss (1999) is shown in Figure 8.115 and expressed as:

$$MSF = 6.9\, \mathrm{e}^{-M/4} - 0.058 \leq 1.8 \tag{8.205}$$

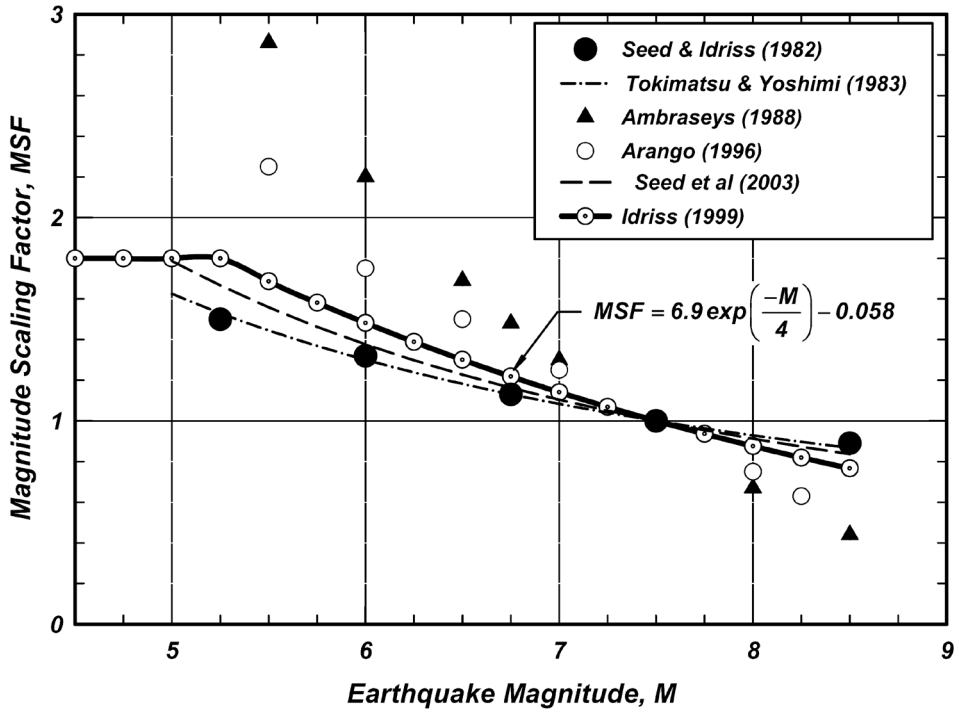

Figure 8.115 Magnitude scaling factor proposed by various investigators (Boulanger and Idriss, 2004)

Determination of r_d factor

The r_d parameter should be expressed in terms of depth and earthquake magnitude (Figure 8.116). The following empirical relation was derived by Idriss (1999):

$$r_d = -1.012 - 1.126 \sin\left(\frac{z}{11.73} + 5.133\right) + M\left[0.106 + 0.118 \sin\left(\frac{z}{11.28} + 5.142\right)\right] \tag{8.206}$$

where:

z = depth (m)
M = magnitude of the earthquake (-)

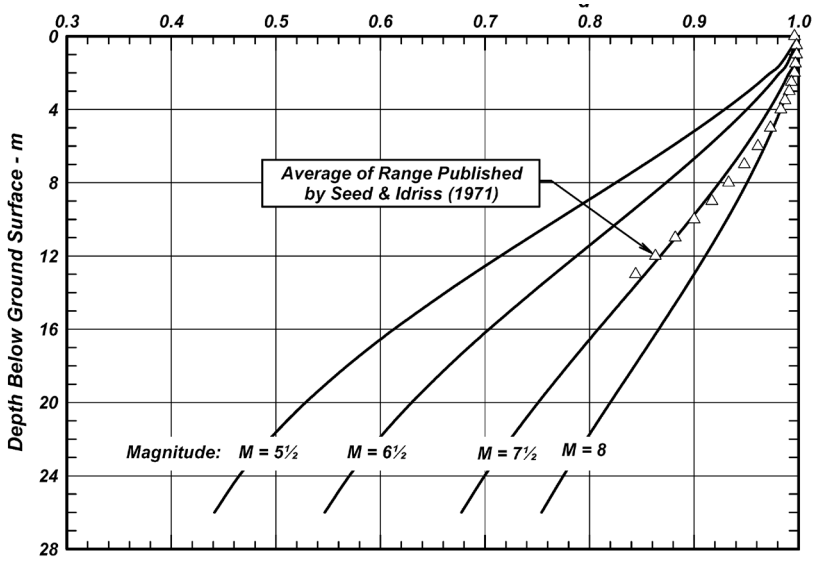

Figure 8.116 Variation of strength reduction factor with depth and earthquake magnitude (Boulanger and Idriss, 2004)

Normalised SPT and CPT resistances

According to Idriss and Boulanger (2004), the effective use of SPT blow count and CPT tip resistance as indices for soil liquefaction characteristics require that the effect of soil density and effective confining stress on penetration resistance be separated. Consequently, Seed *et al* (1975) included the normalisation of penetration resistance in sand to an equivalent σ'_{v0} = 1 atm (101 kPa) as part of the empirical procedure. The purpose of the overburden normalisation is to obtain quantities that are independent of σ'_{v0} and so are more likely to relate to the sands relative density (Boulanger and Idriss, 2004).

SPT test

For SPT tests, this normalisation currently takes the form:

$$N_{1,60} = C_N \frac{E}{E_{60}} N \tag{8.207}$$

where:

C_N = correction factors (-)
E = transmitted SPT energy blow (J)
E_{60} = 60 per cent energy blow efficiency (J)
N = SPR blow count (-)

Boulanger and Idriss (2004) proposed the following expressions for determining correction factor from an iteration process:

$$C_N = \left(\frac{P_a}{\sigma'_{v0}}\right)^{0.784-0.0768\sqrt{N_{1,60}}} \leq 1.7 \tag{8.208}$$

CPT test

The normalised cone tip resistance is given by:

$$q_{c,1N} = C_q \, q_c \tag{8.209}$$

where:

C_q = correction factors (-)
q_c = cone tip resistance (kPa)

The correction factor is also estimated iteratively from the empirical formula:

$$C_q = \left(\frac{P_a}{\sigma'_{v0}}\right)^{1.338-0.249q_{c1N}} \leq 1.7 \tag{8.210}$$

Shear wave velocity test

As for SPT and CPT resistances, the shear wave velocity is normalised as follows:

$$V_{s1} = C_V\, V_s \tag{8.211}$$

with

$$C_V = \left(\frac{P_a}{\sigma'_{v0}}\right)^{0.25} \leq 1.4 \tag{8.212}$$

Determination of cyclic resistance ratio (CRR)

Once the resistances have been normalised, the value of cyclic resistance ratio for a magnitude M = 7.5 and an effective vertical stress σ'_{v0} = 1 atm may be estimated based on the field test data (SPT, CPT, Shear wave velocity) and Equations 8.213 to 8.217 as detailed following.

SPT test

To estimate the cyclic resistance ratio, the SPT penetration resistance is adjusted to an equivalent clean sand value as:

$$N_{1,60cs} = N_{1,60} + \exp\left(1.63 + \frac{9.7}{\text{FC}} - \left(\frac{15.7}{\text{FC}}\right)^2\right) \tag{8.213}$$

where FC is the soil fine content (%) defined as the proportion of fines retained by a no 200 sieve (D < 0.075 mm). The variation of SPT blow count with correction factor, C_N, is shown in Figure 8.117.

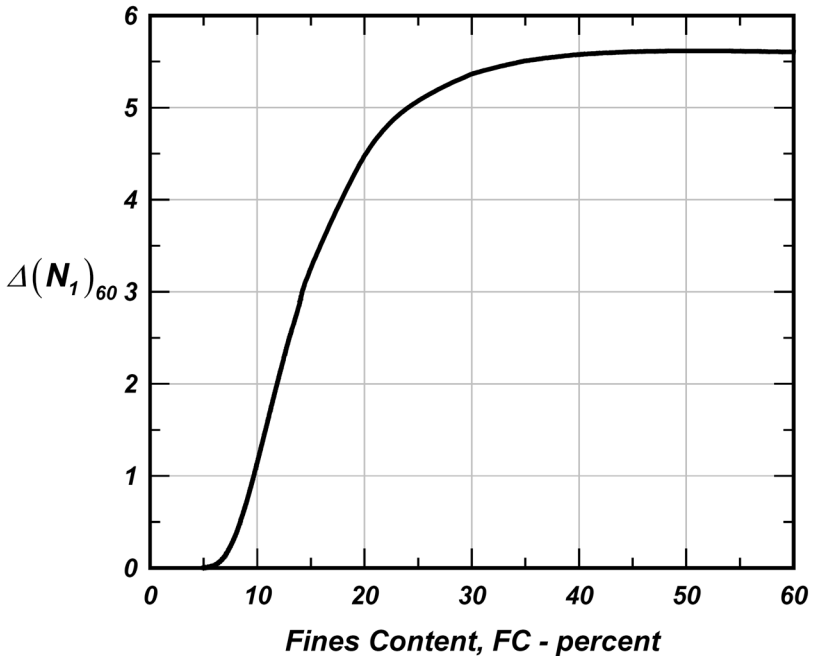

Figure 8.117 Variation of SPT blow count correction factor with fine content (Boulanger and Idriss, 2004)

So, following Boulanger and Idriss (2004), the cyclic resistance ratio is shown in Figure 8.118 and expressed as:

$$CRR_{7.5} = \exp\left(\frac{N_{1,60cs}}{14.1} + \left(\frac{N_{1,60cs}}{126}\right)^2 - \left(\frac{N_{1,60cs}}{23.6}\right)^3 + \left(\frac{N_{1,60cs}}{25.4}\right)^4 - 2.8\right) \tag{8.214}$$

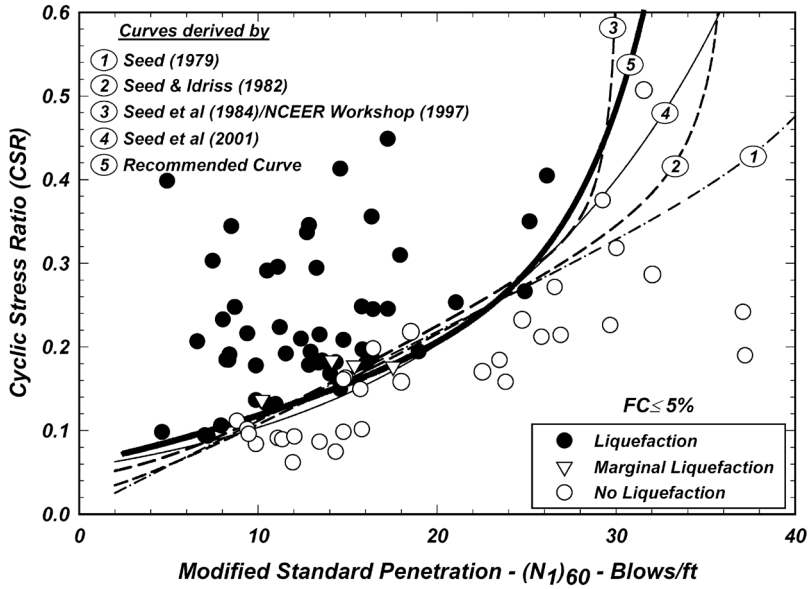

Figure 8.118 Curves relating CRR to $N_{1,60}$ for clean sands and the curves recommended by Boulanger and Idriss (2004) for M = 7.5 and σ'_0 = 1 atm

Figure 8.118 has plotted the corrected SPT blow counts versus the corresponding cyclic stress ratio for numerous field sites where liquefaction was or was not observed following an earthquake. The different lines correspond to different curves proposed to fit the limit between liquefaction and no liquefaction zones.

CPT test

In the case of CPT tests, and for FC ≤ five per cent soils, the expression of cyclic resistance ratio is shown in Figure 8.119 and may be expressed as:

$$CRR_{7.5} = \exp\left(\frac{q_{c1N}}{540} + \left(\frac{q_{c1N}}{67}\right)^2 - \left(\frac{q_{c1N}}{80}\right)^3 + \left(\frac{q_{c1N}}{114}\right)^4 - 3.0\right) \quad (8.215)$$

For fine contents ≥ five per cent, specific procedures may be used to determine CPT resistance, such as Robertson and Wride (1997), which introduce a soil behaviour type index as a function of cone tip resistance and sleeve friction ratio, or Moss (2003), which use CSR and R_f values to estimate the fine content adjustment.

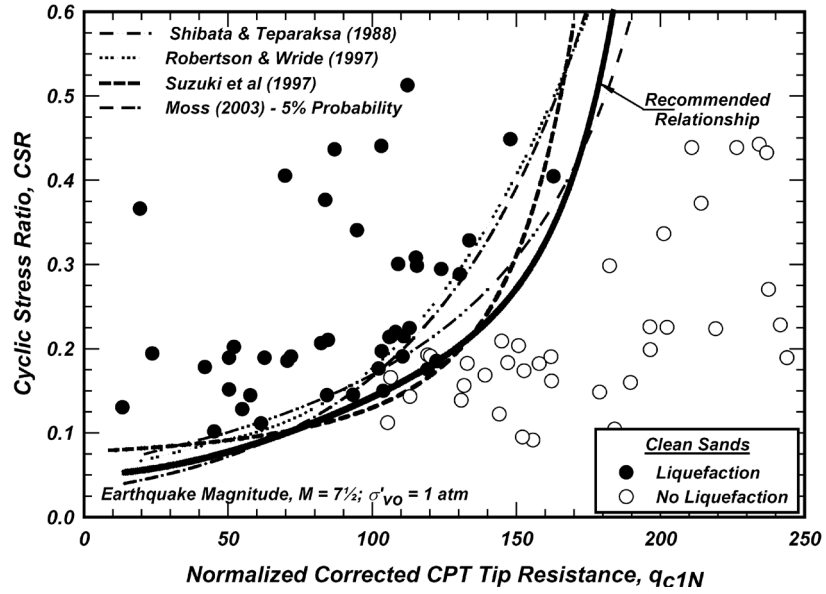

Figure 8.119 Curves relating CRR to q_{c1N} for clean sands and the curves recommended by Boulanger and Idriss (2004) for M = 7.5 and σ'_{v0} = 1 atm

Shear wave velocity test

The cyclic resistance ratio based on shear wave velocity is shown in Figure 8.120 and expressed as:

$$CRR_{7.5} = \left\{ 0.22 \left(\frac{V_{s1}}{100} \right)^2 + 2.8 \left(\frac{1}{V_{s1}^* - V_{s1}} - \frac{1}{V_{s1}^*} \right) \right\} \tag{8.216}$$

with

$$200 \leq V_{s1}^* = 215 - 0.5\,(FC - 5) \leq 215 \tag{8.217}$$

where FC is the soil fine content and V_{s1}^* the limiting upper value of V_{s1} for liquefaction occurrence. The curves recommended by Andrus and Stokoe (2000) are shown in Figure 8.120. On this figure, the dashed line indicates that field performance data are limited. They do not extend much below 100 m/s, because no field data were available to support extending them to the origin. It is important to note that these boundary curves are for extreme behaviour, where boils and ground cracks occur.

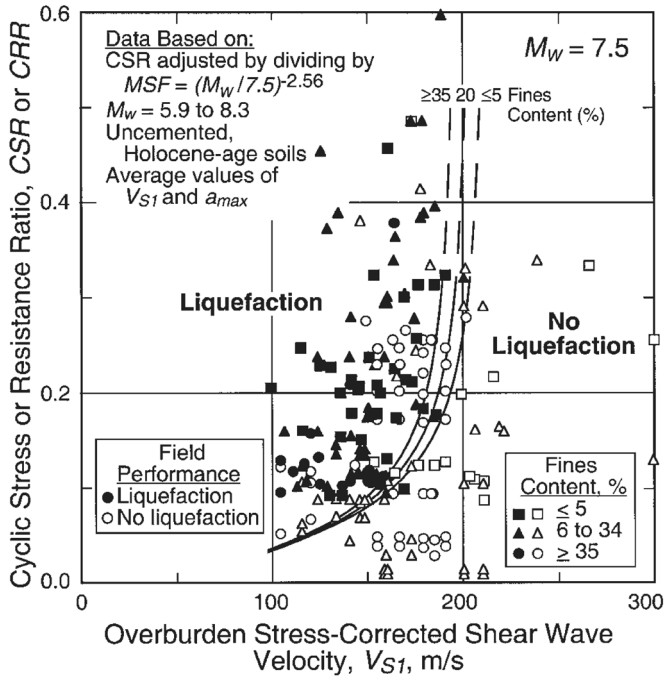

Figure 8.120 Curves relating CRR to V_{s1} for clean sands and the curves recommended by Andus and Stokoe (2000) for M = 7.5 and σ'_{v0} = 1 atm

8.8.4.8 Modelling soil liquefaction

Most commonly used methods of ground response analysis are based on the equivalent linear model (Seed, 1973). This model is a total stress approach and so does not take into account the effect of pore water pressures on soil properties and dynamic response during earthquake or cyclic loading. This was a major factor leading to the development of effective stress analysis models that are able to generate pore water pressures during earthquake or cyclic loading.

Semi coupled models

- **Martin-Finn-Seed model**

The first model of this kind was developed by Martin *et al* (1975) and Seed *et al* (1976). They proposed a relationship between pore water pressure and the number of uniform shear stress cycles that cause liquefaction (determined from cyclic triaxial tests).

It has to be noted that some commercial codes propose successive use of equivalent linear models (eg QUAKE/W) to determine a pore pressure ratio function based on equivalent number of uniform cycles.

The pore pressure ratio is then implemented in slope stability analysis tools (SLOPE/W) to determine the effective shear strength of the soils along a given slip surface. This simplified approach may be useful in the context of a tiered approach.

- **Pecker model**

The basic idea of this model (Pecker *et al*, 2001) consists of splitting the time into two separate scales associated with (a) the cyclic loading (fast time) and (b) with the steady pore pressure increase and dissipation (slow time). The fastest phenomena (pore pressure build-up or pore pressure dissipation) will govern the residual pore pressure at any time. Under constant mean pressure, the pore pressure increment depends on the bulk modulus of soil skeleton and the volumetric strain increment.

Fully coupled constitutive models

Various constitutive models have been developed that can capture the liquefaction behaviour of sands (Jefferies 1993, Drescher *et al*, 1995, Byrne *et al*, 1995, Gudehus, 1996, Wolffersdorff, 1996, Drescher and Mróz, 1997, Puebla *et al*, 1997, Niemunis and Herle, 1997, Beaty and Byrne, 1998, Yu, 1998, Boukpeti and Drescher, 2000, Boukpeti *et al*, 2002, Jefferies and Shuttle, 2002, Mróz *et al*, 2003, and Imam *et al*, 2005). The practical application of a constitutive model for a geotechnical problem is only possible when the model is implemented in a finite element/finite difference program. Some of the constitutive models that are implemented (as user defined soil models) in commercial finite element/difference codes are described here:

- **UBCSAND Model**

This model was developed at the University of British Columbia (Byrne *et al*, 1995, Puebla *et al*, 1997, and Beaty and Byrne, 1998). It is an elastic–plastic model developed specifically for liquefaction behaviour of sand. The model is implemented in the commercial computer code FLAC (Fast Lagrangian analysis of Continua, ITASCA 2005). The UBCSAND model has also been implemented (Tsegaye, 2010) in the finite element program PLAXIS (Brinkgreve *et al*, 2010).

- **Hypoplastic model for sand**

Hypoplasticity is a newly developed framework for constitutive modelling of granular materials. Unlike elasto-plasticity, hypoplasticity does not make use of the concepts such as yield surface and plastic potential (Kolymbas, 2000). There are several versions of hypoplasticity available in literature. The Hypoplastic model (Wolffersdorff, 1996) has been implemented (Masin, 2010) in the finite element program PLAXIS.

- **NorSand model**

NorSand is a critical state elastic-plastic constitutive model (Jefferies, 1993, and Jefferies and Shuttle, 2002). NorSand has been used for modelling a range of soils from clayey silt to sand (Shuttle and Jefferies, 2010). This model is capable of capturing the liquefaction behaviour of sands.

- **CASM – a unified state parameter model for clay and sand**

CASM (clay and sand model) is a critical state elastic-plastic model developed by Yu (1998) and further extended by Yu *et al* (2006). CASM is capable of predicting the behaviour of clay and sand under both drained and undrained loading conditions. CASM has been implemented (Khong, 2004) into the finite element program CRISP (CRItical State soil mechanics Program).

Limitations of phenomenological models

It has been shown (Finn, 1999) that comparison between observed cyclic response and model predictions for general loading paths were largely disappointing. In fact, despite the theoretical generality of these models, the predictions of elastic-plastic methods can be strongly path dependant. The predictions are good for loading paths close to those used to calibrate the models, but for paths far from these the predictions are often poor.

8.9 STABILITY OF FLOOD WALLS

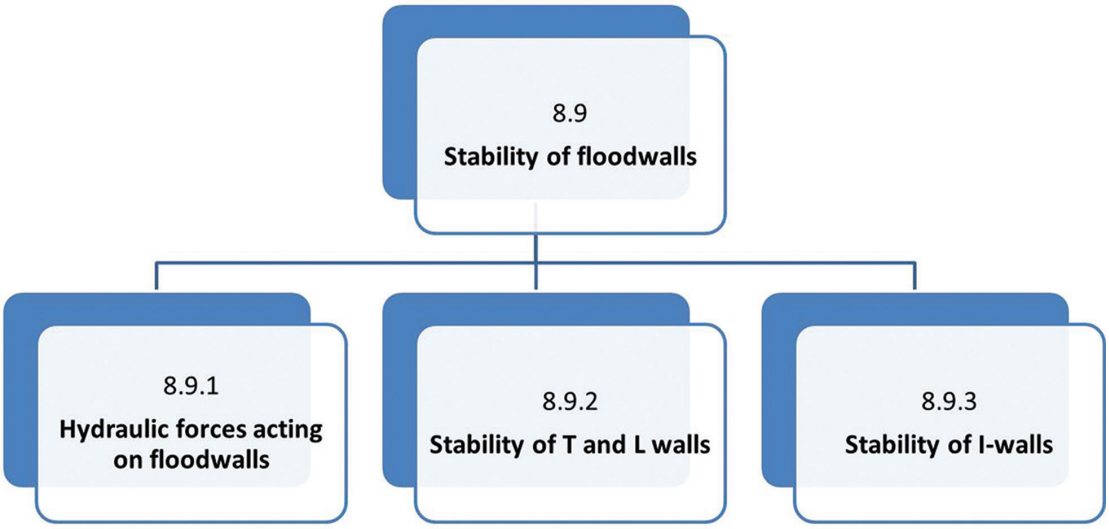

Flood walls are often an integral part of a flood protection system and are of particular concern when they are embedded into the levee section or form transitions with a levee segment. This section will detail the stability of flood walls as presented in the flow chart.

8.9.1 Hydraulic forces acting on flood walls

Analysis and design of flood wall components of levee systems requires consideration of both static and dynamic forces. Static forces result when the structure contains a level of water on one side that is stationary so pressures over the face of the wall are hydrostatic.

Where the water is moving, additional dynamic forces come into play. These wave forces are primarily estimated using impulse-momentum methods, often using empirical methods developed specifically for estimating wave forces on vertical walls.

Wave action on the wall is the primary dynamic loading to be considered for flood walls (USACE, 1989). In the case of waves, a distinction is made between the action of nonbreaking, breaking, and broken waves, where the methods are recommended for calculation of wave forces on vertical walls. Wave forces on other types of walls (ie sloping, stepped, and curved) are less well understood, so general analytical design methods may need further extension. For these instances, a coastal engineer should be involved in establishing wave forces for the design of important structures where wave forces can be expected.

8.9.1.1 Hydrostatic forces

The horizontal force produced by water acts perpendicular to the surface of the object containing it (in this case the flood wall). The pressure that water exerts on a vertical surface can be calculated by multiplying the density of water, γ, with the depth of water at the point of interest, y, as indicated in Equation 8.218. The pressure varies linearly with depth increase as indicated in Figure 8.121. The water density may be assumed constant for depths associated with flood walls, but will be determined by whether the water body is composed of fresh, brackish, or seawater in the case of rivers, estuaries, and oceans, respectively.

$$p(y) = \gamma\, y \tag{8.218}$$

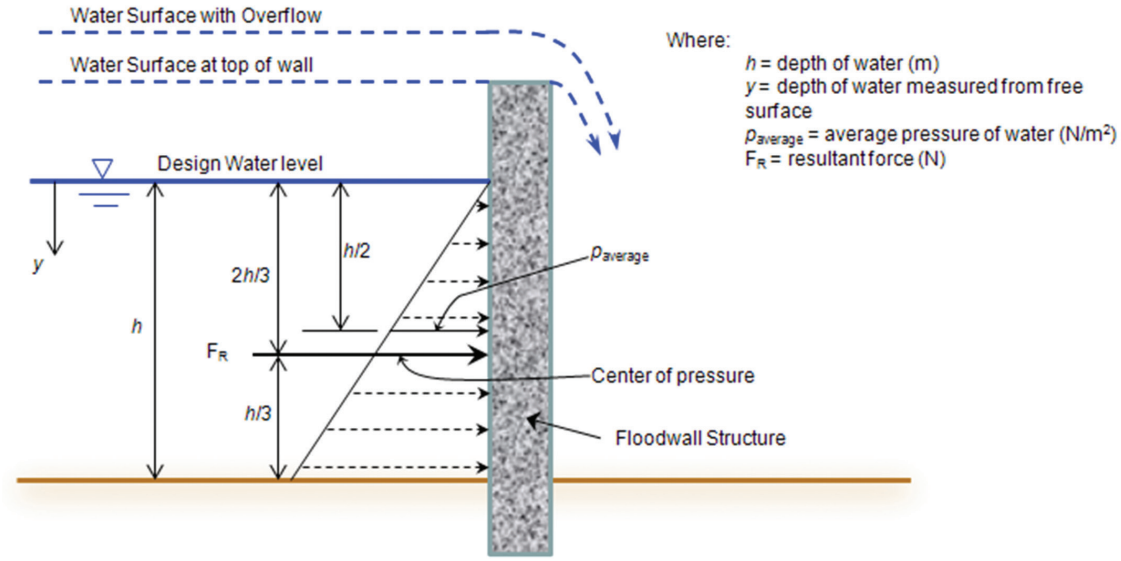

Figure 8.121 Hydrostatic pressure acting on vertical flood wall

The horizontal force acts at the centroid of the pressure distribution, which is 2/3×h below the water surface (Figure 8.121) for a vertical wall. In general, the force at any point on a vertical wall is a function of the depth of water to the point of interest. Where a flood wall has a sloped face on the waterside, both horizontal and vertical forces must be considered. The same methodology can be applied where curved or other irregularly shaped flood wall sections may exist. The reader is referred to classical hydraulics texts for formula needed for calculating centroids and areas for these shapes.

Due to the uncertainty associated with estimating the magnitude of flow on river levee systems, it is recommended that forces acting upon flood walls are calculated for:

- the design water level
- the water levels equal to the top of the flood wall crest and
- the maximum possible water level that results in overflow, if applicable (Figure 8.121).

The critical loading case to be considered for design should be where h equals the full height of the wall or the highest anticipated water level if greater than the wall height.

8.9.1.2 Dynamic forces

It has been appreciated for many years that apparently similar wave conditions may give rise to dramatically different wave pressures or forces depending on the form of wave breaking at, onto, or close to the wall. Under wind waves, there will inevitably be a wide range of wave breaking, but it is generally convenient to use categories of wave load/breaking conditions from the following:

1 Nonbreaking or pulsating.
2 Impulsive breaking or impact.
3 Broken waves.
4 Post breaking or bore waves.

Wave pressures on a vertical wall for two of these breaking types are illustrated in Figure 8.122 – nonbreaking versus impulsive. The simplest case, (type a), is generally when the wave is nonbreaking, also termed reflecting or pulsating. For this condition, the wave motion is relatively smooth, and the main processes can be predicted by simple wave theories. Simple prediction methods for pulsating wave loads by Goda or Ito generally predict average pressures up to about $p_{av} = 2\rho g H_s$ where H_s is the incident (local) significant wave height.

Much more intense wave forces/pressures arise if the wave can break directly against the wall, termed plunging, breaking, impulsive or impact (type b). Research studies in Europe have measured local wave impact pressures up to or greater than $p_{impact} = 40\rho g H_s$, much higher than would be predicted by simple design methods (Allsop and Vicinanza, 1996 and Allsop *et al*, 1996a). In extremis, tests by Kirkgoz (1995) suggest impact pressures up to $p_{impact} = 100\rho g H$, although these are highly unlikely in practice.

Impulsive breaking is strongly influenced by any mound, berm, or steep bed slope in front of the wall with conditions difficult to predict, and producing significant variability/uncertainty. In the past, these variations have led to significant lack of clarity in advice on wave forces.

Rather lower forces arise if waves have already broken before reaching the wall (type c). The wave motion is turbulent, but often highly aerated. Predictions of broken wave loads are uncertain, with relatively few laboratory or field data. The last class is the post-breaking or bore wave (type d) usually applied to a wall where the toe is above the static water level, but where the run-up bore can still reach the wall.

Broken waves occur when the local water depth is insufficient to support unbroken waves. For simple vertical walls with no significant mound, waves may start to break when the local wave height to depth exceeds, for example, $H_{si}/d > 0.35$. As local wave conditions approach the breaking limit, so the proportion of broken waves increases, and the probability of a large but un-broken wave reduces.

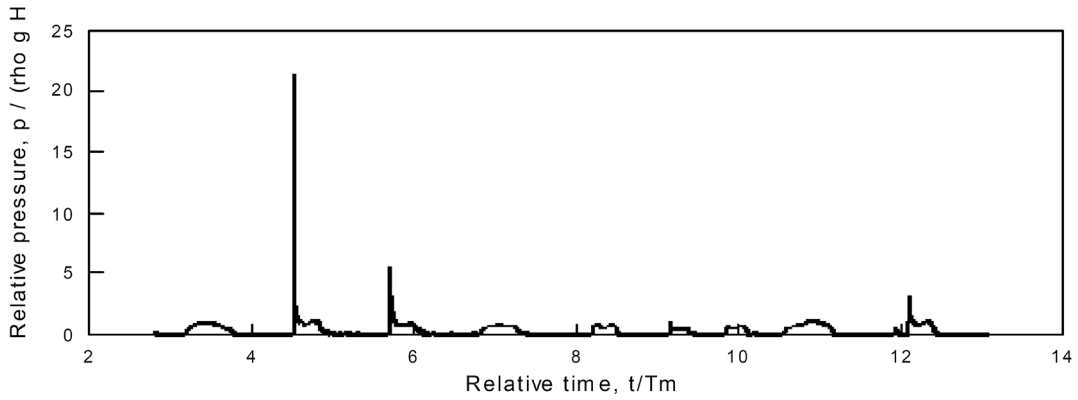

Figure 8.122 Example wave pressure traces on a vertical wall with toe berm: model test results (after Allsop et al, 1996a)

Predicting types of wave load

A method to identify the occurrence of some types of breaking and wave load, was developed in the PROVERBS project (Allsop *et al*, 1999), and is shown in Figure 8.123.

The version shown in Figure 8.123 was derived for approach slopes no steeper than 1:50. The parameter map indicates that wave impacts are most likely to occur for three categories of conditions:

- vertical walls with large waves ($H_{si}/d > 0.35$)
- walls on low mounds with large waves ($0.65 < H_{si}/d < 1.3$)
- high mounds with moderate berm widths ($0.14 < B_{eq}/L_{pi} < 0.4$) and large waves ($0.65 < H_{si}/d < 1.3$).

Using this general approach, methods to predict wave forces on vertical wall and, where applicable, are described in the following guidance:

- Goda (1985)– use for nonbreaking waves
- Takahashi modification to Goda (Takahashi *et al*, 1994) – use when a berm may cause impulsive breaking of waves
- Allsop and Vicinanza (1996) – estimate impulsive force of breaking waves
- Cuomo *et al* (2010a and b, and 2011) – estimate impulsive force of breaking waves
- Blackmore and Hewson (1984) – estimate force when wave action is broken before reaching the wall
- Camfield (1991) – estimate force when a breaking/broken bore travels over a slope or beach.

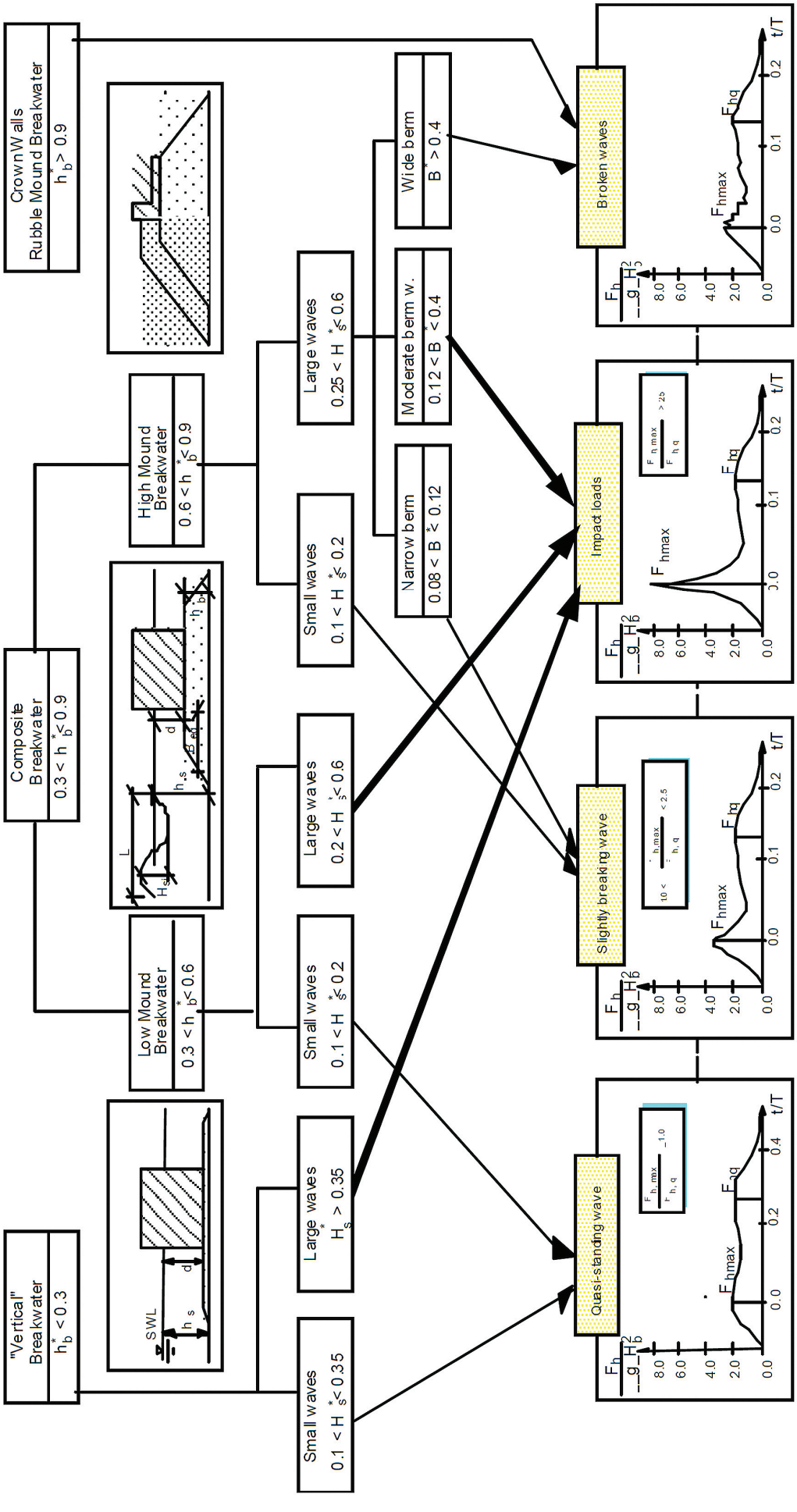

Figure 8.123 Parameter map to predict occurrence of wave load types (after Allsop et al, 1999)

Pulsating (or non-impulsive) wave loads

The main default method to calculate quasi-static wave loads should be Goda's, or Takahashi's modified version of Goda's method.

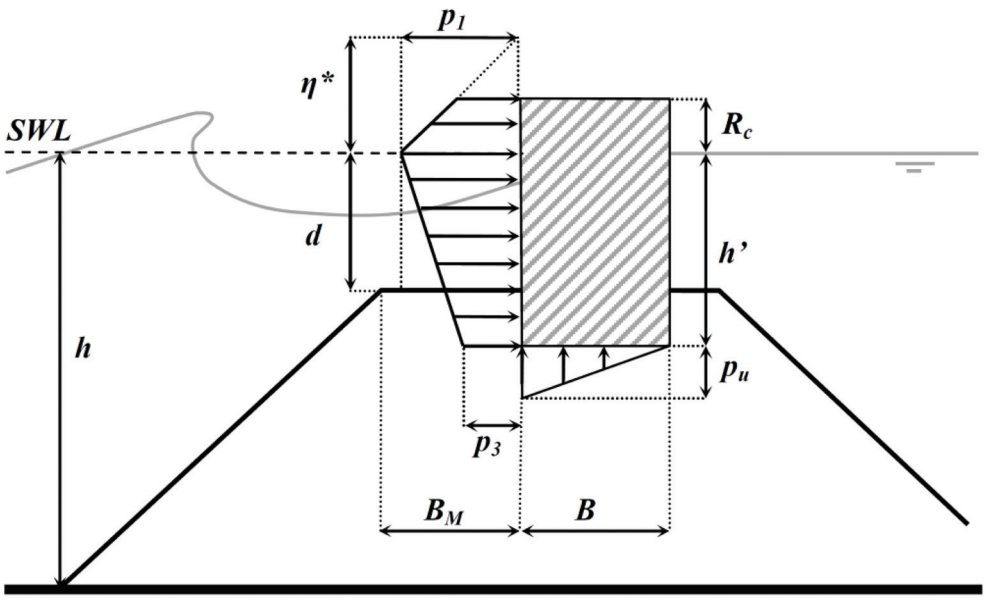

Figure 8.124 Nomenclature used in Goda's wave load prediction method (Goda, 1985)

The most robust (and most widely accepted) prediction method for wave loads on vertical and composite walls is that developed by Goda (1974 and 1985). This method assumes that wave pressures on the front face can be represented by a trapezoidal distribution, reducing from p_1 at the still water level (SWL) to p_3 at the caisson base, see Figure 8.124. At points above SWL, wave pressures reduce to zero at the notional run-up point given by a height η^* above SWL.

If wave pressures can penetrate under the wall, uplift pressures at the waterside edge might be determined by a separate expression, and may be less than pressures calculated for the toe of the waterside face. In Goda's method, uplift pressures are distributed triangularly from the waterside edge to zero at the rear heel. The method was developed from hydraulic model tests where wave pressures were measured, and from a larger set of sliding tests on model breakwater caissons. The resulting prediction formulae were then calibrated by comparison with field experience. The main response parameters determined in Goda's method are:

$$\eta* = 0.75\,(1+\cos\beta)\,H_{max} \tag{8.219}$$

$$p_1 = \frac{1}{2}\,(1+\cos\beta)\left(\alpha_1+\alpha_2\cos^2\beta\right)\gamma_w H_{max} \tag{8.220}$$

$$p_3 = \alpha_3 p_1 \tag{8.221}$$

where the coefficients α_1, α_2 and α_3 are determined from:

$$\alpha_1 = 0.6 + 0.5\left[\frac{4\pi H_s/L}{\sinh\left(4\pi H_s/L\right)}\right]^2 \tag{8.222}$$

$$\alpha_2 = \min\left\{\frac{h_b-d}{3h_b}\left(\frac{H_{max}}{d}\right)^2;\frac{2d}{H_{max}}\right\} \tag{8.223}$$

$$\alpha_3 = 1-\frac{h'}{H_s}\left[1-\frac{1}{\cosh\left(2\pi H_s/L\right)}\right] \tag{8.224}$$

where η^* is the maximum elevation above SWL (m) to which pressure could be exerted (taken by Goda as $\eta^* = 1.5\ H_{max}$ for normal wave incidence) β is the angle of wave obliquity in plan (°). The design wave height, H_{max}, is taken as $1.8H_s$ for all positions waterside of the surf zone. In conditions of broken waves, H_{max} should be taken as $H_{max,b}$. The water depth H is taken at the toe of the mound, and d over the mound at the front face of the wall, but h_b is taken $5H_s$ waterside of the wall.

The total horizontal force, F_h, is calculated by integrating pressure p_1 over the height h_f of the front face. Similarly, where appropriate, the total uplift force is calculated by integrating $p = p_u$ at the front edge to p = 0 at the rearward edge, giving a total uplift force: $F_u = 0.5\ p_u\ B$. All force and pressures calculated by Goda's method represent a 1/250 exceedance level, $F_{1/250}$.

For mounds with a relatively large height, the water depth over the mound, d, may be sufficiently smaller than the depth in front of the mound, h, to cause impulsive breaking. Takahashi *et al* (1994) have devised an adaptation of α_1 in Goda's equations, where:

$$\alpha_1 = \alpha_{10}\ \alpha_{11} \tag{8.225}$$

where α_{10} is given by $\alpha_{10} = H/d$ for $H/d \leq 2$, or $\alpha_{10} = 2$ for $H/d > 2$ and α_{11} is given by the diagram in Figure 8.125. Coefficient α_{11} takes a maximum value of 1 when $d/H = 0.4$ and $B_M/L = 0.12$. The impulsive breaking coefficient α_1 takes values between 0 and 2, with larger values giving larger wave forces.

When calculating wave forces using Goda's method modified by Takahashi, α_1 is used in place of α_2 when $\alpha_1 > \alpha_2$.

It should be noted that the Goda formula deals with wave action only. The hydrostatic action of water on both sides of the flood wall has to be added in order to calculate the resultant action of water.

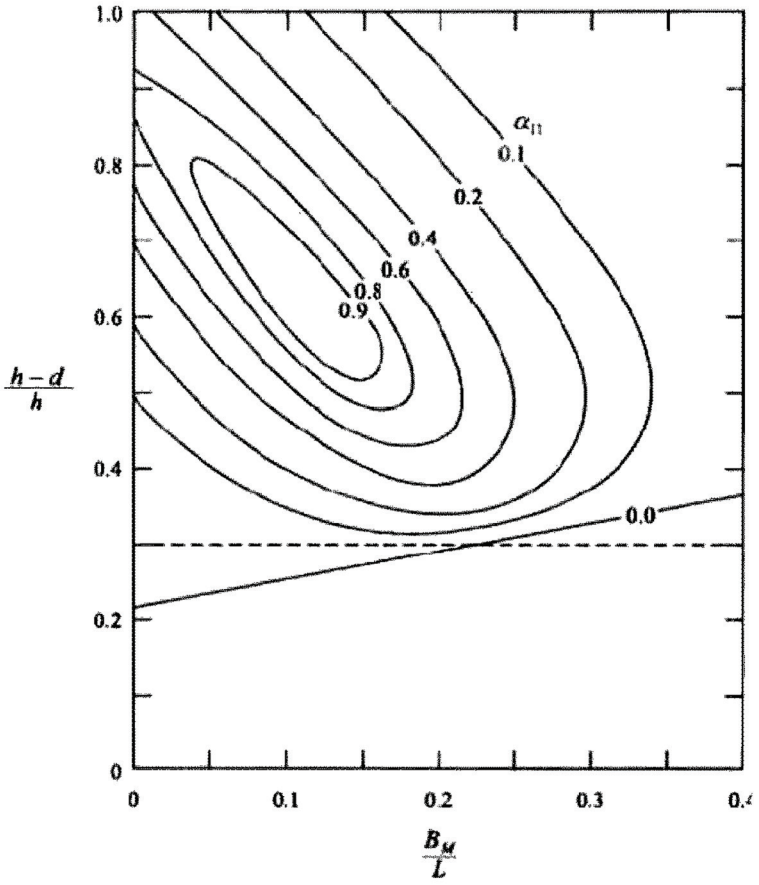

Figure 8.125 Impulsive breaking wave pressure coefficient α_{11} (after Takahashi et al, 1994)

Impulsive wave loads

A simple and robust method to predict wave impact pressures was derived by Allsop and Vicinanza (1996) based on testing by Allsop *et al* (1996a). They noted that for waves close to breaking given by $0.35 < H_{si}/d < 0.6$, other prediction methods underestimate measured forces. Differences are greatest where the incident wave conditions approach the breaking limit, approximated for shallow bed slopes by $H_{si}/H_s \approx 0.55$. A simple prediction curve using Equation 8.226 was fitted to test results for composite walls (vertical wall with a toe berm/mound) for $0.35 < H_{si}/d < 0.6$, see Figure 8.126.

$$F_{h,1/250} = 15\,\gamma_w\,d^2\left(\frac{H_{si}}{d}\right)^{3.134} \tag{8.226}$$

Fortunately, this equation also gives a good description of wave impact forces for walls on low mounds given by $0.3 < h_b/H_s < 0.6$, and higher relative wave heights given by $0.6 < H_{si}/d \leq 1.3$.

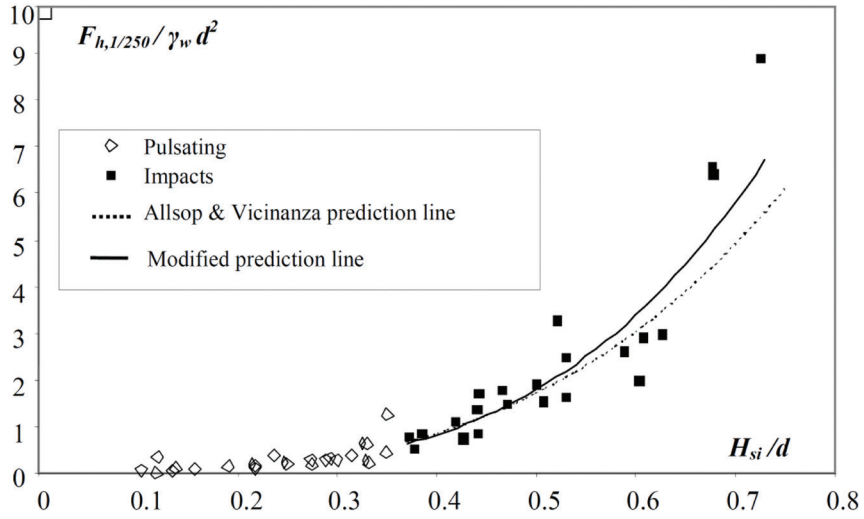

Figure 8.126 Impulsive wave load (after Allsop and Vicinanza, 1996)

Recently Cuomo *et al* (2010a, 2010b and 2011) have improved the prediction of impulsive loads using results from the Big-VOWS large-flume experiments resulting in:

$$F_{h,imp,1/250} = \gamma_w\,H_{m0}\,L_{hs}\left(1 - \frac{|h_b - d|}{d}\right) \tag{8.227}$$

where L_{hs} is the wave length at the toe of the structure, and the water depth at breaking, h_b, is evaluated using:

$$h_b = \frac{1}{k}\arctan\left(\frac{H_{m0}}{0.14L_{hs}}\right) \tag{8.228}$$

where $k = 2\pi/L_{hS}$.

Broken wave conditions

For many coastal seawalls, and for some breakwaters, the design wave condition may be limited by depth in front of the structure. In these cases, the larger waves at the structure will be broken and it is most unlikely that wave impact loads will occur. A method to estimate an average wave pressure from broken wave loads was developed by Blackmore and Hewson (1984).

$$p_{i,max} = \lambda\,\rho\,T_p\,C_b^2 \tag{8.229}$$

where λ (s^{-1})is an aeration for which values are suggested in Table 8.27, ρ is the water density, T_p is the peak wave period, C_b is the velocity of the breaker, and d is the depth at the wall. The simplest formula for breaker celerity may be given by shallow water wave theory:

$$C_b = \sqrt{gd} \tag{8.230}$$

Table 8.27 Aeration coefficients for broken wave loads (Blackmore and Hewson, 1984)

	Approach slope		
Foreshore conditions	1:5 to 1:10	1:30 to 1:50	1:100
Smooth bed, sand	1.5	0.9	0.7
Rough, rocky	0.5	0.3	0.24
Very rough, emergent rocks	0.13	0.18	0.14

These methods may be used to make an initial estimate of the horizontal wave force under broken waves, $F_{h,broken}$, to be applied only if $F_{h,broken} < F_{h,Goda}$:

$$F_{h,broken} = h_f \, p_{i,max} \tag{8.231}$$

Bore wave conditions

Where the wall (toe) is above the static water level, there is a single method cited in USACE (2006a), which was developed by Camfield (1991) and based on earlier work by Cross (1967) for wave loads on back-beach seawalls. The method requires a wave run-up limit on the beach to be calculated, from which a wave 'surge height' (H_w) at the wall is deduced. Wave run-up levels are subject to significant measurement uncertainties, and to some debate. The classic method for estimating wave run-up on beaches or shallow slopes is that ascribed to Hunt (1959), perhaps as re-stated by Battjes (1974). The 'surge' force, F_{surge}, is calculated from a 'surge height', H_{surge}, by:

$$F_{surge} = 4.5 \, \gamma_w \, H_{surge} \tag{8.232}$$

where:

$$H_{surge} = 0.2 \, H_b \left(1 - \frac{x_1}{x_2}\right) \tag{8.233}$$

where x_1 is the horizontal distance from shoreline to toe of the wall, and x_2 from the shoreline to the notional run-up point without the wall.

In its original application, on shallow beaches, the breaking wave height was approximated to be $H_b = 0.78 h_s$, but this would not be a safe estimate of H_b on slopes steeper than 1:50. Camfield (1991) recommends the method for slopes between 1:100 and 1:10, but notes that waves "on composite slopes should be investigated on a case-by-case basis".

This method gives no indication of the height over which the load applies, or of the average pressure, so simple rectangular distribution over the full wall height is generally assumed. The calculation of bore wave load is rather subjective, and it is not known whether it has been validated by any measurements, either field or laboratory, so its reliability is unknown.

Box 8.21 provides an example for the evaluation of wave loads on a reservoir wall.

Box 8.21 *Wave loads on a reservoir wave wall*

The wave wall

An embankment dam at the western end of a reservoir faces approximately east to south-east. Prevailing winds are generally away from the dam, but waves along the main fetch (650 m) of the reservoir may break directly onto the 1 m high vertical wave wall at the crest of the 1:3 embankment slope.

There is no simple prediction method for wave forces on this wall, which is within range for the particular geometry of dam slope, wave wall position, and water level. None of the usual prediction methods are strictly valid for the particular configuration given. So, it was necessary to apply a number of methods, all involving extrapolating from their original ranges.

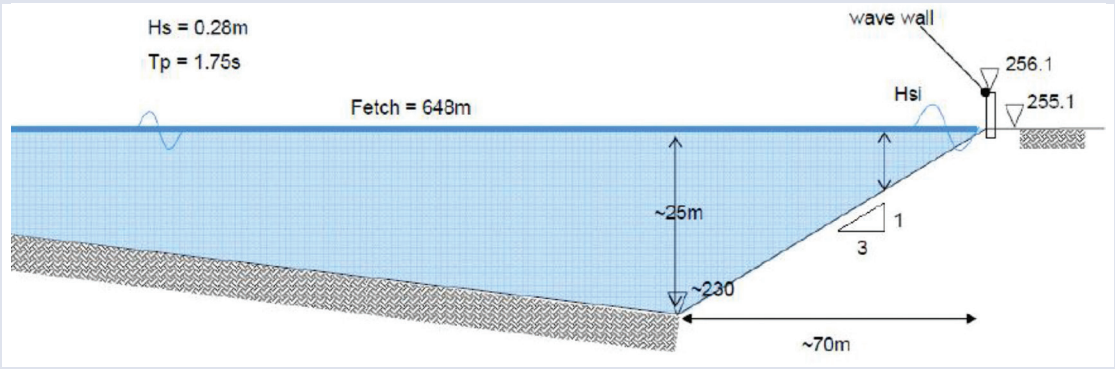

Figure 8.127 *Schematic of dam and wave wall – input conditions for the calculations*

The key 'given' data are summarised in Figure 8.127. The water level coincides with the toe of the 1 m high vertical wall, and the crest of the embankment slope. This coincidence is unfortunate as no generic prediction method for either vertical walls or plane slopes is within range, so there is a need to extrapolate different methods out of their intended range.

The approach to wave load calculations is summarised:

- determine the effective wave condition at $5H_s$ waterside from the structure
- calculate the momentum-driven horizontal Goda load (F_{hGoda}) and pressures
- if the geometry has a noticeable berm, which may cause impulsive breaking, apply the Takahashi modification to Goda's method to give an enhanced quasi-static load of $F_{hG\&T}$
- if impulsive wave loads are possible, use simple methods by Allsop and Vicinanza (1996), or Cuomo et al, to estimate $F_{impulsive}$ and an impulsive load duration
- if the wave can be broken by the time it reaches the wall, use the method by Blackmore and Hewson (1984) to calculate $F_{hB\&H}$
- if the wall is only reached after a breaking/broken bore has travelled over a slope or beach, estimate the load by Camfield's method (1991), $F_{hCamfield}$.

The default load should always be F_{hGoda} or $F_{hG\&T}$ either of which may be taken as a quasi-static load. Any impulsive load should be taken as an additional load case, not replacing the default load. High-intensity impulsive loads are limited in duration so have to be treated as dynamic loads.

Assumptions and results

In the first stage, a check was made on wave conditions at positions from the dam toe to a depth of 0.1 m below the wall toe (note extending the calculations to the wall would simply give zero wave height in zero water depth, a pointless calculation). The Goda location of $5H_s$ away from the wall toe was position 8 in these calculations with a 'bed' level at 254.6 mODN.

There are no validated methods to predict shoaling and depth-limited breaking on a 1:3 slope. So, calculations of incident wave height in Table 8.28 used a simple depth-limiting check for the steepest slope available at 1:10 to test whether waves will have broken before or at the analysis position.

Table 8.28 *Summary wave condition check*

Position	Bed level (mODN)	Local depth (m)	H_{si} (m)	H_{max} (m)
6	254.2	0.9	0.28	0.50
7	254.4	0.7	0.28	0.50
8	254.6	0.5	0.28	0.50
9	254.8	0.3	0.24	0.44

Wave conditions in Table 8.28 were then used to calculate Goda momentum-driven wave loads in Table 8.29. These calculations inherently assume that the wall is shifted 'seawards' such that the wall toe is below water level. So the wall height used to calculate the total horizontal force will be over-estimated, as will the calculated values of $F_{h1/250}$ itself. The indicative wave pressure at the

Box 8.21 *Wave loads on a reservoir wave wall (contd)*

waterline, p_1, will not however be significantly distorted by these (slight) changes to the structure geometry.

Table 8.29 *Goda wave load check*

Position	Bed level (mODN)	Local depth (m)	H_{max} (m)	$F_{н1/250}$ (kN/m)	p_1 (at SWL) (kN/m²)
6	254.2	0.9	0.50	3.6	3.5
7	254.4	0.7	0.50	3.6	3.9
8	254.6	0.5	0.50	3.7	4.7
9	254.8	0.3	0.44	3.4	5.6

It is interesting to note that, while values of the wave pressure at the water line may increase 'landward' of position 8 (eg p_1 = 5.6 kN/m² at position 9), this does not increase the total horizontal force, improving confidence in the calculation of $F_{h1/250}$ = 3.7 kN/m as the representative quasi-static loading at position 8.

As impulsive breaking is likely, the Takahashi extension of Goda's method was applied for an (assumed) berm of 0.2 m height and 0.25 m width. The changes to $F_{h1/250}$ *and* p_1 are however small (Table 8.30).

Table 8.30 *Goda and Takahashi wave load check*

Position	Bed level (mODN)	Local depth (m)	H_{max} (m)	$F_{н1/250}$ (kN/m)	p_1 (at SWL) (kN/m²)
6	254.2	0.9	0.50	3.80	3.36
7	254.4	0.7	0.50	3.78	3.64
8	254.6	0.5	0.50	3.81	4.11
9	254.8	0.3	0.44	3.12	4.15

In the last set of calculations summarised in Table 8.31, methods by Allsop and Vicinanza (1996) for impulsive loadings, Blackmore and Hewson (1984) for broken waves, and Camfield (1991) for wave bores were applied. The calculation of broken wave loads with Blackmore and Hewson used a coefficient λ = 0.5, and the bore wave load calculated by Camfield used a Hunt (1959) wave run-up limit for H_s.

As expected, the impulsive loads (A&V) increase as the depth decreases, while the broken wave load (B&H) reduces with decreasing depth. Load estimations using Camfield's method are very much lower than Goda's loads, and are not regarded as realistic.

Table 8.31 *Impulsive, broken waves, and wave bore load check*

Position	Bed level (mODN)	Local depth (m)	Allsop and Vicinanza		Blackmore and Hewson		Camfield
			$F_{A\&V}$ (kN/m)	p_{av} (kN/m²)	$F_{B\&H}$ (kN/m)	p_{av} (kN/m²)	$F_{Camfield}$ (kN/m)
	(mODN)	(m)					
6	254.2	0.9	6.9	4.2	13	7.7	0.45
7	254.4	0.7	8.5	5.8	8.7	6.0	0.45
8	254.6	0.5	11.1	8.8	5.4	4.3	0.45
9	254.8	0.3	11.5	12	2.5	2.6	0.34

Recommendations

Given the unusual configuration (for wave load calculations), and the potential for plunging wave action onto the wall, the minimum load that should be considered is the Goda load of $F_{h1/250}$ = 3.7 kN/m, taken as a quasi-static load. The possibility of two alternative loads should also be considered.

If it can be demonstrated that these waves will break before the wall, then the broken wave load of $F_{B\&H}$ = 6.4 kN/m should be applied, taken as effectively a static load.

However, if the wave can plunge direct against the wall, then impulsive loads should be estimated, eg $F_{A\&V} \approx$ 11 kN/m, $p_{av} \approx$ 9kN/m². This will only be of short duration, so must not be applied as a static load, but as an impulsive load with appropriate duration.

8.9.1.3 Scour depth

Scour in front of vertical walls is more severe than for slopes/mound, driven by enhanced bed pressures/velocities/turbulence. This mechanism uses simple rules to estimate scour depth of granular materials under wave attack.

For normally incident, nonbreaking, regular waves incident upon an impermeable vertical wall (Xie, 1981 and 1985):

$$S_m = 0.4 \frac{H_s}{[\sinh(kh)]^{1.35}} \tag{8.234}$$

where:

S_m = maximum scour depth at node (L/4 from wall) (m)
H_s = incident regular wave height (m)
k = incident regular wave number (-)
h = water depth (m)

For normally incident, nonbreaking irregular waves (Hughes and Fowler, 1991):

$$S_m = 0.05 \frac{\langle u_{rms} \rangle_m}{[\sinh(k_p h)]^{0.35}} \tag{8.235}$$

where:

k_p = wave number associated with the spectral peak by linear wave theory (-)
$<u_{rms}>_m$ = root-mean-square of horizontal bottom velocity

The value of $< u_{rms} >_m$ was given by Hughes (1992) as:

$$\langle u_{rms} \rangle_m = \frac{\sqrt{2}}{4\pi} \frac{g\, k_p\, T_p\, H_{m0}}{\cosh(k_p h)} \left[0.54 \frac{(1.5 - k_p h)}{2.8} \right] \tag{8.236}$$

where:

T_p = wave period of the spectral peak (s)
H_{m0} = zero-th moment wave height (m)
g = gravitational constant (9.81 m/s^2)

8.9.2 Stability of T-walls

In the analysis of T-walls the following limit states shall be considered:

- bearing resistance failure
- failure by sliding
- failure by overturning
- loss of overall stability
- structural failure.

In this handbook, focus is given only on the first three limit states. The overall stability is discussed in Section 8.6, and the reader may refer to relevant national or other design standards for the structural resistance assessment tools.

8.9.2.1 Bearing capacity

General considerations

Depending on the stiffness of the foundation soil and depth of the foundation, three modes of failure may be experienced:

- general shear failure
- local shear failure
- punching shear failure.

Considering that the T-walls are founded on shallow foundations, consideration of the general shear failure pattern may only occur. Therefore, bearing resistance limit state verification is made through the verification that the vertical stress applied by the structure does not exceed the ultimate limited strength of the soil:

$$q \leq q_{ult} \tag{8.237}$$

Bearing resistance can be obtained either by:

- analytical methods
- semi-empirical methods
- numerical models.

Analytical methods

Determination of ultimate bearing capacity (q_{ult}) for shallow foundations on soil is regarded as a problem of equilibrium of rigid-plastic solids. The solutions rely on a physical understanding of the failure mode, which is generally considered under the general pattern described in Figure 8.128.

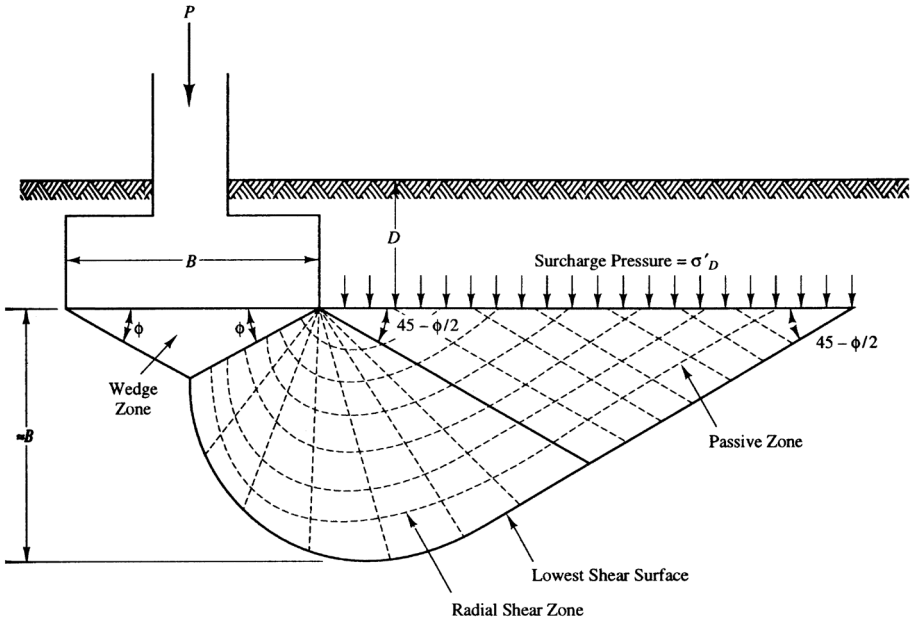

Figure 8.128 General bearing capacity failure pattern (after Terzaghi, 1943)

The subsequent equation of the bearing capacity, first proposed by Terzaghi and extended by several authors (Meyerhof, Hansen, Vesic), may be expressed, for frictional soils, as:

$$q_{ult} = c\,N_c\,s_c\,d_c\,i_c\,g_c + q\,N_q\,s_q\,d_q + \frac{1}{2}\gamma\,B'\,N_\gamma\,s_\gamma\,d_\gamma\,i_\gamma\,g_\gamma \tag{8.238}$$

where:

q = overburden pressure at base of the footing (kPa)
c = average cohesion of the soil (kPa)
B' = corrected width of the footing (m)

The parameters N_c, N_q and N_γ are bearing capacity factors representing the influence of cohesion, soil unit weight and overburden pressure respectively. The other factors can take into account the footing shape (s_i), the footing embedment depth (d_i), the load inclination (i_i) and the sloping ground (g_i). The load

eccentricity is taken into account by reducing the dimensions on the footing: $B' = B–2e_B$ and $L' = L–2e_L$ with e_B and e_L as the eccentricity in the minimum and maximum dimensions of the footing respectively. The bearing capacity and other correction factors are detailed in Table 8.32 and Figure 8.129.

Table 8.32 Bearing capacity and correction factors

Bearing capacity factor		$N\gamma$	N_q	N_c
Formula	φ (°)	$N_\gamma = 2(N_q - 1)\tan\varphi$	$N_q = e^{\pi \tan\varphi} \tan^2(\pi/4 - \varphi/2)$	$N_c = (N_q - 1)\cot\varphi$
Values	0°	0.0	1.0	5.1
	5°	0.11	1.6	6.5
	10°	0.5	2.5	8.3
	15°	1.6	3.9	11.0
	20°	4.6	6.4	14.8
	25°	9.0	10.7	20.7
	30°	20.1	18.4	30.1
	35°	45.2	33.3	46.1
	40°	106.1	64.2	75.3
	45°	267.8	134.9	133.9
Shape factor		$s_\gamma = 1 - 0.3\frac{B'}{L'}$	$s_q = 1 + \frac{B'}{L'}\sin\varphi$	$s_c = \frac{s_q N_q - 1}{N_q - 1}$
Depth factor (1)		$d_\gamma = 1.0$	$d_q = 1 + 2k\tan\varphi\cos^2\varphi$	$d_c = 1 + 0.4k$
Inclination factor (2)		$i_\gamma = \left[1 - \frac{H}{V + B'L'\cot\varphi}\right]^{m+1}$	$i_q = \left[1 - \frac{H}{V + B'L'\cot\varphi}\right]^{m}$	$i_c = i_q - \frac{1 - i_q}{N_c}\tan\varphi$
Sloping ground factor		$g_\gamma = (1 - \tan\beta)^2$	$g_q = g_\gamma$	$g_c = i_q - \frac{1 - i_q}{(\pi + 2)\tan\varphi}$

Notes :
The load applied to the footing is decomposed in three components : H, V and M which are the horizontal, vertical forces and the momentum acting on the footing.
(1) Values of k parameter depend on the embedment depth D_e as follows : if $\frac{D_e}{B'} < 1$ then $k = \frac{D_e}{B'}$, otherwise $k = \tan^{-1}\left(\frac{D_e}{B'}\right)$.
(2) Values of the m parameter depend on the orientation of the load as follows :

- when H is oriented in the direction of B : $m = m_B = 2 + \frac{B'/L'}{1 + B'/L'}$
- when H is oriented in the direction of L : $m = m_L = 2 + \frac{L'/B'}{1 + L'/B'}$
- when the horizontal force is oriented with an angle θ : $m = m_L \cos^2\theta + m_B \sin^2\theta$

For purely cohesive soils, the ultimate bearing capacity becomes:

$$q_{ult} = (\pi + 2)\, s_u\, (1 + s'_c + d'_c - i'_c - g'_c) + q \tag{8.239}$$

where s_u is the undrained shear strength. The correction factors depend on soil characteristics, footing geometry etc. The values of the factors depend on national standards and the reader is referred to those standards.

Figure 8.129 Bearing capacity factors for analytical determination of bearing capacity (from Chai, 2000)

ϕ	N_c	N_q	$N_{\gamma(M)}$	$N_{\gamma(H)}$	$N_{\gamma(V)}$	$N_{\gamma(C)}$	N_q/N_c	tan ϕ
0	5.14	1.00	0.00	0.00	0.00	0.00	0.19	0.00
1	5.38	1.09	0.00	0.00	0.07	0.07	0.20	0.02
2	5.63	1.20	0.01	0.01	0.15	0.16	0.21	0.03
3	5.90	1.31	0.02	0.02	0.24	0.25	0.22	0.05
4	6.18	1.43	0.04	0.05	0.34	0.35	0.23	0.07
5	6.49	1.57	0.07	0.07	0.45	0.47	0.24	0.09
6	6.81	1.72	0.11	0.11	0.57	0.60	0.25	0.11
7	7.16	1.88	0.15	0.16	0.71	0.74	0.26	0.12
8	7.53	2.06	0.21	0.22	0.86	0.91	0.27	0.14
9	7.92	2.25	0.28	0.30	1.03	1.10	0.28	0.16
10	8.34	2.47	0.37	0.39	1.22	1.31	0.30	0.18
11	8.80	2.71	0.47	0.50	1.44	1.56	0.31	0.19
12	9.28	2.97	0.60	0.63	1.69	1.84	0.32	0.21
13	9.81	3.26	0.74	0.78	1.97	2.16	0.33	0.23
14	10.37	3.59	0.92	0.97	2.29	2.52	0.35	0.25
15	10.98	3.94	1.13	1.18	2.65	2.94	0.36	0.27
16	11.63	4.34	1.37	1.43	3.06	3.42	0.37	0.29
17	12.34	4.77	1.66	1.73	3.53	3.98	0.39	0.31
18	13.10	5.26	2.00	2.08	4.07	4.61	0.40	0.32
19	13.93	5.80	2.40	2.48	4.68	5.35	0.42	0.34
20	14.83	6.40	2.87	2.95	5.39	6.20	0.43	0.36
21	15.81	7.07	3.42	3.50	6.20	7.18	0.45	0.38
22	16.88	7.82	4.07	4.13	7.13	8.32	0.46	0.40
23	18.05	8.66	4.82	4.88	8.20	9.64	0.48	0.42
24	19.32	9.60	5.72	5.75	9.44	11.17	0.50	0.45
25	20.72	10.66	6.77	6.76	10.88	12.96	0.51	0.47
26	22.25	11.85	8.00	7.94	12.54	15.05	0.53	0.49
27	23.94	13.20	9.46	9.32	14.47	17.49	0.55	0.51
28	25.80	14.72	11.19	10.94	16.72	20.35	0.57	0.53
29	27.86	16.44	13.24	12.84	19.34	23.71	0.59	0.55
30	30.14	18.40	15.67	15.07	22.40	27.66	0.61	0.58
31	32.67	20.63	18.56	17.69	25.99	32.33	0.63	0.60
32	35.49	23.18	22.02	20.79	30.21	37.85	0.65	0.62
33	38.64	26.09	26.17	24.44	35.19	44.40	0.68	0.65
34	42.16	29.44	31.15	28.77	41.06	52.18	0.70	0.67
35	46.12	33.30	37.15	33.92	48.03	61.47	0.72	0.70
36	50.59	37.75	44.43	40.05	56.31	72.59	0.75	0.73
37	55.63	42.92	53.27	47.38	66.19	85.95	0.77	0.75
38	61.35	48.93	64.07	56.17	78.02	102.05	0.80	0.78
39	67.87	55.96	77.33	66.75	92.25	121.53	0.82	0.81
40	75.31	64.19	93.69	79.54	109.41	145.19	0.85	0.84
41	83.86	73.90	113.98	95.05	130.21	174.06	0.88	0.87
42	93.71	85.37	139.32	113.95	155.54	209.43	0.91	0.90
43	105.11	99.01	171.14	137.10	186.53	253.00	0.94	0.93
44	118.37	115.31	211.41	165.58	224.63	306.92	0.97	0.97
45	133.87	134.97	262.74	200.81	271.74	374.02	1.01	1.00
46	152.10	158.50	328.73	244.64	330.33	458.02	1.04	1.04
47	173.64	187.20	414.32	299.52	403.65	563.81	1.08	1.07
48	199.26	222.30	526.44	368.66	495.99	697.93	1.12	1.11
49	229.92	265.49	674.91	456.40	613.13	869.17	1.15	1.15
50	266.88	319.05	873.84	568.56	762.85	1089.46	1.20	1.19

Note
Subscripts refer to different methods to calculate Nγ: (M) Meyerhof, (H) Hansen, (V) Vesic, (C) Chen

The main issue concerning this approach is that the different methods give a wide range of Nγ values. Also, the choice of the angle of friction (from triaxial or plane strain solicitations) is an important source of uncertainty. This point has been discussed in detail by Droniuc and Magnan (2002). Finally, the controversial aspect of Nγ determination is that it does not include compressibility of the soil. In addition, some comparisons of predicted solutions against model footing test results were found inconclusive.

Semi-empirical methods

Different semi-empirical methods can be used to obtain the bearing capacity q_{ult} of a shallow foundation. Some examples are given in the following paragraphs. The general expression is as follows:

$$q_{ult} = i_\delta \, i_\beta \, K_s \, (B, L, D_e, D_w) \; q_e + \sigma'_{v0} \tag{8.240}$$

where:

q_e = averaged soil resistance 1.5B below the shallow foundation
σ'_{v0} = vertical effective stress at the base of the footing
B = width of the footing
L = length of the footing
D_e = embedment depth
D_w = water table depth

The expressions of the correction factor K_s depend primarily on soil type and *in situ* test. The reader may refer to the relevant standards, with an example from France given in Box 8.22.

Two additional correction factors, i_δ and i_β, can be introduced to take into account inclination of the applied load and proximity of a slope respectively. An example of curves allowing selection of the reduction factor i_δ due to inclination δ of applied load is given in Figure 8.130.

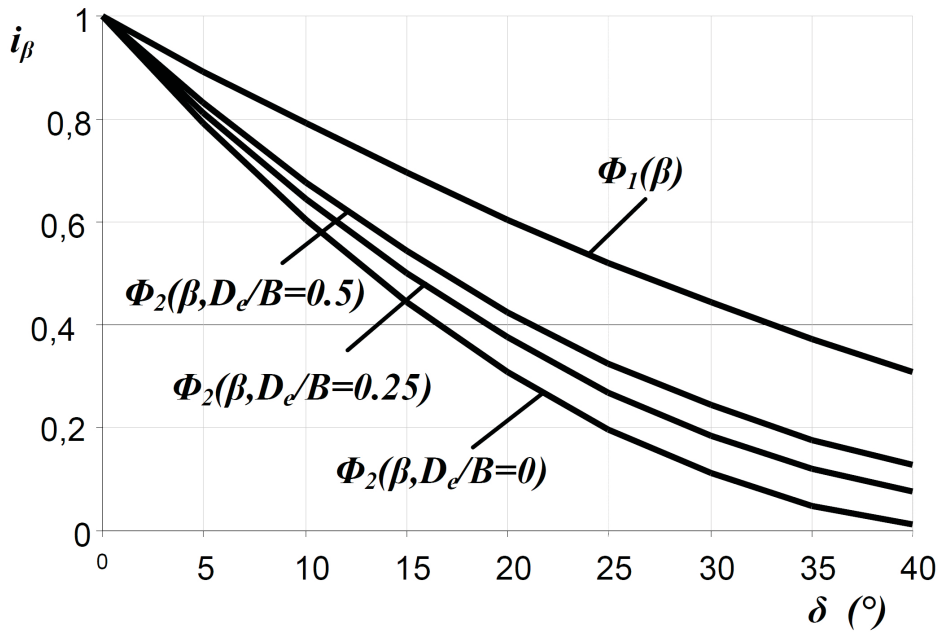

Figure 8.130 Reduction factor i_δ (curves Φ_1 for cohesive soils, Φ_2 for non-cohesive soils)

Values of the reduction factor i_β due to inclination β of a close slope can be obtained through the following formulae (hypothesis shown in Figure 8.131 are used).

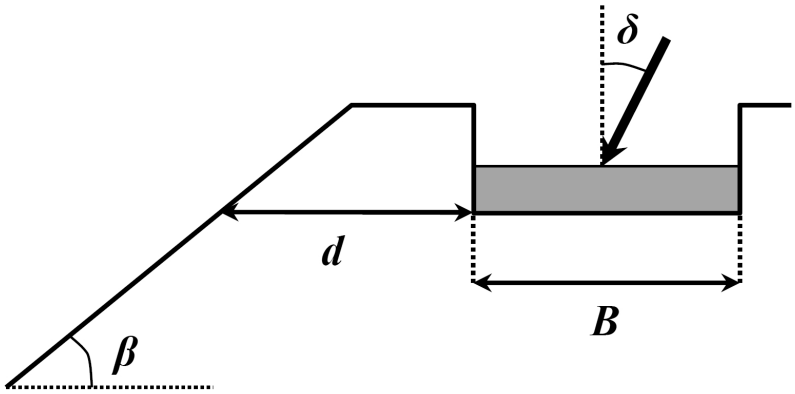

Figure 8.131 Hypothesis used for reduction factor i_β

- for cohesive soils: $$i_\beta = 1 - \frac{\beta}{\pi}\left(1 - \frac{d}{8B}\right)^2 \quad (8.241)$$
- for non-cohesive soils: $$i_\beta = 1 - 0.9\tan\beta\,(2 - \tan\beta)\left[1 - \frac{d + D_e/\tan\beta}{8B}\right]^2 \quad (8.242)$$

Box 8.22 Example of the French standards

Pressuremeter method

Ultimate bearing capacity is directly correlated with the limit pressure p_l measured *in situ* (Bustamante and Gianeselli). For a homogeneous soil layer, q_e, is defined as the interpolation value of net limit pressure (pl-p0) at *2B/3*. For a heterogeneous soil formation, the equivalent net limit pressure is estimated with a geometric mean over the measured values, obtained as follows:

$$q_e = \left(\prod_{i=1}^{n} p_{l,i}\right)^{\frac{1}{n}} \quad (8.243)$$

The correction factor k_p depends on soil under the shallow foundation, on the foundation shape and on the equivalent depth of the foundation, D_e, which is as follows:

$$D_e = \frac{1}{q_e}\int_0^D p_l(z)\,dz \quad (8.244)$$

The correction factor is expressed under the general formula:

$$K_s = \alpha\left[1 + \beta\left(0.6 + 0.4\frac{B}{L}\right)\frac{D_e}{B}\right] \quad (8.245)$$

where α and β depend on the soil type (Table 8.33).

Table 8.33 Limit pressure values to estimate the correction factor K

Soil category	p_l-p_0 (MPa)	α	β
Clay and silts	< 0.7	0.8	0.25
	1.2–2.0		0.35
	> 2.5		0.50
Sand and gravel	< 0.5	1.0	0.35
	1.0–2.0		0.50
	> 2.5		0.80

Cone penetration test based method

Cone static penetrometer can be used to estimate ultimate bearing capacity (Tandetal, Bouafia, and Bustamante and Gianeselli). The equivalent cone penetration resistance is estimated with a geometric mean over the measured values, given as follows:

Box 8.22 *Example of the French standards (contd)*

$$q_e = \frac{1}{1.5B} \int_D^{1.5B} q_c(z)\, dz \tag{8.246}$$

The correction factor K depends on the depth of the foundation, on the soil under the shallow foundation and on the foundation shape. It is generally comprised between 0.31 and 0.44. It can also be obtained based upon the equivalent depth of the foundation D_e, which is given as follows:

$$D_e = \frac{1}{q_e} \int_0^D q_c(z)\, dz \tag{8.247}$$

Table 8.34 gives some examples to determine the correction factor K, for different soils and shapes of the foundation.

Table 8.34 *Correction factor K for cone penetration based method*

Soil category	q_c (MPa)	α	β
Clay and silts	–	0.8	0.35
Sand and gravel	< 5	0.14	0.35
	8–15	0.11	0.50
	> 20	0.08	0.80

An example of determining the allowable bearing pressure from SPT measurements is given in Box 8.23.

Box 8.23 *Meyerhof-Bowles method from SPT blow counts*

Other methods have been developed from SPT measurements. In the USA, the following method is widely used. The net allowable bearing pressure q_f (MPa), for B ≥ 1.22 m, may be expressed as follows (Meyerhof, 1965, and Bowles, 1977):

$$q_f = \left(\frac{3.28\, B + 1}{3.28\, B}\right)^2 11.98\, N_{60}\, \frac{s}{0.025} \tag{8.248}$$

where:

B = equivalent width of the foundation (m)

N_{60} = normalised blow count for a 60 per cent transferred energy (-)

s = tolerable settlement (m)

In the case of an embedded foundation, the net bearing capacity pressure has to be multiplied by the depth factor $1 + 0.33 D_e/B \leq 1.33$.

8.9.2.2 Horizontal sliding

The following inequality shall be satisfied where the loading is not normal to the foundation base, foundations shall be checked:

$$H \leq A_c\, c + (V - U) \tan \frac{\varphi}{k} + R_p \tag{8.249}$$

where H, V and U are the horizontal, vertical and uplift forces, R_p is the resistance caused by earth pressure in front of the foundation. Its value should be related to the scale of movement anticipated under the limit state of loading considered and reflect the anticipated life of the structure. The parameter k defining the design friction angle may be assumed equal to $k = 1$ for cast *in situ* concrete foundations, but for smooth precast foundations, it may be equal to $k = 2/3$. For drained conditions, any effective cohesion C should be neglected, but for undrained conditions, the cohesion term may be replaced by the undrained shear strength S_u.

8.9.2.3 Overturning

Avoiding failures by overturning is reached by limiting the eccentricity of loadings e (m). For ultimate states and strip footings, the simple following criteria could also be used:

$$e < \frac{B}{10} \tag{8.250}$$

where B is the width of the footing (m). This method requires special care to design values of actions and magnitude of construction tolerances in order to determine the accurate location of the foundation.

8.9.3 Stability of I-walls

In the analysis for stability of I-walls the following limit states shall be considered:

- failure by rotation (overturning)
- loss of overall stability
- seepage and uplift
- structural failure.

An I-wall is defined as a slender cantilever flood wall, deeply embedded in the ground or in an embankment. The wall rotates when loaded and is stabilised by reactive lateral earth pressures. A design goal is to limit wall deflection to tolerable levels during loading. This is typically achieved by designing the wall using the limit equilibrium method based on lateral earth pressures at their limit state, after applying a safety factor to the soil shear strength. Advanced soil-structure interaction (SSI) approaches, such as modelling I-walls using springs or finite elements/finite difference techniques, are available for more rigorous solutions and are discussed briefly in Section 8.9.3.5.

When hydraulic forces are applied to I-walls founded in soils that exhibit cohesion, a gap may form between the I-wall and waterside soil resulting in a loading that exceeds the active lateral earth pressure (Duncan *et al*, 2008). The authors indicate that the formation of the gap is an important feature and so it needs to be considered in all failure modes. This is because wall loading may be increased, thereby reducing stability, and seepage paths may be shortened increasing the potential for heave and uplift. Hydrostatic pressures within the gap are applied to the wall and to the soil face to the full gap depth at a point where the hydrostatic pressure within the gap is equal or less than the total active lateral earth pressure. Gaps are not considered in cohesionless soils as saturated granular soils have no free-standing height and will displace and remain in contact with the wall as it deflects.

8.9.3.1 Overturning

General considerations

It should be demonstrated by equilibrium calculations that embedded walls have sufficient penetration into the ground to prevent rotational failure. In addition to active lateral earth pressure other actuating/driving forces causing rotation towards the landward side include:

- hydrostatic pressure
- hydrodynamic loads
- seepage effects
- vessel or debris impacts
- ice forces.

In the rotational failure mode the wall rotates as a rigid body about a point somewhere in its embedded depth typically near the tip of the wall. Equilibrium is achieved by a balance of driving loads and of active and passive soil pressures that depend on the wall relative deflection. Driving loads are primarily from the water (flood) force, and resisting pressures are the passive pressures near the ground surface

on the landward side of the wall and near the tip of the sheet pile on the watersideside of the wall. The following sections are based on information from Dawkins (1991).

Hydraulic loads

Water loads are applied to the wall above and below the ground surfaces on both the water and landward sides. These are applied as pressures due to hydrostatic head on either side of the wall, hydrodynamic distributions from wave impacts, pore water pressure on the embedded part of the wall and seepage induced forces (where applicable) that are incorporated in the computation of lateral earth load.

Hydraulic forces acting on the wall above the ground are discussed in Section 8.9.1. Pore water pressures and effects of seepage below the ground surface are included in a simplified manner and determined separately for the waterside (driving) of the wall and for the landward (resisting) side as shown in Figure 8.132 with associated net water pressure diagrams. Hydrostatic loading within a potential flood side gap must also be considered, and the hydrostatic loading within the gap is used instead of the active lateral earth pressure when it exceeds that value.

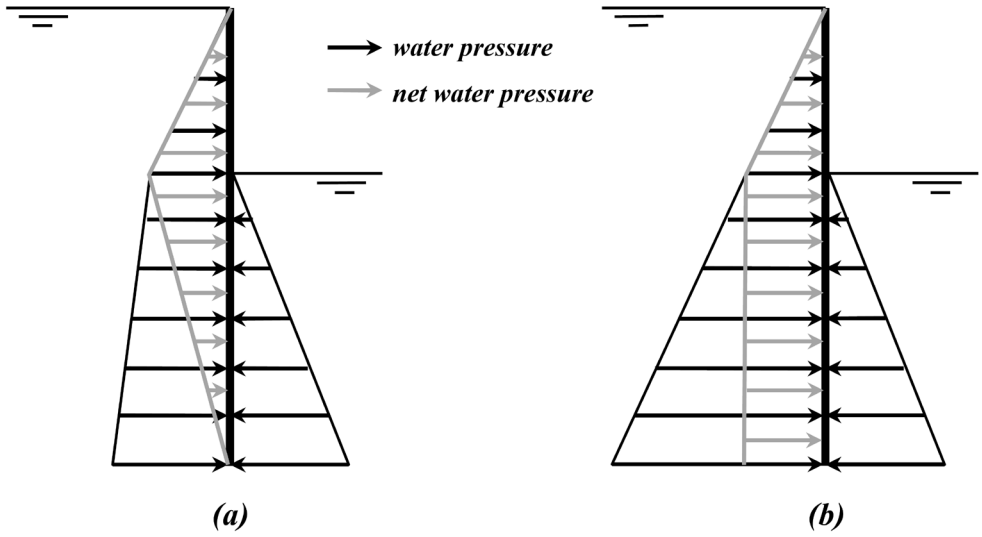

Figure 8.132 Water pressure diagrams and net pressure, sand with seepage (a), and clay without seepage (b)

Earth loads

The pressures on both sides of the wall are computed using lateral earth pressure theory based on mobilised shear strengths (Equations 8.253 and 8.255), and the point of rotation is found that simultaneously provides force and moment equilibrium. Analyses are performed using either effective or total stresses. As the wall is loaded by a flood loading the top of wall rotates towards the landward side and pivots about a point above the sheet pile toe. As the wall rotates away from the waterside active pressures develop, on the watersideside while passive pressures exist on the landward side. Likewise, below the point of rotation passive pressures develop on the waterside and active on the resisting landward side. The differences between passive and active pressures on the waterside and on the resisting side of the wall are computed and these pressure differences on each side of the wall are the net earth pressures that can exist (note that seepage forces tend to increase the effective unit weight of soil on the waterside while reducing the effective unit weight on the landward side resulting in differing lateral earth loads on each side of the wall). With the net water pressure diagrams and the maximum passive pressure diagrams the point of rotation is computed considering horizontal force and moment equilibrium. The lateral earth pressures and embedment depth of wall are computed as follows:

$$\varphi_m = \arctan\left(\tan\varphi / F_s\right) \tag{8.251}$$

$$c_m = c/F_s \tag{8.252}$$

where:

φ = angle of internal friction (°)
φ_m = mobilised angle of internal friction (°)
c = cohesion (kPa)
c_m = mobilised cohesion (kPa)
F_s = given or required factor of safety (-)

Several different methods can be used to determine the limiting values of earth pressures. For a vertical wall with horizontal ground surfaces and soil layers and zero wall/soil adhesion, limit values of earth pressure may be calculated using Coulomb's earth pressure coefficients as follows:

For active limit state:

$$\sigma'_a = \left(K_a\,\sigma'_v - 2\,c_m\,\sqrt{K_a}\right)\cos\delta_a \tag{8.253}$$

where σ'_v is the effective vertical stress (kPa) calculated using the effective soil-unit weight (including seepage effects), δ_a the angle of friction along the wall (°), and K_a the active earth pressure coefficient (-). The active earth pressure coefficient may be calculated from different methods, which have to account for the real geometry of the levee. When the crest is large enough, the following formula may be used:

$$K_a = \left[\frac{\cos\varphi_m}{1+\sqrt{\dfrac{\sin\left(\varphi_m+\delta_a\right)\sin\varphi_m}{\cos\delta_a}}}\right]^2 \frac{1}{\cos\delta_a} \tag{8.254}$$

For passive limit state:

$$\sigma'_p = \left(K_p\,\sigma'_v + 2\,c_m\,\sqrt{K_p}\right)\cos\delta_p \tag{8.255}$$

where K_p is the passive earth pressure coefficient (-).When the crest is large enough, the following formula may be used:

$$K_p = \left[\frac{\cos\varphi_m}{1-\sqrt{\dfrac{\sin\left(\varphi_m+\delta_p\right)\sin\varphi_m}{\cos\delta_p}}}\right]^2 \frac{1}{\cos\delta_p} \tag{8.256}$$

The calculation using Coulomb's passive earth pressure coefficient (based on a linear failure surface) may overestimate the passive resistance. Log spiral failure mechanisms should be checked as they often return a less passive pressure. When the ground surface is not horizontal or other limiting assumptions are not valid, earth pressures may be calculated using the Wedge method (Section 8.6.3.1) where the active or passive load is either analytically or numerically optimised.

Hydrostatic water pressures may be altered by seepage. When seepage effects are included, the excess hydrostatic head is assumed to be dissipated by vertical flow downward on the waterside and upward on the landward side. The seepage gradient i (-) is assumed to be constant at all points in the soil on either side of the wall. Under this assumption, the effect of seepage is to alter the effective unit weight of water (and the unit weight of soil) in the region of flow. On the waterside of the wall:

$$\gamma_{we} = \gamma_w\left(1-i\right) \tag{8.257}$$

and on the landward side:

$$\gamma_{we} = \gamma_w\left(1+i\right) \tag{8.258}$$

where:

γ_{we} = effective unit weight of water used to calculate σ'_v (kN/m^3)
γ_w = unit weight of water (kN/m^3)
i = seepage gradient (equals zero under hydrostatic conditions) (-)

Figure 8.133 shows the maximum earth pressure diagrams for the landward side and waterside of the wall and the resulting net pressure diagram needed to achieve horizontal force and moment equilibrium about a point of rotation denoted as Point O. Solving for the location of Point O to achieve equilibrium is an iterative process that requires varying embedment depth until the required factors of safety are achieved.

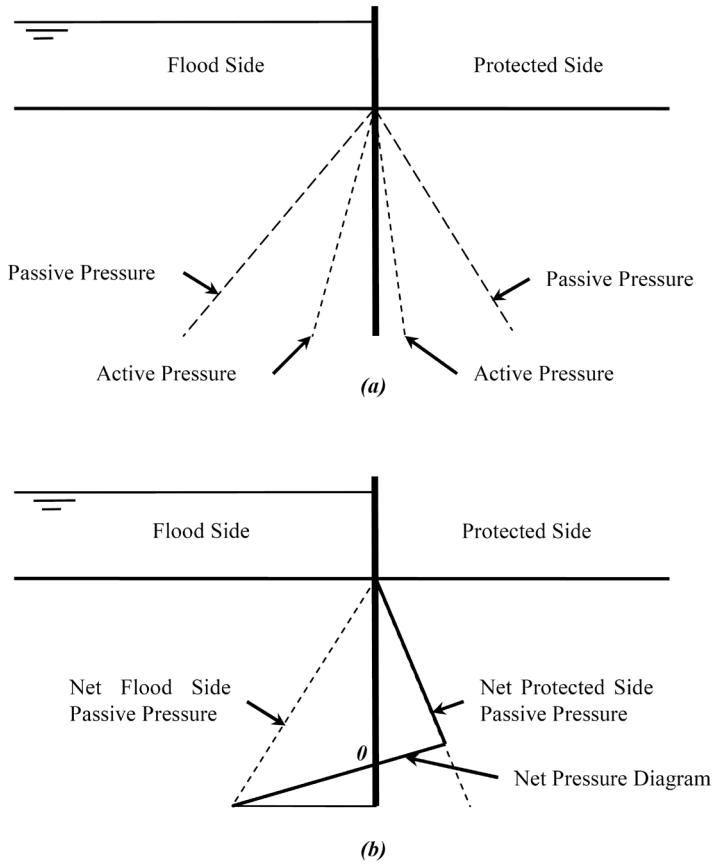

Figure 8.133 Lateral earth pressure diagrams active and passive pressures (a), and maximum passive pressure with resulting net pressure diagram (b)

Vessel or debris impacts and ice loads

These loads may be estimated and included with hydraulic loads and lateral earth pressures when solving for horizontal force and moment equilibrium. The determination of these loads is project specific and not discussed further.

8.9.3.2 Overall stability

Overall, global, or deep-seated stability are terms used to describe a failure mode where the wall is assumed to displace along with the soil mass in which it is embedded when it slides or rotates under a slope stability type failure mechanism. This failure mode is most likely to be critical when I-walls are located within levees in very soft soils. Global stability is evaluated using typical slope stability software for the gap and no-gap analyses as presented in Figure 8.134. The methods used to evaluate global stability shall satisfy all conditions of static equilibrium. The no-gap condition is evaluated using typical or routine slope stability analysis procedures but incorporation of the gap can add complexity and is discussed in more detail as follows. A waterside water-filled gap can be included by removing the waterside soil to the bottom of the gap and replacing it with a mechanical pressure to represent the hydrostatic water load against the wall. Tension crack options in software packages can be used but should be checked for correctness regarding the treatment of submerged tension cracks.

Methods for determining gap depths are considered approximate, so global stability needs to be checked for the no-gap and full-gap conditions and possibly the partial gap condition. Under the no-gap and full-gap conditions stability is performed assuming either that no waterside gap develops or that a gap will extend to the bottom of the sheet piling. Because saturated granular soils will not sustain a gap, a gap is not presumed to develop in these materials and a gap is not included in modelling. When cohesive soils overlie granular soils, the gap depth may propagate to the top of the granular layer but no deeper (Figure 8.134). The condition where cohesive soils underlie granular soils is not fully understood. However, the previous assumption that the gap will extend to the bottom of the sheet pile or to the bottom of the fine-grained material is recommended.

Figure 8.134a presents the gap and no-gap critical slip surfaces for the composite levee system shown. The no-gap slip surface is constrained below the wall toe, preventing potential slip surfaces from passing through the wall. In soft soils or where high pore water pressures in sand result in low shear strength, this is a reasonable assumption as the stiffness of the wall is expectedly higher than that of surrounding soil. Figure 8.134b presents the partial gap stability model showing soil removed to the toe of the wall and the slip surface initiating at that point. In this analysis the gap did not extend completely to the wall toe but instead to the top of the sand strata, and hydrostatic water pressure is included to this depth. Seepage and associated head loss within the sand layer is shown as less than hydrostatic from the top of sand to the toe of the wall. In this analysis an active effective horizontal lateral earth pressure is calculated and applied to the model in the sand strata (Brandon *et al*, 2008).

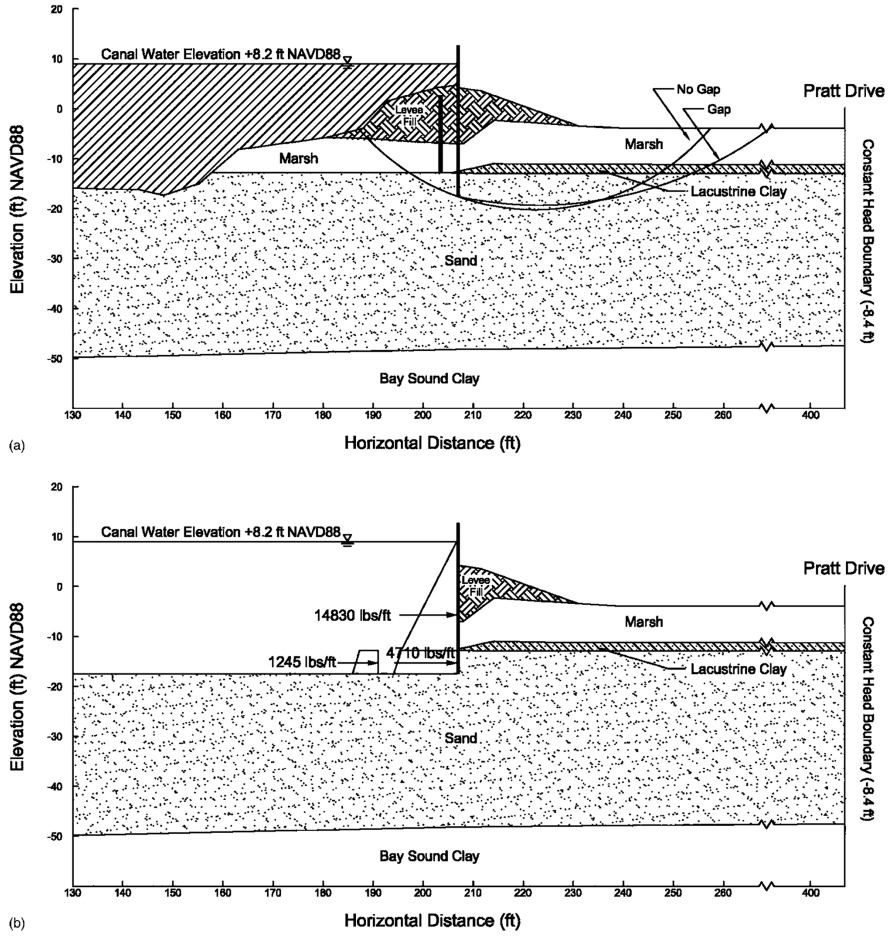

Figure 8.134 Slope stability analyses with and without gap formation (Brandon et al, 2008)

8.9.3.3 Seepage and uplift

Seepage and associated heave or uplift for levees is described in Section 8.6. The same underlying principles apply to seepage around I-walls with the additional concern of gap formation. The formation of a waterside gap in cohesive soils adjacent to I-walls can create a direct connection to underlying sand layers (Duncan *et al*, 2008), and increase the potential for heave or uplift.

Several procedures are available to analyse seepage and uplift. Graphical methods (flow nets), analytic or closed-form solutions that have been solved for specific conditions, method of fragments, and finite elements are common tools. Advances in hardware and software associated with modern computers have greatly reduced the time and effort to perform numerical analyses. Also, analysis of seepage by finite elements has become routine for many designers. Finite elements are often used where the substrata system is considered too complex for generalised characterisation, and the waterside gap for seepage analysis is easily incorporated with this method. Several computer programs couple results from finite element seepage analysis with limit equilibrium slope stability programs to aid in estimating pore water pressures for global stability analyses.

8.9.3.4 Structural failure

Steel sheet pile and reinforced concrete elements of the I-wall are designed to resist the strength limit states of bending and shear. Bending and shear forces in the I-wall are determined from the limit equilibrium analysis for rotation. However, the designer should recognise the factors of safety that are included in the analysis. Moment and shear forces produced from the limit equilibrium analysis to determine required tip depth using mobilised soil strength values already include a factor of safety. The design must consider the total factor of safety when combined with live load factors or allowable stresses for structural strength design from design codes. Typically limit equilibrium analyses are performed without including a factor of safety in order to determine moment and shear for the design of the structural elements.

I-walls are often constructed with a reinforced concrete wall above the ground surface and steel sheet pile driven below the ground surface. Besides designing for bending and shear forces in the sheet pile and reinforced concrete portions alone, the wall must be designed to transfer moment and shear from the reinforced concrete section to the sheet pile section. Methods for designing this connection vary but normally depend on a length of sheet pile to extend into the concrete wall (typically a metre or more) with reinforcing bars passed through holes cut into the sheet pile or shear studs welded to the flange of the sheet pile.

8.9.3.5 Advanced soil-structure interaction methods

Advanced soil-structure interaction (SSI) methods may be used for the design of I-walls but it is recommended that simpler limit equilibrium methods also be performed to complement the more advanced methods. Finite element/difference methods have been used to perform complete SSI analyses. Modelling the soil as a continuum requires the characterisation of stress-strain behaviour in addition to soil strength. Foundation investigation and testing must consider the parameters needed to support the constitutive model selected for performing the analysis. The simplest constitutive model considered acceptable for I-wall analysis and design is the Mohr-Coulomb (linearly elastic, perfectly plastic) model. In addition to using traditional Mohr-Coulomb shear strength properties this model incorporates properties for linear elasticity, such as Young's modulus and Poisson's ratio or shear and bulk modulus.

When constructing the FEM model it is important to include appropriate interfaces that allow slip and separation at the wall/soil contacts, but in order to capture potential overall stability concerns it is also important to allow the toe of the wall to move, such as by extending an interface below the wall or horizontally at the wall toe. Loading is applied as mechanical pressures acting normal to the ground surface and normal to the wall face. When a gap is included between the soil and I-wall a horizontal mechanical pressure is added to both the soil and the wall to the depth of the gap. Gap development is modelled following the procedure used in a report by USACE (2006b). The total horizontal stress in the element adjacent to the wall is compared to the hydrostatic pressure that would exist if a gap were present. If the hydrostatic water pressure exceeds the total horizontal stress it is assumed that a gap would form. Starting at the flood side ground surface, each underlying element is checked as water levels are incrementally raised. Water levels are raised in small increments (ie 0.3 to 0.6 m or 1 to 2 ft) and the gap is deepened in small steps as needed. The protocol for loading and gap initiation and progression is as follows:

- the model is brought into equilibrium and nodal displacements and velocities are reset to zero at the initial water level
- the water level is incrementally raised until loading is applied to the wall (ie no gap is allowed to form until water levels reach the wall)
- when water loads the wall the gap criteria is checked and the gap is deepened in small increments until the horizontal stress exceeds the hydrostatic water pressure that would exist at that depth
- the water level is incrementally raised and the need for extending the gap is checked
- once a gap has been extended to depth it is assumed the gap will not close (ie the depth of gap never reduces).

When using FEMs for evaluation or design the criteria for acceptable performance includes allowable stress in the structural elements but also allowable deflection of the wall. Confidence in calculated deflection is a concern and performing field load tests may be useful for calibrating models on critical structures. In lieu of field load testing conservative stress-strain parameters can be assumed from *in situ* and laboratory testing. Also, factor of safety calculations can be performed using a strength reduction technique and maintaining a reasonably high factor of safety as used in limit equilibrium analyses for wall rotation. The allowable amount of wall deflection should be selected based on a serviceability limit state.

Software involving reactive loads from springs rather than a soil continuum has been developed and is available for evaluation and design. When using these tools designers are encouraged to perform limit equilibrium analyses for comparison purposes.

Box 8.24 presents an example of gap analysis for an I-wall.

Box 8.24 Example of composite levees, New Orleans, USA

As reported by Duncan et al (2008), failures of I-walls during Hurricane Katrina were responsible for many breaches in the flood protection system in New Orleans, USA. An important factor in all of the cases investigated was development of a gap behind the wall as the water rose against the wall and caused it to deflect. Formation of the gap increased the load on the wall, because the water pressures in the gap were higher than the earth pressures that had acted on the wall before the gap formed. Where the foundation soil was clay, formation of a gap eliminated the shearing resistance of the soil on the flood side of the wall, because the slip surface stopped at the gap. Where the foundation soil was sand, formation of the gap opened a direct hydraulic connection between the water in the canal and the sand beneath the levee. This hydraulic short circuit made seepage conditions worse, and erosion due to under-seepage more likely. It also increased the uplift pressures on the base of the levee and marsh layer on the landward side of the levee, reducing stability. Because gap formation has such important effects on I-wall stability, and because gaps behind I-walls were found in many locations after the storm surge receded, the presence of the gap should always be assumed in I-wall design studies.

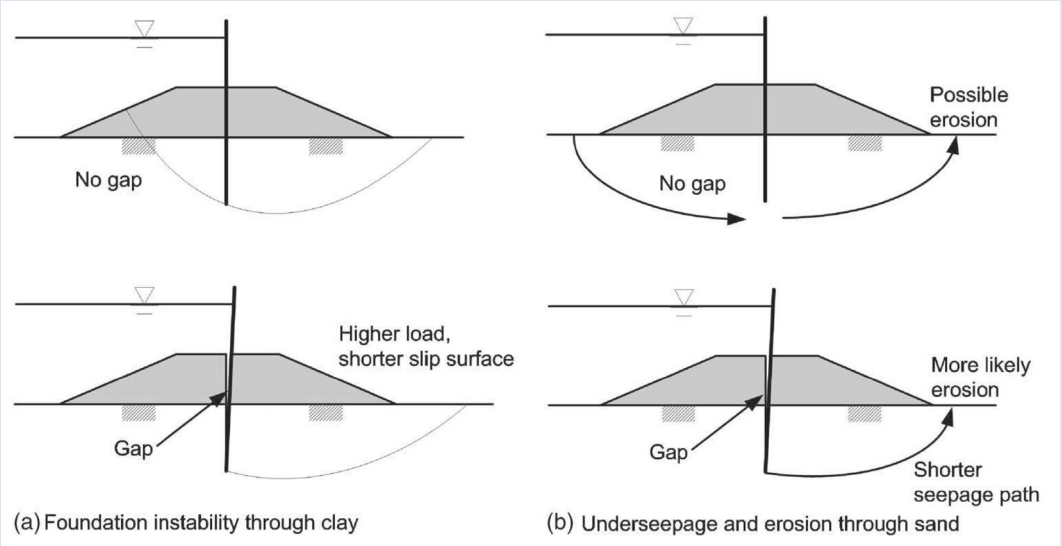

Figure 8.135 Potential I-wall failure mechanisms (from Duncan et al, 2008)

8.10 BREACH

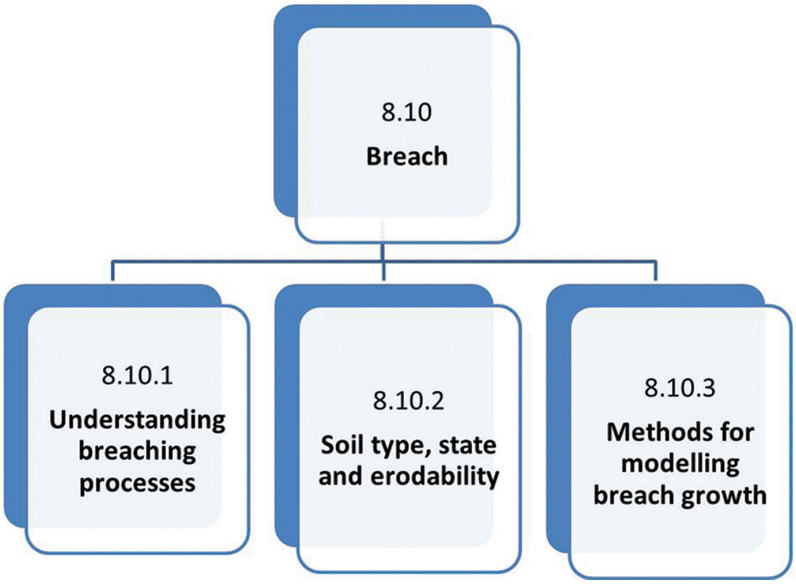

The reliable prediction of breach processes (rate at which a breach forms, volume and rate of release of floodwater) is fundamental to many activities such as flood risk assessment, emergency planning and flood event management. There are a range of issues to be taken into account when considering breach prediction.

Uncertainty

The degree of uncertainty associated with breach prediction methods can be large in comparison to, for example, the prediction of river flood levels through numerical modelling. Significant uncertainty exists in the prediction of breach because:

- uncertainties and variabilities exist in natural and constructed soil conditions
- breach processes involve a complex interaction of hydraulic, soil and structure behaviour
- a single prediction of breach may only be one possible scenario within a wider range of possibilities

Understanding the uncertainty within breach prediction should help to determine which methods of breach prediction are appropriate for use in a given situation. Where a large degree of uncertainty may be acceptable, it is likely that the simpler, rapid methods of breach estimation may be acceptable. Where a greater degree of certainty is required, more complex methods of analysis, perhaps combined with data collection, might be appropriate. Sensitivity analysis to provide a distribution for potential breach conditions can assist by narrowing the limits of uncertainty.

Relevance of different aspects of breach prediction to different end users

Different methods for predicting breach, and in particular simplified methods, ignore certain aspects of the overall process. So, it is important to appreciate which processes are of priority to end users when considering how to predict breach. For example:

- in a **high level flood risk assessment**, the focus is on establishing indicative areas at risk of flooding, and so an estimate of breach flood volume distributed across the inundation area may be acceptable. Details of the breach itself would not be as important as an estimate of the flood hydrograph
- in **flood risk assessments for local development control decisions**, exact boundaries for flooding become important and so does reducing any uncertainty within the flood hydrograph prediction
- for use in **emergency planning**, determining the approximate timing, duration and peak flood conditions becomes relevant

- in **emergency event management (evacuation and repair)**, exact timing, extent of flooding and rates of draw-down after the flood becomes of interest. Where breach is taking place and needs repair, a reliable prediction of breach dimensions, including rate of growth and maximum size, becomes important.

8.10.1 Understanding breaching processes

Three steps can be identified for levee breaching, which apply to breach growth through both headcut and surface erosion processes.

1 **Breach initiation:** with overflow or overtopping, surface protection measures, such as grass or rock cover, fail and soil starts to erode from the surface of the levee. Inside the levee, seepage flow increases slowly as material is gradually eroded from the body or foundation. Outflow remains relatively small but increases slowly as sediment is eroded. This stage can last for hours, days, or months if load conditions are not extreme, but can occur quickly if load conditions continue to increase.

2 **Breach formation:** occurs once erosion under the initiation stage starts to affect the hydraulic control. For breach overflow or overtopping this is when surface erosion starts to lower the crest or when headcut cuts back through the upstream slope. During breach formation, both the flow and erosion increase rapidly often resulting in catastrophic breach. For internal erosion, this stage occurs once a pipe is formed and flow and erosion increases rapidly. As the pipe grows, the roof collapses resulting in open breach formation.

3 **Breach widening:** once breach formation occurs, erosion typically cuts down to the base of the levee very quickly and flow through the levee increases rapidly. Breach widening then occurs, where the focus for erosion is undercutting and removal of material from the sides of the breach. Breach widening will continue while there is sufficient flow through the breach to erode material from the sides. Flow and erosion will slow and eventually stop as the flow subsides, either because flood loads reduce or because the breach becomes drowned by floodwater from the downstream side.

Inundation hydrograph and breach growth

The two main factors that dictate the type of hydrograph are:

- soil erodibility
- stage duration relationship for the hydraulic loading (or in the case of a reservoir, the stage-area or stage-volume relationship).

Resulting hydrograph shapes include:

- **low peak discharge:** where the upstream water level can drop at the same rate as soil erosion lowers the levee crest, the flood hydrograph will be relatively slow and long duration
- **high peak discharge:** where the release of water does not immediately affect the upstream water levels, the rapid increase in discharge being associated with rapidly increasing size of breach.

Where there is an ability to control the 'soil erodibility' and/or the upstream load conditions, this can be used to ensure that, in the event of a breach, the speed and peak of the flood hydrograph can be reduced to a minimum, even though the overall flood volume released may remain the same. In the area close to the breach this is likely to reduce the risk of damage and loss of life.

The impact of drowning on breach flow and formation can be significant and, where likely, should be considered as an integral part of the breach analysis. This is because when water levels downstream of a breach rise they act to drown the flow through the breach and so reduce discharge. This reduction in discharge in turn reduces the rate of erosion and breaches growth. Drowning of the breach will typically occur when downstream levels raise above two-thirds the depth of the upstream level relative to the breach invert level.

Breach initiation timing

At the breach initiation stage overflow, overtopping or seepage flow starts to erode the soil, removing any surface protection if present. When the erosion is sufficient to significantly affect the hydraulic control of the levee (for example, loss of crest elevation or an increasingly large pipe through or under the levee) then the increase in flow starts to accelerate and breach formation occurs. The timing at which breach formation occurs in relation to the timing of the peak of the flood event is significant. If the timing is coincident, then worse flooding from the breach may arise than if the breach formation occurred after the peak of the flood.

Factors affecting size and location of a breach

Factors that affect breach location include:

- variation in the crest level of the levee – low points in a crest, whether as a result of construction, settlement or erosion through animal or human use, will provide a focal point for overflow driven surface erosion
- variations in the quality of surface protection, especially of grass cover and/or of more erodible areas of soil
- structures through or over the levee (transitions), which often provide an opportunity for seepage at interfaces or a focal point for surface erosion
- transitions in surface protection measures, which also provide a focal point for erosion.

For coastal levees, additional factors affecting breach location include:

- local focusing of wave action due to wave refraction processes (Section 7.4)
- steep bathymetry in front of the levee increasing the force of breaking waves.

A study of historical breaches may provide useful guidance on making assumptions on breach location. Historical breach analysis in a catchment is also useful for assessing breach size, as the size depends upon the soil erodibility and hydraulic load conditions. Within a natural river system, where levee construction may have used broadly similar soils, analysis of historic breach events may show increasing sizes of breach down through the catchment. As the size of the catchment upstream increases, so will the volume of floodwater that might pass through a breach during a given storm event.

Box 8.25 gives an example of historic breach analysis to determine breach location.

Box 8.25 ***Historic analysis of breach location, River Loire, France***

The location of potential breaches initiated by overflowing can be easily located by comparing a longitudinal profile of the crest elevation to a longitudinal profile of the water elevation along the levee for various different flood events. However, there are many other factors that affect breach location, and analysis of the history of a levee will help to detect some of these weaker points in the levee system.

An analysis of historical failures of the levee will provide information on both the breach location and their characteristics, including the main cause, breach dimensions etc. For example, an analysis of the historical breaches along the levees of the River Loire, France (Gaullier and Piney, 2011) identified from archives details of most of the breaches that occurred during the three major floods of the 19th century. Also, some recurring features could be identified including:

- overflowing was the main cause of breaches on the Loire but that internal erosion was also identified as the cause for some breaches
- the widths of breaches varied from a few metres to several hundred metres (600 m for the widest).

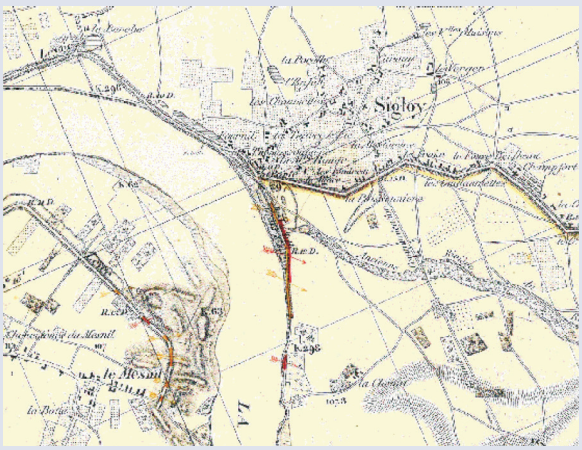

Figure 8.136 ***Extract of a historical map of the River Loire levees (first edition in 1850) showing positions of breaches (arrows), infiltrations and limits of flooded areas (dotted and yellow lines), occurred during the main 19th century flood events in 1846, 1856 and 1866***

Historic breach locations can be considered as preferential locations for future breaches because of repairs that provide weaker points within the levee or simply because those locations correspond to points where specific factors make breach formation more likely to occur. These factors could be the location of higher water elevations (relative to crest level), scour at the toe of the levee, high water velocities (corresponding to a narrowing of the river channel, development of vegetation or vegetation jams, the outside bank of a river bend etc). So in addition to historical analysis, morphological and geotechnical analyses can help to identify possible locations of breaches. However, of the many potential breach locations identified, judgement is required to select those associated with higher potential consequences for more detailed consideration. Alternatively, a systematic assessment of flood risk along the entire levee system may be performed. Such an analysis considers the performance of all levees under a range of load conditions, and the likelihood and consequences of failure. By attributing flood risk from each of the thousands of scenarios considered to the breached levee or flood defence being analysed, the system model can build a picture of the flood risk associated with each section of levee or flood defence, providing a valuable tool to assist in asset management.

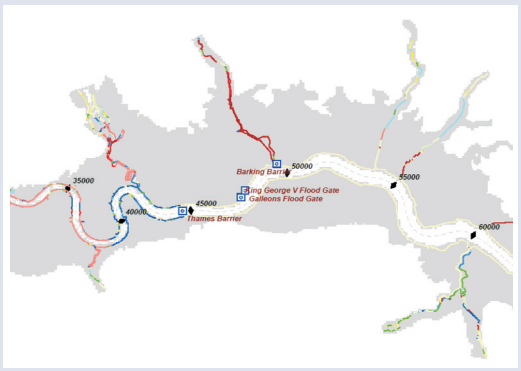

Figure 8.137 ***An example of system modelling showing river channel, flood risk area (shaded) and colour coded flood defences representing flood risk attribution***

8.10.2 Soil type, state and erodibility

As previously discussed, the type and nature of soil within a levee determines the erodibility of that soil and this in turn affects the rate and type of erosion that will occur during breach initiation and

formation. So, natural variations within the soil, or variations introduced through construction, can create areas of strength or weakness in relation to erodibility. Since soil erodibility is significantly influenced by compaction energy and soil moisture content during construction, consideration of these parameters will allow more erosion resistant levees to be constructed. However, changes in these parameters over time (deterioration) will also affect erodibility.

Levee erosion will typically be in the form of surface or headcut erosion, depending upon the nature of the soil (Hahn *et al*, 2000, and Hansen *et al*, 2005a and b). A highly erodible soil, such as a soil with low cohesion and a high sand or gravel content, will erode rapidly and typically through erosion of the exposed surfaces, including erosion of the crest. A highly erosion-resistant soil, such as clay with high cohesive strength, will erode slowly, typically through headcut formation, whereby a step erodes on the downstream face of the levee and recedes towards and through the crest. As the crest of the levee controls the rate of overflow during breach formation, an erosion process that lowers the crest will probably result in catastrophic breach sooner than, for example, a headcut process where catastrophic failure only occurs after the headcut has receded through the crest into the upstream face.

These processes are fuelled by the removal of sediment from the levee body. This can occur via three mechanisms (de Vroeg *et al*, 2002, Mostafa, 2003, Mostafa *et al*, 2008, and Morris, 2009):

1 Sediment erosion.
2 Mass erosion.
3 Soil wasting.

Sediment erosion occurs when sediment is removed from the surface of the embankment and held in suspension by the flow. Mass erosion occurs when small lumps of soil, rather than individual particles, are removed from the embankment surface by the flow. This process is particularly affected by the structure of the soil, including any fissuring that may have occurred. Soil wasting occurs when large blocks of soil are undercut and collapse into the breach flow. These are then quickly removed via a mixture of sediment and mass erosion.

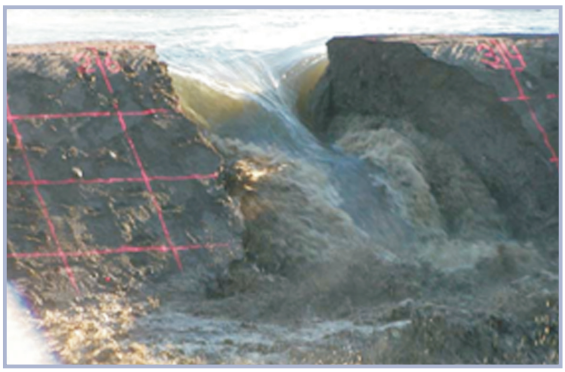

a Sediment erosion by turbulent flow along base of breach sides

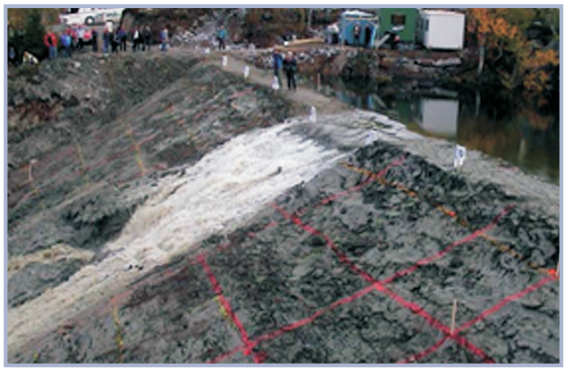

b Mass erosion – small lumps of soil/clay being removed

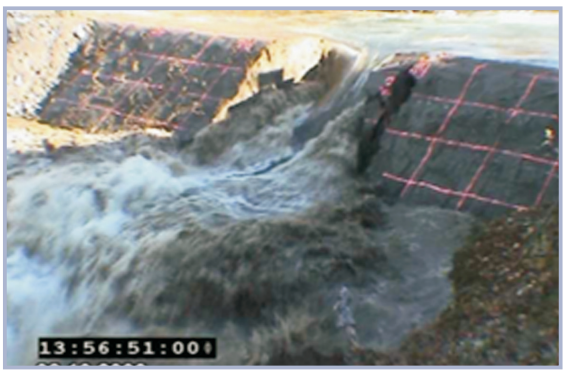

c Soil wasting – block failure on left face of breach

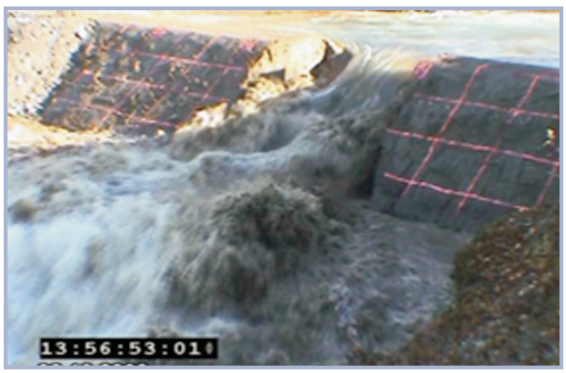

d Soil wasting – block failure on left face of breach 2s after failure of block breach (ie block has been removed)

Figure 8.138 Small scale erosion mechanisms (courtesy M Morris)

These processes can be seen in different scales of embankment or levee; for example, headcut and block failure during failure of the El Guapo dam (Figure 8.139) shows similar processes to those seen during tests on five to six metre high levees (Figure 8.138).

Figure 8.139 Failure of the El Guapo Dam, Venezuela, December 1999 (courtesy M Morris)

Until recently (~2005), a majority of levee erosion models have used equilibrium sediment transport (EST) equations. The problem with the use of these equations is that they have been developed for the long-term prediction of river bed morphology rather than the prediction of short-term, dynamic conditions typical of catastrophic levee erosion. EST relationships have typically been established by studying equilibrium sediment transport conditions in a flume, where sediment is fed into and collected from a flume under steady state flow conditions in order to establish what bed material load and wash load transport rate occurs for a given sediment and flow condition. This process relies upon a balance being established between sediment inflow and outflow. It is also based upon flow over a sediment bed, rather than flow across a levee or through a breach, where erosion may occur along the breach sides resulting in soil wasting, where a mass of sediment is injected into the flow.

Critically, the rate of levee erosion towards breach can be seen to be highly dependent upon soil state, for example, a highly compacted soil as compared to a loosely placed soil, will take much longer to erode (Hanson, 1992, and Hanson, *et al*, 1997). EST equations do not offer the flexibility of allowing for soil state, because the equations are based upon the soil being in flux along a river bed. So, the use of erosion equations rather than EST equations for simulating levee erosion offers a better solution that more closely represents the physical processes that occur. Erosion equations relate the rate of sediment removal to the shear stress applied by the surface flow and are applicable to non-equilibrium conditions.

A common form of erosion equation as used by Chen and Anderson (1986) and Hanson *et al* (2005b) is given here:

$$E = K_d b(\tau - \tau_c)^a \qquad (8.259)$$

where:

E = erosion rate, bulk volume hence rate of bed elevation change or retreat ($m^3/s/m^2$)
K_d = erodibility or detachment coefficient (-)
τ = effective shear stress (kPa)
τ_c = critical shear stress (kPa)
a, b = empirical coefficients dependent upon soil properties (-)

Hanson assumes that a = b = 1. The only variables in calculating the rate of erosion are the critical shear stress (τ_c), and the erodibility of the soil (K_d).

The use of such an erosion equation has two advantages:

1 The equation reflects a dynamic erosion process and is not based upon steady state equilibrium conditions, which clearly do not apply.

2 The erodibility parameter, K_d, can be used to reflect variations in erosion as a function of soil state (compaction, moisture content etc) (Hanson and Hunt, 2006).

It can be seen that soil erodibility is highly dependent upon soil compaction and moisture content, Figure 8.140.

Embankment Test	Soil Classification[1]	Sand[1] > 75µm (%)	Fines[1] > 2µm (%)	Fines[1] < 2µm (%)	PI[2]
P1	SM	64	29	7	NP
P4	CL	25	49	26	17

Note: Based on ASTM : [1]D 2487, [2]D 4318.

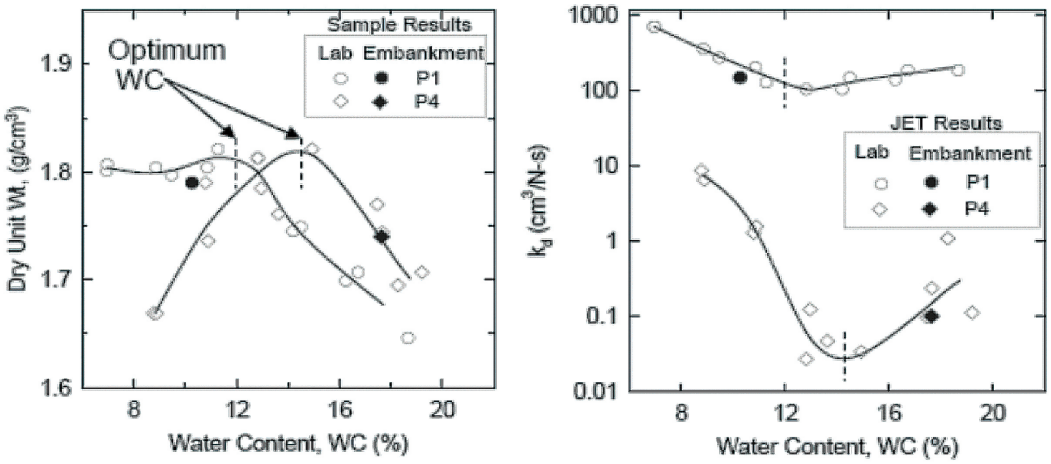

Figure 8.140 Example analyses showing relationship between soil erodibility (K_d) and soil type, density and water content (Hanson et al, 2010)

The drawback to using an equation based upon an erodibility coefficient, such as K_d is the need to define a value for K_d. To date this has been undertaken through laboratory or field testing (Hanson *et al*, 2005a) but there are several different methods by which this might be done and results are not yet consistent between approaches (Regazzoni *et al*, 2008b, Wahl, 2008, and Wahl *et al*, 2009). The two main approaches are jet testing (JET) (Hanson) for erodibility relating to surface or headcut erosion, and hole erosion testing (HET) (Fell) for internal erosion erodibility.

Simple guidance on the likely range of erodibility for a given soil and state is available, but this is indicative and care should be taken to assess the impact of uncertainty in these values on any particular study. Temple and Hanson have undertaken programmes of research into soil and vegetation performance at the USDA Agricultural Research Service centre in the USA. As part of this work they have produced some indicative and qualitative descriptions of soil erodibility, as shown in Equation 8.260 and Tables 8.35 and 8.36. Equation 8.260 provides an approximate method for estimating erodibility (K_d) based upon percentage clay content and soil density (Temple and Hanson, 1994).

$$K_d = \frac{10\gamma_w}{\gamma_d} exp\left[-0.121(C_{\%})^{0.406}\left(\frac{\gamma_d}{\gamma_w}\right)^{3.10}\right] \quad (8.260)$$

where:

K_d = erosion rate (cm³/N-s)
$C_{\%}$ = per cent clay
γ_d = dry unit weight (mg/m³)
γ_w = unit weight of water (mg/m³)

When using Equation 8.260, a value of τ_c is also required (Table 8.37). An approximation is to assume that $\tau_c = 0$ or to use Equation 8.261 (Hanson and Simon, 2001, and Hanson and Hunt, 2006).

$$K_d = 0.2\tau_c^{-0.5} \quad (8.261)$$

where:

K_d = erosion rate (cm^3/N-s)

τ_c = critical shear strength (Pa)

Given the uncertainty associated with a clear description and measure of erodibility, an alternative approach is to adopt qualitative descriptions of erodibility and to allow for this uncertainty when considering modelling results such as shown in Figure 8.141.

Table 8.35 Qualitative descriptions of values for K_d modified from (Hanson et al, 2010)

Description	K_d (cm^3/N-s)
Extremely rapid	1000
Extremely rapid	100
Very rapid	10
Moderately rapid	1
Moderately slow	0.1
Very slow	0.01
Extremely slow	0.001

Table 8.36 Approximate values of K_d (cm^3/N-s) relative to compaction and % clay (Hanson et al, 2010)

	Modified compaction (27.5 kg-cm/cm^3)		Standard compaction (6.0 kg-cm/cm^3)		Low compaction (kg-cm/cm^3)	
Clay (%)	*≥ Optimum water content%*	*< Opt WC%*	*≥ Opt WC%*	*< Opt WC%*	*≥ Opt WC%*	*< Opt WC%*
>25	0.05	0.5	0.1	1	0.2	2
14–25	0.5	5	1	10	2	20
8–13	5	50	10	100	20	200
0–7	50	200	100	400	200	800

Table 8.37 Approximate values of τ_c (Pa) relative to compaction and % clay (Hanson et al, 2010)

	Modified compaction (27.5 kg-cm/cm^3)		Standard compaction (6.0 kg-cm/cm^3)		Low compaction (kg-cm/cm^3)	
Clay (%)	*≥ Optimum water content%*	*<Opt WC%*	*≥Opt WC%*	*< Opt WC%*	*≥ Opt WC%*	*< OptWC%*
> 25	16	0.16	4	0.04	1	0.01
14–25	0.16	0.01	0.04	0	0.01	0
8–13	0.0	0	0	0	0	0
0–7	0	0	0	0	0	0

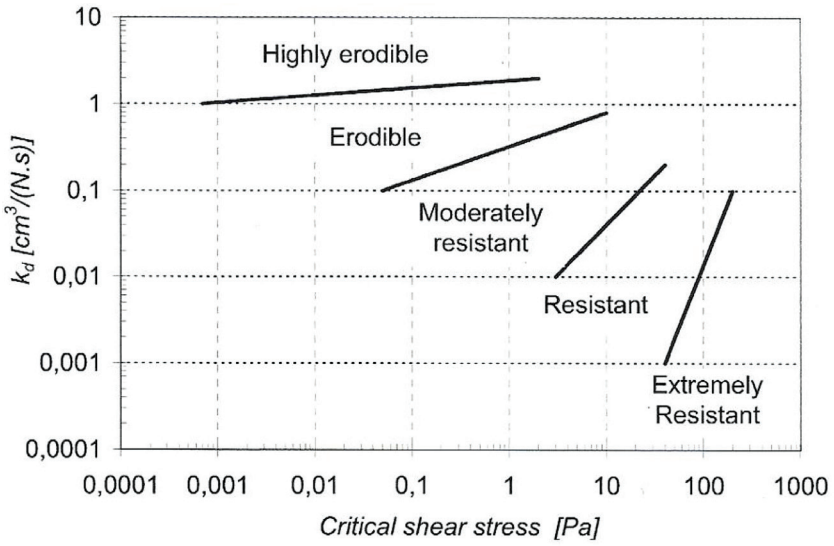

Figure 8.141 Erodibility of soil (from Hanson and Simon, 2001)

8.10.3 Methods for modelling breach growth

There are a variety of different types of model (or method) for predicting breach conditions. These may be broadly categorised as:

- non-physically based, empirical models
- semi-physically based, analytical and parametric models
- physically based models.

Non-physically based or empirical models

Such methods are usually based upon data collected from a series of documented breach events. Breach parameters (eg peak discharge, beach width etc) are estimated from predictor equations, derived through regression analysis using historic case study or laboratory data. The advantage of these equations is their simplicity – there is no need to run computer models. However, this simplicity is also one of their main weaknesses, because there can be considerable uncertainty within the predictions. Users often have little knowledge of the data that the equations were based upon, so any constraints for application and the suitability for application to site specific cases are hidden or unknown. An additional limitation of these equations is that they only predict specific parameter values, for example, peak discharge rather than the whole outflow hydrograph, or final breach width rather than the time varying growth of width. Wahl (2004) provides a review and comparison of these equations, recommending the Froehlich (1995b) equation as the least uncertain:

$$Q_p = 0.607 V_w^{0.295} h_w^{1.24} \quad (8.262)$$

where:

Q_p = peak outflow (m³/s)
V_w = volume of water stored above breach invert at the time of failure (m³)
h_w = depth of water above breach invert at the time of failure (m).

This equation has been developed by regression analysis against a record of 22 dam failures, so it is unclear how applicable this would be to smaller levees. Note that the key parameters (V_w and h_w) relate to volume and depth of water retained by a dam. Wahl (2004) suggested that the uncertainty in use of this equation was in the order of 0.53 to 2.3 with a hypothetical value of 1.0. Additional equations predicting final breach width and time to failure are also available. The uncertainty in time prediction is greater at 0.38 to 7.3 with a predicted value of 1.0. So applying such an equation to levee conditions offers a quick, simple estimate but with potentially large uncertainties.

All of the equations compared relate to breach formation through dams rather than levees. The suitability for cross application has not been studied and it is likely that considerable errors may be introduced to an already uncertain method of breach prediction. Research work by Verheij (2002) provides a simple relationship between predicted breach width B (m) and time t (s) for sand and clay dikes, based on field and laboratory tests (Figure 8.142),

For sandy dikes: $$B = 67 \log\left(\frac{t}{522}\right) \tag{8.263}$$

For clayey dikes: $$B = 20 \log\left(\frac{t}{288}\right) \tag{8.264}$$

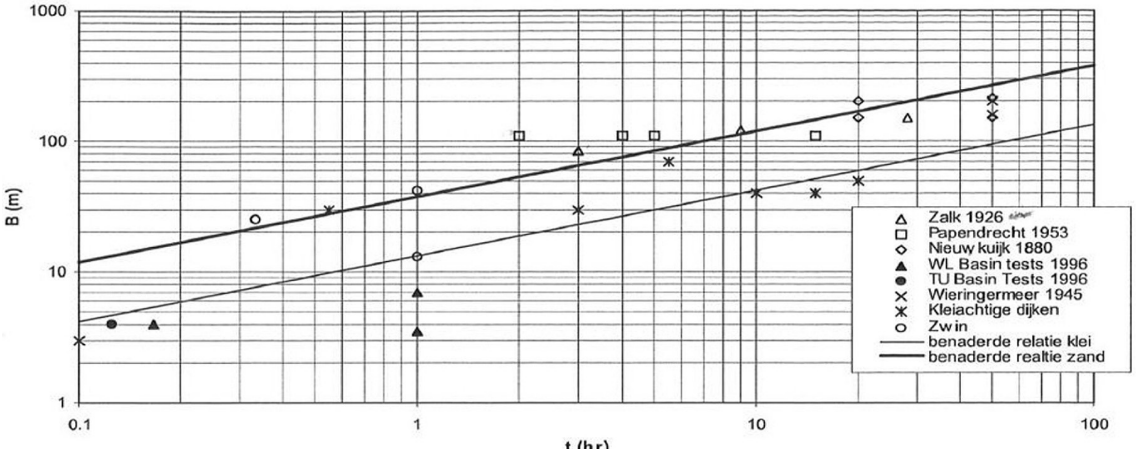

Figure 8.142 Breach width (B) as a function of time (t) and soil type (upper curve: sand, lower curve: clay) (Verheij, 2002)

Semi-physically based, analytical and parametric models

The large range of uncertainty associated with the non-physically based methods prompted development of more complex models. These were based on physical processes, but with simplified assumptions to represent the failure of the dam or levee so as to not unduly complicate the calculation process. Assumptions usually include use of a weir equation to represent the flow over the embankment, so that critical flow conditions exist on the embankment crest. However, these models often also require the input of erosion rate for the growth of breach, or the time taken to form the breach, and the final dimensions of a breach shape. Some models then simply predict a growth pattern to fit these parameters and subsequently produce a flood hydrograph. So their values may vary and are highly dependent upon the user. While these models appear to provide a more accurate prediction of the flood hydrograph in comparison to empirical equations, they simply reflect the data provided by the user, and can also include large degrees of uncertainty.

Examples of this approach can be seen within the original DAMBRK code and the Hydrologic Engineering Center River Analysis System (HEC-RAS) (USACE, 2011). Sensitivity analysis is usually performed using several methods of parameter estimation to develop an expected range of breach behaviour, and then try to determine the range of uncertainty within the approach.

Physically based models

Physically based numerical models simulate the failure of embankments based on the processes observed during failure, such as the flow regimes, erosion and slope instability processes. In the last four decades many models have been developed to simulate the failure of dams and levees. These models differ in their complexity, assumptions involved, and techniques used. Morris (2011) provides a summary of these models.

The CEATI Dam Safety Interest Group funded a research project to review and evaluate breach models for industry use (Morris *et al*, 2012b). After an international review, this research focused upon the

performance of two models – the HR BREACH model (Mohamed, 2002, and Morris *et al*, 2012b) and the SIMBA model (Hansen *et al*, 2005c). The SIMBA model is now integrated into the WinDAM B software (USDA, 2013) while the 2008 HR BREACH model is integrated into the InfoWorks®RS (Innovyze, 2013) flow modelling package. SIMBA simulates breach formation through headcut, while HR BREACH simulates breach initiation and formation through surface erosion. However, a version of the SIMBA headcut process is also included in HR BREACH, along with prediction of breach growth through pipe formation.

Both SIMBA and HR BREACH are physically based models although they adopt different approaches to simulation. SIMBA runs very quickly, but achieves this by predefining the erosion failure process. HR BREACH takes minutes to run, but allows the model to predict how erosion develops through the levee.

Later developments of HR BREACH (Morris *et al*, 2012b) introduce the ability to predict breach formation processes through zoned or layered levees, where layers of different soil, or soil erodibility, can be seen to significantly affect some breaching processes. Development of a new simplified model called AREBA (van Damme *et al*, 2011) takes a similar approach to SIMBA in predefining the failure process, but includes failure (of homogeneous levees only) by considering surface erosion, headcut or piping. AREBA runs in less than one second, making it a useful tool to aid understanding of how a levee might fail under varying conditions and failure modes.

Although the WinDAM (SIMBA), HRBREACH and AREBA models are some of the most recent physically based breach models, it should be recognised that there are a variety of other models in existence, often developed as part of research programmes. When choosing a particular breach model to use it is important to understand what processes are simulated and what simplifications or assumptions have been made and how these affect your particular case.

The EU FLOODsite project included a substantial programme of research into modelling breach initiation and growth. Conclusions from this work, including guidance on breach models and modelling can be found online (Oumeraci, 2005). A range of associated reports also provide supporting information and offer a good starting point for anyone interested in understanding more about breaching processes. In particular, Oumeraci (2005) provides frame by frame images of various levee failures, highlighting the different processes that occur.

Selecting breach model input parameters

The model input parameters required will depend upon the model being used, ie the simpler the model (or equation) the fewer parameters are required but the greater the uncertainty in prediction. Since breach processes depend upon the hydraulic load, combined with soil erosion and structure response it would be reasonable to assume that parameters reflecting these processes are required in order to model these processes. A key parameter affecting erosion is the soil erodibility, which is affected by parameters such as soil water content, compaction etc. However, in practice, these parameters are often not taken directly into account, instead being reflected by judgement as to the soil type and of potential erodibility. Although this approach offers a practical approach to breach modelling, care should be taken to include consideration of how erodibility might vary for a given case. Formal sensitivity analysis using a range for key modelling parameters is strongly recommended.

It should be noted that early breach models tended to use sediment transport equations to predict erosion within the breach. In recent years there has been a move by many modellers towards the use of erosion equations, which derive the rate of erosion from the flow stress and soil erodibility, rather than simply particle size. This better reflects the dynamic, rapidly changing conditions within a breach and allows consideration of soil state as well as type.

Integrated breach and flow modelling

To correctly simulate breach conditions within a levee system it is often necessary to integrate the breach and flow modelling together. Where downstream floodwater levels can exceed about two-thirds

the depth of upstream water levels on the breach invert, then the release of water through the breach and the rate of breach growth will be affected. In these situations, the correct prediction of conditions requires a step-by-step analysis of water levels and breach growth throughout the levee system. Very few breach models are truly integrated with flow models to provide breach predictions throughout a levee system. In some situations the effects of drowning on overall flood conditions will be significant.

Examples of different models for breach analysis are given in Boxes 8.26 to 8.27.

Box 8.26 Example of non-physically based or empirical models

For some studies a simple assumption that breach has occurred is made, and flood conditions are then simulated. While simple, this can be unduly pessimistic for assessing the extent and magnitude of flood risk. Figure 8.143 shows an inundation plan generated from such an assumption. These results can be quickly misinterpreted because the degree of detail from the inundation mapping masks the crude assumptions made for breach modelling, which ultimately dictates the volume and rate of floodwater released into the inundated area.

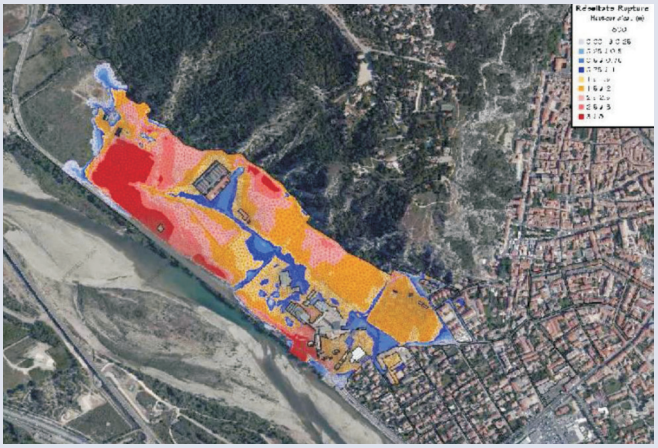

Figure 8.143 Example of zoning of water depths 30 minutes after a levee breach in an urban area (Th. Monier, Sogreah, 2011)

An example of the differences that might be found through predicting breach rather than assuming instantaneous breach are shown in Figure 8.144. The left plot shows breach growth with time, the right plot shows the difference in predicted flood hydrograph. The example was computed by calculating in advance the breach evolution with the code Rupro, developed by Irstea in France (this code is included in the simplified breach modelling code CastorDigue), then by using this evolution in the hydraulic modelling code. This assumption requires that the breach does not drown during formation, because the breach growth and flow modelling are undertaken independently.

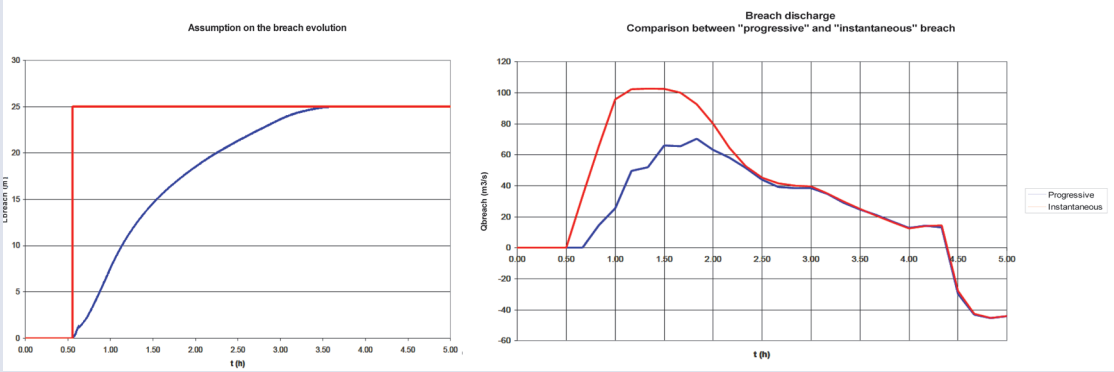

Figure 8.144 Example of breach prediction assuming instantaneous breach (red) or progressive breach growth (blue)

Box 8.27 *Examples of physically based models*

The HR BREACH model was originally developed by Mohamed (2002), and integrated with the InfoWorks®RS flow modelling package in 2008, and extended to simulated breach through zoned embankments by Morris (2011). The model requires a range of parameters to define the hydraulic boundary conditions, embankment structure and soil type and state. Breach simulation takes into account surface protection (grass, rock etc) and simulates breach formation through surface or headcut erosion, and piping. The model predicts conditions at sections through the embankment, uses a soil erosion equation to predict erosion section by section and allows for discrete block failure and removal during the process.

The integrated version of the breach model interacts with a 1D/2D flow modelling package at a time step level so that conditions within the breach and the associated flood cells update interactively (Figure 8.145). Multiple breach units can be run within the flow model simultaneously allowing prediction of multiple breaches within a levee system within a single simulation.

The extended (Morris, 2011) version of the model includes the ability to simulate breach formation through zoned embankment structures. So, where a levee has been constructed using different material in different areas, or where a levee has been extended so that there are layers of different soil, or different soil states (and also erodibility) the model simulates how the rate and shape of breach growth is affected by the various zones. Zones of different material within a single levee can significantly affect the way in which a breach forms.

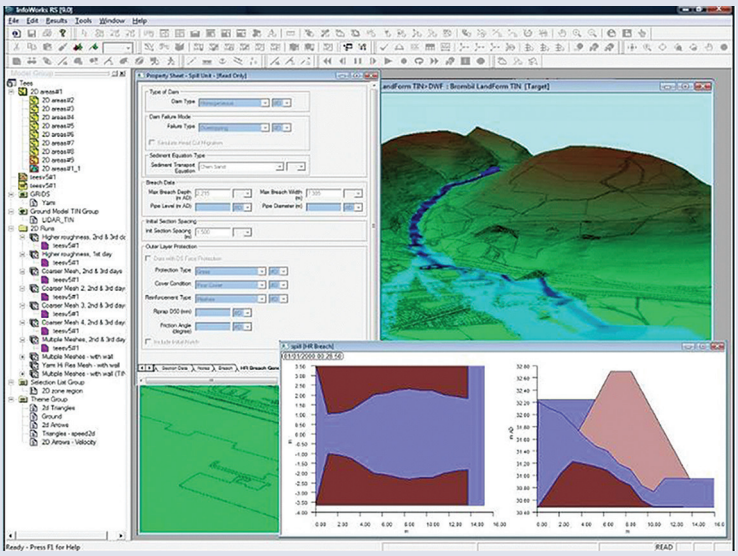

Figure 8.145 *Fully integrated breach and 2D flow model*

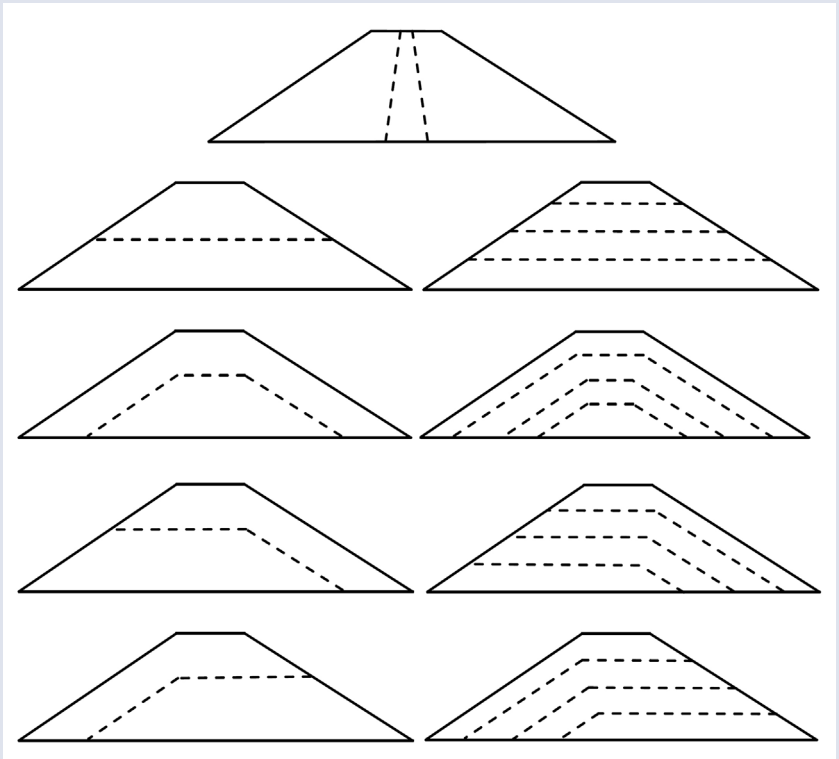

Figure 8.146 *Zoned approach to breach modelling (HR BREACH, 2011)*

Box 8.27 Examples of physically based models (contd)

The WinDAM B code (USDA, 2013) incorporates the SIMBA headcut model. SIMBA simulates headcut erosion through a levee or earthen dam by assuming a predefined failure process. By making these assumptions the model can simulate breach very quickly (a few seconds). The WinDAM B package incorporates the SIMBA model within a framework that allows simulation of a reservoir, including grass resistance to overflow.

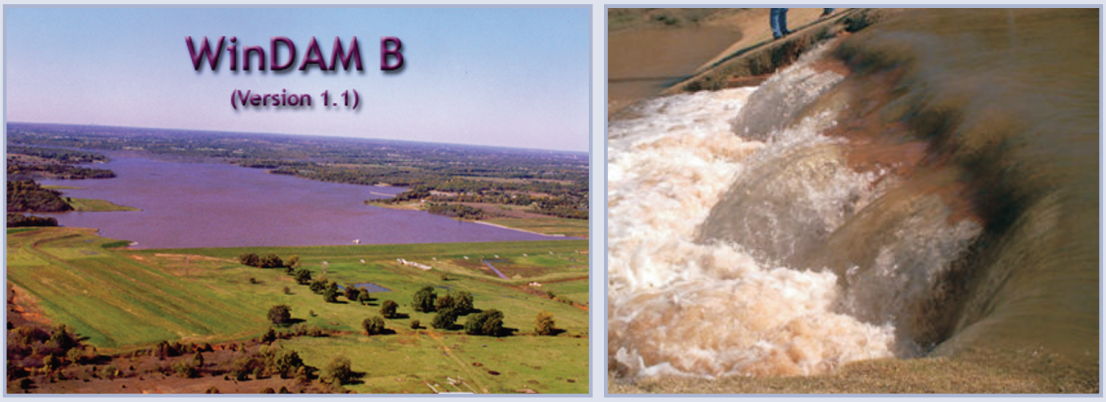

Figure 8.147 WinDAM code for estimating erosion of earthen embankments and auxiliary spillways of dams (from USDA, 2013)

AREBA is a new model that adopts a similar approach to SIMBA in predefining the way in which breach formation occurs, but allows the user to simulate erosion through surface erosion, headcut or internal erosion (pipe formation). The model takes less than a second to run and has been designed for use either within system risk models (ie simulation of flood risk for levee systems) or as a 'standalone' model. At the time of writing (2012), the model was being finalised.

Example of current practice

The second type of model is often used in operational studies because it remains a simple tool but avoids fixing the evolution timescale in a quite arbitrary way. For instance, for the case of La Faute sur Mer (France), the breach model Rupro, which is encapsulated in CastorDigue software (Irstea, 2012) was used (Box 8.28).

Box 8.28 Rupro model

This model relies on the assumption that the breach cross-section can be represented by an average value and does not have to be explicitly defined, which helps to evaluate the linear loss of head along the breach channel. Then, the discharge hydrograph is obtained using the Bernoulli equation while the rate of erosion comes from the sediment discharge calculated using the Meyer-Peter and Müller (1948)'s equation:

$$Q_s = 8\,(\,\beta\psi - 0.047)^{3/2}\sqrt{\left(\frac{\gamma_s}{\gamma_w} - 1\right) g\, d^3} \qquad (8.265)$$

The primary shape of the representative breach cross-section is either circular (such as occurs due to piping) or rectangular (such as occurs due to overtopping). Results from the Cadam and Impact European research projects(blind tests on controlled experiments both field and laboratory) showed that such a simplified model can provide suitable estimates of breach discharges but less reliable results on breach shape development (Paquier and Recking, 2004). From the Impact European project, Paquier (2007) showed that the model can be improved by reducing the erosion rate during the widening step in order to obtain nearly perfect agreement between measured and predicted results (error is of the same order as measurement uncertainty). The limits of such a model and also of most of the models to field applicability are the assessment of model parameters (which are easier to establish in controlled experiments with homogeneous materials). During the Impact European project, the uncertainty assessment of a well-known dam break event (the Tous dam failure in Valencia, Spain) provided a 30 per cent uncertainty for peak discharges at 90 per cent, due to the uncertainty parameters. If the failure scenario is not known, uncertainty will be much higher. Therefore, to reduce uncertainty of breach modelling results, it is important to consider the following factors:

- location of the breach
- estimation of the time for breach development
- assessment of the levee material parameters.

8.11 FLOOD INUNDATION

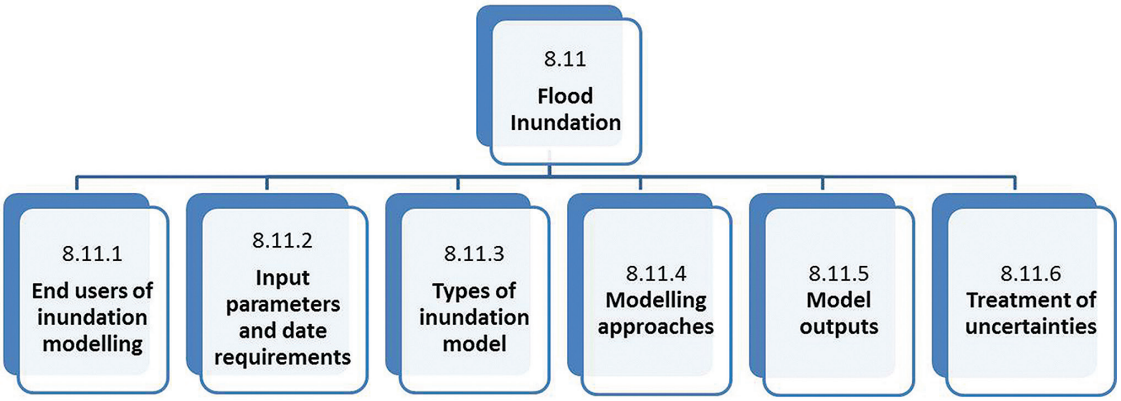

This section provides guidance on how to relate accuracy of modelling results to the end user and be clear on limitations of existing methods, and under which circumstances these methods may be applicable. The section highlights, as appropriate, current efforts undertaken by groups or organisations across the world, especially during the FLOODsite project (Oumeraci, 2005).

8.11.1 End uses of inundation modelling

8.11.1.1 Land use planning

A critical component of risk reduction is minimising the consequences that could occur as a result of a flooding or storm event. A large component in minimising the consequences is increased awareness of all stakeholders (population at risk in addition to any federal, state, and local government entities). So, making information such as flood maps that incorporate breach scenarios available to stakeholders is a prudent step. Flood mapping should be made available to the public and accompanied by information explaining the risk linked to these breaching processes (for example, the flooding of the town of Toulouse in the South of France)

8.11.1.2 Risk analysis

In several countries, national policies are imposed on owners of levees to assess the risk induced in the flooded area by a failure or a breach that may occur in the levee. To do so, 2D inundation modelling is used to determine and localise versus time, maximum velocities and water depths in the flooded area. For life safety, these results are compared to criteria chosen generally to enable safe evacuation (an example of limits is shown in Figure 8.148).

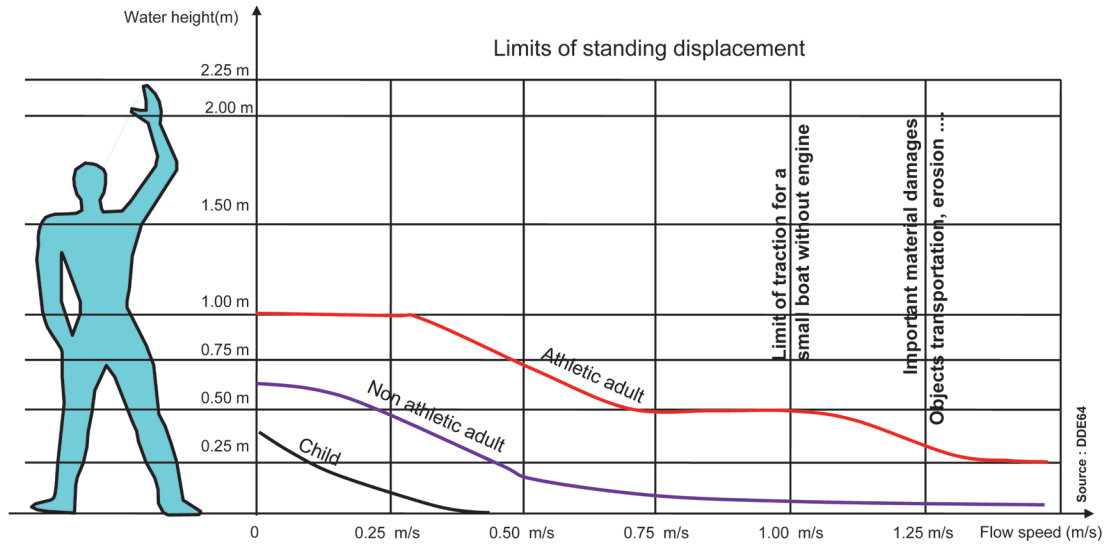

Figure 8.148 Limits of standing evacuations for a child (lower curve), a non-healthy adult or a stressed healthy adult (upper curve) regarding water depth or flow velocity

This kind of criteria can be used to estimate casualties and material damage. An example of a map used to communicate flood inundation is given in Box 8.29.

Box 8.29 Example of flood map from a 2D diffusive wave model

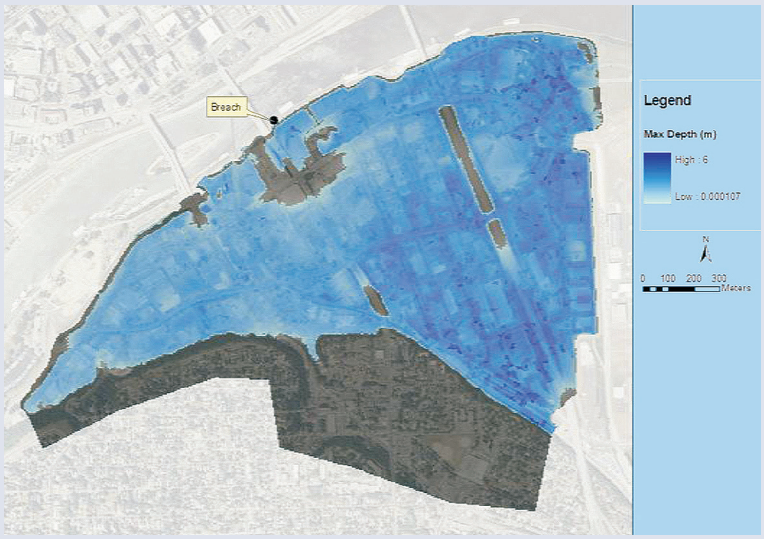

Figure 8.149 Example of a map of maximum depth generated with RFSM, showing the inundation resulting from a breach in a levee protecting an urbanised area in the floodplain

Planning authorities often use inundation mapping to evaluate the potential risk of areas considered for new developments. Insurance companies also use inundation mapping techniques to calculate insurance premiums for individuals and businesses.

8.11.1.3 Flood and risk management

Another type of end user is the emergency responder that should organise the evacuation of the population in advance. In this context, modelling could be used to highlight the areas with the greatest risk of casualties. Box 8.30 illustrates the use of flood mapping in the case of emergency preparedness.

Box 8.30 ***Inundation mapping for evacuation planning***

A flood inundation map was used for preparing the evacuation plan for a population (provisional results for a municipality in the South of France). Because of the high probability of overtopping in cases of extreme flood and the short period for evacuation (flood peak can occur within one hour from the start of rainfall), the municipality proposed to evacuate the population, starting with the people in the more exposed locations (red, orange, and yellow grids on Figure 8.150). Using a 2D model for the whole area and simulating breaches in various locations, hazard classes due to levee failure were derived from classes for peak water depth and peak velocity. Due to the low water head upstream the levees are located very close to the river where most of the more risky areas are, within 100 m of the levees. The computational mesh is shown in Figure 8.150.

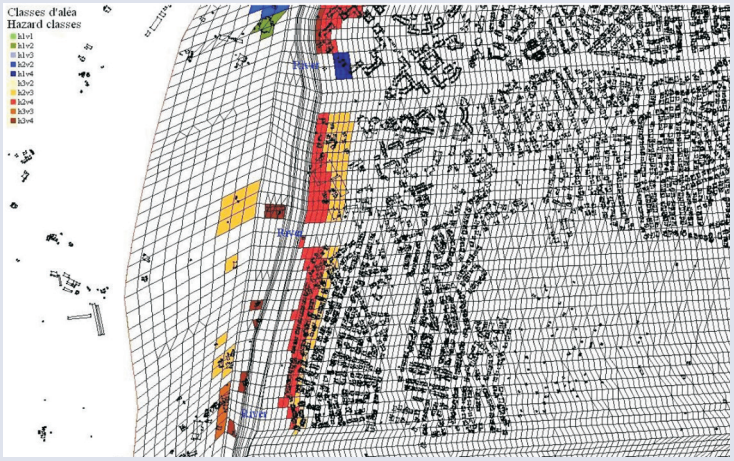

Figure 8.150 *Flood map showing high risk areas due to levee failure calculated from 2D hydraulic model*

8.11.2 Input parameters and data requirements

8.11.2.1 Input data

The primary data representation for inundation modelling is the digital terrain model (DTM). It gives a numerical representation of the topography and is usually acquired from the air (airplane or satellite). The most common format is a regular grid, but triangular irregular networks (TIN) also exists. LiDAR (Light Detection and Ranging) is currently the most accurate type of DTM, with horizontal resolution as low as 0.5 m (or even lower), and vertical accuracy of 0.1 m. But this means that the amount of topographical data available can be much greater than the data the inundation model can take into account. Other types of DTM available include SAR (Synthetic Aperture Radar) and ASTER (Advanced Spaceborne Thermal Emission and Reflection Radiometer), which are more widely available, cheaper to purchase (or free), and cover extensive areas. A DTM can also be created by digitising points using a detailed topography (paper) map if no DTM can be sourced at the required resolution. Alternatively, depending on the type of model used, cross-sections can be given to represent the topography. These will usually be measured perpendicular to the river and cover the river and the floodplain.

A land use dataset is useful to help the modeller to assign the friction coefficient values. In urban areas, the network of streets and the location of buildings have a key influence on the propagation of the flood. Being able to use a polygon dataset indicating the contours of the buildings is important to build a detailed inundation model, and can be obtained from national cartographic institutes or from the internet. Bridges are not captured properly in a DTM, as this will show only the top of the bridge. Manual editing might be needed to restore the terrain elevation under the bridge and avoid artificial blockages. Also it is possible in some software to insert a 1D structure within the 2D mesh to represent the bridge opening.

The flow model should include the whole area that is influenced by the breaching process. In the case of breaching a levee along a river during a flood, breaching will influence the whole flooding process downstream from the breach, so the extent of the breach model including breaching will be similar to the extent of the general flood model. Due to the high velocities close to the breach, any obstacle in the floodplain involves a rise of the water elevation upstream and a drop downstream, so it is important to

describe the floodplain in detail near the breach. In the case of a flood flowing through an urban area, the flow will be concentrated in the streets and straight streets can generate high velocities. The location of the breach in relation to the street directions influences the flood results (El kadi Abderrezzak *et al*, 2009).

Initial conditions (level and velocity) in the river and the floodplain are needed for the numerical model to start the simulation, although the floodplain is usually assumed to be dry at the start. Boundary conditions are also needed at the upstream and downstream end of the river (upstream discharge, downstream level or rating curve) and at the limits of the floodplain (no flow, free flow).

8.11.2.2 Model assumptions

Other parameters influencing the inundation cannot always be measured and some assumptions need to be made. The main assumptions are:

- location of the breach in the dike
- moment of the beginning of the breach (if the evolution of the breach is modelled) or moment of the breach (if an instantaneous breach is assumed)
- maximum depth of the breach
- maximum width of the breach.

Some of these assumptions can be helped by using existing studies (eg hazard studies required for some dikes in France). The number of assumptions can be large and these can influence the results such as water level or velocity in the floodplain or the flooded area. For this reason it is often considered that a precise modelling of the breach evolution is not always needed.

8.11.3 Types of inundation models

8.11.3.1 Model requirements

The aim of a flood model consists in providing the time evolution of water depth and flow velocity in any point of the floodplain. Flow coming from a breach failure, such as flash-floods in urban areas, is generally characterised by high velocity and high water level. Both factors lead to an increased risk compared to an assessment using water depth only. In terms of constraints for modelling, the fast flows imply that the numerical model needs to cope with the changes of regime from subcritical to supercritical and conversely.

If all the physical processes are considered, the flood model should also consider sediment transport, sediment coming from the breach and sediment eroded downstream of the breach. Even if sediment transport is not included in the modelling, it is better to integrate the breach model with the flood model in order to have the right upstream condition for the flood model (breach discharge hydrograph), but above all in order to obtain the right upstream and downstream hydraulic conditions for the breach model. Also, such integration or coupling is necessary in cases where the flow is going from upstream to downstream of the levee by other means or processes than a breach (overflow, piping, connecting hydraulic structure etc).

8.11.3.2 Choice of the hydraulic model

First of all, the modeller has to choose a hydraulic model that is suited to the considered inundation. Because of the configuration of a breach and, usually, an extended floodplain, the flow is essentially 2D horizontal. This means that 2D models are relevant (or 3D if the vertical distribution of velocity is considered) in most cases. In the case of flood wave propagation due to dam break, a 1D model is acceptable, but this is not the case for flood wave propagation due to a dike breach, because the flow is spreading in the floodplain and no preferential direction can be assumed. 3D models are more expensive to create than 2D models, and are not always necessary. Indeed, in some situations a model may not be needed at all. Given gauged water surface elevations along a reach, or water surface elevations predicted, based on flood frequency analysis, a similar interpolation to that used by Werner

(2001 and 2004) can be created. This estimates the flood wave as a plane (or series of planes), which is intersected with the DEM to give extent and depth prediction.

Models that solve the shallow water equations (Bates *et al* 2010), (either 1D or 2D), are preferred as they can represent both subcritical and supercritical flows. Advanced models have shock capturing capabilities to represent more accurately the flow regime changes (hydraulic jump). Infoworks (Innovyze, UK), Telemac and Mascaret (EDF, France and consortium), Rubar20 (Irstea, 2013) are a few examples. Although when the levee failure is progressive, the flood hydrograph is less extreme and a simplified flow algorithm can be used. Examples are Lisflood at the University of Bath (Bates *et al*, 2010) and RFSM-EDA from HR Wallingford (Jamieson *et al*, 2012a and b), based on the diffusive wave approximation with a local acceleration term.

Examples of flood maps produced with three different models are shown in the Boxes 8.31 and 8.32.

8.11.3.3 Computation set-up

Advances in computational hardware in recent years have led to a reduction of model run-times. Faster processors and large amounts of RAM contribute to model acceleration, but parallel processing is the main factor. Parallel processing involves splitting the computation between multiple concurrent processes, and reducing the total time needed for the whole process. There is a small overhead in doing so, meaning that the total reduction in run-time is not equal to the number of processes, as the calculations from each process need to be merged at the end of a time step. Three computation approaches are commonly used to achieve parallel processing:

- multi-core
- multi-computer distributed
- graphics processing unit (GPU).

Usually model software supports only one parallel processing approach. Some inundation models can run in parallel such as Telemac and Infoworks.

8.11.4 Modelling approaches

Different options are available when modelling the flood caused by a dike breach:

- model the breach evolution and the flood wave propagation in the floodplain simultaneously by coupling a breach model and a hydraulic model
- estimate a realistic hydrograph at the breach, by means of a separate calculation, and use this hydrograph as an inflow into the floodplain
- assume an instantaneous breach and propagate the flood wave in the floodplain.

The first solution is more elegant from a scientific point of view, but it requires combining a soil or breach erosion model with a hydraulic model, and as mentioned previously, the uncertainty of the sediment or soil parameters is high in these models. Also, the physical phenomenon of breach formation and evolution are not completely understood. Research on this issue is still ongoing (ie research programmes FLOODsite and ERINOH in Europe, or LEVEES and DOFEAS in France).

The second solution is more practical, but the disadvantage is that only a part of the hydraulic system is integrated in the model. This solution does not take into account the interactions between the river, the dike and the floodplain. These interactions can influence the breach discharge, water level and velocities in the floodplain, which cannot be taken into account if the hydrograph is set at the breach.

The third solution is easier to implement, because the breach is assumed instantaneous. This assumption is acceptable especially in the case of concrete or masonry structures. In the case of earth levees, the breach is generally not instantaneous, but it is not obvious that this assumption has great influence on

the impact in the floodplain, in particular on the flooded area at the end of the simulation. Also, this assumption is favourable from a safety point of view, because the water levels and velocities should be overestimated compared with a progressive breach assumption.

It is preferable to model the whole flood system including the river and the floodplain to its left and right, the dike, and the landward zone, which could be flooded in case of breach in the dike, in order to capture all the processes involved and their interaction.

8.11.4.1 Model coupling

Coupling can be achieved by four methods:

- linking breaching and flow software by external coupling through the upstream and downstream water elevations.
- linking breaching and flow software by an exchange protocol such as the OpenMI Association, allowing a dynamic interaction between the two models
- using flow software (generally solving the 2D shallow water equations) that treats the breach as a hydraulic structure evolving in time:
  - **Rubar 20** software (Paquier, 2009 and 2010), developed by Irstea (2013) that integrates the simplified breach model Rupro (the parameters of the hydraulic structures representing the breach are assigned *a priori*)
  - **Infoworks®RS** software, developed by Innovyse (2013) that includes HR BREACH developed by HR Wallingford.
- using a sediment transport model in which the embankment is treated as an ordinary bed area. Generally, this kind of model is based on 2D shallow water equations with additional equations to simulate bed load or suspended load. This kind of modelling allows assessment of the erosion and deposition processes downstream of the breach, which can influence the water elevation. Alternatively models including the sediment as a fluid phase can be used. Although they bring some advantages in terms of coupling various very unsteady processes, these models are not fully operational, or still need an empirical parametrisation and a sensitivity analysis when used in operational situations. A benchmark of some of this software was performed at a PIRE workshop in Belgium (Soares-Frazaoa, 2012), which allowed evaluation of the corresponding uncertainty for further spreading of sediment.

8.11.4.2 Multiple breaches

For operational purposes, it should be considered that flooding can be caused either by one or several breaches at the same time. A first step should be to select the scenarios corresponding to the aim of the study. If there are many possible scenarios, this step is not obvious and a simplified model can be used (such as CastorDigue developed by Irstea, 2013, or AREBA developed by HR Wallingford and University of Oxford) to evaluate which scenarios should be studied in a detailed way. This selection can be based on a comparison of the breach outflows. Alternatively, select the breaches that will start first.

8.11.4.3 Specific modelling of urban areas

Buildings and streets have a great impact on flood propagation in urban areas as they create preferential flow directions. Urban areas can be represented in various ways by inundation models. The three following approaches are the most common and are used in both consultancy and research applications:

1 **Raised ground:** the ground elevation in the footprint of the building is raised, to the real elevation of the top of the building or to a generic value, such that water never flows through the building footprint. This can be done as a direct use of a digital surface model (DSM) or by modifying the DTM elevations using the dataset of building polygons. However, using a DSM can be a challenge as it will also show the elevation of the top of the trees rather than the ground. This approach can cause stability problems in some models if computational cells straddle the edge of the building, as they will have very steep slopes.

2 **Increased friction:** here the individual buildings are not represented in the computational mesh, but the whole urban area is represented by an extremely high friction coefficient to account for the reduction in conveyance through the urban area (low Strickler coefficient or high Manning coefficient). However, this approach does not account for the reduction in storage in the urban area.

3 **Voids:** the building footprints are used to create holes or voids in the computational mesh. The effect is similar to the raised ground approach, but this avoids issues with steep slopes at the building edges. It also requires a flexible meshing technique (unstructured mesh usually).

Sanders *et al* (2008a) describe a comparison between the raised ground and voids approaches. The increased friction and voids approaches are compared in Soares-Frazao *et al* (2008).

The following approaches are also possible but are less common:

- **porosity:** some models use a modified version of the shallow water equation that includes a porosity coefficient. This porosity coefficient can be different in each cell, it can be isotropic or anisotropic (Guinot and Soares-Frazao, 2006, and Sanders *et al*, 2008b). It is usually constant with time and with the water depth. This approach means that buildings are not represented individually in the mesh, reducing the number of computational cells and the run-time. Both conveyance and storage reduction are represented correctly. Schubert and Sanders (2012) present a comparison of the three approaches previously mentioned, with the porosity approach.
- **sub-cell topography:** instead of having one average ground elevation, each computational element is assigned a range of ground levels that captures the topography inside the element (Hartnack *et al*, 2009, and Jamieson *et al*, 2012b). Both conveyance and storage reduction are represented correctly, and this approach is also useful outside of urban areas. This allows use of large computational elements while still capturing accurately the topography, reducing the run-times.
- **multi-layer:** in this approach complex building footprints are finely captured using simple polygons contained in multiple layers (Chen *et al*, 2012). This allows use of a coarse mesh while still accounting accurately for the buildings, hence reducing the run times.

8.11.5 Model outputs

Water depth, level and velocity are the variables calculated by all models. Time series of water depth and velocity are produced by the models and allow understanding and visualising the evolution of the flood. Maximum depth and maximum velocity are often used for the production of flood maps.

Hazard to people is usually considered to be related to the product of flow depth and velocity (Ramsbottom *et al*, 2004). This can be calculated by the inundation model at each time step and saved with the other outputs. It is more accurate to calculate the maximum hazard as the maximum in the hazard time series, rather than as the product of maximum velocity and maximum depth. This is because the timing of the peak depth and peak velocity can be completely different, and the product of the maximum values can greatly overestimate the maximum hazard. Hazard can then be considered alongside vulnerability to estimate the risk to people. Similarly, building failure can be estimated by the inundation model using flow depth and velocity, plus some parameters describing the resistance of the buildings.

The outputs from the inundation model can then be used as inputs to an evacuation model (for example, life safety model (LSM) from BC Hydro – Canada, and the Utah Water Research Laboratory model). Using a description of the population (eg age, location, transport mode, decisions) and the road network, the arrival of the flood wave triggers the evacuation of the population. The evacuation model routes people through the road network towards 'safe havens', and estimates the number of casualties from drowning, cars being washed away and building collapse. The LSM model has been applied to various study cases in Europe and North America and proved to give reasonable estimates of the number of casualties (Lumbroso *et al* 2010 and 2011). An example output from LSM is shown in Box 8.33.

8.11.6 Treatment of uncertainties

In order to develop the data required to understand probability of occurrence and uncertainty, techniques such as the Monte Carlo simulation are used. In a Monte Carlo simulation the variability of the various input parameters are represented and a large number of model runs are carried out with each input parameter sampled from its underlying distribution, so the data generated by the total set of model runs can be analysed probabilistically. In this way, the sensitivity of the overall outputs (such as inundation depth and timing) to specific parameters can also be evaluated, and the different components of risk can be assessed. A significant amount of effort has been undertaken recently to refine Monte Carlo simulation techniques to allow more complete and more complicated evaluation of input parameters. HEC-RAS (USACE, 2011) and similar hydraulic models provide deterministic results for specified input conditions, ie a single set of input (flow, channel conditions, breach formation parameters) is provided and the characteristics of flow are generated for that specified condition.

A Monte Carlo approach can also be incorporated in breach software. HR BREACH can give a distribution of likely outcomes (fail/not fail) and a range of shapes and peak values for the hydrograph in failure cases, depending upon the knowledge of the embankment properties and a given probability distribution for the input parameters.

Monte Carlo simulation can be applied not only to the hydrologic and hydraulic modelling, but throughout the flood assessment process wherever appropriate understanding of uncertainty is required. Froehlich (2008) presents a method to use Monte Carlo simulation to evaluate the effects of breach parameter uncertainty within an inundation analysis. Determination of the nature of the expected distribution, and possible spatial correlation of relevant input parameters, is an important consideration when conducting failure assessments. Levee fragility analysis incorporates Monte Carlo simulation of structural soundness as reflected in 'fragility curves'. Fragility curves display the probability of failure of a levee segment due to one or more mechanism over the full range of loads it is likely to experience. Curves can be developed based on analyses of specific locations, but general curves can also be developed based on generic levee type where more specific information is not available. Such an approach has been used for the UK National Flood Risk Assessment (NaFRA). Monte Carlo simulations for flood breach analysis would apply probabilities to each reach of levee, which would be converted into an elevation where failure will occur for that run. Unsteady floodwater level profiles would be input and breach locations for each run would be determined. The summation of output from a large number of runs would indicate which reaches of levee are most likely to breach under the chosen flood conditions.

Box 8.31 *Example of flood map from 2D finite element software*

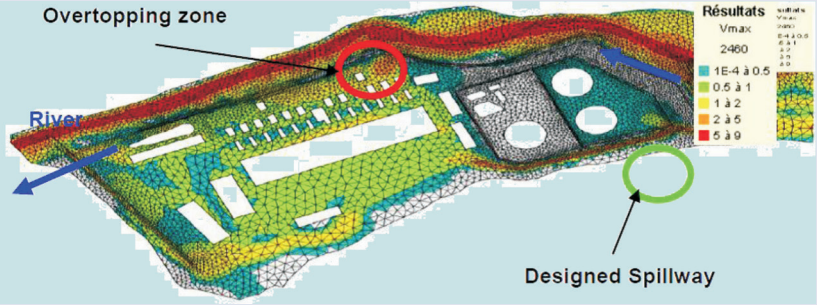

Figure 8.151 *Example of flood map showing maximum flow velocities due to levee overtopping calculated from 2D finite element software (Telemac) for which the computational mesh is shown (EGIS Eau for EDF PEI, 2009)*

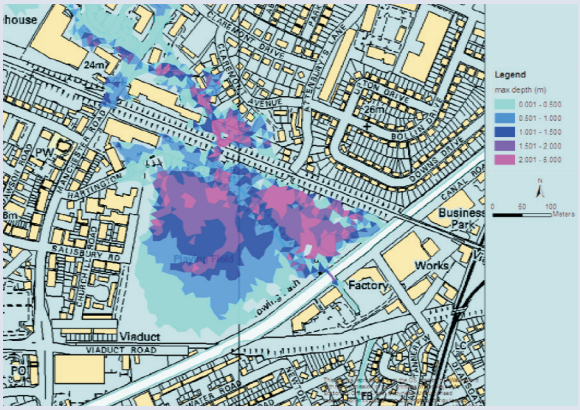

Figure 8.152 *Example of a map of maximum depth generated with InfoWorks®RS, showing the inundation resulting from a breach in a canal embankment (from Innovyze, 2013)*

Box 8.32 *Example of implementation of a 2D hydraulic modelling of the flood wave due to a breach in a dike*

In the case of an open source code, ie when the user can modify subroutines to model a breach, the instantaneous breach modelling is rather easy to do. The user has only to locate the nodes (in the case of a finite elements mesh) or the elements (in the case of a structured mesh) and to modify the field elevation when the breach occurs. Figure 8.153 illustrates the modelling of breach in a sea dike, before the breach, just after the breach, at the maximum level of the sea and at the end of the event.

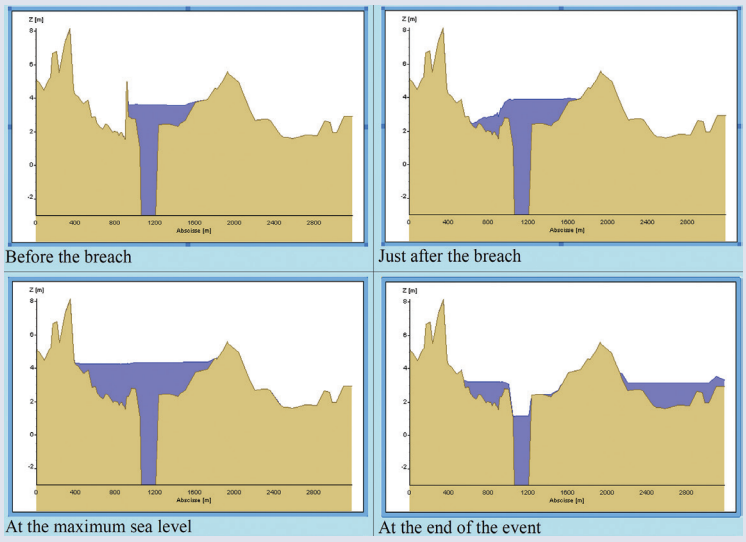

Figure 8.153 *Breach modelling in a sea dike with the 2D code Telemac*

Progressive breach modelling is also possible, but its utility has to be compared to the aims and precision needed. Use of such a model is more difficult to do than an instantaneous breach model and sometimes not justified. The following example has been developed by first calculating in the breach evolution using Rupro, developed by Irstea in France (this code is included in the simplified breach modelling code CastorDigue, Irstea, 2012), then by using this evolution in the hydraulic modelling code. Figure 8.154 presents the breach evolution calculated with the code Rupro.

Box 8.32 Example of implementation of a 2D hydraulic modelling of the flood wave due to a breach in a dike (contd)

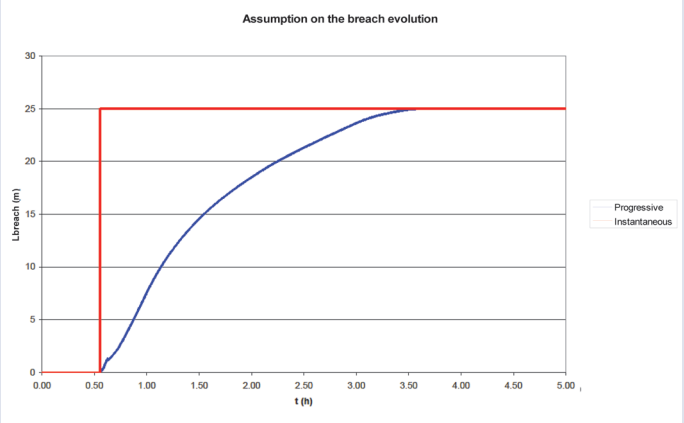

Figure 8.154 Assumption on the breach evolution

Figure 8.155 presents the calculated hydrograph at the breach in the case of a progressive breach evolution (calculated using Rupro) and in the case of an instantaneous breach.

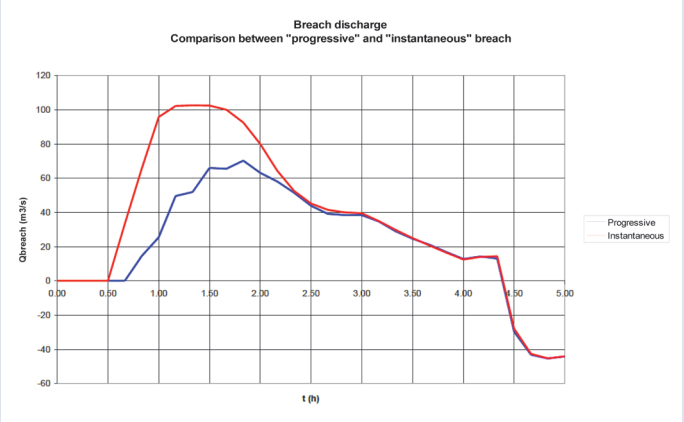

Figure 8.155 Breach discharge

In this example, the breach discharge with an instantaneous breach is higher than with a progressive breach, which is favourable from a safety point of view. The question is to know if this assumption is acceptable or not. By considering the hydraulic conditions downstream of the breach, especially the maximum water level or velocity, it can be noted that this assumption is conservative. Figures 8.156 and 8.157 present the maximum water level and the maximum velocity downstream of the breach.

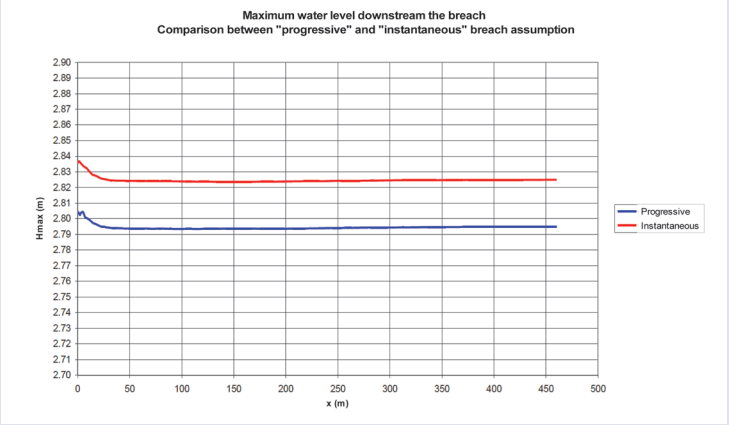

Figure 8.156 Maximum water level downstream the breach

Box 8.32 Example of implementation of a 2D hydraulic modelling of the flood wave due to a breach in a dike (contd)

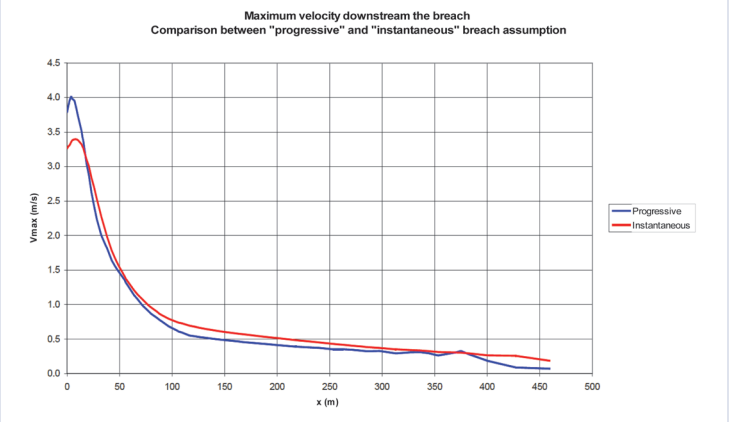

Figure 8.157 Maximum velocity downstream the breach

From these figures, it can be noted that the water level differs by a few centimetres and that the velocities are very close.

Other case studies available such as TMFlood Inundation modelling, River Durance – 2D flood wave Modellisation of St Jacques Levee in Cavaillon (France).

Box 8.33 Example of outputs from an evacuation model

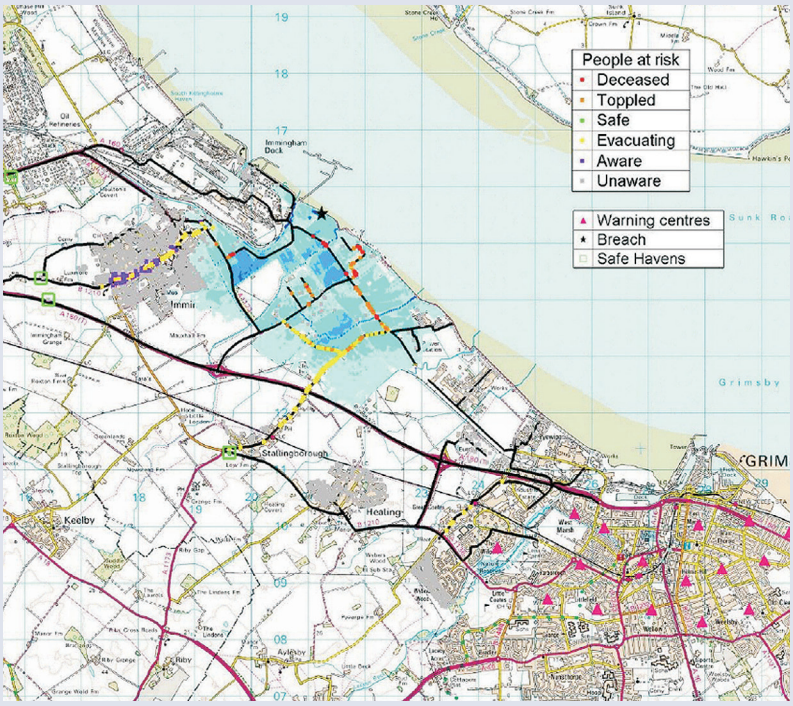

Figure 8.158 Output from the life safety model showing people evacuating the flooded area and travelling towards the safe havens

8.12 REFERENCES

AFNOR (1993) NF G 38-061: *Détermination des caractéristiques hydrauliques et mise en oeuvre des géotextiles et produits apparentés utilisés dans les systèmes de drainage et de filtration – Articles à usages industriels – recommandations pour l'emploi des géotextiles et produits apparentés*

AHRENS, J P (1981) *Irregular wave runup on smooth slopes*, CETA No. 81-17, US Army Corps of Engineers, Coastal Engineering Research CEnter, Fort Belvoir, VA, USA

ALLSOP, N W H (1990) "Reflections performance of rock armoured slopes in random waves". In: *Proc 22nd int conf on coastal engineering*, 2–6 July, Delft, ASCE, New York, pp 1460–1471

ALLSOP, N W H (2000) "Wave forces on vertical and composite wall". In: J B Herbich (ed), Chapter 4, *Handbook of coastal engineering*, McGraw-Hill, New York (ISBN: 0-07-134402-0), pp 4.1–4.47

ALLSOP, N W H and Channell, A R (1989) *"Wave reflections in harbours: reflection performance of rock armour slopes in random waves, Report OD 102*, HR Wallingford, Wallingford, UK

ALLSOP, N W H and VICINANZA, D (1996) "Wave impact loadings on vertical breakwaters: development of new prediction formulae". In: *Proc 11th int harbour congress, Antwerp, Belgium*, pp275–284

ALLSOP, N W H, VICINANZA, D and MCKENNA, J E (1996a) *Wave forces on vertical and composite breakwaters,* Research Report SR 443, HR Wallingford, Wallingford, UK

ALLSOP, N W H, MCKENNA, J E, VICINANZA, D and WHITTAKER, T J T (1996b) "New design formulae for wave loadings on vertical breakwaters and seawalls". In: *Proc 25th int conf on coastal engineering,* 2–6 September 1996, Orlando, Florida, USA

ALLSOP, N W H, KORTENHAUS, A, OUMERACI, H and MCCONNELL, K (1999) "New design methods for wave loadings on vertical breakwaters under pulsating and impact conditions". In: *Proc Coastal Structures '99: Proceedings of an international conference*, Santander, Spain, 7–10 June, 1999, I J Losada (ed), Taylor & Francis, UK, pp 592–602

ALLSOP, N W H, BRUCE, T, PEARSON, J and BESLEY P (2005) "Wave overtopping at vertical and steep seawalls". In: *Proc of the IC – Maritime Engineering*, vol 158, **3**, Institution of Civil Engineers, UK, pp 103–114

AMBRASEYS, N N and MENU, J M (1988) "Earthquake-induced ground displacements", *Earthquake Engineering & Structural Dynamics*, vol 16, **7**, John Wiley & Sons, UK, pp 985–1006

ANDREWS, D C A and MARTIN, D R (2000) "Criteria for liquefaction of silty soils". In: *Proc of the 12th world conf on earthquake engineering (12WCEE2000)*, Auckland, New Zealand, 30 January to 4 February 2000. Go to: **www.iitk.ac.in/nicee/wcee/article/0312.pdf**

APMANN, R P (1972) "Flow processes in open channel bends", *Journal of the Hydraulics Division*, vol 98, **5**, American Society of Civil Engineers (ASCE), New York, USA, pp 795–810

ANDRUS, R D and STOKOE, K H (2000) "Liquefaction resistance of soils from shear-wave velocity", Journal of *Geotechnical and Geoenvironmental Engineering*, vol 126, **11**, American Society of Civil Engineers (ASCE), New York, USA, pp 1015–1025

ARNESON, L A, ZEVENBERGEN, L W, LAGASSE, P F and CLOPPER, P E (2012) *Evaluating scour at bridge, fifth edition*, Publication No. FHWA-HIF-12-003, Hydraulic Engineering Circular No. 18, US Department of Trasportation, Federal Highway Administration, USA. Go to: **www.fhwa.dot.gov/engineering/hydraulics/pubs/hif12003.pdf**

ASCE (1966) "Nomenclature for bed forms in alluvial channel, report of the task force on bed forms in alluvial channels of the committee on sedimentation", *Journal of the Hydraulics Division*, vol 93, **2**, March/April 1967, American Society of Civil Engineers (ASCE), New York, USA, pp 72–77

ASHMORE, P and PARKER, G (1983) "Confluence scour in coarse braided streams" *Water Resources Research*, vol 19, **2**, Wiley Online, UK, pp 392–402

ASAOKA, A (1978) "Observational procedure of settlement prediction", *Soils and foundations*, vol 18, **4**, The Japanese Geotechnical Society, Japan, pp 87–101

BAKER, R and GARBER, M (1978) "Theoretical analysis of the stability of slopes" *Géotechnique*, vol 28, **4**, Institution of Civil Engineers, London, pp 395–411

BATES, P, HORRITT, M and FEWTRELL, T (2010) "A simple inertial formulation of the shallow water equations for efficient two-dimensional flood inundation modelling", *Journal of Hydrology*, vol 387, **1–2**, Elsevier BV, UK, pp 33–45

BATTJES, J A (1974) "Surf similarity". In: *Proc 14th coastal engineering conf*, Copenhagen, American Society of Civil Engineers (ASCE), New York, USA, pp 466–479

BEGUIN, R (2011) *Etude multi-échelle de l'érosion de contact au sein des ouvrages hydrauliques en terre*, PhD Thesis, University of Grenoble, France

BEGUIN, R, PHILIPPE, P and FAURE, Y-H (2013) "Pore-scale flow measurements at an interface between a sandy layer and a model porous medium: Application to statistical modeling of contact erosion", *Journal of Hydraulic Engineering*, vol 139, **1**, American Society of Civil Engineers (ASCE), New York, USA, pp 1–11

BELL, J M (1966) "Dimensionless parameters for homogeneous earth slopes", *Journal of the Soil Mechanics and Foundations Division*, vol 92, **5**, American Society of Civil Engineers (ASCE), New York, USA, pp 51–66

BENAHMED, N and BONELLI, S (2012) "Investigating concentrated leak erosion behavior of cohesive soils by performing hole erosion tests", *European Journal of Environmental and Civil Engineering*, vol 16, **1**, pp 43–58

BEZUIJEN, A, KLEIN BRETELER, M, and BAKKER, K J (1987) "Design criteria for placed block revetments and granular filters". In: *Proc 2nd COPEDEC*, China Ocean Press, vol 2, pp 1852–1866

BISCH, P, CARVALHO, E, DEGEE, H, FA JFAR, P, FARDIS, M, FRANCHIN, P, KRESLIN, M, PECKER, A, PINTO, P, PLUMIER, A, SOMJA, H and TSIONIS, G (2011) *Eurocode 8: Seismic design of buildings. Worked example*, JRC Scientific and Technical Reports, Lisbon

BISHOP, A W (1955) "The use of the slip circle in the stability analysis of slopes", *Géotechnique*, London, vol 5, **1**, Institution of Civil Engineers, London, pp 7–17

BLACKMORE, P A and HEWSON, P (1984) "Experiments on full scale impact pressures", *Coastal Engineering*, vol 8, **4**, Elsevier BV, pp 331–346

BLIGH, W G (1927) T*he practical design of irrigation works*, Van Nostrand Co., New York

BLR (1970) "Soil's hydraulic". In: *Bulletin of Roads Laboratories – Special N, Proceedings of soil's hydraulic journeys, 27–29 November 1968*, LCPC. Go to: www.lcpc.fr/english/information-sources

BONELLI, S (ed) (2012) *Erosion of geomaterials*, Irstea (French Environmental Sciences and Technologies Research Institute), France (ISBN: 978-1-84821-351-7)

BONELLI, S and BENAHMED, N (2011) "Piping flow erosion in water retaining structures", *International Journal of Hydropower and Dams*, vol 18, **3**, pp 94–98

BONELLI, S and BRIVOIS, O (2008) "The scaling law in the hole erosion test with a constant pressure drop", *International Journal for Numerical and Analytical Methods in Geomechanics*, vol 32, **13**, John Wiley & Sons, UK, pp 1573–1595

BONELLI, S, BRIVOIS, O, BORGHI, R and BENAHMED, N (2006) "On the modelling of piping erosion", *Comptes rendus de Mécanique*, vol 334, **8–9**, Elsevier Masson SAS, Cedex, France

BONELLI, S, COURIVAUD, J-R, DUCHESNE, L, FRY, J-J and ROYET, P (2012) "Internal erosion on dams and dikes: lessons from experience and modelling". In: *Proc 24th ICOLD Congress,* Kyoto, Japan, 6–8 June 2012, International Commission on Large Dams, Japan

BOULANGER, R W and IDRISS, I M (2004) *Evaluating the potential for liquefaction or cyclic failure of silts and clays*, Report No UCD/CGM-04/01, Department of Civil and Environmental Engineering, University of California at Davis, USA

BOULANGER, R W and IDRISS, I M (2006) "Liquefaction susceptibility criteria for silts and clays", *Journal of Geotechnical and Geoenvironmental Engineering,* vol 132, **11**, American Society of Civil Engineers (ASCE), New York, USA, pp 1413–1426

BOWLES, J E (1977) *Foundation analysis and design*, second edition, McGraw-Hill, New York (ISBN: 978-0-07118-844-9)

BRANDON, T L, WRIGHT, S G and DUNCAN, J M (2008) "Analysis of the stability of I-walls with gaps between the I-wall and the levee fill", *Journal of Geotechnical and Geoenvironmental Engineering*, vol 134, **5**, Special issue: Performance of Geo-Systems during Hurricane Katrina, American Society of Civil Engineers (ASCE), New York, USA, pp 692–700

BRAUNS, J (1985) "Erosionsverhalten geschichteten Bodens bei horizontaler", Durchstromung, *Wasserwirtschaft 75*, pp 448–453

BRAY, J D (2007) "Simplified seismic slope displacement procedures", Chapter 14, K D Pitilakis (ed) *Earthquake geotechnical engineering. 4th International Conference on Earthquake Geotechnical Engineering-Invited Lectures, Geotechnical, Geological and Earthquake Engineering series*, vol 6 (ISBN: 978-1-4020-5893-6), Springer, UK, pp 327–353

BRAY, J D and TRAVARASOU, T (2007) "Simplified procedure for estimating earthquake-induced deviatoric slope displacement", *Journal of Geotechical and Geoenvironmental Engineering*, vol 133, **4**, American Society of Civil Engineers (ASCE), New York, USA, pp 1165–1177

BRIAUD, J-L, TING, F, CHEN, H C, CAO, Y, HAN, S-W and KWA,K K (2001) "Erosion function apparatus for scour rate predictions", *Journal of Geotechnical and Geoenvironmental Engineering*, vol 127, **2**, American Society of Civil Engineers (ASCE), New York, USA, pp 105–113

BURENKOVA, V V (1993) "Assessment of suffosion in non-cohesive and graded soils". In: *Proc 1st int conf on "geo-filters",* Karlsruhe, Germany, 20–22 October 1992, J Brauns and U Schuler (eds) *Filters in geotechnical and hydraulic engineering*, A A Balkema, Rotterdam (ISBN: 978-9-05410-342-4), pp 357–360

BROWN, S A and CLYDE, E S (1989) *Design of riprap revetment,* Report No. FHWA-IP-89-016-HEC-11, Federal Highway Administration, McLean, VA, USA

CAMFIELD, F E (1991) "Wave forces on wall", *Journal of Waterway, Port, Coastal and Ocean Engineering*, vol 117, **1**, American Society of Civil Engineers (ASCE), New York, USA, pp 76–79

CARTER, R K (1971) *Computer oriented slope stability analysis by method of slices*, MSCE Thesis, Purdue University, West Lafayette, Indiana, USA

CAVOUNIDIS, S (1987) "On the ratio of factors of safety in slope stability analysis", *Géotechnique*, vol 37, **2**, Institution of Civil Engineers, London, pp 207–210

CERC (1984) *Shore protection manual*, US Army Corps of Engineers, Washington DC, USA

CFBR (2010) *Earthen dams and levees stability justification – Recommendations guideline*, French Comity for Dams and Reservoirs, France

CHANG, H H (1988) *Fluvial processes in river engineering*, revised edition, Krieger Publishing Company, USA (ISBN: 978-1-57524-302-3)

CHEN, Z Y (2007) "The limit analysis in soil and rock: a mature discipline of geomechanics", *Journal of Zhejiang University*, Science A, vol 8, **11**, China

CHEN, Y H and ANDERSON, B A (1986) *Development of a methodology for estimating embankment damage due to flood overtopping*, FHWA/RD-86/126, Federal Highway Administration, US Department of Transport, USA. Go to: **http://isddc.dot.gov/OLPFiles/FHWA/009466.pdf**

CHEN, Z and MORGENSTERN, N R (1983) "Extension to the generalized method of slices for stability analysis", *Canadian Geotechnical Journal*, vol 20, **1**, Canadian Science Publishing, Canada, pp 104–109

CHEN, A S, EVANS, B, DJORDJEVIĆ, S and SAVIĆ, D A (2012) "Multi-layered coarse grid modelling in 2D urban flood simulations", *Journal of Hydrology*, vol 470–471, Elsevier BV, UK, pp 1–11

CHING, R K H and FREDLUND, D G (1983) "Some difficulties associated with the limit equilibrium method of slices", *Canadian Geotechnical Journal*, vol 20, **4**, Canadian Science Publishing, Canada, pp 661–672

CHOW, V T (1959) *Open channel hydraulics*, The Blackburn Press, New York (ISBN: 978-1-93284-618-8)

CHUGAEV, R R (1971) "Seepage through dams". In: V T Chow (ed), *Advances in Hydroscience*, vol 7, 1971, Academic Press, New York, USA, pp 283–325

COLEMAN, S E (1991) *The mechanics of alluvial stream bed forms*, PhD thesis, Department of Civil Engineering, University of Auckland, Auckland, New Zealand.

COLEMAN, S E and MELVILLE, B W (1994) "Bed-form development", *Journal of Hydraulic Engineering*, vol 120, **5**, American Society of Civil Engineers (ASCE), New York, USA, pp 544–560

COLORADO DEPARTMENT OF TRANSPORTATION (2004) *Drainage design manual,* CDOT, Denver, Colorado, USA. Go to: **www.dot.state.co.us/DesignSupport/Drainage Design Manual**

CORREIA, R M (1988) "A limit equilibrium method for slope stability". In: *Proc 5th ISL Switzerland*, vol 1, pp 595–598

CROSS, R H (1967) "Tsunami surge forces", *Journal of Waterways and Harbors Division,* vol 93, **WW4**, American Society of Civil Engineers (ASCE), New York, USA, pp 201–231

CUOMO, G, ALLSOP, N W H and TAKAHASHI, S (2010a) "Scaling wave impact pressures on vertical walls", *Coastal Engineering*, vol 57, **6**, Elsevier BV, UK, pp 604–609

CUOMO, G, ALLSOP, N W H, BRUCE, T and PEARSON, J (2010b) "Breaking wave loads at vertical sea walls and breakwaters", *Coastal Engineering*, vol 57, **4**, Elsevier BV, UK, pp 424–439

CUOMO, G, PISCOPIA, R and ALLSOP, N W H (2011) "Evaluation of wave impact loads on caisson breakwaters based on joint probability of impact maxima and rise times", *Coastal Engineering*, vol 58, **1**, Elsevier BV, UK, pp 9–27

CIRIA; CUR; CETMEF (2007) *The Rock Manual. The use of rock in hydraulic engineering (2nd edition),* C683, CIRIA, London (ISBN: 978-0-86017-683-1). Go to: **www.ciria.org**

DAWKINS, W P (1991) *User's guide: computer program for design and analysis of sheet-pile walls by classical methods (CWALSHT) including Rowe's moment reduction*, Instruction Report ITL-91-1, Information Technology Laboratory (ITL), Department of the Army, US Army Corps of Engineers (USACE), Mississippi, USA. Go to: **www.dtic.mil/dtic/tr/fulltext/u2/a243811.pdf**

DEGOUTTE, G (2012) *Les déversoirs sur les digues fluviales (Spillways on river flood protection levees)*, QUAE Editions, France (ISBN: 978-2-7592-1885-1)

DELINGER, R P and IVERSON, R M (1990) "Limiting equilibrium and liquefaction potential in infinite submarine slopes", *Marine Geotechnology*, vol 9, 4, Taylor & Francis, UK, pp 299–312

DE LOOFF, A K, HART, R T, MONTAUBAN, K C and VAN DE VEN, M F C (2006) "GOLFKLAP, a model to determine the impact of waves on dike structures with an asphalt concrete layer". In: *Proc 30th int conf on coastal engineering*, San Diego, USA, vol 4, pp 241–263

DE LOOFF, A K, VAN DE VEN, M F C and HART, R T (2011) "Resistance of aged asphalt concrete to wave attack". In: *Proc 6th int conf Coastal Structures 2011*, 5–9 September, Yokohama, Japan, Takahashi, S, Isobe, M, Kobayashi, N, Shimosako, K-I (eds) *Coastal structures 2011*, World Scientific Publishing Company, Tokyo, Japan (ISBN: 978-9-81441-220-9)

DE VROEG, J H, KRUSE, G A M and VAN GENT, M R A (2002) *Processes relating to breaching of dikes,* DC030202/H3803, Delft, the Netherlands

DE WAAL, J P and VAN DER MEER, J (1992) "Wave run-up and overtopping on coastal structures". In: *Proc 23rd conf on coastal engineering, Venice, Italy*, vol 23, American Society of Civil Engineers (ASCE), New York, USA, pp 1758–1771

DRONIUC, N and MAGNAN, J-P (2002) "About the assessment of the angle of shearing resistance for shallow foundation design". In: *Int symp on identification and determination of soil and rock parameters for geotechnical design; PARAM 2002*, 2–3 September 2002, LCPC, Paris, France (ISBN: 2-72086-003-4), pp 531–540

DUNCAN, J M (1996) "State of the art: limit equilibrium and finite-element analysis of slopes", *Journal of Geotechnical Engineering*, vol 122, **7**, American Society of Civil Engineers (ASCE), New York, USA, pp 577–596

DUNCAN, J M, BRANDON, T L, WRIGHT, S G and VROMAN, N (2008) "Stability of I-walls in New Orleans during Hurricane Katrina", *Journal of Geotechnical and Geoenvironmental Engineering*, vol 134, **5**, Special issue: Performance of Geo-Systems during Hurricane Katrina, American Society of Civil Engineers (ASCE), New York, USA, pp 681–691

ESCARAMEIA, M and MAY, R W (1992) *Channel protection: turbulence downstream of structures*, Report SR 313, HR Wallingford, Wallingford, UK

FANNIN, R J and LI, M (2006) "Comparison of two criteria for internal stability on granular soil"*Canadian Geotechnical Journal,* vol 45, **9**, Canadian Science Publishing, Canada, pp 1303–1309

FAURE, R M (1985) "Analyse des contraintes dans un talus par la method des perturbations", *Revue Française de Géotechnique*, vol 33, Comité Français de Mécanique des Roches (CFMR), INSA – Université de Lyon, France, pp 49–59

FELLENIUS, W (1936) "Calculations of the stability of earth dams", *Transactions of the 2nd congress on large dams*, Washington DC, USA, vol 4, pp 445–465

FINN, W D L (1999) "Evolution of dynamic analysis in geotechnical earthquake engineering". In: *Proc of the TRB workshop on new approaches to liquefaction analysis*, 10 January 1999, Washington DC, USA

FOSTER, M and FELL, R (2001) "Assessing embankment dam filters that do not satisfy design criteria", *Journal of Geotechnical and Geoenvironmental Engineering*, vol 127, **5**, American Society of Civil Engineers (ASCE), New York, USA, pp 398–407

FREDLUND, D G and KRAHN, J (1977) "Comparison of slope stability methods of analysis", *Canadian Geotechnical Journal,* vol 14, **3**, Canadian Science Publishing, Canada, pp 429–439

FROEHLICH, D C (1995a) "Peak outflow from breached embankment dam" *Journal of Water Resources Planning and Management*, vol 121, 1, American Society of Civil Engineers (ASCE), New York, USA, pp 90–97

FROEHLICH, D C (1995b) "Embankment dam breach parameters revisited". In: Proc *1st int conf on water resources engineering*, 14–18 August 1995, San Antonio, Texas, US, American Society of Civil Engineers (ASCE), New York, USA, pp 887–891

FROEHLICH, D C (2008) "Embankment dam breach parameters and their uncertainties", *Journal of Hydraulic Engineering*, vol 134, **12**, American Society of Civil Engineers (ASCE), New York, USA, pp 1708–1721

GALAY, V J, YAREMKO, E K and QUAZI, M E (1987) "River bed scour and construction of stone riprap protection". In: C R Thorne, J C Bathurst and R D Hey (eds) *Sediment transport in gravel-bed rivers*, John Wiley & Sons, New York, USA (ISBN; 978-0-47190-914-9)

GAULLIER, M and PINEY, S (2011) *Etude de dangers des digues de classe. A de la Loirse moyenne*, DREAL Cenrre, Journees techniques Polytech 'Oreleans, France

GHIASSIAN, H and GHAREH, S (2008) "Stability of sandy slopes under seepage conditions", *Landslides*, vol 5, **4**, Journal of the International Consortium on Landslides, Springer, UK, pp397–406

GIROUD, J-P (1973) *Charts for foundations design*, Tome II, Dunod, Paris

GIROUD, J-P (1982) *Filter criteria for geotextiles, proceedings of the second international conference on geotextiles"*, vol 1, Las Vegas, Nevada, USA, August 1982, pp 103–108

GIROUD, J-P (1988) "Review of geotextile filter criteria". In: *Proc first Indian geotextiles conference*, Bombay, India, 8–9 December 1988, Indian Institute of Technology, Bombay, International Geotextile Society, International Society of Soil Mechanics and Foundation Engineering

GIROUD, J-P (2003) "Filter criteria", Jubilee Volume, 75th anniversary of K. Terzaghi's "Soil mechanics", H Brandl (ed), *Reports of the institute for soil mechanics and Geotechnical Engineering*, Technical University of Vienna, Austria

GODA, Y (1971) "Expected rate of irregular wave overtopping of seawalls", *Coastal engineering in Japan*, vol 14, JSCE, Tokyo, pp 45–51

GODA, Y (1974) "New wave pressure formulae for composite breakwaters". In: *Proc 14th int conf on coastal engineering*, 24–28 June, Copenhagen, Denmark, ASCE, New York, pp 1702–1720

GODA, Y (1985) "Random seas and maritime structures, third edition", *Advanced Series on Ocean Engineering*, vol 33, World Scientific Publishing Company, Tokyo, Japan (ISBN: 978-9-81428-240-6)

GRAHAM, D S (1983) "Review of status of knowledge on scour in constrained rivers". In: *Proc workshop on bridge hydraulics*, Banff School of Fine Arts, Alberta, Canada, pp 1–22

GRIFFITHS, D V and KIDGER, D J (1995) "Enhanced visualization of failure mechanisms by finite elements", *Computers and Structures*, 55, **2**, Elsevier BV, UK, pp 265–268

GUIDOUX, C, FAURE, Y H, BEGUIN, R and HO, C (2010) "Contact erosion at the interface between granular coarse soil and various base soils under tangential flow condition", *Journal of Geotechnical and Geoenvironmental Engineering*, vol 136, **5**, American Society of Civil Engineers (ASCE), New York, USA, pp 741–750

GUINOT, V and SOARES–FRAZAO, S (2006) "Flux and source term calculation in two-dimensional shallow-water models with porosity on unstructured grids", *International Journal of Numerical Methods in Fluids*, vol 50, **3**, John Wiley & Sons, UK, pp 309–345

HAGER, W H (1987) "Lateral outflow over side weirs", *Journal of Hydraulic Engineering*, vol 113, **4**, American Society of Civil Engineers (ASCE), New York, USA, pp 491–504

HAHN, W, HANSON, G J and COOK, K R (2000) "Breach Morphology observations of embankment overtopping tests", *Building Partnerships: transactions of the American Society of Civil Engineers (ASCE)*, New York, USA, pp 1–10

HANSON, G J (1989) "Channel erosion study of two compacted soils", *Transactions of ASAE*, vol 32, **2**, American Society of Agricultural and Biological Engineers, St. Joseph, Michigan, USA, pp 485–490

HANSON, G J (1992) "Erosion resistance of compacted soils", Transportation Research Record No. 1369, *Advance in geotechnical engineering*, Transportation Research Board, USA (ISBN: 0-30905-410-9)

HANSON, G J and TEMPLE, D M (2002) "Performance of bare-earth and vegetated steep channels under long duration flows", *Transactions of ASAE*, vol 45, **3**, American Society of Agricultural and Biological Engineers, St. Joseph, Michigan, USA, pp 695–701

HANSON, G J and HUNT, S L (2006) "Lessons learned using laboratory jet test method to measure soil erodibility of compacted soils". In: *Proc theASABE Annual International Meeting*, 9–12 July 2006, Portland, Oregon, USA

HANSON, G J and SIMON, A (2001) "Erodibility of cohesive streambeds in the loess area of the midwestern United States", *Hydrological Processes*, vol 15, **1**, Taylor & Francis, UK, pp 23–38

HANSON, G J, ROBINSON, K M and COOK, K R (1997) "Headcut migration analysis of a compacted soil", *Transactions of ASAE*, vol 40, **2**, American Society of Agricultural and Biological Engineers, St. Joseph, Michigan, pp 355–361

HANSON, G J, COOK, K R and HUNT, S L (2005a) "Physical modeling of overtopping erosion and breach formation of cohesive embankments", *Transactions of the ASAE*, vol 48, **5**, American Society of Agricultural and Biological Engineers, St. Joseph, Michigan, USA, pp 1783–1794

HANSON, G J, TEMPLE, D M, MORRIS, M W and HASSAN, M A A M (2005b) "Simplified breach analysis model for homogeneous embankments: Part II, Parameter inputs and variable scale model comparisons", In: *Proc of the 2005 US Society on Dams (USSD) annual meeting and conference*, 6–10 June 2005, Salt Lake City, Utah, USA

HANSON, G J, TEJRAL, R D, HUNT, S L and TEMPLE, D M (2010) "Internal erosion and impact of erosion resistance" In: *Proc of the 30th US Society on Dams annual meeting and conference*, 12–16 April 2010, Sacramento, California, pp 773–784

HENDERSON, F M (1966) *Open channel flow*, Macmillan Series in Ocean Engineering, Prentice Hall, New York, USA (ISBN: 978-0-02353-510-9)

HENKEL, D J (1959) "The relationships between the strength, pore-water pressure, and volume-change characteristics of saturated clays", *Géotechnique*, vol 9, **3**, Institution of Civil Engineers, London, pp 119–135

HEWLETT, H W M, BOORMAN, L A and BRAMLEY, M E (1987) *Design of reinforced grass waterways*, R116, CIRIA, London (ISBN: 978-0-86017-285-7). Go to: **www.ciria.org**

HEY, R D, BATHURST, J C and THORNE, C R (1982) *Gravel-bed rivers: fluvial processes, engineering, and management*, John Wiley & Sons Inc, New York, USA (ISBN: 978-0-47110-139-0)

HOFFMANS, G J C M and VERHEIJ, H J (1997) *Scour manual,* A A Balkema, Rotterdam, the Netherlands (ISBN: 978-9-05410-673-9)

HOLMAN, R A and SALLENGER, A H (1985) "Set-up and swash on a natural beach", *Journal of Geophysical Research: Oceans*, vol 90, **C1**, American Geophysical Union, USA, pp 945–953

HR WALLINGFORD (2008a) *Understanding the lowering of beaches in front of coastal defence structures*, Stage 2 Technical Note 3, Defra/EA R&D Project Record FD1927/PR3, Department for the Environment, Food and Rural Affairs, London.
Go to: **http://sciencesearch.defra.gov.uk/Document.aspx?Document=FD1927_7463_PR.pdf**

HR WALLINGFORD (2008b) *Understanding the lowering of beaches in front of coastal defence structures*, Stage 2 Technical Note 9. Defra/EA R&D Project Record FD1927/PR9, Department for the Environment, Food and Rural Affairs, London.
Go to: **http://sciencesearch.defra.gov.uk/Document.aspx?Document=FD1927_7469_PR.pdf**

HR WALLINGFORD (2008c) *Understanding the lowering of beaches in front of coastal defence structures*, Stage 2 Technical Note 5, Defra/EA R&D Project Record FD1927/PR5, Department for the Environment, Food and Rural Affairs, London.
Go to: **http://sciencesearch.defra.gov.uk/Document.aspx?Document=FD1927_7465_PR.pdf**

HUGHES, S A (1992) "Estimating wave-induced bottom velocities at vertical wall", *Journal of Waterway, Port, Coastal and Ocean Engineering*, vol 118, **2**, ASCE, USA, pp 175–192

HUGHES, S A (2008) *Combined wave and surge overtopping of levees: flow hydrodynamicsand articulated concrete mat stability*, ERDC/CHL TR-08-10, U.S. Army Engineer Research and Development Center, USACE, Vicksburg, Mississippi, USA

HUGHES, S. A and FOWLER, J E (1991) "Wave-induced scour prediction at vertical walls". In: *Proc A specialty conference on quantitative approaches to coastal sediment processes*, 25–27 June 1991, Seattle, Washington, USA. Kraus, N C, Gingerich, K J, Kriebel, D L (eds) *Coastal sediments '91*, ASCE, vol 2, pp 1886–1900

HUGHES, S A and NADAL, N C (2008) "Laboratory study of combined wave overtopping and storm surge overflow of a levee", *Coastal Engineering*, vol 56, **3**, US Army Engineer Research and Development Center, USACE, Vicksburg, Mississippi, USA, pp 244–259

HUNGR, O, DALGADO, F M and BYRNE, P M (1989) "Evaluation of a three dimensional method of slope stability analysis", *Canadian Geotechnical Journal*, vol 26, **4**, Canadian Science Publishing, Canada, pp 679–686

HUNT, J A (1959) "Design of seawall and breakwaters", *Journal of Waterway, Port, Coast and Ocean Engineering*, vol 85, American Society of Civil Engineers (ASCE), New York, USA, pp 123–152

HUTCHINSON, D L (1972) *Physics of erosion of cohesive soils*, vol 30, School of Engineering, University of Aukland, New Zealand

ICE (1984) *Flexible armoured revetments incorporating geotextiles. Proceedings of the international conference organised by the Institution of Civil Engineers and held in London on 29–30 March 1984*, Thomas Telford, London (ISBN: 978-0-72770-226-5)

ICOLD (2010) *Selecting seismic parameters for large dams – guidelines*, Bulletin 72 (1989), Revised Bulletin 148, International Commission on Large Dams (ICOLD), Paris, France. Go to: **www.icold-cigb.net**/

IDRISS, I M (1999) "An update of the Seed-Idriss simplified procedure for evaluating liquefaction potential" In: *Proc of the workshop on new approaches to liquefaction analysis*, 10 January 1999, Washington DC, USA

IKEDA, S (1984) "Prediction of alternate bar wavelength and height", *Journal of Hydraulic Engineering*, vol 110, **4**, American Society of Civil Engineers (ASCE), New York, USA, pp 371–386

INDIAN ROADS CONGRESS (1966) *Standard specifications and code of practice for bridges*, University of Michigan, USA. Go to: **http://glbajajgroup.org/downloads/ce-IRC&ISCODES-01.pdf**

INNOVYZE (2013) *InfoWorks®RS*. Go to: **www.innovyze.com/products/infoworks_rs/**

IRSTEA (2012) *CASTORDIGUE: CAlcul Simplifié pour le Traitement des Ondes de Rupture de digue*, Irstea, France. Go to: **www.irstea.fr/castordigue**

IRSTEA (2013) *Rubar 20*, Irstea, France. Go to: **www.irstea.fr/rubar20**

ISHIHARA, K and YAMAZAKI, A (1984) "Wave-induced liquefaction in sea-bed deposits of sand", *Seabed Mechanics*, Proc of a symposium, sponsored jointly by the International Union of Theoretical and Applied Mechanics (IUTAM) and the International Union of Geodesy and Geophysics (IUGG), and held at the University of Newcastle upon Tyne, 5–9 September, 1983

ISHIHARA, K and MITSUTOSHI, Y (1992) "Evaluation of settlements in sand deposits following liquefaction during earthquakes", *Soils and Foundations*, vol 32, **1**, The Japanese Geotechnical Society, Japan, pp 173–188

ITO, Y (1971) "Stability of mixed type breakwater – a method of probable sliding distance", *Coastal engineering in Japan*, vol 14, JSCE, Tokyo, pp 53–61

IZBASH, S V and KHALDRE, KY (1970) *Hydraulics of river channel closure*, Butterworths, London

JAMIESON, S R, WRIGHT, G, LHOMME, J and GOULDBY, B (2012a) "Validation of a computationally efficient 2D inundation model on multiple scales". In: *Proc of the int conf on floodrisk*, 20–22 November, Rotterdam, the Netherlands

JAMIESON, S R, LHOMME, J, WRIGHT, G and GOULDBY, B (2012b) "A highly efficient 2D flood model with sub-element topography", *Proceedings of the ICE – Water Management*, vol 165, 10, Institution of Civil Engineers, UK, pp 581–595

JANBU, N (1973) "Slope stability computations", *Embankment dam engineering*, *Casagrande volume,* R C Hirschfeld and S J Poulos (eds) John Wiley and Sons, New York, USA (ISBN: 978-0-47140-050-9)

JIANG, G L and MAGNAN, J P (1997) "Stability analysis of embankments: comparison of limit analysis with methods of slices", *Géotechnique*, vol 47, **4**, Institution of Civil Engineers, London, pp 857–872

JIANG, J C, BAKER, R and YAMAGAMI, T (2003) "The effect of strength envelope nonlinearity on slope stability computations", *Canadian Geotechnical Journal*, vol 40, Canadian Science Publishing, Canada, pp 308–325

JIBSON, R W and KEEFER, D K, (1993) *Analysis of the seismic origin of landslides: examples from the New Madrid seismic zone*, Bulletin 105, Geological Society of America, USA, pp 521–536

JOSSEAUME, H (1970) "Earthen levees", *Hydraulic of soils*. Bulletin des laboratoires Routiers, Numero spécial, April 1970

JULIEN, P Y and KLAASSEN, G J (1995) "Sand-dune geometry of large rivers during floods", *Journal of Hydraulic Engineering*, vol 121, **9**, American Society of Civil Engineers (ASCE), New York, USA, pp 657–663

KENNEY, T C and LAU, D (1985) "Internal stability of granular filters", *Canadian Geotechnical Journal*, vol 22, **2**, Canadian Science Publishing, Canada, pp 215–225

KEZDI, A (1979) *Soil physics – selected topics*, Elsevier Scientific Publishing Company, Amsterdam (ISBN: 978-0-44499-790-6)

KIRKGOZ, M S (1995) "Breaking wave impact on vertical and sloping coastal structures", *Ocean Engineering*, vol 22, **1**, Elsevier BV, UK, pp 35–48

KLEIN BRETELER, M and BEZUIJEN, A (1991) "Simplified design method for block revetments". In: *Coastal structures and breakwaters: proceedings of the conference organis+ed by the Institution of Civil Engineers, and held in London on 6–8 November 1991*, Institution of Civil Engineers (eds), Thomas Telford, UK (ISBN: 978-0-72771-672-9)

KLEIN BRETELER, M, PILARCZYK, K W and STOUTJESDIJK, T (1998) "Design of alternative revetments". In: *Proc Coastal Engineering 1998 conf*, 22–26 June 1998, Copenhagen, Denmark, B L Edge (ed), *Section: Part III: Coastal Structures*, American Society of Civil Engineers (ASCE), New York, USA, pp1587–1600

KRAMER, S L (1996) Geotechnical Earthquake, Prentice Hall, (ISBN: 978-0-13374-943-4)

KRAMER, S L and ELGAMAL, A W (2001) *Modelisation soil liquefactioon hazards for performance-based earthquake engineering*, PEER-2001/13, Pacific Earthquake Engineering Research Center, University of California, Berkeley, 2001-02. Go to: **http://peer.berkeley.edu/publications/peer_reports/reports_2001/0113.pdf**

KRAMER, S L and SMITH, M W (1997) "Modified Newmark model for seismic displacements of compliant slopes", *Journal of Geotechical and Geoenvironmental Engineering*, vol 123, **7**, American Society of Civil Engineers (ASCE), New York, USA, pp 635–644

LACEY, G (1930) "Stable channels in alluvium", *Minutes of the proceedings*, vol 229, 1930, 1 January 1930, Institution of Civil Engineers, UK pp 259–292

LAMBE, T W (1964) "Methods of estimating settlement", *Soil Mechanics, and Foundation Engineering*, vol 90, American Society of Civil Engineers (ASCE), New York, USA, pp 47–71

LANE, E W (1935) "Security from underseepage: masonary dams on earth foundation", *Transactions of the American Society of Civil Engineers*, vol 100, **1**, American Society of Civil Engineers (ASCE), New York, USA, pp 1235–1272

LANE, E W, BROWN, C, GIBSON, G C, HOWARD, C S, KRUMBEIN, W C, MATTHES, G H, RUBEY, W W, TROWBRIDGE, A C and STRAUB, L G (1947) "Report of the sub-committee on sediment terminology of the stream dynamics committee of the American Geophysical Union", vol 28, **6**, American Geophysical Union, USA

LARSON, M, CAPOBIANCO, M, JANSEN, H, ROZYNSKI, G, SOUTHGATE, H N, STIVE, M, WIJNBERG, K M and HULSCHER, S (2003) "Analysis and modelling of field data on coastal morphological evolution over yearly and decadal time scales. Part 1: Background and linear techniques", *Journal of Coastal Research*, vol 19, **4**, Coastal Education & Research Foundation (CERF), USA, pp 760–775

LI, M (2008) *Seepage induced instability in widely graded soils*, PhD Thesis, University of British Columbia, Vancouver, Canada

LI, M and FANNIN, R J (2008) "A comparison of two criteria for internal stability of granular soils", *Canadian Geotechnical Journal*, 45, **9**, Canadian Science Publishing, Canada, pp 1303–1309

LI, Y-C, CHEN, Y-M, ZHAN, T L T, LING, D-S and CLEALL, P J (2010) "An efficient approach for locating the critical slip surface in slope stability analyses using a real-coded genetic algorithm", *Canadian Geotechnical Journal*, 47, **7**, Canadian Science Publishing, Canada, pp 806–820

LINDENBERG, J (1983) *Stability of Armorflex block slope protection mats under wave attack*, Report M1910, Delft Hydraulics, the Netherlands

LOWE, J and KARAFIATH, L (1960) "Stability of earth dams upon draw-down". In: *Proc 1st Pan-American conference on soil mechanics and foundation engineering*, Mexico City, Mexico, 7–12 September 1959, International Society of Soil Mechanics and Geotechnical Engineering (ISSMGE), pp 537 – 552

LUBOCKOV, E A (1965) "The calculation of suffusion properties of non-cohesive soils when using the non-suffosion analogue". In: *Proc int conf on hydraulic research*, Brno, Czech Republic, pp 135–148

LUMBROSO, D M, JOHNSTONE, W, DE BRUIJN, K, DI MAURO, M, LENCE, B and TAGG, A (2010) "Modelling mass evacuations to improve the emergency planning for floods in the UK, the Netherlands and North America". In: *Proc int conf on emergency preparedness (InterCEPt), the challenges of mass evacuation*, 21–23 September 2010, University of Birmingham, UK

LUMBROSO, D M, SAKAMOTO, D, JOHNSTONE, W M, TAGG, A F and LENCE, B J (2011) "The development of a life safety model to estimate the risk posed to people by dam failures and floods, dams and reservoirs", *Dams and Reservoirs*, June 2011, Journal of the British Dam Society, UK

MADEJ, J S (1984) "On the accurate solution of the limit equilibrium slope stability analysis". In: *Proc 4th ISL*, Toronto, 2, pp 457–462

MAKDISI, F I and SEED, H B (1978) "Simplified procedure for estimating dam and embankment earthquake-induced deformations", *Journal of the Geotechnical Engineering Division*, vol 104, **7**, American Society of Civil Engineers (ASCE), New York, pp 849–867

MANZARI, M T and NOUR, M A (2000) "Significance of soil dilatancy in slope stability analysis", *Journal of Geotechnical and Geoenvironmental Engineering*, vol 126, **1**, American Society of Civil Engineers (ASCE), New York, USA, pp 75–80

MARTIN, G R, FINN, W D L and SEED, H B (1975) "Fundamentals of liquefaction under cyclic loading, journal of the geotechincal engineering division", *ASCE*, vol 101, **GT5**, pp 423–483

MAYNORD, S T (1993) "Corps riprap design guidance for channel protection", *Preprints of internationl riprap workshop: Theory, policy and practice of erosion control using riprap, armour stone and rubble*, Fort Collins, CO, USA

MAYNORD, S T (1996) "Toe-scour estimation in stabilized bendways", *Journal of Hydraulic Engineering*, vol 122, **8**, American Society of Civil Engineers (ASCE), New York, USA, pp 460–464

MAYNORD, S T and HUBBARD, L C (1993) *Outer-bank velocity estimation on Mississippi River revetted bends*, Technical Report HL-93-8, US Army Engineers, Waterways Experiment Station, Vicksburg, MS, USA

MCCONNELL, K J (1998) *Revetment systems against wave attack: a design manual*, Thomas Telford, London (ISBN: 978-0-7277-2706-0)

MCCONNELL, K J and ALLSOP, N W H (1999) "Revetment protection for embankments exposed to wave attack". In: *Proc MAFF Keele conf of river and coastal engineers, MAFF*, London

MCDOUGAL, W G, KRAUS, N C and AJIWIBOWO, H (1996) "The effects of seawalls on the beach: Part II, numerical modeling of SUPERTANK seawall tests", *Journal of Coastal Research*, vol 12, **3**, Coastal Education & Research Foundation, Inc, USA, pp 702–713

MELBY, J A (2012) *Runup prediction for flood hazard assessment*, ERDC/CHL TR-12-X, Engineers Research and Development Centre, US Army Corps of Engineers, Vicksburg, USA.
Go to: http://greatlakescoast.org/pubs/reports/Melby_Runup_TR_fema.pdf

MELVILLE, B W and COLEMAN, S E (2000) *Bridge scour*, Water Resources Publications, LLC, Colorado, USA (ISBN: 978-1-88720-118-6)

MEYER-PETER, E, and MÜLLER, R (1948) "Formulas for bed-load transport". In: *Proc 2nd meeting of the International Association for Hydraulic Structures Research*, Delft, the Netherlands, pp 39–64

MEYERHOF, G G (1965) "Shallow foundations", *Journal of Soil Mechanics and Foundation Division*, vol 91, SM2, American Society of Civil Engineers (ASCE), New York, USA, pp 21–31

MICHALOWSKI, R L (1989) "Three-dimensional analysis of locally loaded slopes", *Géotechnique*, vol 39, **1**, Institution of Civil Engineers, London, pp 27–38

MICHALOWSKI, R L (1993) "Limit analysis of weak layers under embankments", *Soils and Foundations*, vol 33, **1**, 1993 Japanese Society of Soil Mechanics and Foundation Engineering, Japan, pp 155–168

MILNE-THOMSON, H (1960) *Theoretical hydrodynamics,* Macmillan Co., New York, USA (ISBN: 978-0-48668-970-8)

MISHRA, G. and SINGH, A. (2005) "Seepage through a Levee", *International Journal of Geomechanics*, vol 5, **1**, ASCE, New York, USA, pp 74–79

MLYNAREK, J, LAFLEUR, J, ROLLIN, A and LOMBARD, G (1993) "Filtration opening sizes of geotextiles by hydrodynamic sieving", *Geotechnical Testing Journal*, vol 16, **1**, ASTM SEDL, USA, pp 61–69

MOHAMED, M A A (2002) *Embankment breach formation and modelling methods,* PhD Thesis, The Open University, UK

MORRIS, M W (2009) *Breach initiation and growth: physical processes*, FLOODsite Report T06-08-11. UK. Go to: **www.floodsite.net**

MORRIS, M W (2011) *Breaching of earth embankments and dams,* PhD Thesis, The Open University, UK

MORRIS, H M and WIGGERT, J M (1963) *Applied hydraulics in engineering*, Ronald Press, USA (ISBN: 978-0-82606-305-2)

MORRIS, M W, HASSAN, M A A M and ESCARAMEIA, M (2012a) *The performance of vegetation on flood embankments*, FloodProBE Report WP03-01-10-06, the Netherlands. Go to: **www.floodprobe.eu**

MORRIS, M W, HASSAN, M A A M, WAHL, T L, TEJRAL, R D, HANSON, G J and TEMPLE, D M (2012b). Evaluation and development of physically based embankment breach models" In: *Proc FLOODrisk 2012*, 20–22 November 2012, Rotterdam, the Netherlands

MORGENSTERN, N R (1992) "The evaluation of slope stability – a 25 year perspective". In: *Stability and performance of slopes and embankments II* (Geotechnical Special Publication (GSP) No. 31) R B Seed and R W Boulanger (eds) *A Specialty Conference*, 29 June to 1 July 1992, Berkeley, California, USA (ISBN: 978-0-87262-872-4), pp 1–26

MORGENSTERN, N R and PRICE, V E (1965) "The analysis of stability of general slip surface", *Géotechnique*, vol 15, **1**, Institution of Civil Engineers, UK, pp79–93

MOSS, R E S (2003) *CPT-based probabilistic assessment of seismic soil liquefaction initiation*, PhD Dissertation, University of California, Berkeley, California, USA

MOSTAFA, T M S (2003) *Experimental modelling of local scour in cohesive soils*, PhD Thesis, University of South Carolina, USA

MOSTAFA, T M S, IMRAN, J, CHAUDHRY, M H and KAHN, I B (2008) “Erosion resistance of cohesive soils”. *Journal of Hydraulic Research*, vol 46, 6, Taylor & Francis, UK, pp 777–787

NEILL, C R (1973) (ed) *Guide to bridge hydraulics*, Transportation Association of Canada, Toronto, Canada (ISBN: 978-0-72773-262-0)

NEWMARK, N M (1965) “Effects of earthquakes on dams and embankments”, *Géotechnique*, vol 15, **2**, Institution of Civil Engineers, UK, pp139–160

ORDIN, C F and ALGERT, J H (1965) “Geometrical properties of sand waves: discussion”, *Journal of the Hydraulics Division*, vol 91, **HY3**, American Society of Civil Engineers (ASCE), New York, USA, pp 367–374

OFEG (2003) *Documentation de base pour la vérification des ouvrages d’accumulation aux séismes*, Version 1.2, série eaux, Rapports de l’OFEG, Office Federal des Eaux et de la Geologie, Ittigen, Suisse

OSTERBERG, J O (1957) “Influence values for vertical stresses in a semi-infinite mass due to an embankment loading”. In: *Proc fourth int conf on soil mechanics and foundation engineering*, London, vol 1, American Society of Civil Engineers (ASCE), New York, USA, pp 393–396

OWEN, M W (1980) *Design of sea walls allowing for wave overtopping*, Report EX 924, HR Wallingford, Wallingford, UK

OWEN, M W (1982) “Overtopping of sea defences”. In: *Proc conf on hydraulic modelling of civil engineering structures*, Coventry, UK, pp 469–480

PAN, J Z (1980) *The stability of structures against sliding and slope stability analysis*, Hydraulic Publishing Co, Japan

PAQUIER, A (2007) “Testing a simplified breach model on impact project test cases”. In: *Proc 32nd congress of IAHR*, 1–6 July, 2007, Venice, Italy

PAQUIER, A (2009) “Rupture d’une digue en milieu fluvial (Agly en 1999)”. *Chapitre 10 De la goutte de pluie jusqu’à la mer, traité d’hydraulique environnementale, Volume 7 Applications des modèles numériques en ingénierie, 1*, Hermes/Lavoisier, Paris (ISBN: ISBN 978-2-74622-337-0), pp 127–138

PAQUIER, A (2010) “Failure of a Dike in a Flood Environment (Agly 1999)” *Practical Applications in Engineering*, vol 4, John Wiley & Sons Inc, New Jersey, USA (ISBN: 978-1-11855-779-2)

PAQUIER, A and RECKING, A (2004) “Advances on breach models by Cemagref during impact project”. In: *Proc 4th IMPACT Workshop*, 3–5 November 2004, Zaragoza

PECKER, A, PREVOST, J H and DORMIEUX, L(2001) “Analysis of pore pressure generation and dissipation in cohesionless materials during seismic loading”, *Journal of Earthquake Engineering*, vol 5, 4, World Scientific Publishing Company, Tokyo, Japan, pp 441–464

PHILIPPE, P and RICHARD, T (2008) “Tart and stop of an avalanche in a granular medium subjected to an inner water flow”, *Physical review E,* vol 77, 4 (041306), American Physicla Society, USA

PHILIPPONNAT, G and HUBERT, B (2003) *Géotechnique, Fondation et ouvrages en terre*, fourth edition, Eyrolles, France (ISBN: 978-2-21207-218-1)

PIANC (1987) *Guidelines for the design and construction of flexible revetments incorporating geotextiles for inland waterways*, Report of Working Group 4 of the Permanent Technical Committee I, Permanent International Association of Navigation Congresses, Brussels (ISBN: 978-2-87223-000-6)

PILARCZYK, K W (1995) “Simplified unification of stability formulae for revetments under current and wave attack”. In: C R Thorne, S R Abt, F B J Barends, S T Maynord and K W Pilarczyk (eds) *River, coastal and shoreline protection: erosion control using riprap and armourstone*, John Wiley & Sons, New York, USA (ISBN: 978-0-471-94235-1)

POHL, R (1997) “Wellenauflauf im Übergangsbereich zwischen Brandung und Reflexion”, *Hansa*, Nr. 134, S. pp 62–64

POHL, R and HEYER, T (2005) “Der Auflauf unregelmäßiger Wellen im Übergangsbereich zwischen Branden und Schwingen”, *Wasser und Abfall*, S., pp 34–38

POHL, R and BORNSCHEIN, A (2012) “Wave run-up of breaking and non-breaking waves with longshore current”, In: *Proc Coastlab12*, Ghent, Belgium

POWELL, K A (1987) *Toe scour at seawalls subject to wave action: a literature review*, Report SR 119, Hydraulic Research, HR Wallingford, Wallingford, UK

POWELL, K A (1989) "The scouring of coarse sediments at the toe of seawalls". In: *Proc seminar on seawall design ands SWALLOW*, Hydraulics Research, HR Wallingford, UK

POWELL, K A and LOWE, J P (1994) "The scouring of sediments at the toe of seawalls". In: *Proc of the Hornafjordur International Coastal Symposium*, Iceland, 20–24 June 1994, G Viggosson (ed), pp 749–755

PRAKASH, S (1981) *Soil dynamics*, McGaw Hill Higher Education, New York, USA (ISBN: 978-0-07050-658-9)

PRZEDWOJSKI, B, BLAZEJEWSKI, R AND PILARCZYK, KW (1995) *River training techniques. Fundamentals, design and applications*, AA Balkema, Rotterdam

PULLEN, T, ALLSOP, N W H, BRUCE, T, KORTENHAUS, A, SCHUTTRUMPF, H and VAN DER MEER, J W (2007) *EurOtop. Wave overtopping of sea defences and related structurs: assessment manual, Die Kuste*, Environment Agency, UK, Expertise Netwerk Waterkeren, the Netherlands, and Kuratorium fur Forschung im Kusteninhenieurwesen, Germany (ISBN: 978-3-8042-1064-6). Go to: **www.overtopping-manual.com**

RAMSBOTTOM, D, WADE, S, BAIN, V, HASSAN, M, PENNING-ROWSELL, E, WILSON, T, FERNANDEZ, A, HOUSE, M and FLOYD, P (2004) *Flood risks to people,* Phase 2, FD2321/IR2, Department for the Environment, Food and Rural Affairs, London and Environment Agency, Bristol, UK.
Go to: **www.rpaltd.co.uk/documents/J429-RiskstoPeoplePh2-Guidance.pdf**

RAUDKIVI, A J (1990) *Loose boundary hydraulics*, 3rd edition, Taylor & Francis, New York, USA (ISBN: 978-9-05410-448-3)

REDDI, L N, LEE, I M and BONALA, M V S (2000) "Comparison of internal and surface erosion using flow pump tests on a sand-kaolinite mixture", Geotechnical Testing Journal, vol 23, **1**, ASTM International Committee, American Society for Testing and Materials, USA, pp 116–122

REEVE, D E, SOLIMAN, A and LIN, P Z (2008) "Numerical study of combined overflow and wave overtopping over a smooth impermeable seawall", *Coastal Engineering*, vol. 55, **2**, Elsevier BV, UK, pp 155–166

REGAZZONI, P L, HANSON, G, WAHL, T, MAROT, D and COURIVAUD, J R (2008) "The influence of some engineering parameters on the erosion of soils". In: *Proc 4th int conf on scour and erosion (ICSE-4),* 5–7 November 2008, Tokyo, Japan

REGAZZONI, P L, MAROT, D, COURIVAUD, J R, HANSON, G and WAHL, T (2008) "Soils erodibility: a comparison between the jet erosion test and the hole erosion test". In: *Proc inaugural international conference of the Engineering Mechanics Institute,* Minneapolis, MN, USA, 18–21 May 2008

ROBERTSON, P K, and WRIDE, C E (1997) "Cyclic liquefaction and its evaluation based on the SPT and CPT". In: T L Youd and I M Idriss (eds) *Proceedings of the NCEER workshop on evaluation of the liquefaction resistance of soils (NCEER-97–0022)*, National Center for Earthquake Engineering Research (NCEER), Buffalo, USA

ROLLEY, R, KREITMANN, H, DUNGLAS, J, PIERREJEAN, A, ROLLAND, L, VILLEPIQUE, LOUDIÈRE, D, OBERLIN, G, RIEUL, L, ALONSO, E, CHEYLAN, COLIN, E, COVA, R, DAUGE, M, KERN, F, LALANNE, MICHEL, C, PERRIN, J and POCHAT, R (1977) *Technique des barrages en aménagement rural*, Ministère de l'Agriculture, France

SANDERS, B F, SCHUBERT, J E, SMITH, M J and WRIGHT, N G (2008a) "Unstructured mesh generation and land cover-based resistance for hydrodynamic modeling of urban flooding", *Advances in Water Resources*, vol 31, **12**, Elsevier BV, UK, pp 1603–1621

SANDERS, B F, SCHUBERT, J E and GALLEGOS, H A (2008b) "Integral formulation of shallow-water equations with anisotropic porosity for urban flood modelling", *Journal of Hydrology,* vol 362, **1–2**, Elsevier BV, UK, pp 19–38

SARMA, S K (1973) "Stability analysis of embankments and slopes", *Géotechnique*, vol 23, **3**, Institution of Civil Engineers, UK, pp 423–433

SARMA, S K and BHAVE, M V (1974) "Critical acceleration versus static factor of safety in stability analysis of earth dams and embankments", *Géotechnique*, vol 24, **4**, Institution of Civil Engineers, UK, pp 661–665

SAVILLE, T (1957) "Wave run-up on composite slopes". In: *Proc of the 6th conference on coastal engineering*, Gainesville, Florida, No 6, **1957**, American Society of Civil Engineers (ASCE), New York, USA, pp 691–699

SCHMITZ, S (2007) *Zur hydraulischen kontakterosion bei bindigen basiserdstoffen*, PhD Thesis,Universität der Bundeswehr, Munich, Germany

SCHUBERT, J E and SANDERS, B F (2012) "Building treatments for urban flood inundation models and implications for predictive skill and modeling efficiency", *Advances in Water Resources*, vol 41, Elsevier BV, UK, pp 49–64

SCHÜTTRUMPF, H (2001) *Wellenüberlaufströmung bei Seedeichen – Experimentelle und Theoretische Untersuchungen*, PhD-Thesis

SCHÜTTRUMPF, H, MÖLLER, J, OUMERACI, H, GRÜNE, J and WEISSMANN, R (2001) "Effects of natural sea states on wave overtopping of seadikes". In: *Proc of the 4th int symposium on waves 2001, Ocean wave measurement and analysis*, American Society of Civil Engineers (ASCE), New York, USA, pp 1565–1574

SEED, H B (1979) "Considerations in the earthquake resistant design of earth and rockfill dams", *Géotechnique*, vol 29, **3**, Institution of Civil Engineers, UK, pp 215–263

SEED, H B and IDRISS, I M (1971) "Simplified procedure for evaluating soil liquefaction potential", *Journal of the Soil Mechanics and Foundations Division*, vol 97, **9**, American Society of Civil Engineers (ASCE), New York, USA, pp 1249–1273

SEED, H B and IDRISS, I M (1971) "Simplified procedure for evaluating soil liquefaction potential", *Journal of the Soil Mechanics and Foundations Division*, vol 97, 9, American Society of Civil Engineers (ASCE), New York, USA, pp 1249–1273

SEED, H B, LEE, K L, and IDRISS, I M (1973) "Analysis of the slide in the San Fernando dams during the earthquake of February 9, 1971", Earthquake Engineering Research Center 73–2, University of California, Berkeley, California

SEED, H B and IDRISS, I M (1982) *Ground motions and soil liquefaction during earthquakes (engineering monographs on earthquake criteria, structural design, and strong motion records)*, Earthquake Engineering Research Institute, California, USA (ISBN: 978-0-94319-824-8)

SEELIG, W N (1983) "Wave reflection from coastal structures". In: *Proc conf on coastal structures '83*, Arlington, USA, American Society of Civil Engineers, New York, pp 961–973

SELLMEIJER, J B and KOENDERS, M A (1991) "A mathematical model for piping", *Applied Mathematical Modelling*, vol 15, **11–12**, Elsevier BV, UK, pp 646–651

SCHMERTMANN, J H (2000) "The no-filter factor of safety against piping through sands" *ASCE Geotechnical Special Publication No. 111, Judgment and innovation*, F Silva and E Kavazanjian (eds), American Society of Civil Engineers, New York, USA (ISBN: 978-0-78440-537-6)

SHEN, H W, SCHNEIDER, V R and KARAKI, S S (1969) "Local scour around bridge piers", *Journal of the Hydraulics Division*, vol 95, **6**, American Society of Civil Engineers (ASCE), New York, USA, pp 1919–1940

SHERARD, J L and DUNNIGAN, L P (1985) "Filters and leakage control in embankment dams, seepage and leakage from dams and impoundments", *Proceedings of the ASCE Symposium on seepage and leakage from dams and impoundments*, Denver, CO, USA (ISBN: 978-0-87262-448-1), pp 1–29

SHERARD, J L and DUNNIGAN, L P (1989) "Critical filters for impervious soils", *Journal of Geotechnical Engineering*, vol 115, **7**, American Society of Civil Engineers (ASCE), New York, USA, pp 927–947

SHIELDS, A (1936) *Anwendung der Ähnlichkeitsmechanik und der Turbulenzforschung auf die Geschiebebewegung (Application of similarity principles and turbulence research to bedload movement),* Mitteilungen der Preußischen Versuchsanstalt für Wasserbau und Schiffbau, Berlin

SIMON, A (1994) "Width adjustment: relative dominance in unstable alluvial streams" In: *Proc of the 1994 Conference of the Hydraulics Division*, 1–5 August 1994, Buffalo, New York, USA. G V Cotroneo and R R Rumer (eds) Hydraulic Engineering (1994), American Society of Civil Engineers (ASCE), New York, USA (ISBN: 978-0-7844-0037-1) pp 974–978

SIMON, A (1995) "Adjustment and recovery of unstable alluvial channels: identification and approaches for engineering management", *Earth Surface Processes and Landforms*, vol 20, **7**, John Wiley and Sons Ltd, New Jersey, USA, pp 611–628

SIMONS, D B and RICHARDSON, E V (1966) Resistance to flow in alluvial channels, Geological Survey Professional Paper 422-J, US Department of the Interior, US Government Printing Office, Washington, DC, USA

SKEMPTON, A W and BJERRUM, L (1957) "A contribution to settlement analysis of foundation on clay", *Géotechnique* vol 7, **4**, Institution of Civil Engineers, London, pp 168–178

SOARES-FRAZÃOA, S, CANELASB, R, CAOC, Z, CEAD, L, CHAUDHRYE, H M, DIE MORANF, A, EL KADIG, K, FERREIRAH, R, CADÓRNIGAI, I F, GONZALEZ-RAMIREZJ, N, GRECOK, M, HUANGL, W, IMRANM, J, LE COZN, J, MARSOOLIO, R, PAQUIERP, A, PENDERQ, G, PONTILLOR, M, PUERTASS, J, SPINEWINET, B, SWARTENBROEKXU, C, TSUBAKIV, R, VILLARETW, C, WUX, W, YUEY, Z and ZECHZ, Y (2012) "Dam-break flows over mobile beds: Experiments and benchmark tests for numerical models", *Journal of Hydraulic Research*, vol 50, **4**, Taylor & Francis, UK, pp 364–375

SOARES-FRAZAO, S, LHOMME, J, GUINOT, V and ZECH, Y (2008) "Two-dimensional shallow-water model with porosity for urban flood modelling", *Journal of Hydraulic Research*, vol, 46, **1**, Taylor & Francis, UK, pp 45–64

SUMER, B M and FREDSOE, J (2002) *The mechanics of scour in the marine environment*, World Scientific, Singapore (ISBN: 978-9-81024-930-4)

SUTHERLAND, J and O'DONOGHUE, T (1998) "Wave phase shift at coastal structures", *Journal of Waterway, Port, Coastal, and Ocean Engineering*, vol 124, **2**, American Society of Civil Engineers (ASCE), New York, USA, pp 90–98

SUTHERLAND, J, BRAMPTON, A and WHITEHOUSE, R (2006) "Toe scour at seawalls: monitoring prediction and mitigation". In: *Proc the 41st Defra Flood and Coastal Management Conference*, 4–6 July 2006, York, UK, pp 03b.1.1–03b.1.12

SUTHERLAND, J, BRAMPTON, A H, OBHRAI, C, DUNN, S and WHITEHOUSE, R J S (2007) *Understanding the lowering of beaches in front of coastal defence structures*, stage 2, Joint Defra/EA Flood and Coastal Erosion Risk Management R&D Programme, R&D Technical Report FD1927/TR, Department for the Environment, Food and Rural Affairs, London

SWAISGOOD, J R (2003) "Embankment dam deformations caused by earthquakes" In: *Proc of the 2003 Pacific conf on earthquake engineering*, 13–15 February 2003, Christchurch, New Zealand, New Zealand, National Society for Earthquake Engineering, Wellington, New Zealand

TAKAHASHI, S, TANIMOTO, K and SHIMOSAKO, K (1994) "A proposal of impulsive pressure coefficient for the design of composite breakwaters". In: Un'yushō Kōwan Gijutsu Kenkyūjo, Engan Kaihatsu Gijutsu Kenkyū Sentā, Doboku Gakkai, Yokosuka-shi (eds), *Hydro-Port '94: Proceedings of the international conference on hydro-technical engineering for port and harbor construction,* 19–21 October 1994, Yokosuka, Japan, Volume 2, Coastal Development Institute of Technology, University of California (ISBN: 978-4-90030-204-4), pp 489–504

TEMPLE, D M (1985) "Stability of grass-lined channels following mowing". In: American Society of Agricultural and Biological Engineers, St. Joseph, Michigan, USA, vol 28, 3 pp 750–754

TEMPLE, D M (1997) "Earth spillway erosion model", Chapter 51, Part 628 *Dams, National Engineering Handbook*, US Department of Agriculture (USDA), Washington DC, USA.
Go to: **http://directives.sc.egov.usda.gov/OpenNonWebContent.aspx?content=18378.wba**

TEMPLE, D M, ROBINSON, K M, AHRING, R M and DAVIS, A G (1987) *Stability design of grass-lined open channels*, Agriculture Handbook Number 667, Agricultural Research Service, US Department of Agriculture, Fort Worth, Tx, USA. Go to: **http://rpitt.eng.ua.edu/Class/Erosioncontrol/Module5/contents.pdf**

TEMPLE, D M and HANSON, G J (1994) "Headcut development in vegetated earth spillways", *ASABE Applied Engineering in Agriculture*, vol 10, **5**, American Society of Agricultural and Biological Engineers, Michigan, USA, pp 677–682

TERZAGHI, K (1943) *Theoretical soil mechanics*, John Wiley & Sons, UK (ISBN: 0-471-85305-4)

TERZHAGI, K (1953) *Investigation of filter requirements for underdrains*, Technical Memo 3–360, US Waterways Experiment Station, USACE, Vicksburg, Mississippi, USA

THORNE, C R (1988) *Bank processes on the Red River between Index, Arkansas and Shreveport*, LA, Final Report to US Army European Research Office, Queen Mary College, London, England

THORNE, C R and ABT, S R (1993) *Velocity and scour prediction in river bends*, Contract Report HL-93-1, US Army Engineers, Waterways Experiment Station, Vicksburg, Mississippi, US

THORNE, C R, MAYNORD, S T and ABT, S R (1995) "Prediction of near-bank velocity and scour depth in meander bends for design of riprap revetments", C R Thorne, S R Abt S T Maynord, K Pilarcyzk and F Barends (eds) *River, coastal and shoreline protection: erosion control using riprap and armourstone*, J Wiley and Sons, Chichester, UK (ISBN: 978-0-471-94235-1), pp 115–136

TOKIMATSU, K and SEED, H B (1987) "Evaluation of settlements in sand due to earthquake shaking", *Journal of Geotechnical Engineering*, vol 113, **8**, American Society of Civil Engineers (ASCE), New York, USA, pp 861–878

TRAVASAROU, T, and BRAY, J D (2003) "Optimal ground motion intensity measures for assessment of seismic slope displacements". In: *Proc 2003 Pacific conference on earthquake engineering*, Christchurch, New Zealand

TSUKAMOTO, Y and ISHIHARA, K (2010) "Analysis on settlement of soil deposits following liquefaction during earthquakes", *Soils and Foundations*, vol 50, **3**, Elsevier BV, UK, pp 399–411

USACE (1989) *Engineering and design of retaining and flood walls*, EM 1110-2-2502, US Army Corps of Engineers, Washington, DC. Go to: **http://publications.usace.army.mil/publications/eng-manuals/**

USACE (1992) *Hydraulic design of spillways*, EM 1110-2-1603, US Army Corps of Engineers, Washington DC, USA. Go to: http://publications.usace.army.mil/publications/eng-manuals/

USACE (1993) *Seepage analysis and control for dams*, EM110-2-1901, US Army Corps of Engineers, Washington DC, USA. Go to: **http://publications.usace.army.mil/publications/eng-manuals/**

USACE (1994) *Hydraulic design of flood control channels*, EM 1110-2-1601, US Army Corps of Engineers, Washington DC, USA. Go to: **http://publications.usace.army.mil/publications/eng-manuals/**

USACE (2003) *Slope stability*, EM 1110-2-1902, US Army Corps of Engineers, Washington DC, USA. Go to: **http://publications.usace.army.mil/publications/eng-manuals/**

USACE (2006a) *Coastal engineering manual,* EM 1110-2-1100, US Army Corps of Engineers, Washington DC, USA. Go to: **http://chl.erdc.usace.army.mil/cem**

USACE (2006b) *Performance evaluation of the New Orleans and Southeast Louisiana Hurricane Protection System*. Draft final report of the Interagency Performance Evaluation Task Force. Volume VII: the consequences, US Army Corps of Engineers, Washington DC, USA.
Go to: http://media.nola.com/hurricane_katrina/other/060106corps_vol7.pdf

USACE (2008) *Hurricane and storm damage reduction system design guidelines*, interim report, New Orleans District, US Army Corps of Engineers, New Orleans, USA.
Go to: **http://www2.mvn.usace.army.mil/ENG/entiredocument.pdf**

USACE (2010) *HEC-RAS 4.1 user manual*, Hydrologic Engineering Center, US Army Corps of Engineers, Washing DC, USA

USACE (2011) *Hydrologic Engineering Center River Analysis System (HEC-RAS)*, US Army Corps of Engineers, Washing DC, USA. Go to: **www.hec.usace.army.mil/software/hec-ras/**

USDA (2013) *WinDAM B Software*, Natural Resource Conservation Service, US Department of Agriculture, USA. Go to: **http://go.usa.gov/8Oq**

VAN, M A (2001) "New approach for uplift induced slope failure". In: *Proc 15th int conf on soil mechanical and geotechnical engineering*, Istanbul, 27–31 August 2001, vol 3, AA Balkema, Lisse, the Netherlands, pp 2285–2288

VAN, M A, KOELEWIJN, A A and BARENDS, F B J (2005) "Uplift phenomenon: model and validation", International Journal of Geomechanics, vol 5: special issue on soft clay engineering and soft clay improvement, American Society of Civil Engineers (ASCE), New York, USA, pp 98–109

VAN BEEK, V M, KNOEFF, H and SELLMEIJER, J B (2011) "Observations on the process of backward erosion piping in small, medium and full-scale experiments", European Journal of Environmental and Civil Engineering, vol 15, 8, Taylor & Francis, UK, pp 1115–1138

VAN DAMME, M, MORRIS, M W and HASSAN, M A A M (2011) *A new approach to rapid assessment of breach driven embankment failures*, FRMRC2–WP 4.4, Flood Risk Management Research Consortium.
Go to: **http://web.sbe.hw.ac.uk/frmrc/downloads/FRMRC2_WP4_4_ScienceReport.pdf**

VAN DER MEER, J (1988) *Rock slopes and gravel beaches under wave attack*, PhD Thesis (Delft Hydraulics Publication No. 396), Delft University of Technology, the Netherlands.
Go to: **www.vandermeerconsulting.nl/downloads/stability_b/1988_vandermeer_doctoralthesis.pdf**

VAN DER MEER, J W (2002) *Wave run-up and wave overtopping at dikes*, technical report, Technical Advisory Committee for Flood Defence in the Netherlands (TAW), Delft, the Netherland

VAN DER MEER, J W and JANSSEN, W (1995) "Wave run-up and wave overtopping at dikes", Kobayashi, Demirbilek (ed) *Wave forces on inclined and vertical wall structures*, Task Committee on forces on inclined and vertical wall structures of the committee on waves and wave forces of the Waterway, Port, Coastal and Ocean Engineering Division, American Society of Civil Engineers (ASCE), New York, USA (ISBN: 978-0-78440-080-7), pp 1–27

VAN DER MEER, J M, HARDEMAN, B, STEENDAM, G J, SCHÜTTRUMPF, H and VERHEY, H (2010) "Flow depths and velocities at crest and landward slope of a dike, in theory and with the wave overtopping simulator". In: *Proc 32nd int conf on coastal engineering*, ICCE 2010, 20 June to 5 July 2010, Shanghai, China

VAN DER MEIJ, R and SELLMEIJER, J B (2010) "A genetic algorithm for solving slope stability problems : from Bishop to a free slip surface". In: *Proc 7th European Conference on Numerical Methods in Geotechnical Engineering (NUMGE 2010)*, Trondheim, Norway, 2–4 June 2010

VAN HERPEN, J A (1998) "Bituminous revetments". In: K W Pilarczyk (ed), *Dikes and revetments. Design, maintenance and safety assessment*, A A Balkema, Rotterdam, the Netherlands (ISBN: 9-05410-455-4), pp 249–289

VAN GENT, M (2000) *Wave runup on dikes and berms*, Technical Report H3609, WL Delft Hydraulics, Rijkwaterstaat, the Netherlands

VAN GENT, M (2001) *Wave runup on dikes and shallow foreshores, Journal of Waterway, Port, Coastal and Ocean Engineering*, vol 127, **5**, American Society of Civil Engineers (ASCE), New York, USA, pp 254–262

VAN RIJN, L C (1984) "Sediment transport, Part III: Bed forms and alluvial roughness", *Journal of Hydraulic Engineering*, vol 110, **12**, American Society of Civil Engineers (ASCE), New York, USA, pp 1733–1754

VAN RIJN, L C, WALSTRA, D J R, GRASMEIJER, B, SUTHERLAND, J, PAN, S and SIERRA, J P (2003) "The predictability of cross-shore bed evolution of sandy beaches at the time scale of storms and seasons using process-based profile models", Coastal Engineering, vol 47, **3**, Elsevier BV, UK, pp 295–327

VANONI, V A (ed) (1975) *Sedimentation engineering (classic edition), Manuals and Reports on Engineering Practice*, No. 54, American Society of Civil Engineers (ASCE), New York, USA (ISBN: 978-0-78440-823-0)

VERHEIJ, H (2002) "Time-dependent breach development in cohesive material". In: *Proc the 2nd IMPACT project workshop*, 12–13 September 2002Mo-i-Rana, Norway, WL | Delft Hydraulics, the Netherlands.
Go to: **www.impact-project.net**

VERHEIJ, H J, KRUSE, G A M, NIEMEIJER, J H, SPRANGERS, J T C M and DE SMIDT, J T (1997) "*Technical report erosion resistance of grassland as dike covering*" TAW Guideline TPG130510, Rijkswaterstaat, the Netherlands

WAHL, T L and ERDOGAN, Z (2008) *Erosion indices of soils used in ARS piping breach tests*, Hydraulic Laboratory Report HL-2008-04, US Department of the Interior, Bureau of Reclamation, Denver, Colorado, USA

WAHL, T L (2004) "Uncertainty of predictions of embankment dam breach parameters", *Journal of Hydraulic Engineering*, vol 130, **5**, American Society of Civil Engineers (ASCE), New York, USA, pp 389–397

WALLIS, M, WHITEHOUSE, R and LYNESS, N (2009) "Development of guidance for the management of the toe of coastal defence structures". In: *Proc of the coasts, marine structures and breakwaters 2009 conference*, 16–18 September 2009, EICC, Scotland

WAN, C F and FELL, R (2004a) *Experimental investigation of internal instability of soils in embankment dams and their foundations*, UNICIV Report No. R-429, the University of New South Wales, Sydney, Australia

WAN, C F and FELL, R (2004b) "Experimental investigation of internal erosion by the process of suffusion in embankment dams and their foundations", ANCOLD Bulletin No. 126, The Australian National Committee on Large Dams Incorporated, Australia, pp 69–78

WAN, C F and FELL, R (2008) "Assessing the potential of internal instability and suffusion in embankment dams and their foundations", *Journal of Geotechnical and Geoenvironmental Engineering*, vol 134, **3**, American Society of Civil Engineers (ASCE), New York, USA, pp 401–407

WANG, W S (1979) *Some findings in soil liquefaction*, Earthquake Engineering Department, Water Conservancy and Hydroelectric Power Scientific Research Institute, Beijing

WASSING, F (1957) "Model investigation on wave run-up carried out in the Netherlands during the past twenty years". In: *Proc 6th int conf on coastal engineering*, ASCE, Gainesville, Florida, USA

WERNER, M G F (2001) "Impact of grid size in GIS based flood extent mapping using a 1D flow model", *Physics and Chemistry of the Earth Part B – Hydrology, Oceans and Atmospheres*, vol 26, **7–8**, Elsevier BV, UK pp 517–522

WERNER, M G F (2004) *Spatial flood extent modelling, a performance-based comparison*, PhD Thesis Technical University Delft, Delft University Press, the Netherlands

WHITMAN, R V and BAILEY, W A (1967) "Use of computers for slope stability analysis", *Journal of the Soil Mechanics and Foundations Division*, vol 93, SM4, American Society of Civil Engineers (ASCE), New York, USA, pp 475–498

WILLIAMS, D T and COZAKOS, D (1994) "Use of HEC-2 and HEC-6 to determine levee heights and revetment toe scour depths". In: *Proc of the 1994 Conference of the Hydraulics Division*, 1–5 August 1994, Buffalo, New York, USA. G V Cotroneo and R R Rumer (eds) *Hydraulic Engineering (1994),* American Society of Civil Engineers (ASCE), New York, USA (ISBN: 978-0-7844-0037-1) pp 1075–1079

WILSON, R C and KEEFER, D K (1985) "Predicting the areal limits of earthquake-induced landsliding". In: J I Ziony (ed) *Evaluating earthquake hazards in the Los Angeles Region – an earth science perspective*, U.S. Geological Survey, Paper 1360, pp 316–345

WHITEHEAD, E (1976) *A guide to the use of grass in hydraulic engineering practice,* TN071, CIRIA, London (ISBN: 978-0-86017-012-9) (out of print). Go to: **www.ciria.org**

WHITEHOUSE, R (1998) *Scour at marine structures: a manual for practical applications*, Thomas Telford Publications, London (ISBN: 978-0-72772-655-1)

WÖRMAN, A and OLAFSDOTTIR, R (1992) "Erosion in a granular medium interface", *Journal of Hydraulic Research*, vol 30, 5, Taylor & Francis, UK, pp 639–655

XIE, S-L (1981) *Scouring patterns in front of vertical breakwaters and their influences on the stability of the foundations of the breakwaters*, Department of Civil Engineering, Delft University of Technology, Delft, the Netherlands

XIE, S-L (1985) *Scouring patterns in front of vertical breakwaters*, vol 4, **1**, Acta Oceanologica Sinica, Springer, UK, pp 153–164

YALIN, M S (1964) "Geometrical properties of sand waves", *Journal of the Hydraulics Division*, vol 90, **5**, American Society of Civil Engineers (ASCE), New York, USA, pp 105–119

YALIN, M S (1992) *River mechanics*, Pergamon Press, New York, USA (ISBN: 978-0-08040-190-4)

YARDE, A J, BANYARD, L S and ALLSOP, N W H (1996) *Reservoir dams: wave conditions, wave overtopping and slab protection*, Report SR 459, HR Wallingford, UK

VAUGHAN, N, ALBERT, J and CARLSON, R F (2002) Impacts of ice forces on stream bank protection, Report FHWA-AK-RD-02-03, prepared for Alaska Department of Transportation and Public Facilities, Statewide Research Office, Juneau, AK, USA

YOUD, T L and PERKINS, D M (1978) "Mapping liquefaction-induced ground failure potential", *Journal of the Geotechnical Engineering Division*, vol 104, **4**, American Society of Civil Engineers (ASCE), New York, USA, pp 433–446

YU, H S, SALGADO, R and SLOAN, S W (1998) "Limit analysis versus limit equilibrium for slope stability", *Journal of Geotechnical and Geoenvironmental Engineering*, vol 124, **1**, American Society of Civil Engineers (ASCE), New York, USA, pp 1–11

ZHENG, H, THAM, L G and LIU, D (2006) "On two definitions of the factor of safety commonly used in the finite element slope stability analysis", *Computers and Geotechnics*, 33, **3**, Elsevier BV, UK, pp 188–195

ZHU, Y H (2006) *Breach growth in clay dikes*. PhD Thesis, Delft University of Technology, Delft, the Netherlands

ZHU, D Y and LEE C F (2002) "Explicit limit equilibrium solution for slope stability", *International Journal for Numerical and Analytical Methods in Geomechanics*, vol 26, **15**, John Wiley and Sons, UK, pp 1573–1590

ZHU, D Y, LEE, C F and JIANG, H D (2003) "Generalised framework of limit equilibrium methods for slope stability analysis", *Géotechnique*, vol 53, **4**, Institution of Civil Engineers, UK, pp 377–395

ZIENKIEWICZ, O C and TAYLOR, R L (1991) *The finite element method for solid and structural mechanics*, volume 2, fourth edition, Butterworth-Heinemann, UK (ISBN: 978-0-75066-321-2)

Statutes

BS EN 13383-1:2002 *Armourstone. Specification*

BS EN 1998-1:2004 *Eurocode 8.Design of structures for earthquake resistance. General rules, seismic actions and rules for buildings*

BS EN 1998-5:2004 Eurocode 8 Design of structures for earthquake resistance. Foundations, retaining structures and geotechnical aspects

BS EN 1997-1 Eurocode 7 *Geotechnical design*

8.13 FURTHER READING

Internal erosion

CEDERGREN, H R (1967) *Seepage, drainage and flow nets*, John Wiley & Sons, New York, USA (ISBN: 978-0-47118-053-1)

FELL, R and FRY, J-J (2007) *Internal erosion of dams and their foundations*, Taylor & Francis, London (ISBN: 978-0-41543-724-0)

HOFFMANS, I G (2012) *The influence of laminar flow on piping*, pers. comms

ICOLD (2012) *Internal erosion in existing dams, levees, and dikes, and their foundations*, Bulletin 161, International Commission on Large Dams (ICOLD), Paris, France

ICE (2012) *Manual of geotechnical engineering, volume I, geotechnical engineering. Principles, problematic soils and site investigation*, Insitution of Civil engineers, Thomas Telford, London

MUALEM, Y (1976) "New model for predicting hydraulic conductivity of unsaturated porousmedia", *Water Resources Research,* vol 12, **3**, Wiley Online, UK, pp 513–522

SCHMERTMANN, J H (2000) *The non-filter factor of safety against piping through sands*, ASCE special publication, no 111, *Judgment and Innovation*, American Society of Civil Engineers (ASCE), New York, USA

VAN GENUCHTEN, M TH (1980) "A closed-form equation for predicting the hydraulic conductivity of unsaturated soils", *Soil Science Society of America Journal*, 44, **5**, Madison, USA, pp 892–898

Heave and uplift

USACE (1993) *Seepage analysis and control for dams*, EM 1110-2-1901, US Army Corps of Engineers, Washington DC, USA. Go to: **http://publications.usace.army.mil/publications/eng-manuals/**

WUDTKE, R-B and WITT, K J (2006) "A static analysis of hydraulic heave in cohesive soil". In: *Proc 3rd int conf on scour and erosion*, Amsterdam, 1–3 November 2006, S.251

Slope stability

ABRAMSON, L W, LEE, T S, SHARMA, S and BOYCE, G M (1996) *Slope stability and stabilization methods*, second edition, John Wiley and Sons, New York, USA (ISBN: 978-0-47138-493-9)

CELESTINO, T B and DUNCAN, J M (1981) "Simplified search for noncircular slip surface". In: *Proc 10th int conf on soil mechanics and foundation engineering*, A A Balkema, Rotterdam, the Netherlands, vol 3, pp 391–394

CHEN, W-F (1975) *Limit analysis and soil plasticity*, Elsevier Scientific Publishing Company (ISBN: 978-1-93215-973-8)

CHOWDHURY, R N and ZHANG, S (1990) "Convergence aspect of limit equilibrium methods for slopes", *Canadian Geotechnical Journal*, vol 27, Canadian Science Publishing, Canada, pp 145–151

FREDLUND, D G (1984) "Analytical methods for slope stability analysis". In: *Proc of the fourth int symp on Landslides, State-of-the-art*, 16–21 September 1984, Toronto, Canada, pp 229–250

HUANG, S and YAMASAKI, K (1993) "Slope failure analysis using local minimum factor of safety approach", *Journal of Geotechnical Engineering*, vol 119, **12**, American Society of Civil Engineers (ASCE), New York, USA, pp 1974–1989

HUTCHINSON, J N (1987) "Mechanisms producing large displacements in landslides on pre-existing shears", *Memoir of the Geological Society of China*, vol 9, pp 175–200

LOWE, J (1967) "Stability analysis of embankments", *Journal of Soil Mechanics and Foundation Division*, vol 93, SM4, American Society of Civil Engineers (ASCE), New York, USA, pp 1–33

M.A.VAN, A.R. KOELEWIJN AND F.B.J.BARENDS (2005) "Uplift phenomenon: model and validation", *International Journal of Geomechanics*, *Special issue on Soft Clay Engineering and Soft Clay Improvement*, vol 5, June, pp 98–106

MICHALOWSKI, R L (2002) "Stability charts for uniform slopes", *Journal of Geotechnical Geoenvironmental Engineering*, vol 128, **4**, American Society of Civil Engineers (ASCE), New York, USA, pp 351–355

POHL, R (1997) "Wellenauflauf im Übergangsbereich zwischen Brandung und Reflexion", *Hansa*, Nr. 134, pp 62–64

POHL, R and HEYER, T (2003) "Der Auflauf unregelmäßiger Wellen im Übergangsbereich zwischen Branden und Schwingen". In: *Dresdner Wasserbauliche Mitteilungen 26/2003*, TU Dresden, Institut für Wasserbau und Technische Hydromechanik (ISBN: 3-86005-376-0) pp 95–104

SARMA, S K (1987) "A note on the stability of slopes", *Géotechnique*, 37, **1**, Institution of Civil Engineers, UK, pp 107–11

SASAKI, Y (2009) "River dike failures during the 1993 Kushiro-oki earthquake and the 2003 Tokachi-oki earthquake". *Earthquake geotechnical case histories for performance-based design*, CRC Press/Balkema, pp 131–157

SENGUPTA, A and UPADHYAY, A (2009) "Locating the critical faulire surface in a slope stability analysis by genetic algorithm", *Applied Soft Computing* vol 9, pp 387–392

SERRATRICE, J F (2011) *Examples of levees and embankments failures under seismic conditions – pseudo-static equilibrium design (Exemples de ruptures de digues et de remblais sous séismes – calcul des équilibres pseudo-statiques)*, Report no 116000172

SINGH, A (1970) "Shear strength and stability of man-made slopes", *Journal of Soil Mechanic Foundation*, American Society of Civil Engineers (ASCE), New York, USA, vol 96, **6**, pp 1879–1892

SPENCER, E (1967) "A method of analysis of the stability of embankments assuming parallel interslice forces", *Géotechnique*, vol 17, **1**, Institution of Civil Engineers, UK, pp 11–26

SUN, J, LI, J and LIU, Q (2008) "Search for critical slip surface in slope stability analysis by spline-based GA method", *Journal of Geotechnical and Geoenvironmental Engineering*, vol 134, **2**, American Society of Civil Engineers (ASCE), New York, USA, pp 252–256

TAYLOR, D W (1937) "Stability of earth slopes", Journal of Boston Society of Civil Engineers, (reprinted in: Contributions to Soil Mechanics 1925 to 1940, Boston Society of Civil Engineers, USA, pp 337–386

TEMPLE, D M, HANSON, G J, NEILSEN, M L and COOK, K R (2005) "Simplified breach analysis model for homogeneous embankments: Part I, Background and model components". In: *25th United States Society on Dams (USSD) Annual Conference*, 6–10 June, 2005, Salt Lake City, Utah, USA

ZOLFAGHARI, A R, HEATH, A C and MCCOMBIE, P F (2005) "Simple genetic algorithm search for critical non-circular failure surface in slope stability analysis", *Computers and Geotechnics*, vol 32, 3, Eslevier BV, UK, pp 139–152

Settlement

CARTER, B (1991) *Correlations of soil properties,* Pentech Press, 130 p.

ICE (2012) *Manual of geotechnical engineering. Volume 1: Geotechnical engineering principles, problematic soils and site investigation*, Insitution of Civil Engineers, Thomas Telford, London (ISBN: 978-0-72775-707-4)

USACE (1989) Engineering and Design of Retaining and Flood Walls, Engineer Manual 1110-2-2502, US Army Corps of Engineers, Washington, DC.

WAKITA, E and MATSUO, M (1994) "Observational design method for earth structures on soft ground", *Géotechnique*, vol 44, **4**, Institution of Civil Engineers, UK, pp 747–755

Seismic performance

FEMA (2005) *Federal guidelines for dam safety, earthquake analyses and design of dams*, Federal Emergency Management Agency, US Department of Homeland Security, Washington, DC, USA.
Go to: **www.fema.gov/media-library/assets/documents/2482?id=1573**

HYNES, M E and FRANKLIN, F G (1984) *Rationalizing the Seismic Coefficient Method*, Miscellaneous Paper GL-84-13, US Army Corps of Engineers, Waterways Experiment Station, Vicksburg, MS, USA

MAKDISI, F I and SEED, B H (1977) *A simplified procedure for estimating earthquake-induced deformations in dams and embankments*, Earthquake Engineering Research Center Report No. UCB/EERC-77/19, University of California, Berkeley, CA, USa

TOKIMATSU, K and SEED, H B (1984) *Simplified procedures for the evaluation of settlements in clean sands*, Earthquake Engineering Research Center Report No. UCB/EERC-84/16, october 1984 University of California, Berkeley, CA, USA

USACE (2000) *Technical Bases for Regulatory, Guide for Soil Liquefaction*, NUREG/CR-5741, US Army Corps of Engineers, Washington DC, USA

YOUD, T L, IDRISS, I M, ANDRUS, R D, ARANGO, I, CASTRO, G, CHRISTIAN, J T, DOBRY, R, LIAM FINN, W D, HARDER, JR L F, HYNES, M E, ISHIHARA, K, KOESTER, J P, LIAO, S S C, MARCUSSON III, W F, MARTIN, G R, MITCHELL, J K, MORIWAKI, Y, POWER, M S, ROBERTSON, P K, SEED, R B and STOKOE II, K H (2001) "Liquefaction resistance of soils: summary report from the 1996 NCEER and 1998 NCEER/NSF workshops on evaluation of liquefaction resistance of soils", *Journal of Geotechnical and Geoenvironmental Engineering*, vol 127, **10**, American Society of Civil Engineers (ASCE), New York, USA, pp 817–833

Stability of floodwalls

ALLSOP, N W H, MCKENNA, J E, VICINANZA, D and WHITTAKER, T J T (1996a) "New design formulae for wave loadings on vertical breakwaters and seawalls". In: Proc 25th int conf on coastal engineering, September 1996, Orlando, American Society of Civil Engineers (ASCE), New York, USA

ALLSOP, N W H and VICINANZA, D (1996B) "Wave impact loadings on vertical breakwaters: development of new prediction formulae". In: *Proc 11th int harbour congress*, Antwerpen, Belgium

ALLSOP, N W H, VICINANZA, D and MCKENNA, JE (1996c) *Wave forces on vertical and composite breakwaters*, Research Report SR 443, HR Wallingford, Wallingford, UK

ALLSOP, N W H, KORTENHAUS, A, MCCONNELL, K J and OUMERACI, H (1999) New design methods for wave loadings on vertical breakwaters under pulsating and impact conditions". In: *Proc Coastal Structures '99*, Santander, Spain

ALLSOP, N W H (2000) “Wave forces on vertical and composite walls”, Chapter 4, J Herbich (ed) *Handbook of Coastal Engineering,* McGraw-Hill, New York (ISBN: 0-07-134402-0) pp 4.1–4.47

CHAI, J (2000) “Shallow foundations”, W-F Chen and L Duan (eds) *Bridge Engineering Handbook*, CRC Press, Boca Raton

CROSS, R H (1967) “Tsunami Surge Forces”, *Journal of Waterways and Harbors Division*, vol 96, **WW4**, American Society of Civil Engineers (ASCE), New York, USA, pp 201–231

CUOMO, G, ALLSOP, N W H and TAKAHASHI, S (2010) “Scaling wave impact pressures on vertical walls”, *Coastal Engineering*, vol 57, **6**, Elsevier BV, UK, pp 604–609

CUOMO, G, ALLSOP, N W H, BRUCE, T and PEARSON, J (2010) “Breaking wave loads at vertical sea walls & breakwaters”, *Coastal Engineering*, vol 57, **4**, Elsevier BV, UK, pp 424–439

CUOMO, G, PISCOPIA, R and ALLSOP, N W H (2011) “Evaluation of wave impact loads on caisson breakwaters based on joint probability of impact maxima and rise times”, *Coastal Engineering*, vol 58, **1**, Elsevier BV, UK, pp9–27

ITO, Y (1971) “Stability of mixed type breakwater – a method of probable sliding distance”, *Coastal Engineering in Japan*, vol 14, JSCE, Tokyo, pp 53–61

KIRKGOZ, M S (1995) “Breaking wave impact on vertical and sloping coastal structures”, *Ocean Engineering*, vol 22, **1**, Elsevier Science, UK, pp 35–48

US ARMY CORPS OF ENGINEERS (1989) *Engineering and design of retaining and flood walls*, EM 1110-2-2502, US Army Corps of Engineers, Washington, DC

US ARMY CORPS OF ENGINEERS (2006) *Coastal Engineering Manual*, EM 1110-2-1100, US Army Corps of Engineers, Washington, DC. Go to: http://chl.erdc.usace.army.mil/cem

Breach and inundation modeling

D’ELISO, C, OUMERACI, H and KORTENHAUS, A (2006) “Breaching of coastal dikes induced by wave overtopping”. In: **Proc 30th int conf on coastal engineering (ICCE),** San Diego, USA, ASCE, vol. 3, pp.2844–2856

EL KADI ABDERREZZAK, K, PAQUIER, A and MIGNOT, E (2009) “Modelling flash flood propagation in urban areas using a two-dimensional numerical model”, Natural Hazards, vol 50, Springer Science BV, pp 433–460

HARTNACK, J, ENGGROB, H and RUNGO, M (2009) “2D overland flow modelling using fine scale DEM with manageable runtimes”, P Samuels, S Huntington, N W H Allsop and J Harrop (eds) *Flood Risk Management: Research and Practice*, Taylor & Francis Group, London (ISBN: 978-0-41548-507-4)

OUMERACI, H, D’ELISO, C and KORTENHAUS, A (2005) *Breaching of coastal dikes: state of the art*, FLOODSITE final report T06-06-06, TU Braunschweig, the Netherlands.
Go to: **www.floodsite.net/html/publications2.asp?documentType=1**

PAQUIER, A, RENZONI, J and COGOLUEGNES, A (2005) “Quick estimate of flood risk downstream of a dike breaching”. In: Proc 3rd int symp on floods from defence to management, the Netherlands, Nijmegen, Taylor & Françis Group, London, pp 725–730

RENZONI, J, PAQUIER, A and COGOLUEGNES, A (2005) “Un outil d’estimation rapide du risque d’inondation à l’aval d’une digue. Méthodes et premières étapes de validation”, *Ingénieries – E A T, Spécial Sécurité des digues fluviales et de navigation*, pp 47–53

STANCZAK, G and OUMERACI, H (2012a) “Modeling sea dike breaching induced by breaking wave impact-laboratory experiments and computational model”, *Coastal Engineering*, vol 59, **1**, Elsevier BV, UK, pp 28–37

STANCZAK, G and OUMERACI, H (2012b) “Model for prediction of sea dike breaching initiated by breaking wave impact”, *Natural Hazards*, vol 61, Springer Science, pp 673–687

TUAN, T Q and OUMERACI, H (2012) “Numerical modelling of wave overtopping induced erosion of grassed inner sea-dike slopes”, Natural Hazards, vol 63, Springer Science, pp 417–447